

ULTRA-LOW-POWER UWB IMPULSE RADIO DESIGN: ARCHITECTURE,  
CIRCUITS, AND APPLICATIONS

A Dissertation

Presented to the Faculty of the Graduate School

of Cornell University

In Partial Fulfillment of the Requirements for the Degree of

Doctor of Philosophy

by

Rajeev Kumar Dokania

January 2011

© 2011 Rajeev Kumar Dokania

# ULTRA-LOW-POWER UWB IMPULSE RADIO DESIGN: ARCHITECTURE, CIRCUITS, AND APPLICATIONS

Rajeev Kumar Dokania, Ph.D.

Cornell University 2011

Recent advances in home healthcare, environmental sensing, and low power computing have created a need for wireless communication at very low power for low data rate applications. Due to higher energy/bit requirements at lower data-rate, achieving power levels low enough to enable long battery lifetime ( $\sim 10$  years) or power-harvesting supplies have not been possible with traditional approaches. Duty-cycled radios have often been proposed in literature as a solution for such applications due to their ability to shut off the static power consumption at low data rates. While earlier radio nodes for such systems have been proposed based on a type of sleep-wake scheduling, such implementations are still power hungry due to large synchronization uncertainty ( $\sim 1\mu\text{s}$ ).

In this dissertation, we utilize impulsive signaling and a pulse-coupled oscillator (PCO) based synchronization scheme to facilitate a globally synchronized wireless network. We have modeled this network over a widely varying parameter space and found that it is capable of reducing system cost as well as providing scalability in wireless sensor networks.

Based on this scheme, we implemented an FCC compliant, 3-5GHz, time-multiplexed, dual-band UWB impulse radio transceiver, measured to consume only  $20\mu\text{W}$  when the nodes are synchronized for peer-peer communication. At the system level the design was measured to consume  $86\mu\text{W}$  of power, while facilitating multi-

hop communication. Simple pulse-shaping circuitry ensures spectral efficiency, FCC compliance and  $\sim 30$ dB band-isolation. Similarly, the band-switchable,  $\sim 2$ ns turn-on receiver implements a non-coherent pulse detection scheme that facilitates low power consumption with  $-87$ dBm sensitivity at 100Kbps. Once synchronized the nodes exchange information while duty-cycling, and can use any type of high level network protocols utilized in packet based communication.

For robust network performance, a localized synchronization detection scheme based on relative timing and statistics of the PCO firing and the timing pulses (“sync”) is reported. No active hand-shaking is required for nodes to detect synchronization. A self-reinforcement scheme also helps maintain synchronization even in the presence of miss-detections.

Finally we discuss unique ways to exploit properties of pulse coupled oscillator networks to realize novel low power event communication, prioritization, localization and immediate neighborhood validation for low power wireless sensor applications.

## **BIOGRAPHICAL SKETCH**

Rajeev K. Dokania, was born in December 13, 1981 in the district of Banka, Bihar, India. He studied at local school “Bal Vikas Vidyalaya” till his VIIth standard, at “Rani Mahakam Kumari High School till his Xth, and at “Bihar college of Engineering” (now, NIT), Patna till his XIIth standard. He cleared IIT Entrance exam and got into Indian Institute of Technology, Kharagpur in 1999. He graduated from the IIT with a B.Tech(H) degree in 2003 securing the top rank in the Electrical Engineering Department, while working on power management IC Designs. After Graduating from IIT, Rajeev worked with Intel Corporation at Bangalore on their networking and multi-core server products as a component design engineer with focus on DFX (of Analog and Digital blocks) for two years till August 2005. Rajeev was admitted to the school of Electrical and Computer Engineering in Cornell University in August 2005. He started working as a Graduate Research Assistant in Dr. Apsel’s lab from August 2005 itself and started looking at Low Power Circuit Design in optical and wireless communication space. Rajeev received his master’s thesis in 2008 while working on optical interconnects. Rajeev also interned with the silicon photonics group at Intel in 2006-2007 for 6 months and was awarded an Intel PhD Fellowship at Cornell in 2007-2009. For his PhD dissertation Rajeev worked on ultra low power impulse radio design.

To My Dad, Mom, & Brother

## ACKNOWLEDGMENTS

A commitment for five years towards PhD has been an exciting challenge, more so, as I started on it after working in industry for two years. I will forever remain indebted to my professors at IIT Kharagpur, who always wanted me to do a PhD and helped me in pursuing it. To this end I would especially like to acknowledge Dr. Amit Patra, Dr. Soumitro Banerjee, Dr. S. Maka, Dr. T. K. Basu, Dr. A. K. Sinha, Dr. T. K. Bhattacharya, Dr S. Sen, and Dr. S. Sengupta. I would also like to acknowledge my Intel managers, S. Sreedharan, K. Pattabhiraman, and A. Dutta, who assisted me with all the helps that I needed during the application process to embark in this path. I would like to acknowledge my late Dad, who wanted me to be the first in our extended family to have pursued this path and have been the main source of inspiration. I am also grateful to all of my family members for the kind support they extended during this period.

I am indebted to my committee chair, Dr. Apsel for taking me as her graduate student, and providing guidance to do research. I am extremely thankful of her for giving me the opportunity to work on different things, helping me understand the ups and downs of academic research, and listening to my concerns over various aspects of designs very carefully. Due to her very friendly nature, she came across as a very good friend. I am immensely thankful of her for significant contribution to my professional growth as well. I am also thankful to my other advisors Dr. José F. Martínez, Dr. Michal Lipson, and Dr. Alyosha Molnar for their mentorship during the process. I would also like to acknowledge help from Dr. Sam Palermo, my Intel mentor for extending help.

Special thanks to my project-mate Xiao Wang, who first started this project, and assisted me at all the points. I can't imagine getting this far without his help and

will forever be indebted to him. I am also grateful to other project-mates Carlos Dorta-Quinones, Siddharth Tallur, and Wacek Godycki. I would also like to say thanks to my collaborators across different research groups during my initial work. Special thanks to Sasikanth Manipatruni of Dr. Lipson's group, Nevin Kirman & Meyrem Kirman of Dr. José Martínez's group, and Mathew Wattkins of Dr. David Albonesi's group, for collaboration during my initial research in Cornell.

I am also thankful to my other lab-mates, Anand, Zhongtao, Tony, Silvia, Mustansir, Paul, Bo (senior), Bo (junior), Ishita. I would like to acknowledge help from various undergrads and master students, Yi, Sahil, Joe, Brent, Tony, and Jimmy. I would like to acknowledge my various room-mates Manish, Sanjay, Siva, Ravi, Prasanna, Tiju, Biswajeet, Sudip, Nithin, and Milen for making my stay at Cornell enjoyable. I would like to thank all of my other friends in Cornell, across various research groups, also for useful discussions on various topics ranging from technology, economics, culture, and politics.

Lastly, I would also like to say thanks to Intel for their two year fellowship support and would like to acknowledge the support from other funding agencies DARPA, NSF, Welch Allyn, Army Research Lab, and Lockheed Martin.

## TABLE OF CONTENTS

<b>BIOGRAPHICAL SKETCH.....</b>	<b>iii</b>
<b>DEDICATION.....</b>	<b>iv</b>
<b>ACKNOWLEDGEMENTS.....</b>	<b>v</b>
<b>TABLE OF CONTENTS.....</b>	<b>vii</b>
<b>LIST OF FIGURES.....</b>	<b>xiii</b>
<b>LIST OF TABLES.....</b>	<b>xxvi</b>

### CHAPTER1: WIRELESS SENSOR NETWORKS AND LOW POWER RADIOS

1.1 Introduction: Wireless Communication and Applications .....	1
1.2 Dissertation Focus and Chapter Organization .....	3
1.3 Development in Sensing Technologies .....	8
1.3.1 Wireless Sensor Network Requirements .....	8
1.3.1.1 Ad Hoc (Random) Deployment.....	8
1.3.1.2 Low Cost and Low Maintenance Requirements .....	9
1.3.1.3 Range of Communication Requirements.....	9
1.3.1.4 Distributed Processing Requirements.....	10
1.3.1.5 Non-intrusiveness and small form factor .....	10
1.3.1.6 Data Rate Requirements .....	11
1.3.1.7 Unlicensed Spectrum Requirements.....	11
1.3.1.8. Low Power Requirements .....	11
1.4 A Sensor Node: Low Power sensing, processing and communication .....	13
1.5 Shannon’s Theorem & Link-Power Analysis: A Primer.....	15
1.6 A Traditional Radio Design and Its Various Power Consuming Components .....	20
1.7 Minimum Detectable Signal and Link Margin.....	21
1.8 FOM of Receiver and Link Power Optimization .....	22
1.9 Low Power Low Data Rate Radio Designs .....	25
1.9.1 Duty-Cycled/Sleep-Wake Radios.....	26
1.9.2 Sleep/Wake Radios with Asynchronous Periodic Wake-up .....	27
1.9.3 Idle Listening based Wakeup Radio.....	27
1.9.4 Impulse Radios .....	29
1.10. Impulse Radio Vs Continuous Wave Radio from High to Low Data Rate.....	30
1.11 CW Vs Impulse Radio Comparison based on different FOM.....	36
1.12 Synchronization.....	40

1.13 Chapter Summary .....	41
----------------------------	----

**CHAPTER2: GLOBALLY SYNCHRONIZED NETWORK AND PULSE-  
COUPLED OSCILLATOR**

2.1 Introduction .....	43
2.2 Firefly based Synchronization & Pulse-Coupled Oscillator .....	44
2.3 Synchronization and study of the collective dynamics of a network of pulse coupled oscillators: A Primer to existing work .....	46
2.4 Simplified assumptions in Mirollo’s Analysis .....	49
2.5 Motivation for Event Based Simulation .....	50
2.6 Event Based Simulation .....	51
2.7 Synchronization in the presence of Delays & limited connectivity .....	56
2.8 Synchronization in the presence of Frequency Mismatch.....	59
2.9 Synchronization in the presence of jitter or frequency drift.....	61
2.10 Design of Pulse-Coupled Oscillator & realizable timing uncertainty .....	62
2.11 Chapter Summary .....	64

**CHAPTER3: LOW POWER IMPULSE RADIO ARCHITECTURE AND  
DESIGN**

3.1 Introduction .....	65
3.2 Duty-cycled Synchronized Communication.....	65
3.3 System Block Diagram:.....	70
3.4 H-bridge based Transmitter Design.....	71
3.4.1 Measured Bi-Podal (BPSK) Timing Pulses @ Transmitter .....	72
3.5 Rx Gain Stage Design .....	73
3.6 Non-Coherent Peak-Polarity Detector Design .....	74
3.6.1 Detection of Pulses at low and high data rate (Measurement Results) .....	75
3.7 Differentiating Timing and Data Pulses (A Psuedo-Coherent Self-Correlated Signature Detection and Generation mechanism) .....	79
3.7.1 Measurement of the Psuedo-Coherent Self-Correlated Signature Detection ..	80
3.8 BER Measurements .....	81
3.9 Performance summary .....	81
3.10 Problems and Required Improvements .....	84
3.10.1 Bi-Podal Signal Generation and Detection Methodology .....	84

3.10.2 Interference susceptibility .....	85
3.10.3 Unlicensed Spectrum Utilization.....	85
3.10.4 Double Pulsing Scheme and the Required Power .....	86
3.11 Summary.....	87

## **CHAPTER4: AN FCC COMPLIANT DUAL-BAND UWB IMPULSE RADIO DESIGN**

4.1 Introduction .....	88
4.2 UWB communication: A Primer .....	88
4.3 FCC Spectral Mask for UWB communication.....	89
4.4 Different Ways one can utilize the UWB Spectrum: .....	91
4.5 UWB Spectrum utilization for Low Data Rate Applications.....	93
4.6 Towards Proposed Architecture .....	95
4.7 Proposed Modified Radio Architecture & timing Scheme: .....	97
4.8 Transmitter Design.....	99
4.8.1 Pulse-Shaping Requirements.....	100
4.8.1.1 Spectral efficiency .....	100
4.8.1.2 Out-of-Band Emission.....	101
4.8.1.3 Side-Lob Rejection.....	102
4.9 Transmitter System Architecture.....	103
4.9.1 Timing Circuit .....	103
4.9.2 Current-Starved Ring Oscillator.....	103
4.9.3 Triangular Wavelet Generator.....	104
4.9.4 Antenna Driver Circuit.....	105
4.10 Measurement Results.....	106
4.11. Performance Comparison of the Transmitter .....	109
4.12 Study of the effect of Non-Idealities .....	112
4.12.1 Effect of Pulse-width variation.....	112
4.12.2 Effect of Asymmetry in the Triangular wavelet.....	113
4.12.3 Effect of non-linearity in the Triangular wavelet.....	114
4.12.4 Effect of Frequency Mismatch .....	115
4.13 RX-Design: Front End Design .....	116
4.13.1 Gain Stage design & Measurement Results .....	117

4.13.2 Pulse-detection Mechanism.....	119
4.13.3 Peak-detection based self-timed pulse-detection.....	120
4.13.4 Time Domain Measurement Results .....	122
4.13.5 BER Measurement Setup & Methodology.....	123
4.13.6 RX-Sensitivity and Frequency Selectivity Measurements .....	124
4.13.7 Effect of Narrowband Interferer .....	125
4.13.8 Rx-sensitivity Control .....	127
4.14 Performance Summary .....	128
4.15 Summary.....	130

## **CHAPTER5: OTHER SYSTEM REQUIREMENTS AND OVERALL SYSTEM PERFORMANCE**

5.1 Introduction .....	132
5.2 Timing Circuitry Requirements & Measured Overall System Performance.....	132
5.3 Ultra-Wide-Band Antenna Requirements for the System .....	137
5.4 Range of Communication.....	141
5.5 Limits on Range of communication .....	142
5.6 Chapter Summary.....	145

## **CHAPTER6: SYNCHRONIZATION DETECTION AND RETENTION METHODOLOGY**

6.1 Introduction .....	146
6.2 Synchronization Detection .....	147
6.2.1 The Methodlogy for Sync Detection .....	147
6.2.2 Synchronization Retention and facilitating node joining and leaving the network.....	151
6.2.3 Sync State Detection Algorithm.....	151
6.2.4 System Synchronization State Machine .....	153
6.3 Self-Reinforcement.....	156
6.3.1 Self-Reinforcement State Machine.....	157
6.4. Modification while incorporating the PLL locking signal .....	158
6.5 Matlab Simulation of Synchronization state machine.....	160
6.6 Discrete PCO and FPGA Simulations.....	164

6.7 Impact of self-reinforcement for a global network scalability and sync error rate .....	168
6.8 Summary.....	170

## **CHAPTER7: EVENT BROADCASTING APPLICATIONS USING PCO BASED SYNCHRONIZATION**

7.1 Introduction .....	171
7.2 Structure-less Communication of Event Based on PCO Synchronization.....	172
7.2.1 The Development of a Leader Node in the Network .....	172
7.2.2 The Scheme for Event Detection.....	173
7.2.3 Event Classification.....	174
7.2.4 Event Prioritization.....	176
7.2.5 Network Simulation Results.....	176
7.3 Event Broadcasting in Synchronized Environment.....	180
7.3.1 Event Detection, Propagation, and Localization .....	181
7.3.2 Neighborhood Validation .....	185
7.3.3 Simulation Results.....	189
7.3.4 Other Conditions and Analysis.....	193
7.3.4.1 Condition when the event initiator is in the same neighborhood for two nodes.....	193
7.3.4.2 Condition when the event initiator is in the same neighborhood for two nodes.....	193
7.3.4.3 Addition of Event Classification Feature .....	193
7.3.4.4 Multiple pulses in the same bin .....	194
7.3.4.5 Network Size Limitation .....	194
7.3.4.6 Power Saving for Different Activity factor .....	195
7.4 Routing Using the Synchronized Event-broadcasting Mechanism .....	195
7.5 Summary.....	197

## **CHAPTER8: SUMMARY AND FUTURE WORKS**

8.1 Dissertation Summary .....	199
8.2 Future Works .....	200
8.2.1 Offset-spread due to Distance-delay .....	200

8.2.1.1 Solution Direction .....	202
8.2.2 A node-at the threshold of pulse detection-range.....	204
8.2.2.1 Solution Direction .....	204
8.2.3 Two nodes destructively interfering at another node .....	204
8.2.3.1 Solution Direction .....	206
8.2.4 Asymmetric communication .....	206
8.2.4.1 Solution Direction .....	207
8.2.5 Synchronization in the presence of an un-cooperating node (node failures)	208
8.2.5.1. Solution Direction .....	208
8.2.6 Security problem: an unwanted jammer in the network.....	210
8.2.6.1. Solution Direction .....	210
8.2.7 High frequency mismatch & susceptibility of the system to misdetections..	211
8.2.7.1 Solution Direction .....	211
8.2.8 Susceptibility to narrow-band in-band interferers.....	211
8.2.8.1 Solution Direction .....	212
8.2.9 Scaling to higher data rates and optimizing the FCC-mandated power spectrum .....	212
8.2.9.1 Solution Direction .....	213
8.2.10 Summary of Challenges/Future Work.....	213
REFERENCES.....	214

## LIST OF FIGURES

Figure 1.1. Various ways in which wireless communication is being used in Today's world. (Figure adapted from reference [5]).....	2
Figure 1.2. Wireless Sensor Network as a part of bigger network with intermediate point of accesses. [13] .....	9
Figure 1.3. A Wireless Sensor Node [13].....	13
Figure 1.4. Traditional Radio designs, data rate, power and energy/bit planes. (Figure adapted from [20]).....	14
Figure 1.5. Shannon's Channel Capacity Limit for a given, $P_0/N_0$ (normalized to "1"). .....	16
Figure 1.6. Shannon's limit for communication with spectral efficiency and SNR-Per-Bit. ....	17
Figure 1.7. Probability of Bit Error Rate for common modulation schemes, (The figure taken from Ref. [116], Altera Application notes).....	18
Figure 1.8. A Simple Narrow Band Transmitter and Receiver Design-blocks. ....	21
Figure 1.9. shows the power Vs Data Rate for the CW radio, note at low data rate the power is limited by the overhead and leakage power.....	24
Figure 1.10. (a.) Illustration of typical continuous wave radios from high data-rate to low data rate, (b.) the power for the duty-cycled radios.....	26
Figure 1.11. Illustration of a duty-cycled radio, with active and sleep states. ....	26
Figure 1.12. Sleep-wake scheduling, the two nodes periodically wake up for small duration and go back to sleep, if no activity is detected in the channel. Note: the nodes wakeup asynchronously in this case.....	27
Figure 1.13. Data transfer in sleep-wake scheduling based network. The receiving node when intercepts an RTS signal stays awake for the data exchange. ....	27
Figure 1.14. Data transfer in an idle-listening based wakeup radio. ....	28
Figure 1.15. Signaling in the impulse radio compared to the continuous wave radio the signal is only occasionally transmitted,.....	29
Figure 1.16. Illustrative simplified diagram shows how the signals look like in time and frequency domain for the CW and Impulse radio as one move from high data rate (full rate) to low data rate communication. Note: at high data rate the CW and Impulse signaling looks the same in time and frequency domain.....	32

Figure 1.17. Relative power ratio Vs Data rate of the Impulse radio as compared to the CW radio based on equations derived in (31) and (32), for different link margins. At reduced data rate, the Power consumed by the impulse radio is lower in both cases. .	35
Figure 1.18. Relative power ratio Vs Data rate of the Impulse radio as compared to the CW radio based on equations derived in (42) and (43), for different link margins. At reduced data rate, the Power consumed by the impulse radio is lower once the leakage and overhead power is factored in the equations.....	39
Figure 1.19. Different Synchronization topologies, (a.) One master node synchronizing the nodes in the local neighborhood of the master nodes (b.) Two master nodes c.) A globally synchronized network.....	41
Figure 2.1. Nonlinear Dynamical Pulse Coupled Oscillator System of Mirralo and Strogatz [35]. .....	45
Figure 2.2. Illustrative RC relaxation oscillator circuit generating the state function. PCO signal is generated on Node A. External coupling in the form of a current injects extra charge on the node, thereby creating jumps in the state-function. ....	46
Figure 2.3. Depiction of The internal dynamics of the Pulse coupled Oscillators from Non-synchronized to synchronized state for three nodes. ....	46
Figure 2.4. Study of collective dynamics of pulse-coupled oscillators using the concept of the center of gravity. ....	47
Figure 2.5. Simulation of a network of oscillators (~100 nodes) with random phase and evaluation of the “ $r_{cg}$ ” and the trajectory of the movement of the center of the gravity for two different initial states (a, & b). The “red dots” are placed at time instances, whenever any node in the network fires. As, can be seen the center of gravity of the collective dynamics of the network, starting with random trajectory finally settle to a periodic trajectory. In the steady state the “red” dots” appear only per cycle of revolution indicating phase synchronization. ....	48
Figure 2.6. Simulation of the collective dynamics of a network of oscillators (~100 nodes) with random phase and evaluation of the “ $r_{cg}\sin\theta_{cg}$ ” as time progresses. The “red dots” are placed at time instances, whenever any node in the network fires. As, can be seen the radius of the center of gravity in steady state settles to “1”, while only one firing per full evolution is there in the collective dynamics of the network of oscillators indicating phase synchronization. ....	49
Figure 2.7. Event based simulator: simplified algorithmic flow chart. ....	52
Figure 2.8. Dynamics of randomly distributed Pulse-coupled oscillators in a network at different time-instances. The nodes are shown in blue and red asterisk. “red” asterisks show nodes that fired at the given time the snapshot was taken. ....	54

Figure 2.9. Stroboscopic phase view of 6 different nodes relative to one fixed node. The phases of 6 nodes are marked in time, every time the fixed node fires. As, can be seen the nodes finally synchronize their phases in time.....	55
Figure 2.10. Stroboscopic phase view of 6 different nodes relative to one fixed node. The phases of 6 nodes are marked in time, every time the fixed node fires. As, can be seen the nodes create clusters, where the phases are not aligned, i.e. lack of synchronization.....	55
Figure 2.11. Various iterations of simulations done using the event simulator with random connectivity and different initial phase conditions, the nodes synchronized at all time, while the time to synchronization was also fairly limited in it's upper bound, the lower bound is due to minimum time we wait before declairing the advent of synchronization.....	56
Figure 2.12. synchronization/non-synchronization boundaries for a group of oscillators with inter-node delays. The delays and blackout are given as normalized units (normalized to nominal period of oscillation). The region in black shows the parameter space, over which robust synchronization can't be achieved. A large range of blackout value however still exist, over which robust synchronization can be achieved. The simulation also gives the trend for the minimum required blackout time as 2 times the maximum inter-node delays. ....	58
Figure 2.13 : Dynamics of oscillators with large frequency mismatch. At low coupling, the node period doesn't stabilize to the steady state value. As, the coupling is increased, the node settles to the stable frequency/period.....	59
Figure 2.14. Synchronization/non-synchronization boundaries for a group of oscillators with frequency mismatch. The region in black shows the parameter space, over which robust synchronization can't be achieved. A large range of frequency mismatch value and corresponding coupling factor however still exist, over which robust synchronization can be achieved. ....	60
Figure 3.1. Timing and data bin for exchange of information between different nodes. ....	66
Figure 3.2. (a.) Decentralized multi-hop and (b.) centralized cluster-head based network. ....	66
Figure 3.3. Timing Scheme for a centralized Master-slave configuration, different bins can be utilized for dedicated communication between two nodes. ....	67
Figure 3.4. Hidden Terminal problem, node "c" can create collision at node "B" disturbing the existing communication between node "A" and node "B". ....	68
Figure 3.5. Simplified System Block, showing the Tx, Rx and the timing block .....	69

Figure 3.6. Simplified System Block, showing the Tx, Rx, and The timing Block. ....	70
Figure 3.7. (a) Schematic of the antenna driver circuit, (b) timing diagram, (c) signal flow through antenna for a +Ve polarity (“1”) signal. ....	71
Figure 3.8. (Measured) Bi-podal Signal generated by the transmitter @ a data rate of 50Mbps. ....	72
Figure 3.9. Schematic Diagram of the gain stage of 5-stage differential amplifier chain, each providing ~7dB gain. ....	73
Figure 3.10. Measured and Expected gain from the 5-stage gain amplifier. ....	74
Figure 3.11. Schematic of the non-coherent pulse polarity detector and the corresponding timing. ....	75
Figure 3.12. (Measured) Waveform showing, transmission of positive as well as negative polarity signal and the corresponding detection on the Rx at a faster 50Mbps data rate. <u>Vout+</u> and <u>Vout-</u> go high corresponding to the polarity of the detected signal. ....	76
Figure 3.13. (Measured) Waveform with the bi-podal signaling at low data rate with 1100 sequence and the corresponding detection of pulses in time. ....	77
Figure 3.14. (Measured) Pulse detection within a 10ns window of RF-ON, (Relative delays on the scope signals were controlled to correspond to the signal timing at the chip for this measurement). ....	78
Figure 3.15. (Measured) Eye-diagram of the falling edge (active edge), indicating received pulse arrival jitter as compared to the Tx-transmit request. Uncertainty is only ~100ps. ....	78
Figure 3.16. Schematic of Pseudo-Coherent self-correlated signature generation and detection mechanism. ....	79
Figure 3.17. (Measured) waveform showing detection of the signature pulse as well as the normal pulse. <u>Vout+</u> and <u>Vout-</u> go high corresponding to the polarity of the detected signal, while the signature detected signal (active low) is asserted only at detection of the signature pulses. ....	80
Figure 3.18. ( Measured ) Variation of BER with separation between Rx and Tx antennas for single pulsing based communication. ....	81
Figure 3.19. (Measured) Variation of BER with sub-threshold bias voltage of the peak detector for single and double pulsing based communication @ an average Rx received power of -75dBm. ....	82

Figure 3.20. Die Photo of Tx/Rx Test-Chip in 90-nm CMOS process. ....	82
Figure 3.21. ( Measured ) Assymetry in bipodal signal generation, the uptick is stronger than the down-tick. ....	84
Figure 3.22. ( Measured ) Periodic GSM signal, as received by the antenna. ....	85
Figure 3.23. ( Measured ) zoomed out version of the burst of periodic GSM signal, as received by the antenna. ....	85
Figure 3.24. (Measured) Data Signal, and the corresponding echo from a different reflected path (multi-path). ....	86
Figure 4.1. Continuous Wave Vs Impulse based UWB Radio and signaling .....	89
Figure 4.2. FCC mask for UWB communication [55] .....	90
Figure 4.3. Different types of Gaussian Wavelets utilized for impulse based communication. Higher order derivatives are also utilized. ....	92
Figure 4.4. The spectral radiation profile with different derivatives of the Gaussian pulses. ....	93
Figure 4.5. Carrier-based pulsing scheme for impulse generation in UWB Band .....	94
Figure 4.6. A carrier based impulse and indicative spectral profile. ....	94
Figure 4.7. FCC mask and the corresponding utilization with the sub-bands of 500MHz each. ....	94
Figure 4.8. FCC mask and the corresponding utilization with the sub-bands of 500MHz each. ....	95
Figure 4.9. Modified System Architecture. ....	97
Figure 4.10. Timing Scheme for the modified Architecture .....	98
Figure 4.11. Simplest way of generating a wavelet based on carrier-wavelet modulation. ....	99
Figure 4.12. Different Modulation schemes with impulse based UWB communication. ....	100
Figure 4.13. Different pulse wavelets and the corresponding spectral profiles (figure taken from ref. [67]). ....	101
Figure 4.14. MATLAB simulation of the output spectrum with (a) rectangular, and (b) triangular pulse shapes. ....	102

Figure 4.15. Impulse radio transmitter architecture. ....	103
Figure 4.16. Three-stage current-starved ring-oscillator. ....	104
Figure 4.17. Rectangular-to-triangular wavelet generator. ....	105
Figure 4.18. Simple inverter, (b) modulated inverter, and (c) class-C antenna driver circuits. ....	105
Figure 4.19. Die photo of the chip with the two driver circuits. ....	106
Figure 4.20. Measured output (a) without pulse-shaping, and (b) with pulse-shaping. ....	107
Figure 4.21. Measured output spectrum with (a, b, c) rectangular pulse shape, and (d, e, f) triangular pulse shape at 5Mbps for the 3 different frequency bands. ....	108
Figure 4.22. Power Vs Data Rate of different published schemes and comparison to our work. (ref. are [66, 74, 62, 75, 71, 72, 73, 70] in order). ....	110
Figure 4.23. Energy/bit Vs Data Rate of different published schemes and comparison to our work (ref. are [66, 74, 62, 75, 71, 72, 73, 70] in order). ....	111
Figure 4.24. Normalized Energy/bit Vs Data Rate of different published schemes and comparison to our work (ref. are [66, 74, 62, 75, 71, 72, 73, 70] in order). ....	111
Figure 4.25. Spectral profile impact with Impulse wavelet width variations. ....	112
Figure 4.26. Spectral profile impact with asymmetric Impulse wavelet rise and fall time. ....	113
Figure 4.27. Spectral profile impact with non-linearity in the circuit. ....	114
Figure 4.28. Effect of frequency mismatch between the receiver and the transmitter.[68] ....	115
Figure 4.29. Receiver Front-End design, consisting of 5 gain stages followed by a non-coherent detector ....	116
Figure 4.30. Single stage of the 5-stage band-tunable duty-cycleable gain stage. ....	117
Figure 4.31. S11 measurement of the die at various frequencies. ....	118
Figure 4.32. Measured gain of 5-stage gain circuit at different control voltages (Vctl). ....	118

Figure 4.33. Most common pulse detection methodologies, such as analog correlation as well as digital correlation techniques both consume high power either due to very precise timing requirements (~50-100ps) or high sampling rate (~2Gbps). .....	119
Figure 4.34. A survey of non-coherent and coherent receiver design papers. Non-coherent detection schemes tend to be lower power [112].....	120
Figure 4.35. Schematic of non-coherent detection scheme .....	121
Figure 4.36. Time-domain Detection of the signal by the receiver .....	122
Figure 4.37. The eye-diagram of the pulse_det signal .....	122
Figure 4.38. Antenna received signal and corresponding pulse_det signal at an antenna separation of 1.5m. ....	123
Figure 4.39. Measured OOK detection, while duty-cycling. (With RF-ON, the output stage shows a small dip due to turn-on transients.) .....	123
Figure 4.40. BER Measurement Setup for the receiver test-chip.....	124
Figure 4.41. Measured Rx-sensitivity @100kbs for the two bands. ....	125
Figure 4.42. Measured BER Vs Carrier frequency of the input impulse of fixed strength, with channel tuned to the 3.5GHz and 4.5GHz bands respectively. ....	126
Figure 4.43. Measured Signal to narrow-band Interference power ratio (SIR), (instantaneous power) at different frequencies, when the receiver is configured to listen into one of the two bands. ....	126
Figure 4.44. Measured Rx-sensitivity at BER of $10^{-5}$ while varying the Vbiasn for both 3.5GHz and 4.5GHz bands.....	127
Figure 4.45. Measured Rx-sensitivity at BER of $10^{-5}$ while varying the Vbiasp for both 3.5GHz and 4.5GHz bands.....	127
Figure 4.46. Die Photo of the Rx test chip fabricated in a 90nm CMOs process.....	129
Figure 4.47. Energy/bit comparison of the receiver with other recently published results, (figure adapted from ref. [112]). .....	130
Figure 5.1. Timing Scheme of the system, the “red” and “green” colored time instances are the ones where the RF is “ON”, during the duty-cycling mode. ....	133
Figure 5.2. A simple set-reset latch controlling the band-select logic for the receiver and transmitter. At the end of the data-bin the band is set to the “sync”, while at the end of the “sync” bin the band is set to “data”. The band-switching time was simulated	

to and measured to be 50ns (~1-bin) duration, requiring the data-bin and the sync-bin to be apart by at least 1-bin for correct operation of the scheme. ....	134
Figure 5.3. Die Photo of the system chip with different blocks involved in the design, in a 5mmX5mm die, the actual area occupied by the required circuit blocks was 5mmX2mm. ....	135
Figure 5.4. System board with the system chip for system testing. ....	135
Figure 5.5. (a.) Designed vertical monopole antenna with a radius of 2.5cm (b.) radiation profile and the (c.) performance simulation using HFSS. ....	138
Figure 5.6. S11 measurement showing wide-band matching, and the path loss (S21) over 1.2m distance with elliptical monopole antenna. ....	139
Figure 5.7. (a.) A folded-strip monopole UWB antenna. (b.) S11 matching measured Vs simulation (c.) Measured S11 for different dimensions of the antennas. ....	140
Figure 5.8. Channel loss and received signal amplitude for different transmit signal amplitude showing the range of communication possible. ....	141
Figure 5.9. a.) Average power limit at various pulse-repetition rates, and (b.) the corresponding impulse peak-peak swing limit. ....	143
Figure 5.10. Pulse Repetition rate Vs. maximum communication distance achievable using the FCC constraints on the radio. While at high data rates, the range of communication is limited due to average power requirements, at lower data rate the range of communication gets saturated due to peak power radiation constraints. ....	144
Figure 6.1. PCOOut and the Sync(detected) timing in the case of a single isolated node in the network .....	148
Figure 6.2. PCOOut and the Sync (detected) timing at a master node in the network. The sync detected pulse is during the phase of the blackout, thereby effectively not resulting into any coupling at the node.....	148
Figure 6.3. PCOOut and the Sync (detected) timing at a slave node in the network, the time-correlation between the two event is lower than the circuit delays ( $T_{d0}$ ).....	148
Figure 6.4. PCOOut and the Sync(detected) timing, unsynchronized state, as the correlated delay between the two signal is large. ....	150
Figure 6.5. PCOOut and the Sync (detected) timing, unsynchronized state as more than one sync-detected pulses were detected between consecutive firings of the PCO. ....	150

Figure 6.6. Event Generation and detection circuits. These events control the system synchronization state machine.....	152
Figure 6.7. System Synchronization State Machine.....	155
Figure 6.8. PCOOut and the Sync(detected) timing,in case of missed sync pulses, that results in to large deviation in period. ....	156
Figure 6.9. PCOOut and the Sync (detected) timing in case of missed sync pulses, with the incorporation of the fake coupling provided by the PLL, at the expected time of the sync-detection pulse. ....	156
Figure 6.10. Reinforcement implementation scheme (simplified block diagram). ....	157
Figure 6.11. Reinforcement State Machine keeps track of Reinforcements also helps in detecting the loss of synchronization in conjunction with the system synchronization state machine.....	159
Figure 6.12. PCOOut and PLL correlation to generate the PLL-Lock signal .....	160
Figure 6.13. Time evolution of the phase of different nodes (a total of 7 in this case) at different instances of time without reinforcement. Red indicates unsynchronized state, green- synchronized in slave, and black- synchronized in master mode. Nodes start from unsynchronized state, then get synchronized, while losing synchronization due to misdetection, but able to regain synchronization. ....	161
Figure 6.14. Time evolution of the phase of different nodes (a total of 7 in this case) at different instances of time without reinforcement. Red indicates unsynchronized state, green- synchronized in slave, black- synchronized in master mode, yellow- means self-reinforcement was applied (synchronized state). Nodes start from unsynchronized state, then get synchronized, while still maintain synchronization even during misdetections due to self-reinforcement feature.....	162
Figure 6.15. Time Evolution of the period for different nodes in the network, in presence of error injection without the self-reinforcement feature. ....	163
Figure 6.16. Time Evolution of the period for different nodes in the network, in presence of error injection with the self-reinforcement feature enabled. ....	163
Figure 6.17. PCO-counter based implementation concept. Instead of non-linear state-function, a linear, counter based PCO-state function is implemented. While the amount of coupling is tracked by another counter, which increases the coupling count value (the amount of discrete jump in the count value if a pulse is detected) over time, thereby keeping the essence of the PCO dynamics intact for simulation in an FPGA environment (note: no coupling was applied in the actual pco-state diagram above, coupling count shows how much coupling will be applied, if there was a sync pulse detected at a given point of time.....	164

Figure 6.18. A small snapshot of the discrete PCO implementation program in Verilog. The detailed program is given in the appendix. count_pco is the pco state function implemented using a counter. While, the couple is also a counter, but increments it's value from an initial value (couple_init) and in discrete jumps dictated by thres_mod parameter value.....	165
Figure 6.19. ISIM simulation of the discrete-PCO implementation. Note, the 4-PCOs signal starting from a random unsynchronized state move to a synchronized state, following the PCO dynamics as elaborated above in the discrete FPGA implementation. The 4 PCOs had mismatch in their nominal frequency.....	165
Figure 6.20. ISIM Simulation: States of the various pco-clocks and their pco-firing instances, showing error injection and recovery (loss of synchronization to synchronized mode of operation), in case of no self-reinforcement. ....	167
Figure 6.21. ISIM Simulation: States of the various pco-clocks and their pco-firing instances, showing error injection, not resulting into any loss of synchronization, due to self-reinforcement that happens locally at the node. See the change of states at the node that correspond to the dynamics here. ....	167
Figure 6.22. FPGA simulation depiction of the state-machine with discrete PCO with 4 different PCOs. The displays show the states of each pco in different time. State-0 unsynchronized, state-1-synchronized in slave mode, state-2 synchronized in master mode, state-4, synchronized in master (but on lookout for new nodes) and state-3 means reinforcement. Plot c and d are without reinforcement enabled, while the plofc and g. are with reinforcement enabled. ....	169
Figure 7.1. Simulation results showing the randomly distributed frequency of the various nodes (when no coupling is there) for different frequency variations across different runs (iterations) and the corresponding frequency (in red diamond shape) of the network in the synched state after the coupling is enabled. Note the frequency of the synchronized network corresponds to the highest frequency node. ....	173
Figure 7.2. Depiction of frequency distribution in case of the passive communication of events. Nominally frequencies are centered at $f_0 + \Delta f$ , but on the advent of an event the PCO frequencies become $f_1$ or $f_2$ depending upon the type of event sensed.....	174
Figure 7.3. A simplified schematic of possible implementation of the passive event communication methodology. ....	175
Figure 7.4. State Representation of the Passive Event communication. ....	175
Figure 7.5. Matlab simulation of the global period in case of event transition and event recovery. Initially the nodes are all un-synchronized, and so the nominal global period is low. Once synchronized, the node period is nominally $\sim 1$ , when an event happens at any node, the global period goes low, while on recovery it sets itself back to the nominal value. ....	176

Figure 7.6. Matlab simulation of the global period (of all the nodes) in case of event transition and event recovery. Also shown is the case of event 1 and event 2 happening simultaneously (shows event2 prioritization).....	177
Figure 7.7. Shows the scalability of the scheme to more than 2 events. Also, shows a failure mode, in this case for event-7, the network doesn't synchronize, as the coupling wasn't sufficient to counter the increased frequency mismatch.....	178
Figure 7.8. Matlab simulation of power saving at different number of events classification and frequency mismatch for single cycle event transition and recovery. Higher the number of event classification support, lesser is the amount of power saving one can achieve at the receiver. With calibrated oscillators, while supporting 8 different types of events one can still save close to 80-90% of the RF power by duty-cycling the receiver.....	179
Figure 7.9. Illustration of the bin structure for event detection and localization. ....	181
Figure 7.10. Example depiction of 1-node event initiation and the automated hop-count realization for all the nodes in the network. (The shaded area in the Rx, Tx column, means the corresponding circuit is switched "off"). ....	183
Figure 7.11. Figure illustrating the meaning of information received and information transmitted in the case of event propagation and localization methodology as described in the section above. ....	184
Figure 7.12. One example definition of the bin structure for event detection, localization methodology with immediate neighborhood validation. ....	185
Figure 7.13. Example depiction of 1-node event initiation but no neighborhood validator and the corresponding activity at various nodes, showing the event message getting locally dropped. (Shaded region in the Rx, Tx table means the receiver or the transmitter in that particular bin was "turned off"). ....	186
Figure 7.14. Example Depiction of 1-node event initiation and one validator and the corresponding activity at various nodes, showing the event message getting propagated in the network and the automated hop-count realization for all the nodes in the network. (Shaded region in the Rx, Tx table means the receiver or the transmitter in that particular bin was "turned off").....	187
Figure 7.15. Table illustrating the meaning of information received and information transmitted in the case of Event propagation, localization and immediate neighborhood validation methodology as described in section above. ....	188
Figure 7.16. Example simulation of events and the corresponding hop-count estimation from the event-node using the algorithm in a sensor network: (a.) event-node (red diamond shape) at the close to center of the network (b.) event-node at the bottom right-edge. Nodes at various hop-counts are shown in different colors, while	

reusing the color combination after 5-hop-counts. There is a radial symmetry of nodes (shown as dots) located at the same hop-count away from the event-node. .... 189

Figure 7.17. Hop-count Vs actual distance distribution of the nodes from the event-node. As can be seen there is a linear relationship between the hop-count and actual distance of the node with very small error distribution due to discreteness of the hop-count. .... 190

Figure 7.18. Simulation of localization point based on base-stations at the corner of the rectangular sensor network field. Red-diamond shape is the event-node, while the yellow rectangular box shows the estimated value. a.) simulation with dense network (b.) simulation with a less dense network. Sensor nodes are marked as blue asterisk points. .... 191

Figure 7.19. Simulation of maximum errors for various iterations (blue), while varying the node density. The average errors numbers are marked with red-circles for each node density. For sufficient node density the localization error can be reduced to less than max one-hop distance. .... 192

Figure 7.20. One example definition of the bin structure for event detection, localization methodology with immediate neighborhood validation as discussed in section. .... 194

Figure 7.21. Network Event Activity and per node power consumption as % of “fully on” power. .... 195

Figure 7.22. Bucket Passing type of packet routing scheme. .... 196

Figure 8.1. Showing the offset expectation, in the neighborhood of a node “B” in the simple pulsing scheme. Based on different values of “x” for “B” to be able to receive the signal from both “A” and “C” has to open the window for “2x” duration in the data-bin. .... 201

Figure 8.2. (a.) RX-ON window opening requirement with “X” known , using double pulsing (b.) RX-ON window opening requirement with “X” unknown, using double pulsing. Both result into power saving for the receiver, due to lower window opening requirements. .... 202

Figure 8.3. (a.) RX-ON window opening requirement with  $x = d_{avg} + \Delta x$ , in case of single pulsing, (b.) the Rx-On opening requirement with double pulsing in the same situation. .... 203

Figure 8.4. Showing an example network configuration and how a node “C” can have destructive interference from the signal emitted from node “A” and node “B”, making it blind to node “A” and node “B” even though it’s there in the neighborhood of the two nodes. .... 205

Figure 8.5. An Assymmetric network configuration, “A” can receive the signal from “E” directly but “E” can’t receive the signal from “A” directly. .... 207

Figure 8.6. Concept of selective coupling, based on “sync” detected at various instances, a node evaluets the phase-change required, but applies the coupling only after Twait, and applies the coupling corresponding to the closest signal that was received, thereby effectively ignoring the coupling from “sync1” in this case..... 209

Figure 8.7. (a.) spectrum without frequency dithering. (b.) spectrum with frequency dithering..... 213

## LIST OF TABLES

Table 1.1 Average Power Density of various power source and scavenging devices [15][16].....	12
Table 3.1 (Measured) Performance summary and comparison to the best UWB-IR state-of-the-art .....	83
Table 4.1. FCC Spectral Emission Mask Limits for UWB Communication .....	91
Table 4.2 Wave-shapes and the corresponding spectral efficiencies .....	102
Table 4.3 Measured Overall Power performance comparison to other UWB-IR Transmitters.....	107
Table 4.4 Measured Overall Power performance comparison to other UWB-IR Transmitters.....	109
Table 4.5 Performance summary and comparison to the state-of-the-art design .....	128
Table 5.1 Performance Summary of the system and comparison with the state-of-the-art IR-UWB design.....	136
Table 5.2 Measured Timing Performance Parameter of the PCO and PLL.....	137
Table 5.3 Measured Power Performance Summary.....	137

# CHAPTER 1

## WIRELESS SENSOR NETWORKS AND LOW POWER RADIOS

### 1.1 Introduction: Wireless Communication and Applications

Communication of information is one of the most basic traits of all living creatures. Starting with sound and light based means of communication in the primitive age to today's wireless communication; it has undergone an impressive evolution. There have been multiple drivers to the success story of wireless communication; with mobility among the most important reason for large scale deployment of wireless networks of today. Wireless access in addition to allowing mobility also eases constraints where other means of communication cannot be deployed.

While there are many claimants to the innovation/demonstration of first wireless communication, one can safely establish the origin of the concept to be somewhere in early 1870s [1]. In less than 125 years starting from Hertz's spark-plug based low frequency (~50Hz) radios in 1890s [1] to today's 60-GHz radio [2] developments, wireless communication has gone through many incarnations, in which it has been brought to be used in practice. Today it is being used for everything electronic from short-range endoscopic imaging [3] to long-range terrestrial communication [4]. It is being used for low rate sensing applications to moderate rate audio/voice communication to high data rate streaming video communication. From cell-phones to satellites, wireless communication is one of the most prevalent means of communication in today's world (Fig.1.1). User mobility, non-intrusiveness and cost of infrastructure deployment are still the three main driving forces behind various technological developments in this field.

With the growing list of applications where wireless communication holds promise, also comes the requirement to make the solution optimized for the specific application. This optimization for end-user applications has resulted in various types of radio architectures and standards such as GSM, CDMA, GPS, Wi-Fi, WPAN, WLAN, Bluetooth etc., with each application and standard targeting a different type of performance parameter. These performance parameters for a wireless communication network are mostly bounded under spectrum bandwidth, range of communication, power/energy efficiency, and max data rate. Though the idea for an ideal wireless network would be to use as little spectral bandwidth as possible while using the least power and providing the highest data rate, certain fundamental laws of physics govern trade-offs one has to come to terms with based on intended end-usage. The development in radio designs over the years has been to come as close to these

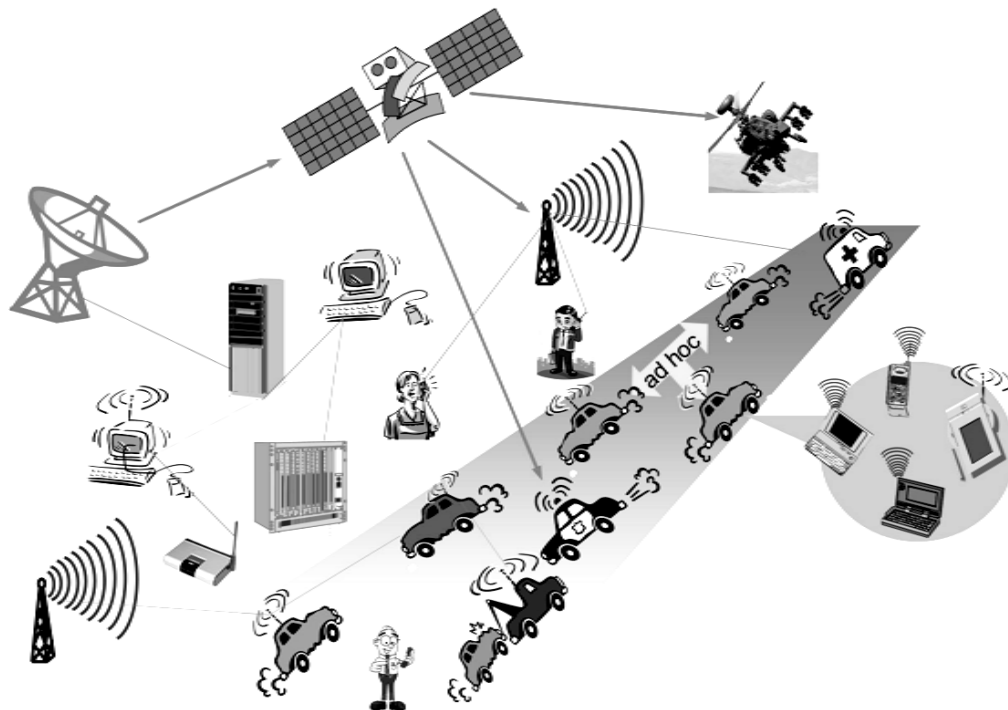


**Figure 1.1. Various ways in which wireless communication is being used in Today's world. (Figure adapted from reference [5]).**

fundamental limits as possible. While, the designers have been coming up with various innovative ways of optimizing designs to provide good performance for any given application, newer applications arising from technological advances in other fields sometime warrant an architectural change. One such technological advance of interest in this work is that of low cost sensing technology.

## **1.2 Dissertation Focus and Chapter Organization**

This dissertation explores the latest advances in wireless sensor network design, and looks in particular for the requirement of low power communication interface for these networks. A survey of various requirements for these wireless sensor networks shows how the need for low power communication is at the center of almost all the research activities in this field. Though low data rate and short-range requirements typically associated of these wireless sensor network applications should have logically meant low power communication, we still don't see radio designs in this space that consume low enough power to sustain long battery life time of 5-10 years. In this dissertation we present the architecture, design and novel applications of ultra low power radio design that cater to the requirements of wireless sensor networks.

In the rest of this chapter (**Chapter1**) of this dissertation we look at wireless sensor networks, and their many requirements. We then look at fundamental limits based on link optimization that govern the communication and energy requirements of a traditional radio design and how it is mostly governed by the overhead power required with the transceiver. We then discuss the potential use of duty-cycled radios as a solution to this problem. We discuss different existing duty-cycled architectures, such as periodic sleep-wake radios, where the radio nodes wake-up asynchronously, as well as the idle-listening based radio architectures. We also discuss the limitations of these architectures and demonstrate the need for impulse based data scheme for

significant power saving. An analytical comparison of impulse radio designs with continuous wave radio designs is also presented to find relative power trends of the two designs that reveal the advantages of impulse radio for low power short range applications. We (with help from project-mate Xiao Wang) then discuss about the synchronization requirements and limitations. While the peer-peer synchronization or a one-master-many slave kind of synchronization can be easily done with the existing methodology, for scalable network and multi-hop architectures a need for global synchronization will then be discussed.

In **Chapter 2** of the dissertation we discuss about various phenomena in nature that lead to global order/synchronization. We specifically focus on southeast-Asian fireflies and the interesting dynamics involved therein that lead to a group of fireflies blinking together in a group. We look at the existing work in understanding this behavior that promises to give a globally synchronized network and look at work done by various groups in mathematical modeling of pulse-coupled oscillators that map the dynamics of these fireflies. In the wake of existing analysis that doesn't incorporate non-ideal effects of frequency mismatch, delay, jitter and limited connectivity; we evaluate the robustness of the synchronization in the presence of these non-idealities. We describe an event based simulator that could incorporate the non-idealities and find the constraints in the system to ensure robust synchronization while doing extensive simulations with randomized parameter space. We present how the constraints placed on the design of the PCOs can be easily achievable, without much degradation on the quality of synchronization. We also discuss the quality of synchronization in the presence of jitter, and discuss the design and measured results of low jitter (high quality) synchronization of a group of oscillators, which can enable aggressive duty-cycling of the RF-frontend.

In **Chapter 3** of the dissertation we present the different ways a globally

synchronized network be used for exchange of information between sensor nodes, and the corresponding requirements for both low data rate, as well as bursty fast pulse generation and detection. We also discuss the need for differentiating the timing and data pulses. Based on these requirements a preliminary design of impulse based duty-cycled, non-coherent transceiver in a 90nm CMOS process is presented. The measured results show only  $19\mu\text{W}$  power consumption at a data-rate of 100kbps. The design was measured to give a BER of  $10^{-5}$  and works for a range of 2.5m at an average Rx-sensitivity of -81dBm, making it useful for low-power short-range wireless sensor networks. The transceiver was designed to enable bi-podal (BPSK) as well as OOK schemes and pseudo-coherent self-correlated signature detection and generation mechanism was also implemented to differentiate between data and timing pulses. While order-of-magnitude better performance was achieved when compared to state-of-the-art designs, operating in unlicensed spectrum limited the performance of this design. Other problems such as larger time-window for the receiver for detection of timing pulses in the presence of multi-path reflections, interference susceptibility and the asymmetry in bi-podal signaling warranted additional modifications in the design.

In **Chapter 4** of the dissertation we discuss the design of an FCC compliant OOK-modulation based UWB Impulse transceiver design that operates in unlicensed band. We also make use of time-multiplexed frequency bands to separate the timing and data pulses, thereby saving additional power associated with larger window sizing in the current design. In this chapter, we specifically look at FCC's UWB spectral mask, and provide design and measurement results of a multi-band radio that operates while complying with the spectral mask constraints placed by the FCC. The receiver and transmitter circuit described in this chapter can be used to implement an ultra-low-power impulse radio optimized for duty-cycled operation of the power-hungry RF circuits. The measured power consumption for the transceiver was found to be  $20\mu\text{W}$

at 100Kbps while using external timing controller. To the best of our knowledge, these operating power levels are far below any other published to date for these data rates, and can enable years of continuous communication with standard batteries or integration with scavenging power supplies.

In **Chapter 5** of the dissertation we present in brief the performance achieved for the overall system with the timing circuitry designed in our lab (by project-mate X. Wang). We talk about the timing and power performance of the timing circuitry and how they stack up in deciding the overall system performance. We then move to the design & measured performance of some of the wide-band Omni-directional antennas required for our application. After the antenna design, we focus on path losses and the expected range of achievable communication by the designed transceiver circuitry. In this chapter we also discuss about how one can increase the range of communication further by increasing the transmitted power due to available margin in the FCC-mask. We then look at scalability of the system for even lower data rate communication and the peak power limit on the transmission power therein which puts constraints on average power at lower data rates based on peak-average power ratio (PAPR).

In **Chapter 6**, we propose a methodology to locally detect the advent of synchronization at a node. The synchronization detection state machine enables the detection of synchronization as well as helps maintain synchronization in combination with the self-reinforcement feature. The self-reinforcement methodology proposed in this chapter uses the time history of the sync-pulses to enable the synch state machine to maintain the synchronization in the event of missing sync pulses. The state-machine was simulated with Matlab as well as FPGA. FPGA was used to have a hardware implementation of the scheme and was also used to implement a discrete PCO and a discrete PLL to enable simulation of the whole system. The scheme was found to be correctly working for the synchronization detection in conjunction with the self-

reinforcement scheme even in the presence of missing pulses.

In **Chapter 7**, we present novel applications for globally synchronized network in the event-broadcasting space for applications such as intrusion detection, temperature exception detection, pressure exception detection, gas leak detection etc. In these types of applications one is primarily interested in knowing if an exception (or an event) occurred at any node. The goal in these applications is to broadcast the occurrence of an event to the entire network in the simplest and fastest way possible. In some applications localization of the event in space is also of importance. In this chapter we propose two different methodologies that rest on the unique properties of the PCO based global synchronization scheme. The first proposed scheme enables structure-less communication of event information to all the nodes in the network without the need of any packet formation. The second scheme can be used in conjunction with any globally synchronized network, and enables not only event propagation, but also localization, neighborhood validation, and fault detection. The scheme makes use of dynamic duty-cycling of the bins as well, thereby facilitating low power communication. We also propose how to use the method while facilitating packet type communication as well as for very low latency routing of the packet to data-collector node in a bucket-passing type of algorithm.

In **Chapter 8**, we discuss various challenges that we came across while designing and analyzing the system. Problems associated with the proposed global synchronization scheme can result into some of the system problems such as symbol self-interference, offset spread, in-band narrowband interference etc. These problems can have significant potential for performance degradation of the system, and are discussed in that context in this chapter. We also propose some solutions that can be pursued to tackle each one of the challenges while presenting the concluding remarks on the dissertation.

### **1.3 Development in Sensing Technologies**

In recent times there have been impressive successes in designing low cost sensors to sense almost anything from pressure [6], temperature [7], humidity, to various biometric information [8]; from motion & intrusion detection [9] to fire hazard [10] and gas leakage detection [11]. Ability to sense these environmental phenomena in a cost effective manner has opened up new research opportunities. Examples of new applications include environmental monitoring, which typically involves soil, water and air monitoring for agriculture; habitat monitoring, military surveillance, border intrusion detection, seismic activity detection, inventory tracking, EEG, ECG and other vital biometric information sensing for early detection of diseases etc [12]. These new applications warrant not just the ability to collect the information but also the ability to disseminate i.e. co-ordinate and communicate the sensed information to a host of wider network systems. This also opens up an opportunity for wireless communication in these fields primarily due to its ease of deployment and non-invasiveness.

#### **1.3.1 Wireless Sensor Network Requirements**

A wireless sensor network is typically made up of a lot of small, low-cost sensor nodes, which collect, process, and propagate sensed information to a wider network (Fig.1.2). As explained before, a wireless sensor network can facilitate remote control and monitoring of various phenomenon of interest. In spite of the diverse applications possible for wireless sensor networks there are some unique technical challenges and requirements associated with the targeted applications.

##### **1.3.1.1 Ad Hoc (Random) Deployment**

Most of the time one is required to deploy sensor nodes with little to no infrastructure. Typical way of deployment in these cases will be to randomly throw

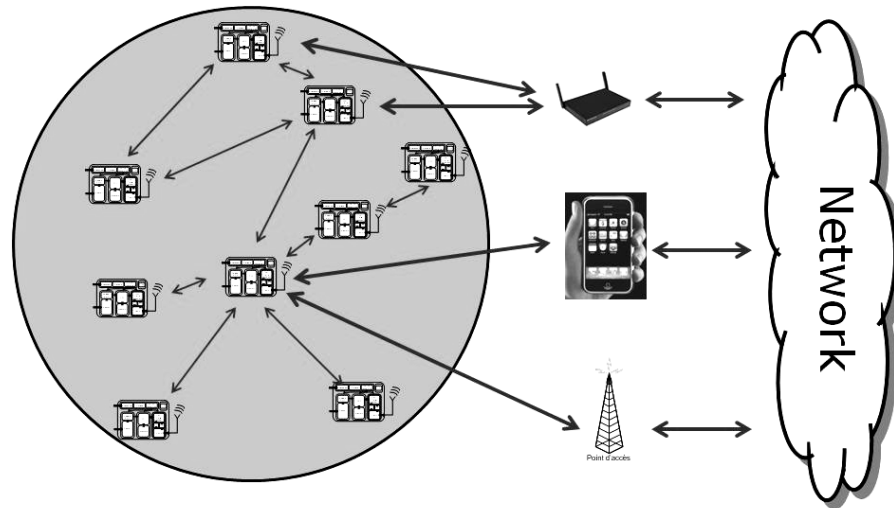


**Figure 1.2. Wireless Sensor Network as a part of bigger network with intermediate point of accesses. [13]**

them in a field/area. In this type of deployment the nodes need to identify connectivity and distribution automatically [12].

### **1.3.1.2 Low Cost and Low Maintenance Requirements**

Due to the distributed nature of sensing in most sensing applications the cost of each node needs to be kept low. One needs to architect not just the network but every individual node in a way that the cost of each node is minimal. Also, once deployed these nodes are expected to work without much human intervention and thus they are responsible for dynamic reconfiguration in response to changes in network connectivity such as addition or failure of nodes in the network as well as changing environmental stimuli [12].

### **1.3.1.3 Range of Communication Requirements**

A wireless sensor network, unlike most traditional radio networks, is very dense due to the distributed nature of sensing and processing requirements of the information that they are deployed to sense. In the past, a sensor network consisted of a small number of sensor nodes that were wired to a central processing station. However, in

recent times, the focus is more on wireless distributed sensing nodes [12]. Distributed sensing can allow more precise localization of a particular phenomenon. The range of communication in most sensing applications is limited due also to limited range of correlation length over which the sensors have their information correlated. This correlation length as well as sensing capabilities for most of the sensors such as motion detectors, fire hazard etc. means the range of communication can be short. Sensors for biometric applications also require only short range of communication, as they can use a larger network through the means of cell phone/PDAs acting as information hubs. A dense deployment of sensing node in these cases means that the sensor is often placed closer to the phenomenon that it is sensing as compared to less dense deployment, and this also reduces the constraints on the sensitivity requirements of the sensor and adds to the accuracy of the sensed information.

#### **1.3.1.4 Distributed Processing Requirements**

Another requirement of sensor networks is distributed processing capability. This is necessary since communication is a major consumer of energy. A centralized system would mean that some of the sensors would need to communicate over long distances, leading to even faster energy depletion. Hence, it would be a good idea to process locally as much information as possible in order to minimize the total number of bits transmitted over long distances [12]. Many applications exist where the sensor nodes are required to be able to process and correlate information locally to see if the sensed information makes sense to the wider network. This reduces the overall network traffic and improves energy efficiency for the sensor nodes.

#### **1.3.1.5 Non-intrusiveness and small form factor**

Sensors deployed for biometric measurement and similar applications must have small form factors. This small size requirement constrains available energy, by limiting the battery size.

### **1.3.1.6 Data Rate Requirements**

While a bio-metric measurement of EEG, ECG recording may warrant a few Hz of communication. The slow time-constants associated with physical parameters such as temperature, pressure and humidity also mean a communication with a data-rate of a few KHz. Similarly, intrusion detection, motion detection, fire hazard or gas leakage detection all these applications require very low data-rates, due to either very low probability of an event to communicate or very slow changing information that they are deployed to sense.

### **1.3.1.7 Unlicensed Spectrum Requirements**

Due to consumer centric but private nature of the network deployments, it's imperative that the sensor network operate on a wireless communication channel that is unlicensed. An unlicensed spectrum for operability is also required to keep deployment cost of the sensor networks as low as possible. This unlicensed use also means the requirement of the network must work under the condition of severe potential interference from another network that might be working on the same spectral band.

### **1.3.1.8. Low Power Requirements**

In most cases, the environment to be monitored in a wireless sensor network does not have an existing infrastructure for either energy or communication. It becomes imperative for sensor nodes to survive on small, finite sources of energy and communicate through each other on a wireless communication channel. Low power requirement becomes extremely important in this case. A sensor node is required in ideal case to be operating at power levels of  $\sim 100\mu\text{W}$ , to enable a power-harvesting based self-sustainable network [14], this power level is largely required as most of the power harvesting techniques available have power densities (Table 1.1), which can facilitate an average power of  $\sim 100\mu\text{W}$ , for a reasonably sized sensor node.

**Table 1.1 Average Power Density of various power source and scavenging devices [15][16].**

Power Source	Power Density ( $\mu\text{W}/\text{cm}^3$ )	Lifetime
Lithium Battery	100	1 year
Micro Fuel Cell	110	1 Year
Solar Cell	10-1500	$\infty$
Vibration Converter	375	$\infty$
Air Flow	380	$\infty$
Temperature Gradients	50	$\infty$

A lot of work has been done, across various streams to shed light on and solve problems associated with sensor networks as discussed above. While information theorists have been working on finding the relationship between optimal range of communication vs optimal node density deployment for a fixed coverage area of a sensor network, the cost metric used in most theory work is still most frequently power/energy efficiency of communication. Similarly scientists, who work on wireless sensor field on algorithms for processing and aggregation of information, also associate cost that is mostly driven by the power optimization techniques. The goal in developing these scheduling and routing algorithm, is to ensure routing that is fair to all the nodes and power efficient, i.e. trying to optimize the activities of all the nodes in the network such that the lifetime of the whole network is maximized.

Thus one can easily see that low power consumption is the most fundamental requirement of a sensor network. For the success of any wireless sensor network one need to look at power consumption in details at every aspect of the system design.

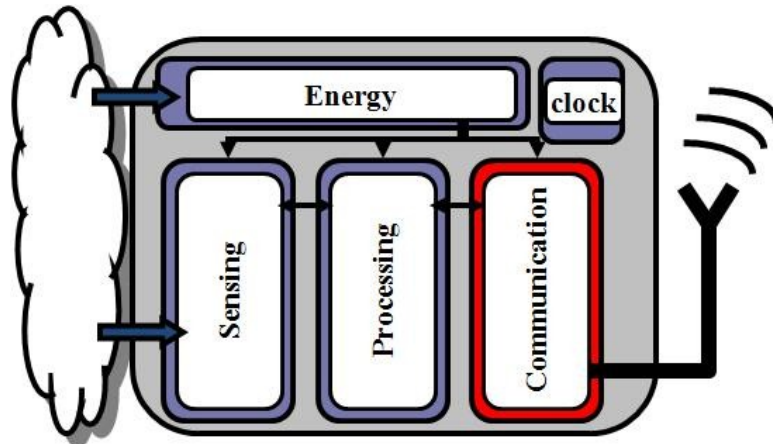


**Figure 1.3. A Wireless Sensor Node [13].**

#### **1.4 A Sensor Node: Low Power sensing, processing and communication**

A sensor node (Fig.1.3) requires a way of taking some information out from the environment, i.e. the information that it is sensing. This information could be any physical information such as temperature, humidity or biometric information depending upon the application. The node also needs a computation block to process information accessed from the environment and a means of communicating that information to the intended destination. Accessing the information from the environment can be done very cheaply, as can be seen from the various works [6-11]. Of late there have also been impressive successes in low power computation fuelled largely by scaling in CMOS processes. We now have computational blocks for sensor networks that can work at almost no power such as the asynchronous network processor designed by Cornell [17]. Similarly, there are other event driven computational processors for sensor network that can work at close to 0.6-1.5pJ/instructions [18-19] while supporting reasonable amount of processing speed. This leaves us with only the challenge of the communication block. This

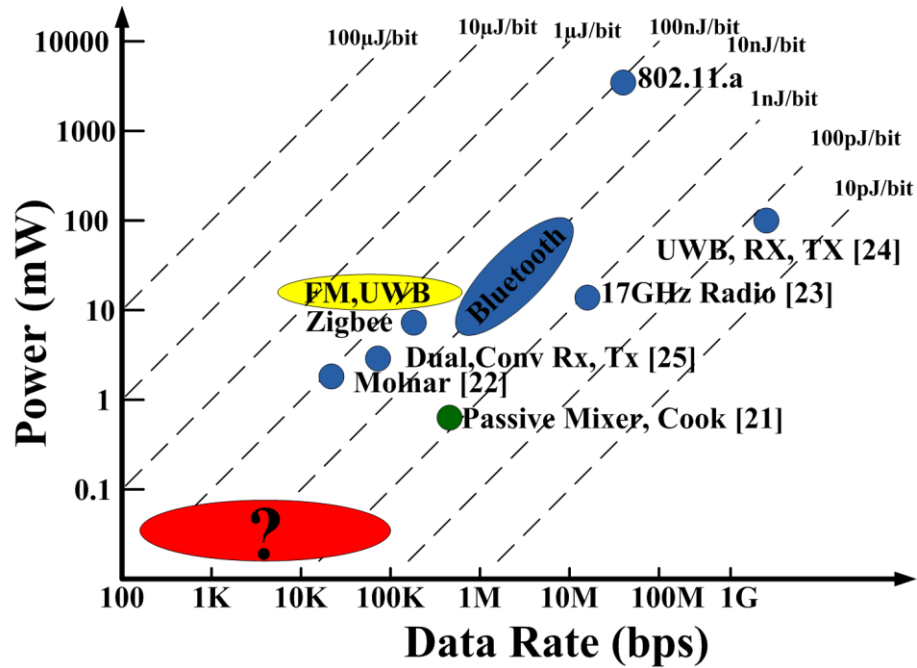


Figure 1.4. Traditional Radio designs, data rate, power and energy/bit planes. (Figure adapted from [20]).

communication block, as elaborated earlier, needs to have very low power consumption to facilitate long battery life time. The low power requirement is also a consequence of the limited size of the sensor node. Most existing sensor nodes consume a lot of power for communication thereby requiring bulky batteries; these bulky batteries are costly and render the sensor node intrusive.

Since the sensor nodes require only low data rate communication, it might sound intuitively clear that they should also naturally be low power. After all, if a node does less work, it should also consume lesser power. But somehow the law of scale doesn't seem to fit the behavior for low data rate, short range radios. If we look at existing radio designs at various data rates and ranges, we see that the design space occupied is very wide. There are designs that operate at very high (~100Mbps) data rates and designs that operate at low data rates (~100 Kbps). There are designs that take wall supply, consuming a few watts of power, while some work on batteries. If one looks at energy per bit requirements of these designs, while some designs operate at 100s of

nJ/bit, some other designs exist consuming only 0.1nJ/bit (Fig.1.4). Now if we plot the range over these designs and examine how they should scale according to the energy/bit requirements we should see designs available working at low data rates while consuming few  $\mu\text{W}$  of powers required by sensor networks. These designs do not exist. The reasons there aren't any designs in this space requires us to consider the consequences of scaling traditional design as we go for lower and lower data rate. Since, Shannon's law governs the limit on the energy efficiency of radio communication and link margin vis-à-vis the channel capacity. It makes sense to have a look at it and then see what constraints the typical radio architectures have which prevent power from scaling for low data rate applications.

### **1.5 Shannon's Theorem & Link-Power Analysis: A Primer**

Shannon's theorem binds channel capacity with information rate and provides us with various fundamental limits and is of importance to understand the link margin for a particular modulation scheme and the tradeoffs associated with them. Considering the following for a data link:

$$\text{Information Rate} = R \text{ bits/sec}$$

$$\text{Continuous Power} = P_0$$

$$\text{Energy/bit} = E_b = P_0/R$$

Now, for a bandwidth limited signal of the following channel/signal characteristics:

$$\text{Signal Bandwidth} = B$$

$$\text{SNR} = \text{Signal to Noise Power Ratio}$$

$$\text{Noise Power /Hz} = N_0 = kT \text{ (For a channel limited by thermal noise)}$$

Shannon's theorem provides an upper bound on maximum information Rate (  $R$  ), in this communication channel in a noisy environment, this upper bound is called the

maximum channel capacity ( $C$  bits/sec) and is given as below(1)[26].

$$C = B * \log_2(1 + SNR) \quad (1)$$

If the channel is assumed to have only Gaussian Noise, then

$$C = B * \log_2 \left( 1 + \frac{P_0}{N_0 * B} \right) \quad (2)$$

$$C = B * \log_2 \left( 1 + \left( \frac{E_b}{N_0} \right)_{sig} * \left( \frac{R}{B} \right) \right) \quad (3)$$

In this equation (3), there are two important ratios, one the  $\left( \frac{E_b}{N_0} \right)_{sig}$  ratio, which is SNR-per-bit and the other  $\frac{R}{B}$  Spectral Efficiency (bps/Hz). Shannon's channel capacity theorem provides us a means of finding the relationship between SNR-per-bit requirements while looking at the tradeoff with the spectral efficiency with common encoding schemes. For a Given signal Power ( $P_0$ ) & Noise Power density  $N_0$ , Channel capacity is limited and is given as  $C_{max}$  by equation below (4).

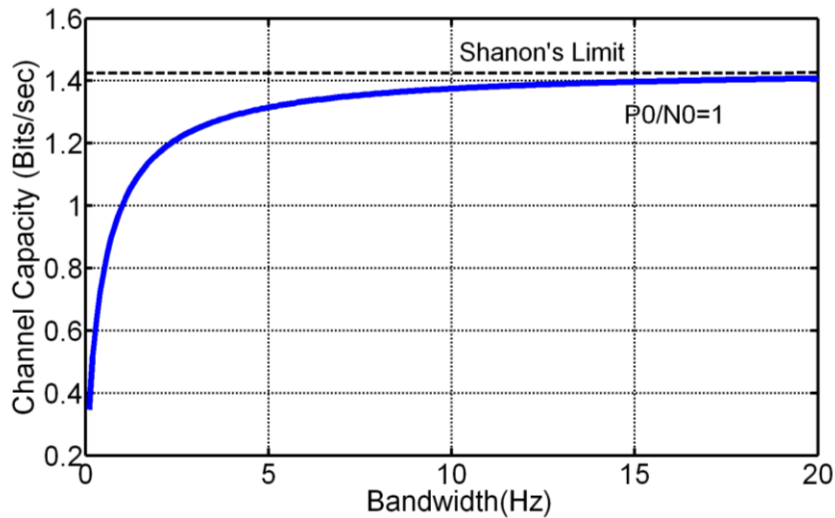


**Figure 1.5. Shannon's Channel Capacity Limit for a given,  $P_0/N_0$  (normalized to "1").**

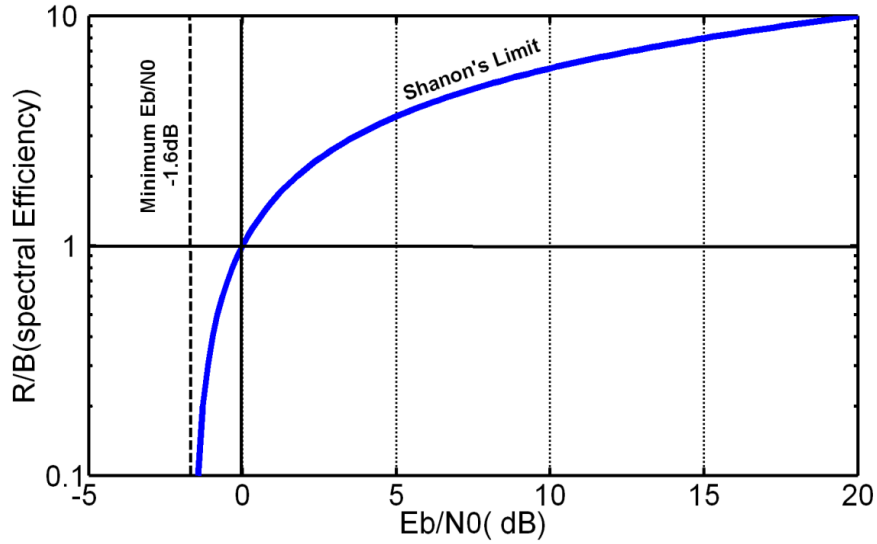


**Figure 1.6. Shannon's limit for communication with spectral efficiency and SNR-Per-Bit.**

$$C_{max} = \left( \frac{1}{\ln 2} \right) * \frac{P_0}{N_0} = 1.44 * \frac{P_0}{N_0} \quad (4)$$

While, this means the maximum channel rate is limited to  $1.44 * \frac{P_0}{N_0}$  (Fig.1.5).

While these fundamental limits are of importance to an information scientist, what is more important in this equation for a low power radio designer is the observation that for the modulation schemes that have very good spectral efficiency; it is likely to require larger energy per bit for successful reception. Thereby, Shannon's theorem establishes a fundamental performance boundary for communication systems based on the relationship between spectral efficiency and energy-per-bit.

As, for a given signal Power ( $P_0$ ), the  $\left( \frac{E_b}{N_0} \right)_{sig}$  is minimized by maximizing the information Rate ( $R$ ) where,  $P_0 = E_b * R$  and  $R_{max} = \frac{1}{\ln 2} * \frac{P_0}{N_0}$ . This gives us the bound between the spectral efficiency and the SNR-per-bit  $\left( \frac{E_b}{N_0} \right)_{sig}$  based on Shannon's' capacity theorem [26].

$$\frac{R}{B} (\text{Spectral Efficiency}) < \log_2\left(1 + \left(\frac{R}{B}\right) * \left(\frac{E_b}{N_0}\right)_{sig}\right)$$

$$\left(\frac{E_b}{N_0}\right)_{sig} (\text{SNR per bit}) > \frac{2^{\frac{R}{B}} - 1}{\frac{R}{B}}$$

A closer look at the spectral efficiency Vs SNR-per-bit provides us the minimum possible  $\left(\frac{E_b}{N_0}\right)_{sig}$  limit to be -1.6dB though at the cost of significant spectral efficiency (Fig.1.6). For a low power design (low  $\left(\frac{E_b}{N_0}\right)_{sig}$ ), one might be tempted to trade the spectral efficiency for lower SNR-per-bit, but that requires significant overhead for encoding, decoding and error correction techniques due to spread spectrum manner of communication in these schemes. One also needs acceptable Bit-Error-Rate for communication, explaining why typical designs don't sit at the fundamental limits of  $\left(\frac{E_b}{N_0}\right)_{sig} = -1.6dB$ . As shown in Fig.1.7, higher than 10dB of  $\left(\frac{E_b}{N_0}\right)_{sig}$  is required for typically used modulation schemes for an acceptable BER in the network.

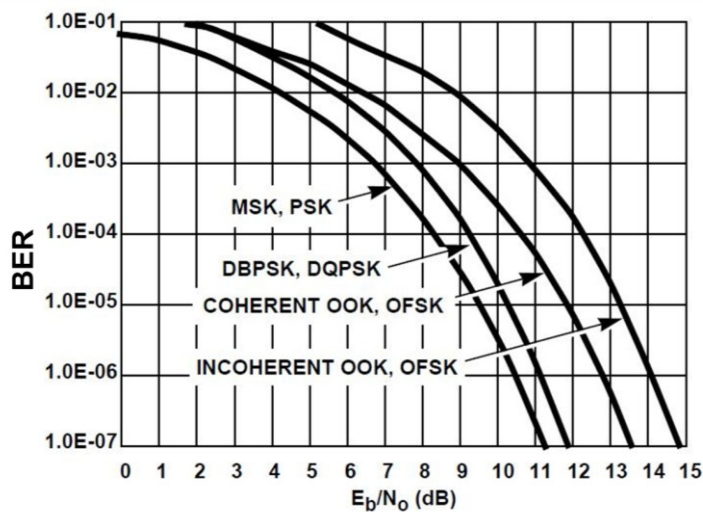


**Figure 1.7. Probability of Bit Error Rate for common modulation schemes, (The figure taken from Ref. [116], Altera Application notes)**

Since a low power radio has to be low on complexity, the typical modulation schemes utilized are either OOK or 2-FSK, and for these schemes the  $\left(\frac{E_b}{N_0}\right)_{sig}$  ratio for a BER of  $>10^{-4}$  is  $\sim 11.5\text{dB}$ . This number gives us a sense of minimum energy required for a signal at the input of the receiver and has its own significance. But what we actually care about is the overall system energy-per-bit, which has to account for the power required for the transmitter and the receiver circuitry as well. Energy-per-bit required for the system,  $(E_b)_{sys}$  can be evaluated as  $\frac{(P_{tx}+P_{rx})}{R}$ , where  $P_{tx}$ ,  $P_{rx}$  are the transmitter and receiver power requirements [26]. For a system with no path loss, 100% efficient transmitter, zero power consumption, and zero noise addition at the receiver the number can be given to be as the same as the energy-per-bit required at the receiver input,  $(E_b)_{sys} = \left(\frac{E_b}{N_0}\right)_{sig} * kT$ . Since there is always a path loss associated with the channel and there are efficiency considerations at the transmitter, the  $(E_b)_{sys}$  is not the same as  $(E_b)_{sig}$  required at the input of the receiver.

The  $(E_b)_{sys}$  at that point is the sum of the energy required at the Transmitter  $(E_b)_{tx}$  and the energy required at the receiver  $(E_b)_{rx}$ .

$$(E_b)_{sys} = (E_b)_{tx} + (E_b)_{rx} \quad (5)$$

Before we find out the power requirement at the transmitter and the receiver it makes sense to look at common transceiver architecture and see different power consuming components to appropriately account for the system power without loss of generality.

## 1.6 A Traditional Radio Design and Its Various Power Consuming Components

As, shown in Fig.1.8, a typical narrowband radio design consists of an oscillator (LO), a means of data modulation (Mixer) and a power amplifier (PA) at the transmitter, while the receiver signal chain consists of low noise amplifier (LNA) + gain stages, a data demodulation scheme (Mixer) and an LO. Power in the transmitter is dominated by three components; power consumed in the power amplifier ( $P_{TX,PA}$ ), the power consumed in the LO and the mixer (Transmit overhead power) ( $P_{TX,OH}$ ), and leakage power ( $P_{TX,Leak}$ ). Power transmitted by the transmitter can be given as in Equation (6). For high data rate designs, the power amplifier at the transmitter is typically the most power hungry block. This block is the one responsible for radiating power in the environment, and is typically designed with an efficiency number ( $\eta_{TX}$ ) of close to 50%. Taking the radiation efficiency ( $\eta_{TX}$ ) into consideration, the transmitter power can be given alternatively as in equation (7) in terms of the radiated power  $P_{TX,rad}$  [26].

$$P_{TX} = P_{TX,PA} + P_{TX,OH} + P_{TX,Leak} \quad (6)$$

$$P_{TX} = \frac{P_{TX,rad}}{\eta_{TX}} + P_{TX,OH} + P_{TX,Leak} \quad (7)$$

Similarly, at the receiver, the power is dominated by the LNA & Gain Stages ( $P_{RX,LNA}$ ), the power consumed in the mixer and LO ( $P_{RX,OH}$ ) (Receiver Overhead Power) and some leakage power ( $P_{RX,Leakage}$ ). Overall, the receiver power can be given as in Equation (8).

$$P_{RX} = P_{RX,LNA} + P_{RX,OH} + P_{RX,Leakage} \quad (8)$$

In the case of a receiver the most power consuming element at moderate and high data rates is the LNA, and can be optimized to provide best system power based on

link budget, data rate, and noise factor (F) as will be explained later.

### 1.7 Minimum Detectable Signal and Link Margin

To calculate the total power for the system, we first need to look at the minimum detectable energy/bit  $(E_b)_{MDS}$  at the receiver taking in to account the finite noise factor, F, associated with the receiver circuit design. The minimum detectable energy/bit  $(E_b)_{MDS}$  for a receiver can be given as in (8). Where, k is the Boltzmann constant and  $\left(\frac{E_b}{N_0}\right)_{sig}$  is the SNR-per bit of the signal at the input of the receiver.

$$(E_b)_{MDS} = kT * F * \left(\frac{E_b}{N_0}\right)_{sig} \quad (8)$$

For a given data rate (R), this gives us the minimum detectable signal power  $P_{MDS}$ , required at the receiver input as in Equation (9).

$$P_{MDS} = kT * F * \left(\frac{E_b}{N_0}\right)_{sig} * R \quad (9)$$

This minimum detectable signal power can be described in terms of the SNR-per-

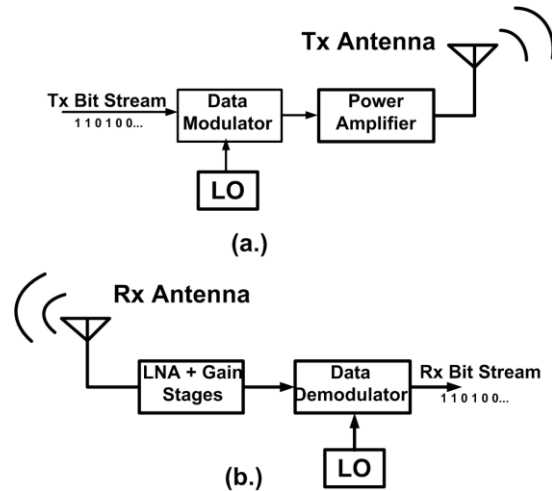


Figure 1.8. A Simple Narrow Band Transmitter and Receiver Design-blocks.

bit  $\left(\frac{E_b}{N_0}\right)_{sig}$  and the spectral efficiency  $\left(\frac{R}{B}\right)$  as given below, where B is the noise bandwidth (5) [26].

$$P_{MDS} = kT * F * B * \left(\frac{E_b}{N_0}\right)_{sig} * \left(\frac{R}{B}\right) \quad (10)$$

Now, for a link of margin M, where M accounts for path losses and any other associated losses, transmitter radiated power ( $P_{TX,rad}$ ) can be given as in equation (11). Where,  $\alpha$  is given as in (12), and is a constant for a link with a fixed BER requirement and chosen modulation scheme.

$$P_{TX,rad} = M * P_{MDS} = M * \alpha * F * B \quad (11)$$

$$\alpha = kT * \left(\frac{E_b}{N_0}\right)_{sig} * \left(\frac{R}{B}\right) \quad (12)$$

As, can be seen from equation (11) the minimum required transmitter radiated power, ( $P_{TX,rad}$ ) is dependent upon the noise-bandwidth (B) and the noise factor of the receiver (F). Depending upon how the noise factor (F) is related to Power consumed at the receiver, a relationship can be worked out between the two to optimize the system power at various data rates.

### 1.8 FOM of Receiver and Link Power Optimization

The most common FOM for LNA designs is given as in equation (13) [27], [28].

$$FOM_{RX,LNA} = \frac{Gain}{(F-1)*P_{RX,LNA}} \quad (13)$$

For a given technology, this means the noise factor (F) can be given as  $(1 + \frac{\gamma}{P_{RX,LNA}})$ . Where  $\gamma$  can be treated as a constant for a design in a given process technology and has units of power [29].

$$\gamma = \frac{\text{Gain}}{FOM_{RX,LNA}}$$

$$F = 1 + \frac{\gamma}{P_{RX,LNA}} \quad (14)$$

Based on equation (14) & (11), the total link power ( $P_{SUM}$ ) can be given as in equation (18), where the sum of Rx and Tx overhead power ( $P_{RXTX,OH}$ ) and the total leakage power ( $P_{RXTX,Leak}$ ) is grouped into a constant “C1”.

$$P_{SUM} = P_{TX} + P_{RX} \quad (15)$$

$$P_{SUM} = P_{TX,PA} + P_{RX,LNA} + (P_{RXTX,OH} + P_{RXTX,Leak}) \quad (16)$$

$$P_{SUM} = M * \alpha * F * \frac{B}{\eta_{TX}} + P_{RX,LNA} + C1 \quad (17)$$

$$P_{SUM} = \frac{M * \alpha}{\eta_{TX}} * \left(1 + \frac{\gamma}{P_{RX,LNA}}\right) * B + P_{RX,LNA} + C1 \quad (18)$$

In order to optimize for a given link margin (M),

$$\frac{dP_{SUM}}{dP_{RX,LNA}} = 0$$

giving,

$$P_{RX,LNA}(\text{optimized}) = \sqrt{M * \alpha * \gamma * \frac{B}{\eta_{TX}}} \quad (19)$$

$$P_{TX,PA}(\text{optimized}) = \frac{M * \alpha * B}{\eta_{TX}} \left(1 + \frac{\gamma}{\sqrt{M * \alpha * \gamma * \frac{B}{\eta_{TX}}}}\right) \quad (20)$$

$$P_{TX,PA}(\text{optimized}) = P_{RX,LNA} \left(1 + \frac{P_{RX,LNA}}{\gamma}\right) \quad (21)$$

$$P_{SUM,CW}(\text{optimized}) = P_{RX,LNA} \left(2 + \frac{P_{RX,LNA}}{\gamma}\right) \quad (22)$$

$$P_{SUM,CW}(optimized) = 2 * \sqrt{M * \alpha * \gamma * \frac{B}{\eta_{TX}}} + M * \alpha * \frac{B}{\eta_{TX}} \quad (23)$$

As, can be seen from the equations (23) the link power for a given link margin has two components, while the first components go as square root of signal-bandwidth, the other component goes as proportionate to the signal bandwidth. Since, for a narrowband communication system the signal-bandwidth is proportionate to “B” (for OOK modulation scheme, data rate “R” is same as signal bandwidth “B”), this means at lower data rate the energy/bit & so the power is expected to be higher (Fig.1.9), compared to the constant energy/bit scaling case.

The higher energy/bit associated with narrow-band radios can also be understood further by looking at the fixed overhead ( $P_{RXTX,OH}$ ) & leakage power ( $P_{RXTX,Leak}$ ) associated with the receiver and transmitter circuitry in traditional narrowband radio designs, which stay constant as one scales the data-rate of communication.

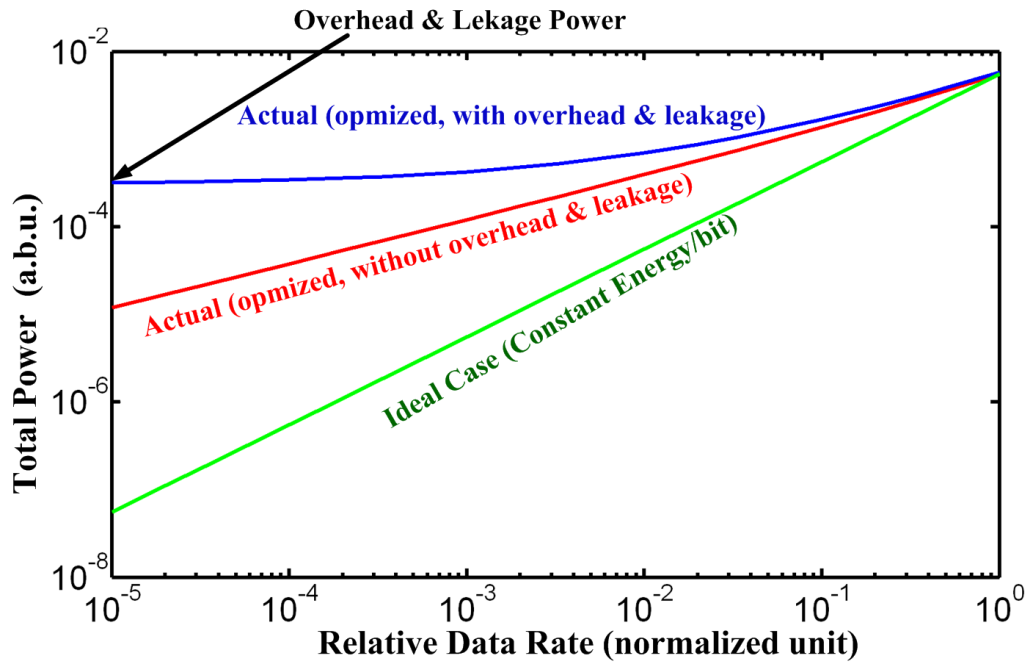


**Figure 1.9. shows the power Vs Data Rate for the CW radio, note at low data rate the power is limited by the overhead and leakage power.**

$$P_{SUM,cw} = 2 * \sqrt{M * \alpha * \gamma * \frac{B}{\eta_{TX}}} + M * \alpha * \frac{B}{\eta_{TX}} + P_{RXTX,OH} + P_{RXTX,Leak} \quad (24)$$

The overhead power associated with even the best transceiver circuit designs is of the order of 300-400 $\mu$ W and for low data rate applications is usually the limiting factor (Fig.1.9). In the presence of this large overhead power associated with the transmitter and receiver designs in typical radio architectures, the key to low power design is to somehow be able to reduce this overhead.

### 1.9 Low Power Low Data Rate Radio Designs

As explained before, the fixed overhead associated with the transmitter and receiver designs and not the fundamental energy/bit limit associated with the exchange of data information between the receiver and the transmitter govern the overall power budget associated with the low data rate link. This explains why at high data rates the energy/bit of typical radio systems is very low, while at low data rates the designs exhibit higher energy/bit (Fig.1.10a).

Since, the laws governing the energy/bit in a given link in a radio system provide the fundamental limit to the dynamic energy/bit requirements of the link, one can think of duty-cycled radio architecture. In such a system the dynamic component of the energy/bit requirement stays the same, but due to switching “on” and “off” of the overhead components in the design one can lower the overall power requirements for the link. The overhead component can also be made rate-dependent, to give a fairly constant energy/bit over large range of data-rates (Fig.1.10b).

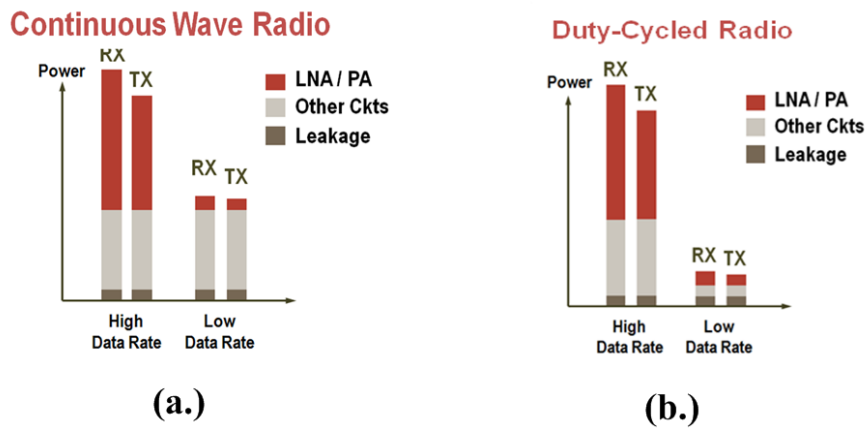


**Figure 1.10. (a.) Illustration of typical continuous wave radios from high data-rate to low data rate, (b.) the power for the duty-cycled radios.**

### 1.9.1 Duty-Cycled/Sleep-Wake Radios

As, shown in Fig.1.10b, a duty-cycled radio, which is active only during the data-transmission while sleeping otherwise can ideally result in scaled behavior for low data-rate applications (Fig.1.11). The trick to implementing this is in knowing when to turn the radio on and off. To do this effectively, the transmitter and receiver blocks must decide together when to put data into the air and when to look for the data. If, for instance, a transmitter has information to send when the receiver it is trying to contact is off, the data will be lost. If the receiver is on when the transmitter has no information to transmit, power will be wasted. Optimizing this communication cycle can be a challenge. There are several approaches to solving this sleep-wake scheduling problem.

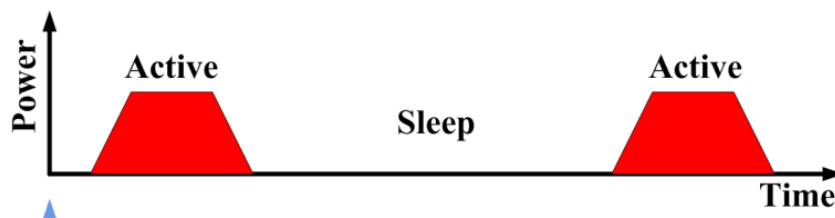


**Figure 1.11. Illustration of a duty-cycled radio, with active and sleep states.**

### 1.9.2 Sleep/Wake Radios with Asynchronous Periodic Wake-up

This approach is based on a regular, periodic waking of the radio nodes. In this type of radio link, all the nodes in the network wake-up periodically for small time duration and go back to sleep mode if no activity is found. For communication between two nodes, a node that wants to communicate with another node sends an RTS (Request To Send) packet, while waiting for a clear signal (CTS- Clear To Send) from the receiving node. If it does not receive a response from the other node, it keeps sending the RTS signal followed by wait duration. At some point when the receiving node wakes up it sends a clear signal, after which the actual data transmission proceeds between the two nodes. After the data transfer the nodes again go back to their normal sleep-wake cycle.

A timing illustration of this scheme is shown in Fig.1.12, 1.13. Depending upon how often the node wakes up, the power consumption for useful transmission of information may still be high with this method. This method is best suited for applications where nodes need to communicate very infrequently (hourly, daily, or even less often) [30].

### 1.9.3 Idle Listening based Wakeup Radio

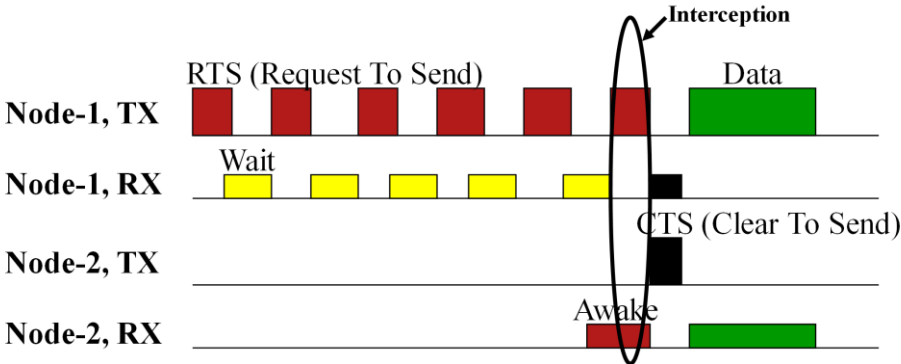


**Figure 1.13. Data transfer in sleep-wake scheduling based network. The receiving node when intercepts an RTS signal stays awake for the data exchange.**

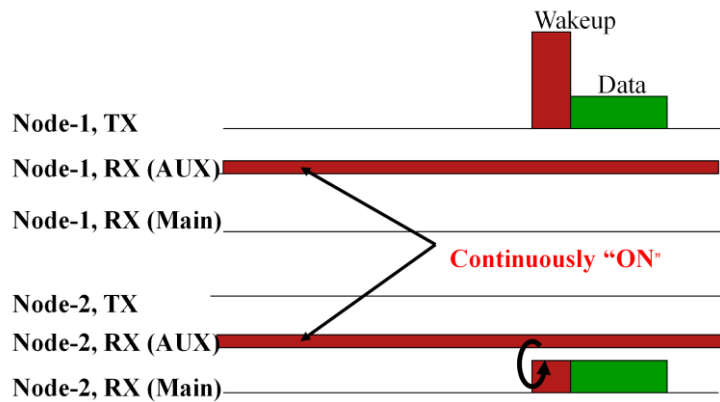


**Figure 1.14. Data transfer in an idle-listening based wakeup radio.**

In this type of wakeup radio designs, a receiver utilizes two types of radio transmitters and receivers in each node. One type of wakeup receiver remains on during idle phase, but is designed for extremely low power and consequently weak amplification of incoming signals. The low power wakeup receiver can only detect a very strong signal. In this kind of system, when a node wants to communicate with other nodes in the system, a strong transmitter sends a very strong signal, which is detected by the wakeup receiver. The wakeup receiver then wakes up the higher power main receiver to facilitate data communication between the two nodes through a stronger receiver and weaker transmitter (Fig.1.14). In this scheme the need for very strong signal for the wakeup receiver means significant power is required each time the radio wakes up. Consequently, this scheme is also best for cases when there is very infrequent communication (hourly, daily, or even less often). Both sleep/wake schemes are subject to regular FCC standards based upon their carrier frequencies. Zigbee-standard based designs also utilize radios based on this principle. Though, this can result in a very low power radio design, the designs are typically asymmetric, as they warrant a very strong transmitter.

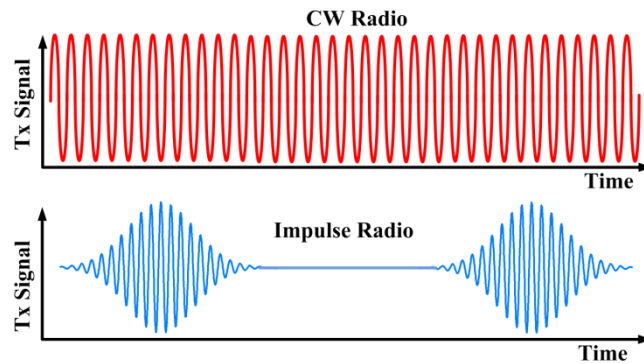


**Figure 1.15. Signaling in the impulse radio compared to the continuous wave radio the signal is only occasionally transmitted,**

### 1.9.4 Impulse Radios

Sleep/Wake radios work well in situations where there are very few events separated by minutes, hours, or longer periods, to be communicated. For example, when detecting the presence of a toxic gas or other dangerous event, sleep/wake radios are effective. However, this type of radio is not as effective when there is a constant level of communication required, such as in a medical monitoring application. In this case, one would like to transmit data at a steady low rate, switching off the transmitter and receiver at regular intervals between transmissions to save power. In order to do this a different type of radio is required. Rather than transmitting a continuous wave, where data is encoded in the phase or frequency of that wave, data can be encoded as the presence or absence of energy within a frequency range at a set time. This way, rather than transmitting many cycles of a wave, one can transmit short bursts of power, called wavelets that are only nanoseconds in duration. By transmitting or not transmitting these wavelets at particular times, as shown in Fig.1.15, digital bits (ones and zeros) are communicated wirelessly from one radio to another. These pulsed radios are known as Impulse Radios, owing to the short duration of their transmitted signals. Alternatively, they are also called Ultra wideband (UWB) radios, because short pulses have a wide spectrum (Fig.1.15). Since the bursts are short in time, they

do not require the transmitter circuitry to be “on” for long duration, thus saving power at the transmitter. In order to receive these bursts, however, the receiver must either be fast and continuously on, consuming large amounts of power, or know to look for the information at approximately the right time, turning off at all other times. The latter can be accomplished if the two (or more) communicating radio transceivers are synchronized to a common clock. Once this is achieved, communication can proceed on a common timescale. In comparison to other packet based synchronization scheme where the two radios can agree on communication along a common time-boundaries but with large synchronization errors the inherent nature of impulse signaling can be utilized to potentially synchronize the radios to very precise accuracy, as seen in many radar applications.

#### **1.10. Impulse Radio Vs Continuous Wave Radio from High to Low Data Rate**

Impulse Radios are the extreme case of the duty-cycled radio architectures and have been found to be of lower power consumption compared to the narrowband continuous wave radios. However, compared to narrowband architectures, impulse radios have wider bandwidth (requiring higher power gain stages) and higher susceptibility to noise. It is not; therefore, immediately obvious as to why a duty-cycled impulse radio architecture should be favored for low power applications. In this section we present an analysis of duty-cycled impulse based communication showing why it ultimately facilitates lower power communication in comparison to the traditional narrowband architectures. We base the analysis on link margin optimization for the two types of radio architecture.

We first compare the power consumed by the CW radio with the Impulse/UWB radio at a given data rate while assuming that power is dominated by the LNA and the power amplifier (PA). In initial derivations, we assume no overhead due to other

circuit components such as the mixer and LO in the receiver and the transmitter mixing blocks for simplification. This simplification allows us to compare signaling schemes on equal footing as only the data rate dependent components are taken into consideration. We later give the derivations that include the effect of the overhead and leakage power as well.

A comparison of signaling methods makes certain tradeoffs apparent. While a CW radio can trade bandwidth,  $B$ , for data rate to save power, in a duty-cycled radio, one can save power by duty-cycling, resulting in shorter on-times at low data rates. Since for an impulse of duration “ $T_{\text{impulse}}$ ”, the bandwidth occupied is  $\sim 1/T$ , we start by comparing this with a CW receiver design that initially has a bandwidth of  $B_0 = 1/T$ . At this point for a data rate of  $R_0=1/T=B$ , the receiver power ( $P_{RX0}$ ) for the CW radio and the duty-cycled radio will be the same, as they both support the same data-rate and the same bandwidth. It is interesting to note that in this degenerate case, the duty-cycled radio mimics a CW radio due to continuous transmission of data as shown in Fig.1.16. Similarly, the power requirement for the transmitter for the two would be the same ( $P_{TX0}$ ). Based on the equation (19) and (21), these values can be given as below.

$$P_{RX0} = \sqrt{M * \alpha * \gamma * \frac{R_0}{\eta_{TX}}} \quad (25)$$

$$P_{TX0} = P_{RX0} \left( 1 + \frac{P_{RX0}}{\gamma} \right) \quad (26)$$

Now, as we scale to a lower data rate ( $R$ ), the two transceivers make different tradeoffs. The CW transmitter sends smaller signal amplitude to save power while the IR sends the same instantaneous power for a shorter duration, saving power by duty cycling. The impulse radio with its inherent duty-cycling at both the receiver and the transmitter will consume power that is reduced by a factor of  $R/R_0$ .

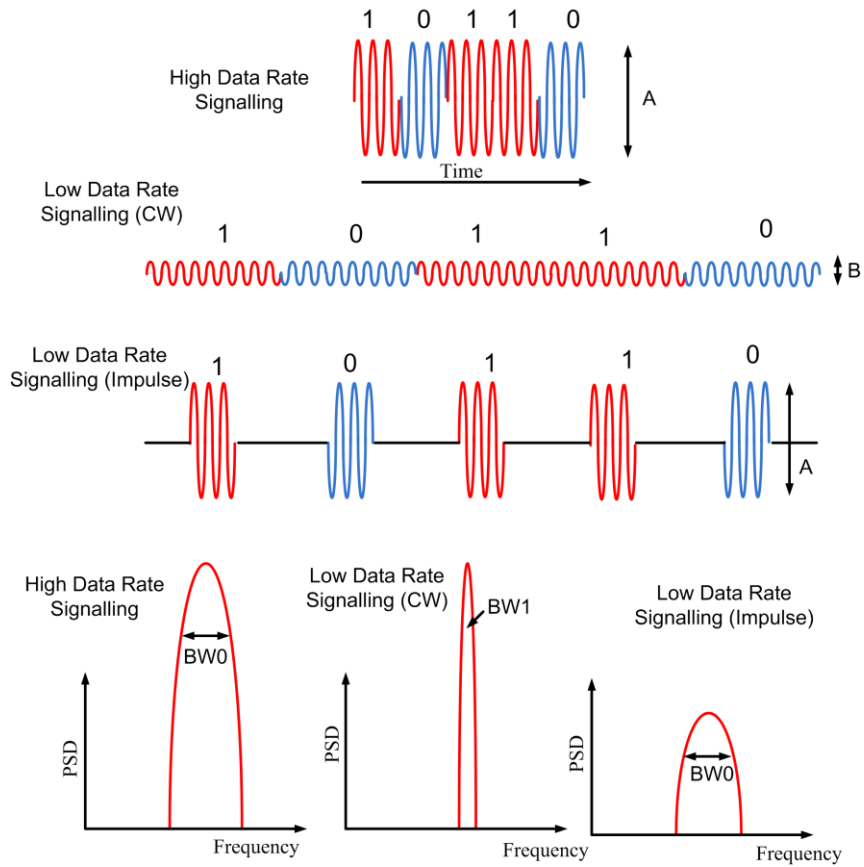


**Figure 1.16. Illustrative simplified diagram shows how the signals look like in time and frequency domain for the CW and Impulse radio as one move from high data rate (full rate) to low data rate communication. Note: at high data rate the CW and Impulse signaling looks the same in time and frequency domain.**

$$P_{SUM,Impulse} = (P_{RX0} + P_{TX0}) * \left(\frac{R}{R_0}\right)$$

$$P_{SUM,Impulse} = P_{RX0} \left(2 + \frac{P_{RX0}}{\gamma}\right) * \left(\frac{R}{R_0}\right) \quad (27)$$

For, the CW radio at various data rates, one can use the equation (19) and (21) to give the optimized power for the receiver and the transmitter by scaling “B” the noise bandwidth due to reduced data rate, as a factor  $R/R_0$ . This allows a smaller signal to be transmitted at the same BER. The receiver power ( $P_{RX,CW}$ ), the transmitter power

$(P_{TX,CW})$  & the total power  $(P_{SUM,CW})$  can be given as below.

$$P_{RX,CW} = (P_{RX0}) * \sqrt{\frac{R}{R_0}} \quad (28)$$

$$P_{TX,CW} = P_{RX0} * \sqrt{\frac{R}{R_0}} * \left( 1 + \frac{P_{RX0}}{\gamma} * \sqrt{\frac{R}{R_0}} \right) \quad (29)$$

$$P_{SUM,CW} = (P_{RX0}) * \sqrt{\frac{R}{R_0}} * \left( 2 + \frac{P_{RX0}}{\gamma} * \sqrt{\frac{R}{R_0}} \right) \quad (30)$$

Thus, the ratio of the  $P_{SUM,Impulse}$  to  $P_{SUM,CW}$  can be given utilizing equation (27) and (30) as below, after simplification (i.e. after cancelling the  $P_{RX0} * \frac{R}{R_0}$  term from both the numerator and denominator).

$$\frac{P_{SUM,Impulse}}{P_{SUM,CW}} = \frac{\left( 2 * 1 + \frac{P_{RX0}}{\gamma} \right)}{\left( 2 * \sqrt{\frac{R_0}{R}} + \frac{P_{RX0}}{\gamma} \right)} \quad (31)$$

$$\frac{P_{SUM,Impulse}}{P_{SUM,CW}} < 1, \quad for \quad \frac{R_0}{R} > 1$$

As, can be seen from equation (31) for low data rate applications the  $(\frac{R_0}{R} > 1)$ , the Impulse radio with its duty-cycled receiver and transmitter will facilitate lower power consumption for a link of given path loss. The same analysis can be done even including the overhead and leakage power, in which the equation for the relative ratio will change to equation (32).

$$\frac{P_{SUM,Impulse}}{P_{SUM,cw}} = \frac{\frac{R}{R_0} * \left(2 + \frac{P_{RX0}}{\gamma}\right) P_{RX0} + P_{RXTX,OH} * \frac{R}{R_0} + (P_{RXTX,Leak})}{\frac{R}{R_0} * \left(2\sqrt{\frac{R_0}{R}} + \frac{P_{RX0}}{\gamma}\right) P_{RX0} + (P_{RXTX,OH} + P_{RXTX,Leak})} \quad (32)$$

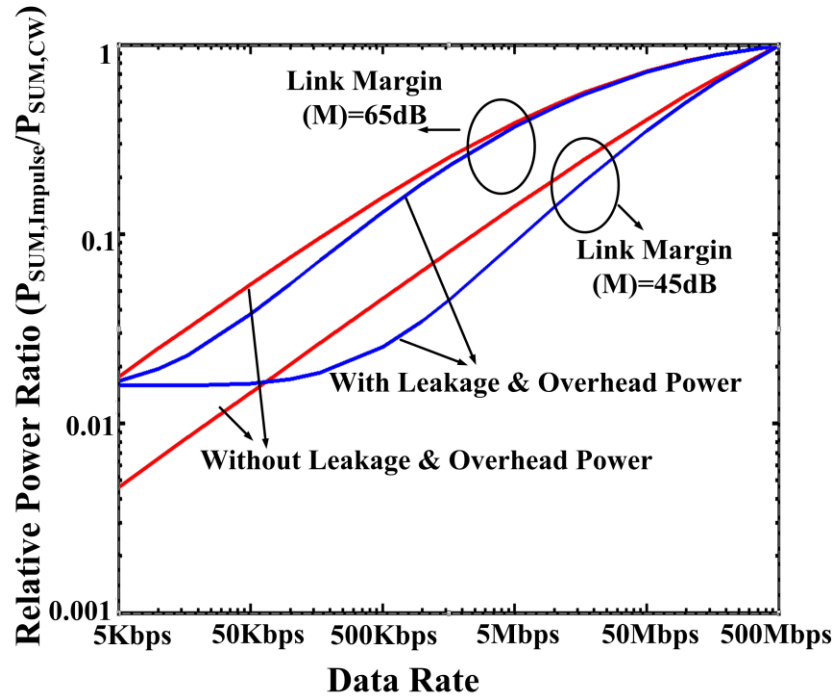
Again, it can be easily seen, that the continuous wave radio consumes higher power than the impulse radio, as  $\frac{R_0}{R} > 1$ .

Fig.1.17 shows the relative ratios of the CW radio as compared to the Impulse radio at lower data rates based on equation (31) & equation (32). The  $\gamma$  value used for the optimization equation can be given approximately as in equation (33) [29].

$$\gamma = \frac{P_{RX,LNA}}{g_m * R_{ANT}} = \frac{VDD * V_{DSAT}}{2 * R_{ANT}} \quad (33)$$

For a 90nm technology,  $VDD = 1V$ ,  $V_{DSAT} = 0.2V$ ,  $R_{ANT} = 50\Omega$ , can be safely assumed. We also assume an OOK modulation scheme with BER requirement of  $10^{-5}$ , which provides the SNR-per-bit  $\left(\frac{E_b}{N_0}\right)_{sig} = 11.5dB$  and spectral efficiency  $\left(\frac{R}{B}\right) = 1$ .

For illustration the link margin is varied between two values of 65dB and 45dB. For leakage power ( $P_{RXTX,Leak} = 5\mu W$ ), we assume the values measured from our design, while the total transceiver overhead power is taken from published data on the best continuous wave radio design [21] as  $P_{RXTX,OH} = \sim 300\mu W$ . Note, the figure gives only the trend, and the absolute values of the parameter selected are not of much importance here and are for illustration only. As can be seen from the figure the Impulse Radio requires significantly less power as compared to the CW radio, especially at low data rates. Looking at the plots in Fig.1.4 for different link margins,



**Figure 1.17. Relative power ratio Vs Data rate of the Impulse radio as compared to the CW radio based on equations derived in (31) and (32), for different link margins. At reduced data rate, the Power consumed by the impulse radio is lower in both cases.**

we can further say, that the power advantages associated with an impulse radio is more enhanced for links with lower link margin (i.e. shorter range communication).

Recent developments in continuous wave radio designs have shown that by modifying the design architecture at the receiver, and having mixer as the first stage, can enable one to control the amplification-bandwidth of the baseband-LNA (or, gain stage), thereby enabling one to design baseband-LNAs with low amplification bandwidth that can trade power at the receiver by trading bandwidth, resulting into a different FOM for these baseband-LNA designs [31] [32]. The analysis associated with relative power comparison of the Impulse radio as compared to the CW radio taking into account this recent development in continuous wave receiver designs, is given in the section below.

### 1.11 CW Vs Impulse Radio Comparison based on different FOM

While doing the analysis earlier we used a figure of merit (FOM) for the LNA that doesn't take into account the amplifier-bandwidth as a trade-off for saving power at the receiver in equation (14). Since, for impulse radio applications the LNA can have wide bandwidth of ~500MHz, one could envision designing LNAs for narrowband CW applications with smaller bandwidths, which could be taken into account in equation (14). Unfortunately due to limited "Q" associated with on-chip inductors the LNA bandwidth is always higher than the minimum required for low data rate applications, which explains why it is not included in the FOM equations. However, as explained before with recent developments with mixer-first architectures [31], [32] the LNA bandwidth (B) can be traded-off for power for the baseband-LNA (or, gain stages). In this section we revisit the optimization equations with a change of FOM for the base-band LNA (or gain stages) as in Equation (34).

$$FOM_{RX,LNA} = \frac{Gain * B}{(F - 1) * P_{RX,LNA}} \quad (34)$$

$$F = 1 + \frac{\gamma 1 * B}{P_{RX,LNA}} \quad (35)$$

Going, by the same formalism as before for optimization of the link power budget in this case, the equations (19), (20) can be given as equations (36), (37) respectively.

$$P_{RX,LNA}(optimized) = \left( \sqrt{M * \alpha * \frac{\gamma 1}{\eta_{TX}}} \right) * B \quad (36)$$

$$P_{TX,PA}(optimized) = \frac{M * \alpha * B}{\eta_{TX}} \left( 1 + \frac{\gamma 1}{\sqrt{M * \alpha * \frac{\gamma 1}{\eta_{TX}}}} \right) \quad (37)$$

We can give the same logic as before for the full rate ( $R_0$ ), the power at the transmitter and receiver for both the impulse and CW radios are supposed to be the same, as the signaling as well as the signal bandwidth for the two at full rate becomes the same. These power numbers, as before, can be given as  $P_{TX0}$  and  $P_{RX0}$  respectively. Now, as we scale to a lower data rate ( $R$ ), the impulse radio with its inherent duty-cycling at both the receiver and the transmitter will consume power that is reduced by a factor of  $R/R_0$  as was explained earlier and thus the overall system power can be given as in equation (38).

$$P_{SUM,Impulse} = (P_{RX0} + P_{TX0}) \left( \frac{R}{R_0} \right) \quad (38)$$

For the continuous wave radio, Equation (37) suggests that one can scale the B as a factor of  $R/R_0$ .

Thus,

$$P_{RX,CW} = (P_{RX0}) \left( \frac{R}{R_0} \right) \quad (39)$$

Similarly, the PA power can be scaled due to similar scaling in this case (40). And so the  $P_{SUM,CW}$  can be given as in equation (41).

$$P_{TX,CW} = (P_{TX0}) \left( \frac{R}{R_0} \right) \quad (40)$$

$$P_{SUM,CW} = (P_{RX0} + P_{TX0}) \left( \frac{R}{R_0} \right) \quad (41)$$

Thus, the ratio of the power for the CW and the Impulse based duty-cycled radio can be given as below in equation (41). As the two values are the same, the two radios can scale power identically at lower data rates. While, the duty-cycled radio receiver can save power at the receiver by duty-cycling the receiver at a reduced rate, the CW

receiver can do the same by reducing bandwidth, thereby requiring lower power at reduced rate. Essentially, while an impulse radio gains from duty cycling, a CW radio gains from averaging and a lower noise floor.

$$\frac{P_{SUM,Impulse}}{P_{SUM,CW}} = \frac{(P_{RX0} + P_{TX0}) \left(\frac{R}{R_0}\right)}{(P_{RX0} + P_{TX0}) \left(\frac{R}{R_0}\right)} = 1 \quad (42)$$

However, the picture in this case changes if we include the overhead and the leakage power in the equation. After including the overhead power and leakage power the modified ratio can be given as in equation (43), where the overhead power can be scaled in the case of Impulse radio in comparison to the CW radio at lower data rates.

$$\frac{P_{SUM,Impulse}}{P_{SUM,CW}} = \frac{(P_{RX0} + P_{TX0}) \left(\frac{R}{R_0}\right) + P_{RXTX,OH} * \left(\frac{R}{R_0}\right) + P_{RXTX,Leak}}{(P_{RX0} + P_{TX0}) \left(\frac{R}{R_0}\right) + P_{RXTX,OH} + P_{RXTX,Leak}} \quad (43)$$

For a given  $R/R_0 < 1$  (i.e. reduced data rate), the ratio indicated in equation (43) can be shown to be  $< 1$ , indicating again the benefit associated with the impulse radio. Fig.1.18 shows the relative ratios of CW and the impulse duty-cycled radio power based on equation (42) and (43). The OOK modulation scheme with a BER of  $10^{-5}$  was assumed to find optimized value for the link with a link margin of 45dB and 65dB. Other parameters were also taken as per the values chosen in earlier section. As, can be seen even in this case the impulse radios perform better as compared to the CW radio due to scaling of the overhead power in impulse radio designs.

In addition to these overhead and leakage powers there are other practical design considerations that can tilt the choice in favor of the duty-cycled radio for several reasons. For one, at low data rate, one cannot physically scale the LNA bandwidth using CMOS components. The design tolerances will eventually require the LNA

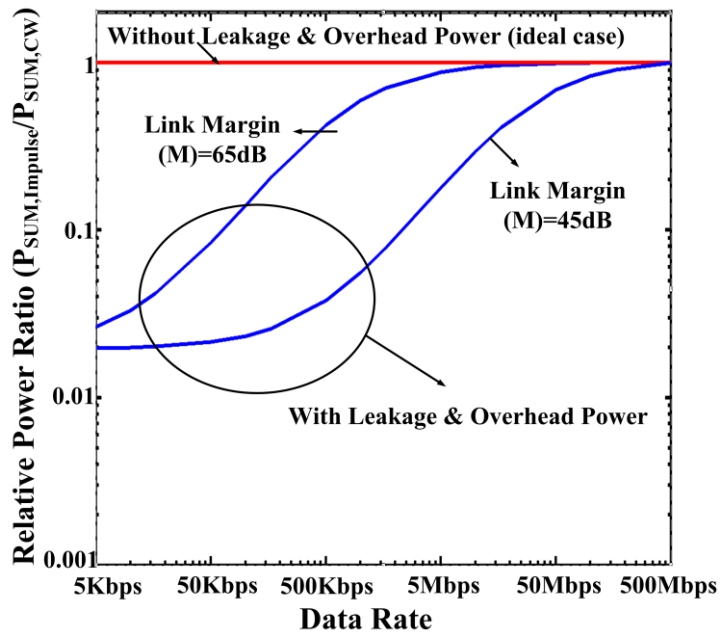


**Figure 1.18. Relative power ratio Vs Data rate of the Impulse radio as compared to the CW radio based on equations derived in (42) and (43), for different link margins. At reduced data rate, the Power consumed by the impulse radio is lower once the leakage and overhead power is factored in the equations.**

bandwidth to be limited to few MHz, requiring very high Q on-chip filters with precise center frequencies in order to achieve the benefits associated with the scaled data rate and FCC compliance. For example a 1MHz bandwidth at 1GHz, means a Q of 1000, while the practical realizable Q's are of the order of 10-20 with on-chip inductors. MEMS based filters with higher Q's have been shown, but they suffer from thermal and process variations. Similarly, for the impulse based UWB communication duty-cycling needs to take into account the uncertainty in timing circuitry, which will require the transmitter and receiver duty-cycle ratio to be less than perfect. Perfect noiseless synchrony of TX and RX are as unlikely as an ideal high Q LNA and oscillator are for the CW case and one need to design the synchronization circuitry very carefully to realize the true advantages associated with duty-cycled impulse radios.

Based on this overall analysis we can say that duty-cycled radios perform better

than CW architectures at low data rates, and enable a designer to push down the limits of low power operation. Impulse radios have some other benefits over the CW radios at lower data rates too. For example, besides lower path loss (due to no impact of multipath), the spectral purity specs for an impulse radio are also not as tight as the CW radio, which can further be utilized for reduction of the overhead power components for low data rate impulse radios. However for realization of all the benefits of the low power impulse radio design one needs good quality synchronization.

### **1.12 Synchronization**

For low power duty-cycled radio designs synchronization is the most important requirement. This synchronization of transmitters and receivers can be accomplished in a variety of ways. Each radio can contain an accurate oscillator that is well matched to other radios. Radios can be synchronized by a master radio sending out a clock signal that other radios use to phase-match their local oscillators (Fig.1.19a.), thereby making a local copy of the common clock within the radio. This limits the network to be useful only for the nodes in the immediate neighborhood of this master node. A situation can be thought of where one places multiple masters (Fig.1.19 (b)), but in this case, there will be multiple disjointed separately synchronized clusters. The nodes which can receive signals from many masters cannot communicate and synchronize. The cluster networks also cannot communicate with each other in this scheme. Ideally what one wants is a globally synchronized network as shown in Fig.1.19.c. In such a network, there should not be ideally any concept of a master node, all the nodes should be identical, and the network should be globally synchronized. In the next chapter we will discuss about how we get to a globally synchronized network.

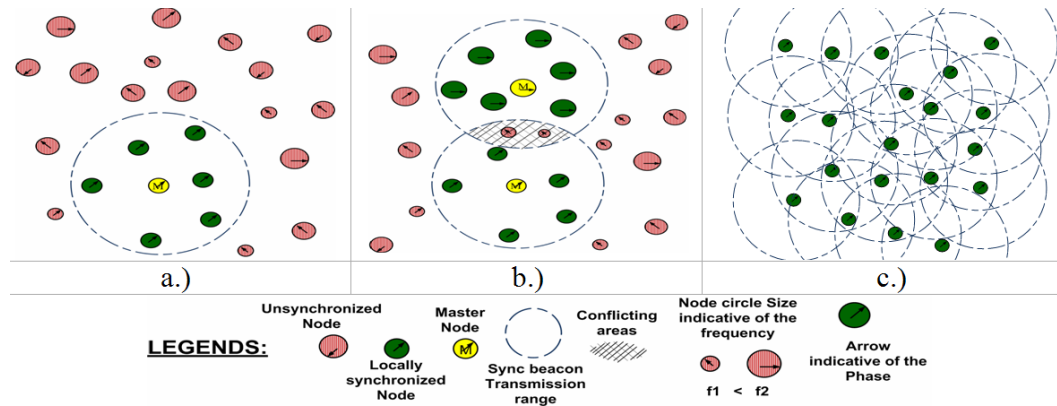


**Figure 1.19. Different Synchronization topologies, (a.) One master node synchronizing the nodes in the local neighborhood of the master nodes (b.) Two master nodes c.) A globally synchronized network.**

### 1.13 Chapter Summary

In this chapter, we discussed wireless communication, wireless sensor networks, and their many requirements. Low power communication was found to be the biggest bottleneck for the realization of low power wireless sensor networks. We then looked at fundamental limits based on link optimization that govern the communication and energy requirements of a radio. For low data rate, low range communication that is warranted by a wireless sensor node, it was found that fundamental limit was governed by overhead power associated with the transmit and receive circuitry that act as a bottleneck in achieving a low power radio. We then discussed the potential use of duty-cycled radios as a solution to this problem. We discussed different existing duty-cycled architectures, such as periodic sleep-wake radios, where the radio nodes wake-up asynchronously, as well as the idle-listening based radio architectures. We discussed the limitations of these architectures and came up with the need for impulse based data scheme for significant power saving. An analytical comparison of impulse radio designs with continuous wave radio designs was also presented to find relative power trends of the two designs that revealed the advantages of impulse radio for low

power short range applications. We then discussed about the synchronization requirements and limitations. While the peer-peer synchronization or a one-master-many slave kind of synchronization can be easily done with the existing methodology, for scalable network and multi-hop architectures a need for global synchronization was discussed. In the next chapter we will talk about the way we propose to achieve a global synchronization scheme.

## CHAPTER 2

# GLOBALLY SYNCHRONIZED NETWORK AND PULSE-COUPLED OSCILLATOR

### 2.1 Introduction

Synchronization is the key bottleneck to realization of duty-cycled radios. In the absence of good synchronization schemes, previous efforts have focused on periodic sleep-wake scheduling that limits overall system performance. Other methods [33,34] utilizing impulse based signaling can guarantee good quality synchronization between two nodes or in a clustered configuration around a single leader node. But, these schemes are limited, as they require a master/leader node in the network with the responsibility to send the “sync” beacons periodically. A network requiring a designated leader node is not a scalable architecture, as it can lead to complications in the network, if the leader node dies. The network connectivity graphs in such cases are also limited to only single hop, as only the nodes in the immediate neighborhood of the leader node are connected to each other. Fully scalable systems need a globally synchronized network. Global synchrony/order exists in nature in multiple forms, such as synchronized firing of neurons, ordered movements of birds, colony formation of ants, crickets chirping together, fireflies flashing etc. It has been shown in many of these cases that a set of local rules bring about a global order. Mirollo and Strogatz, studied these local rules in the context of studying the phenomenon of southeast Asian fireflies blinking together [35]. In this chapter we focus on this phenomenon that promises to facilitate multi-hop global synchronization based upon the analytical framework of Mirollo and Strogatz [35]. They modeled a group of fireflies as a network of pulse coupled oscillators (PCOs) that interact to drive the whole network

into global synchrony. We discuss the unique characteristics of this synchronization scheme and changes required for its potential use in our impulse based communication. Using an event based fast simulator for the network of PCOs, we also study of some non-ideal effects such as delay, frequency mismatch, jitter etc. and their effects on robustness. We also find constraints on various parameters to ensure the system works correctly in the face of non-idealities not considered in prior studies. We also discuss the accuracy to which one can achieve synchronization based on realistic design effects.

## **2.2 Firefly based Synchronization & Pulse-Coupled Oscillator**

One spectacular example of global order that has intrigued many a scientists is that of a south-east Asian fireflies flashing/blinking together [35-41], when in a group. Many studies have been done on this synchronization scheme resulting in practical utilization as well. A prominent example being, that of pace-makers utilizing the model of synchronous firing in biological oscillators first studied by Peskin [42]. Peskin's model of cardiac pacemaker was later mathematically modeled by Mirollo and Strogatz [35] to study the phenomenon in fireflies. Fireflies were modeled as a group of integrate-and-fire oscillators (i.e. electrical equivalent of relaxation oscillators). Mirollo and Strogatz [35] also demonstrated that a group of identical oscillators following a monotonically increasing concave down state function with non-linear coupling synchronize. Fig.2.1 shows one such implementation of pulse coupled oscillators based on RC-charge up. The state function for an oscillator  $i$  is a voltage  $V_i$  that is a function of a normalized time,  $\phi_i = t_i/T_0$ , where  $t_i$  is the time since oscillator  $i$  was last "reset" and  $T_0$  is the time a free running oscillator takes to complete a period. All oscillators start at random initial points on the state curve and travel along the state function at a constant and identical rate. When an oscillator

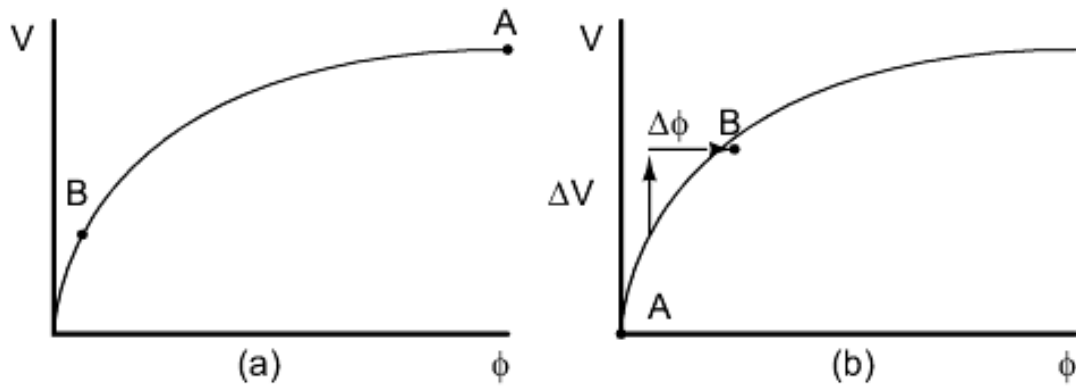


**Figure 2.1. Nonlinear Dynamical Pulse Coupled Oscillator System of Mirralo and Strogatz [35].**

completes a period, it emits an instantaneous coupling  $\Delta V$  to every other oscillator in the system (Fig.2.1b), causing them to advance in state by  $\Delta V$  and its associated  $\Delta \phi_i$ . They then reset to  $t_i=0$ , when the state function reaches the threshold voltage. In this scheme each oscillator firing drives the group of oscillators' phases closer together through the nonlinearity of the state function. Mirralo and Strogatz show that if the state-function is monotonically increasing and concave down, then the system of identical oscillators perfectly phase-locks [35].

A pulse-coupled oscillator circuit can be built in circuit form using an RC relaxation oscillator as shown in Fig.2.2, where the node voltage dynamics at node "A" will implement the concave down state function. The coupling can be implemented using charge injection at the node "A" in the form of extra charge up current, based on detection of pulses/firing of other oscillators in the network, which can easily be implemented by using a switched current source as shown in Fig.2.2. Fig.2.3 shows the simulation of a group of 3 Pulse-coupled-oscillators that start with random phase and finally settle into a synchronized (i.e. phase-frequency locked) state.

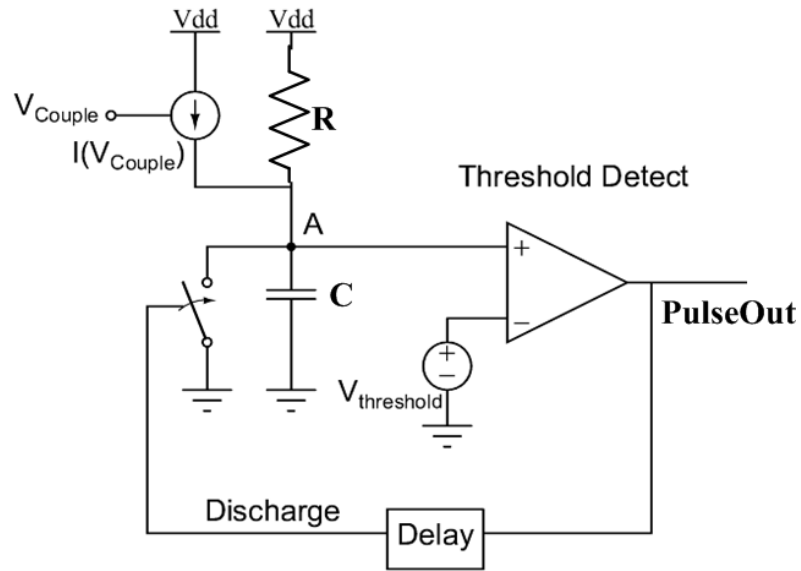


**Figure 2.2. Illustrative RC relaxation oscillator circuit generating the state function. PCO signal is generated on Node A. External coupling in the form of a current injects extra charge on the node, thereby creating jumps in the state-function.**

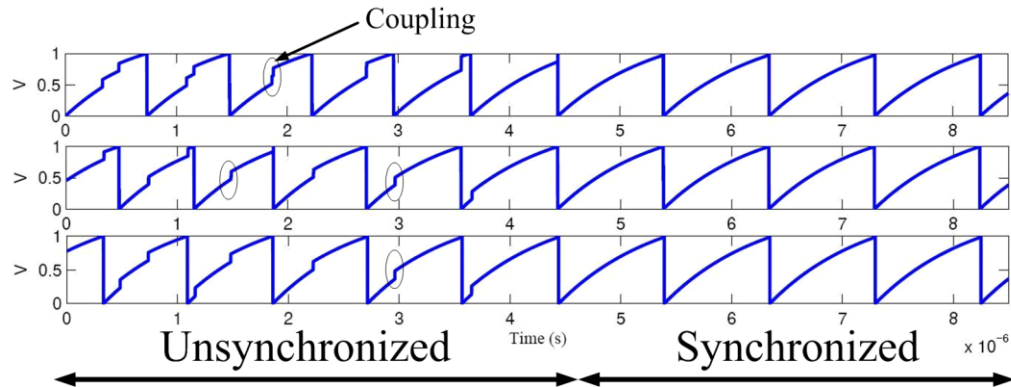


**Figure 2.3. Depiction of The internal dynamics of the Pulse coupled Oscillators from Non-synchronized to synchronized state for three nodes.**

### **2.3 Synchronization and study of the collective dynamics of a network of pulse coupled oscillators: A Primer to existing work**

A number of papers consider the collective dynamics of a network of the pulse-coupled oscillator. In the simplest term the collective dynamics of a network of

oscillators can be understood as multiple nodes travelling at a given rate along the periphery of a circle [35, 43]. If one were to associate a radial vector  $(r_i, \theta_i)$ , with each node “i” in such network of “N” oscillators, then one can evaluate a center of gravity for these oscillator system given as in equation (1) and (2) below.

$$r_{CG} = \frac{1}{N} * \sqrt{\left(\sum_{i=1}^N r_i \cos \theta_i\right)^2 + \left(\sum_{i=1}^N r_i \sin \theta_i\right)^2} \quad (1)$$

$$\theta_{CG} = \tan^{-1} \frac{\sum_{i=1}^N (r_i \sin \theta_i)}{\sum_{i=1}^N (r_i \cos \theta_i)} \quad (2)$$

For a network of oscillators with random phases (unsynchronized, i.e. not moving together), the  $r_{CG}$  can be seen as “0” (Fig.2.4 (a.)), while if the nodes are closer together, the  $r_{CG}$  value starts approaching “1”. In the most ordered state (when all the nodes are moving together) the radius of this centre of gravity becomes “1”. Thus the evaluation of this parameter  $r_{CG}$  can provide insight into the collective dynamics of a network of oscillators. The “ $\theta_i$ ” values can be evaluated with respect to a node crossing some fixed point in the circle, i.e. a chosen node “firing” or “resetting”.

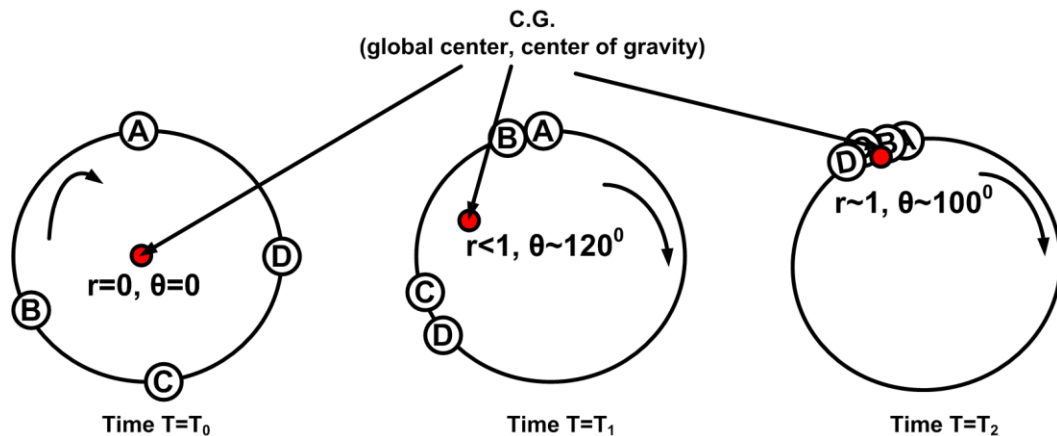


**Figure 2.4. Study of collective dynamics of pulse-coupled oscillators using the concept of the center of gravity.**

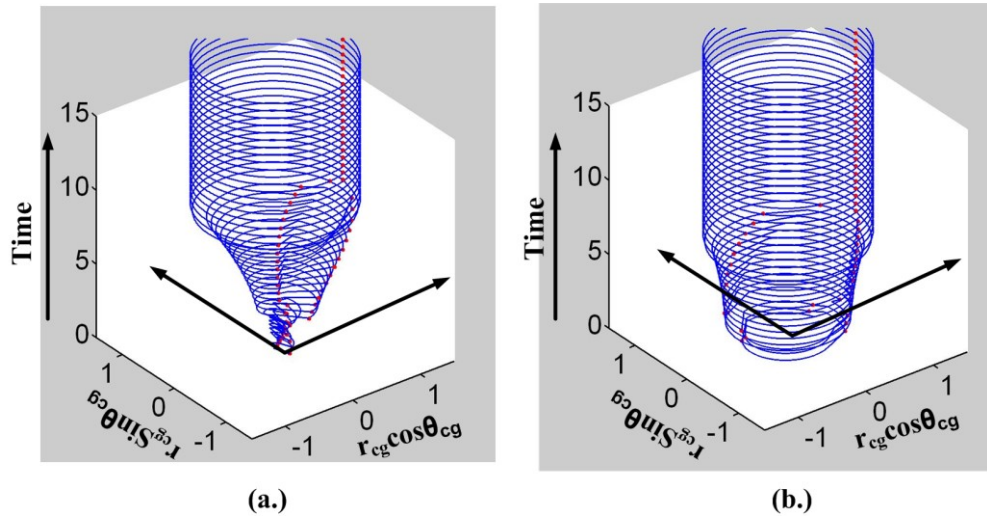


**Figure 2.5. Simulation of a network of oscillators (~100 nodes) with random phase and evaluation of the “ $r_{cg}$ ” and the trajectory of the movement of the center of the gravity for two different initial states (a, & b). The “red dots” are placed at time instances, whenever any node in the network fires. As, can be seen the center of gravity of the collective dynamics of the network, starting with random trajectory finally settle to a periodic trajectory. In the steady state the “red” dots” appear only per cycle of revolution indicating phase synchronization.**

In this configuration one can find the advent of synchronization as a phenomenon when  $r_{CG}$  becomes “1”. When synchronized all the nodes in the network will fire simultaneously thus  $\theta_{CG} = \theta_i$  will hold true for each one of the nodes in the network too at the advent of synchronization or global order.

Fig.2.5 shows a matlab simulation of this concept using a network of coupled oscillators. As can be seen the system reaches a periodic state with the center of gravity radius “ $r_{cg}$ ” settling to a value of “1” in the synchronized state. Fig.2.6 shows the dynamics in a 2-D space for more clarity. An interesting aspect that comes about from close observation of the dynamics of these oscillators is the existence of clustered synchronization. One can see the two distinguishable points over which the activities in the networks are recorded in the initial phase of the synchronization dynamics. These local clusters however eventually merge into one final cluster, in which all the nodes fire together, indicating the advent of synchronization at that point

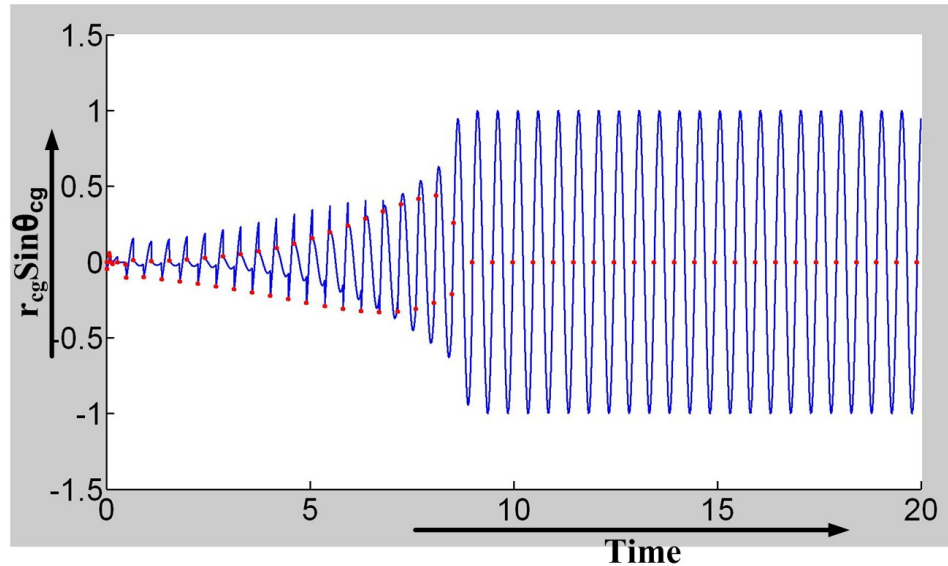


**Figure 2.6. Simulation of the collective dynamics of a network of oscillators (~100 nodes) with random phase and evaluation of the “ $r_{cg}\sin\theta_{cg}$ ” as time progresses. The “red dots” are placed at time instances, whenever any node in the network fires. As, can be seen the radius of the center of gravity in steady state settles to “1”, while only one firing per full evolution is there in the collective dynamics of the network of oscillators indicating phase synchronization.**

for the whole network.

Most of the mathematical models of a network of pulse-coupled oscillators utilize this collective dynamics to find constraints determining synchronization for the network of oscillators. For more detailed study one can refer to the work done in the following references [35, 43-46].

#### **2.4 Simplified assumptions in Mirollo’s Analysis**

While, to the first order Mirollo and Strogatz model demonstrates the working principle of these coupled oscillators [35]. The model makes some simplified assumptions, which are not realistic in a physical system. For example, they consider only identical oscillators. Inherently however oscillators will have mismatch in their frequency. Their derivations have also made the assumption of no path delay whereas

in any physical realization of these PCO network, there will always be path delays. The other short-coming of the model was the assumption of all-all coupling. For large scale sensor network deployment, using these pulse-coupled oscillators for synchronization, scalability rules doesn't allow all-all coupling. The PCO jitter was also not taken into account while establishing the synchronization rules.

## **2.5 Motivation for Event Based Simulation**

In the wake of various unrealistic assumptions in existing studies, we needed to find out if the PCO model will work in a real environment. Different studies have shown existence of various types of synchronization modes for a group of oscillators in a network, while varying the parameter space of frequency mismatch, delays and coupling. The solution space has been found to be sometime aperiodic, sometime resulting in localized clustered solutions and at other times unstable [47-49]. While a complete understanding of the set of possible behaviors of the PCO system is not available yet, it has been found that by placing certain system constraints on the parameters controlling the dynamical behavior of these pulse-coupled-oscillators, a desired mode of synchronization can be achieved.

Though, the existence or non-existence of the synchronization have been studied in detail by various researchers across the world, a detailed analysis of the parameter space, or the boundaries between stable synchronized modes of operation and unstable/undesired mode of synchronization is still missing. This is because a mathematical solution including all parameters without constraints is intractable.

In the absence of a general mathematical theory for a network of random oscillators, we would like to have a behavioral evidence of a large system with random connectivity, delays and frequency mismatch to understand the dynamics and constraints on the system. This requires a simulation interface that randomizes the

parameter space for a randomized network of pulse coupled oscillators to find the steady state solutions. Due to the variability of the parameter space, multiple simulations are required to confidently suggest the stability of a solution for the network of oscillators. This thus requires a simulation environment that is very fast to be able to handle complex dynamics of the large network of these oscillators without losing the precision. In the next section we talk about this fast event based simulator that simulates the behavior of the network with a good time resolution but without consuming too much of simulation time or computing resources.

## **2.6 Event Based Simulation**

We wrote a matlab based event simulator that can initialize a network of nodes with random connectivity as well as with frequency mismatch, delays and jitter to help us gain good insight about synchronization. Since a real time simulator tracking the state-function of each oscillator for a large network is very time-consuming, we make use of the event based simulation to make the simulation faster.

The simulator works on the basis of a global event tracker (an array that evaluates constantly any meaningful events that are supposed to happen at any node). At any node only two types of events occur, namely the firing and coupling. The global tracker has to keep track of only these two types of events on a per node basis. Starting from any initial time ( $t=0$ ), the global event tracker, finds when a node, given their initial states and frequency of oscillations, is supposed to fire next. Based on this information the time of the simulator is advanced to the first such time-point where an event (coupling or firing) occurs. At that time, the new phases of all the PCOs are evaluated, and subsequently, the global event tracker list is updated to find out the next event of importance in the network for any node.

Instead of evaluating the system states with very small timing resolution steps this

methodology enables one to skip time, i.e. adaptively change the time steps, and thereby improves the simulation time of a complex large network of oscillators by orders of magnitude.

Fig.2.7, shows the simplified algorithmic chart of the simulator used for analyzing the system. The actual implementation of the algorithm is however, further simplified

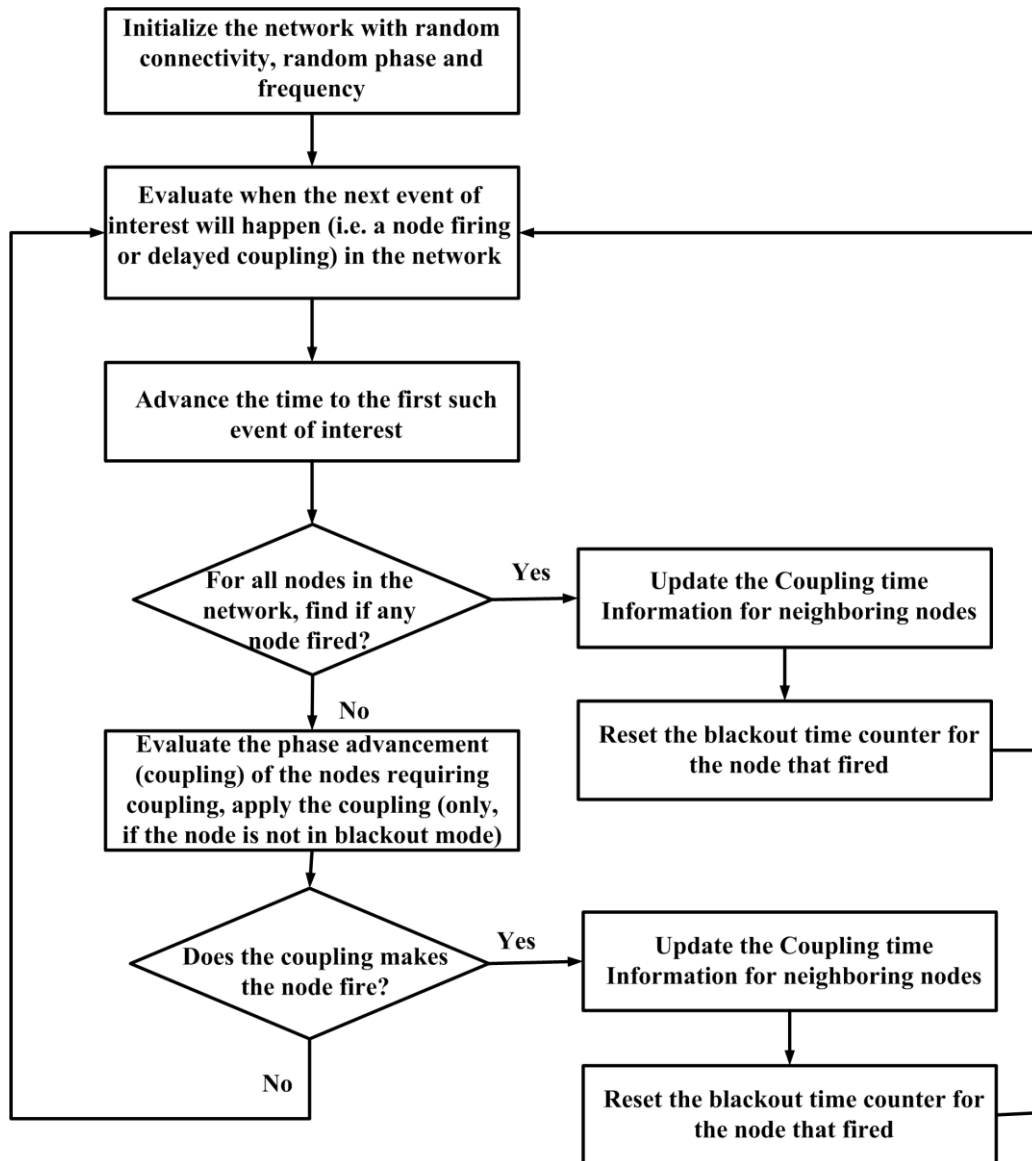
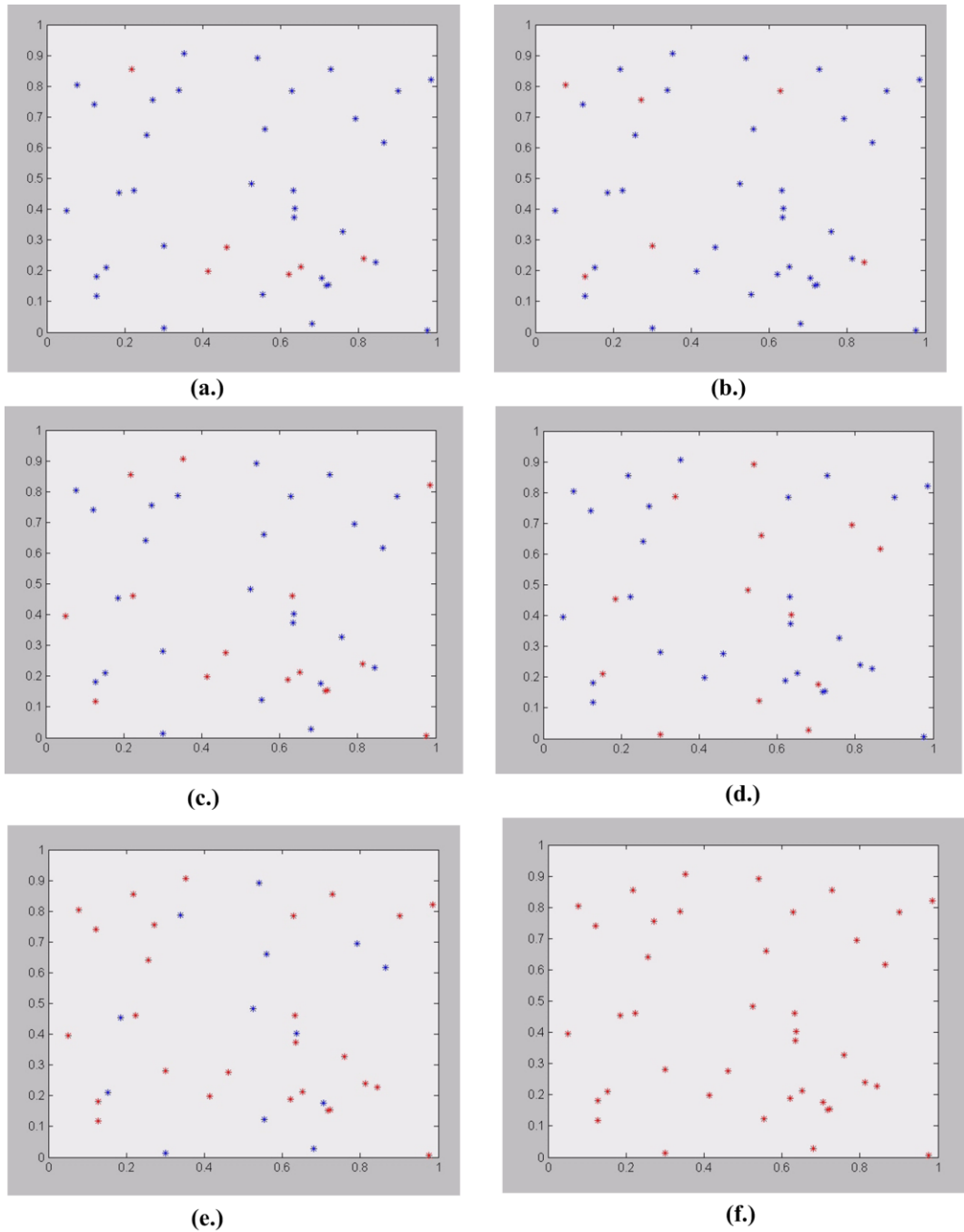


Figure 2.7. Event based simulator: simplified algorithmic flow chart.

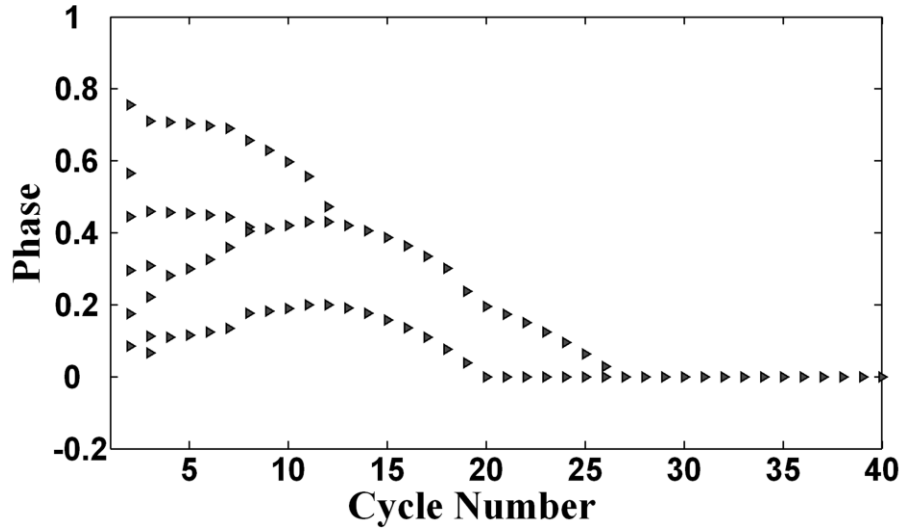
to speed up the simulation performance.

Fig.2.8 shows a simulation of a large network of pulse coupled oscillators modeled using this simulator to show the simulation behavior in time. The figure shows the network snap-shots at different points of time during the evolution of the network dynamics. The nodes are randomly distributed in the network of given area, with limited connectivity. All the nodes are shown at any given point as “blue” or “red” asterisks. The nodes in “red” are the nodes that fired at the point of the snap-shot. As can be seen in different snapshots of the network dynamics increasingly more and more nodes fire together, eventually resulting in all the nodes firing together. Fig.2.9 shows the stroboscopic phase view of a network of 6 PCOs, the phase of other PCOs are shown every time a fixed PCO in the network fires. It can be seen that in the steady state, the phase of all other oscillator go down to “0” indicating all the node firing together in the network, and can be used as an indication of synchronization.

While we could achieve synchronization in this example case, we could also create multiple situations by varying parameters such as coupling, frequency mismatch and delays that resulted in network not converging to a periodic steady state solution. Fig.2.10 shows the stroboscopic view in one such example case, where the synchronization was not achieved. In the later section we focus on these situations and reason why the network fails to synchronize in order to determine what constraints we need to place on the parameter space to ensure the network always synchronizes. We will also show by exhaustive regressive simulation the robustness of the proposed solutions for tackling various situations that can result in loss of synchronization.



**Figure 2.8. Dynamics of randomly distributed Pulse-coupled oscillators in a network at different time-instances. The nodes are shown in blue and red asterisk. “red” asterisks show nodes that fired at the given time the snapshot was taken.**



**Figure 2.9.** Stroboscopic phase view of 6 different nodes relative to one fixed node. The phases of 6 nodes are marked in time, every time the fixed node fires. As, can be seen the nodes finally synchronize their phases in time.

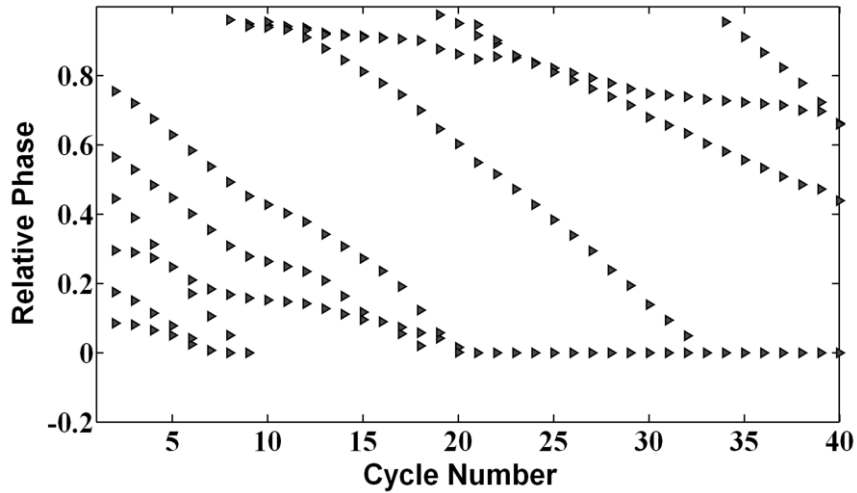


**Figure 2.10.** Stroboscopic phase view of 6 different nodes relative to one fixed node. The phases of 6 nodes are marked in time, every time the fixed node fires. As, can be seen the nodes create clusters, where the phases are not aligned, i.e. lack of synchronization.

## 2.7 Synchronization in the presence of Delays & limited connectivity

As, explained before, for large scale deployment of the sensor network, all-all connectivity will not hold. We created a simulation environment where we could test the synchronization scheme with limited connectivity. For a significantly large number of simulations (~1 million) (Fig.2.11) with random connectivity between varying number of nodes, we could find the synchronization to be completely robust subject to the condition that a node is “connected” to other nodes; a “direct connectivity” to other nodes wasn’t required. These simulations proved a connected network of nodes always resulted in synchronization subject to zero path delays.

We then introduced path delays between nodes in the network, and found that introducing path delays causes synchronization to fail. The problem however was traced to a node coupling to its own echo signal repeated by a neighboring node. For

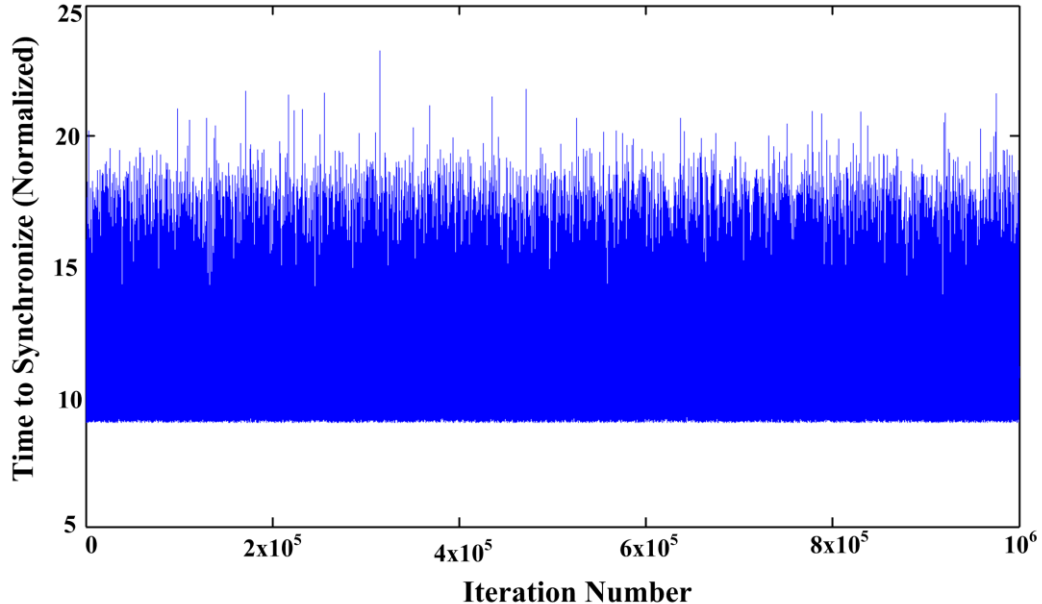


**Figure 2.11. Various iterations of simulations done using the event simulator with random connectivity and different initial phase conditions, the nodes synchronized at all time, while the time to synchronization was also fairly limited in it’s upper bound, the lower bound is due to minimum time we wait before declairing the advent of synchronization.**

example if in a two node system consisting of node “A” and node “B”; node “A” firing thresholds the node “B” and causes it to fire. The resultant firing from “B” should not create a phase-advancement at “A” as otherwise; it can result in a race condition resulting into either non-occurrence of synchronization, or a very fast periodic state, none of which are desired. To work around this problem, we found that we need to create a time-window (blackout window) after a node fires, during which the node is not allowed to couple (i.e. coupling is disabled). This blackout window was already required to prevent self-coupling. In this case, it is required to also ensure that the node doesn’t couple to its own echo signal that has been generated by a node’s neighbors in response to the node’s firing, i.e. prevent an action-reaction type of coupling in a node’s immediate neighborhood.

For the parameter space exploration in the presence of delay we simulated a network of large randomly connected nodes with variable maximum propagation delay between two nodes in the same neighborhood, i.e. limited range of communication. We allowed the blackout time to vary and observed if a synchronous state was achieved in reasonable simulation time. Since the ability of the network to synchronize might be dependent on initial conditions, for each simulated point in the parameter space we perform multiple runs with a uniform distribution of initial node phases and consider synchronization to occur at that point in the parameter space only if all ten runs result in the synchrony. For the parameter pairs of blackout time ( $T_{blk}$ ) and the inter-node propagation delay  $T_d$ , a constraint boundary was found as shown in Fig.2.12, which is blackout equal to two times the maximum single-hop propagation delay and is independent of other system parameters (3).

$$T_{blk} > 2 * T_d \quad (3)$$

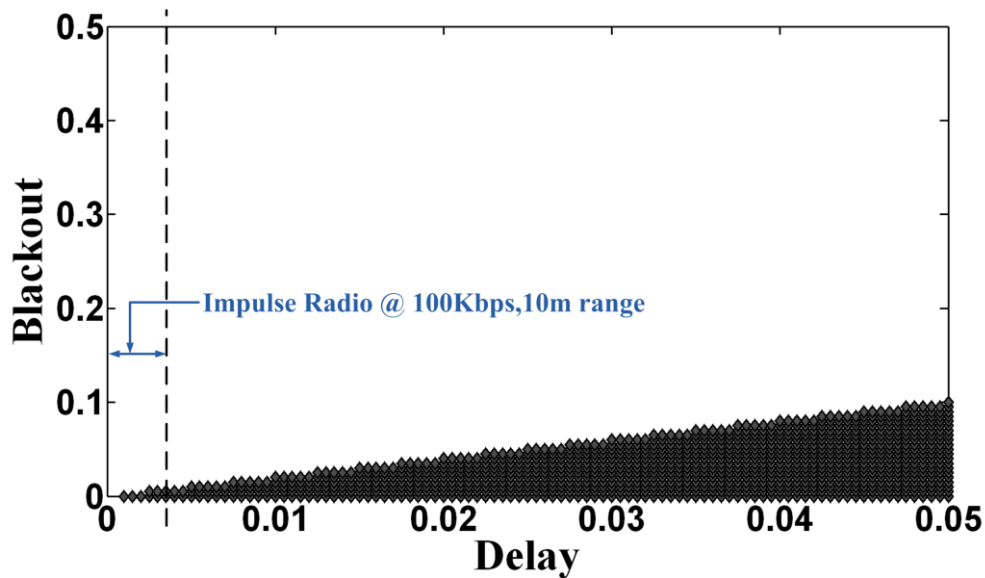


**Figure 2.12. synchronization/non-synchronization boundaries for a group of oscillators with inter-node delays. The delays and blackout are given as normalized units (normalized to nominal period of oscillation). The region in black shows the parameter space, over which robust synchronization can't be achieved. A large range of blackout value however still exist, over which robust synchronization can be achieved. The simulation also gives the trend for the minimum required blackout time as 2 times the maximum inter-node delays.**

An intuitive reason why this boundary exists is because it prevents positive feedback where a node firing triggers the firing of a connected node that subsequently feeds back to the original node and advances its phase, destabilizing the system. We also observed that including sufficient blackout period eliminates the unstable synchronization modes witnessed in [48] that did not incorporate blackout in their simulations. As can be seen a large range of operating conditions exist over which one can achieve robust synchronization. For low data rate, short range communication required for wireless sensor network, these constraints on the parameters are very easily achievable.

## 2.8 Synchronization in the presence of Frequency Mismatch

In simulation, large frequency variations in the pulse-coupled oscillator nodes results in unsynchronized modes (i.e. the nodes didn't settle to a steady state constant period). The failure (non-occurrence) of synchronization was however traced to insufficient coupling. Increasing the coupling resulted in the desired synchronization (Fig.2.13). For example in a two node case, if Node "A" and Node "B" have different initial periods ( $T_0$ ,  $T_1$  respectively,  $T_0 < T_1$ ), once synchronized, they are expected to have same period. Now let's say if "A" and "B" at some point of time start with their zero-state, "A" having smaller period will get to fire first at  $T_0$ , now at that point of time the node "B" needs to have sufficient phase advancement due to the coupling signal received from "A" to negate the time difference of  $T_1 - T_0$ . If the coupling is enough to get "B" to threshold, then the periodicity of oscillation will hold true, as both nodes will start their respective states at the same time again. This means the  $T_{\text{couple}}$  due to the coupling should be at least  $T_1 - T_0$  for the nodes to converge to (4).

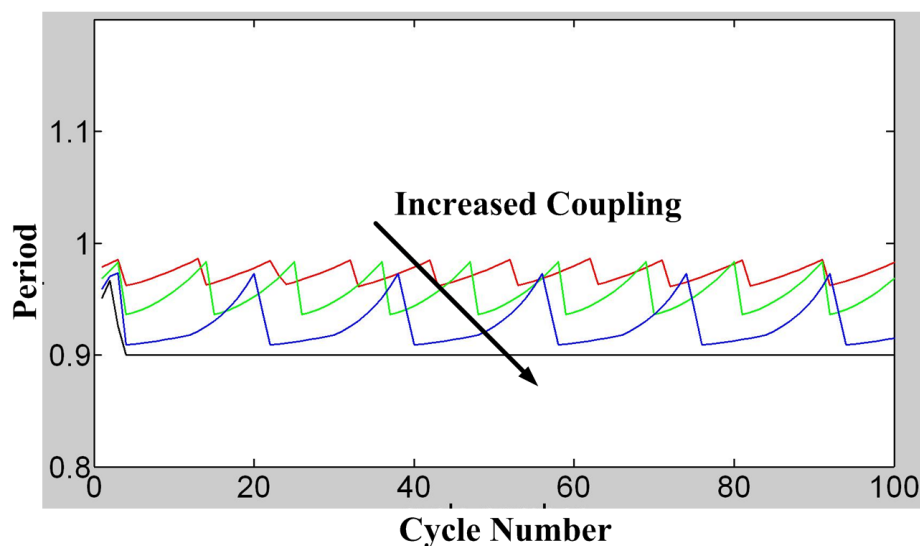


**Figure 2.13 : Dynamics of oscillators with large frequency mismatch. At low coupling, the node period doesn't stabilize to the steady state value. As, the coupling is increased, the node settles to the stable frequency/period.**

$$T_{couple} > T1 - T0 \quad (4)$$

A large scale simulation was done to find the parameter space over which one can achieve robust synchronization for given frequency mismatch. As in the case of blackout and delay earlier, we did the simulation with frequency mismatch and coupling with multiple iterations in any frequency coupling pair to ensure the robustness of the synchronization behavior (Fig.2.14).

A boundary condition for frequency mismatch and coupling co-efficient that mirrors the quadratic shape of the coupling function, and is practically independent of the exact values chosen for ( $T_d$ ,  $T_{blk}$ ) provided they are in a synchronous region is shown in Fig.2.14. This suggests that for synchronization to be maintained the coupling between nodes needs to be strong enough to overcome their intrinsic frequency variations as analyzed earlier in two node case. The boundaries were also independent of the number of nodes in the network, as the simulations were done with

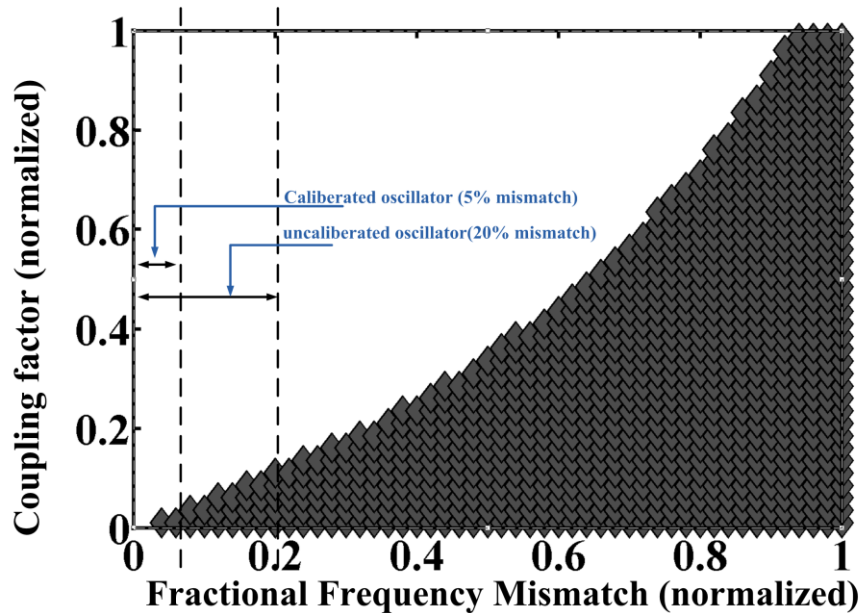


**Figure 2.14. Synchronization/non-synchronization boundaries for a group of oscillators with frequency mismatch. The region in black shows the parameter space, over which robust synchronization can't be achieved. A large range of frequency mismatch value and corresponding coupling factor however still exist, over which robust synchronization can be achieved.**

random number of nodes and random connectivity between them. Based on the results of our simulations, it appears that there is a substantial region of the parameter space to operate the conventional pulse-coupled oscillators with realistic frequency mismatch for the global synchronization of radio nodes (Fig.2.14).

While doing simulations with frequency mismatch we also noted another interesting aspect of the synchronization, we found that in the synchronized mode of network operation, the node that is the fastest in the network, dictates the overall network frequency. The network frequency in the synchronized mode of operation was found to be equal to the fastest node for any given iteration. This means the fastest node can be said to fire first in the synchronized mode of operation, while making all other nodes fire subsequently, it also means the fastest node in the network in synchronized mode of operation doesn't take any coupling from other nodes in the network. We will utilize this interesting property of the pulse-coupled-oscillator networks in chapter-7 for some novel applications.

Overall, the simulation results suggest that robust synchronization can be achieved even in the presence of frequency mismatch by ensuring sufficient amount of coupling between the nodes. Since, one can control the strength of the coupling (Fig.2.2), by changing the strength of the coupling current that injects extra charge at the PCO-node, the criteria can be met very easily.

## **2.9 Synchronization in the presence of jitter or frequency drift**

Timing jitter or frequency drift is another non-ideality that can result in loss of synchronization for a network of practical pulse-coupled oscillators. A network simulation was done with randomly connected pulse-coupled oscillator nodes to see if the network fails over the parameter space.

While, jitter did deteriorate the quality of synchronization, the nodes still

synchronize, with the timing uncertainty of firing of any node in the network limited to the peak-peak timing uncertainty induced by the timing jitter. It was also noticed that in the presence of frequency mismatch between nodes in the network, due to evolution of the fastest node as the master, the network frequency as well as jitter characteristics of the network mimic that of the fastest node. This also leads to the observation that if one could design the fastest node in the network with very low jitter, then the jitter characteristics of each one of the other oscillators in the network will be low as well, irrespective of the intrinsic jitter characteristics of each node if allowed to run freely.

Overall, the network simulation suggested that synchronization can be well maintained even in the presence of the timing jitter; with synchronization quality limited by the amount of jitter in the network, and to this effect synchronization was again found to be robust.

With all the three effects of delay, frequency mismatch and jitter included in a network of random connectivity, we could map a large parameter space, where a robust synchronization of practically realizable pulse-coupled oscillators can be achieved enabling us to use this pulse-coupled oscillators to synchronize a large radio network.

## **2.10 Design of Pulse-Coupled Oscillator & realizable timing uncertainty**

A pulse-coupled oscillator can be designed using an RC-relaxation oscillator, as shown in Fig.2.2, the disabling of the coupling can be easily implemented by disabling the couple signal, after a node fires by using delay element to control the blackout width. The most important design specs that one need to however be careful about in designing a PCO is that of timing jitter. Since, the timing jitter directly affects the quality of synchronization, which thereby affects the amount of duty-cycling one can

do, designing the PCO for low jitter is very important. Since, timing jitter is a function of noise injection at various oscillator nodes, careful design is warranted to ensure low level of noise injection. For a relaxation oscillator based on RC time constant one can keep the timing uncertainties to a low value by increasing the size of the capacitor, while reducing the resistance value. A larger value of the capacitor though also means larger power consumption in charging and discharging the capacitor, and thus design optimization is required to ensure low power as well as low timing jitter. Care also is required to ensure close to zero residual charge in the capacitor when resetting the capacitor after the PCO reaches the trip point (Fig.2.2). This is because; an uncertainty in residual charge after resetting the capacitor can have large timing-uncertainty effects (at the trip-point) due to exponential characteristics of the RC-charge-up.

By careful consideration of noise injection at various nodes and after taking good care of the residual charge uncertainty we were able to achieve pulse-coupled oscillators with only  $\sim 1$ ns timing errors for PCOs operating at  $\sim 150$ KHz ( $6.5\mu$ s) for a power consumption of only  $3\mu$ W in our lab. The design work was done by my project-mate Xiao, and more details about the design can be found at ref. [50].

At only  $3\mu$ W power consumption the overhead power associated with the PCO circuitry is extremely low. A network of pulse-coupled oscillators was also demonstrated to synchronize with high accuracy with designs fabricated in a 90nm CMOS process [50]. We also validated the blackout requirement and coupling strength based analysis presented here with real physical network of PCOs, albeit with a limit of only 4 nodes in the network, due to complexity associated with packaging multiple chips [50], and found the trend to be as expected from the analysis presented here.

With the high quality of demonstrated synchronization using these pulse coupled oscillators, we can design the RF circuitry that can be duty-cycled heavily to save

power. In the next chapter we will talk about the design of the duty-cycled transceivers that can utilize the high quality synchronization achieved by the network of pulse-coupled oscillators.

## **2.11 Chapter Summary**

In this chapter we discussed about various phenomenons in nature that lead to global order. We specifically focused on southeast-Asian fireflies and the interesting dynamics involved therein that lead to a group of fireflies blinking together in a group. We looked at the existing work in understanding this behavior that promises to give a globally synchronized network and looked at work done by various groups in mathematical modeling of pulse-coupled oscillators that map the dynamics of these fireflies. In the wake of existing analysis that doesn't incorporate non-ideal effects of frequency mismatch, delay, jitter and limited connectivity; we found the need to evaluate the robustness of the synchronization in the presence of these non-idealities. We wrote an event based simulator that could incorporate the non-idealities and found the constraints in the system to ensure robust synchronization while doing extensive simulations with randomized parameter space. The constraints placed on the design of the PCOs were found to be easily achievable, without much degradation on the quality of synchronization. We also discussed the quality of synchronization in the presence of jitter, and discussed the design and measured results of low jitter (high quality) synchronization of a group of oscillators, which can enable aggressive duty-cycling of the RF-frontend. With the global synchronization achieved using a network of pulse-coupled oscillators in the next chapter, we will propose a radio architecture and various ways this synchronization can be used in implementing low power radios and the corresponding duty-cycle-able RF-frontend design.

## CHAPTER 3

### LOW POWER IMPULSE RADIO ARCHITECTURE & DESIGN

#### 3.1 Introduction

As discussed in previous chapter, pulse-coupled-oscillators can be utilized for global synchronization of multiple radio nodes. In conjunction with the proposed synchronization scheme, in this chapter, we discuss various ways that global synchronization can be used to facilitate low power communication between radio nodes, the radio architecture, and the corresponding requirements of a duty-cycle-able RF frontend. Based on these requirements we discuss the design and measurement results of a preliminary duty-cycled non-coherent impulse transceiver designed in a 90nm CMOS process to be used in conjunction with the proposed architecture.

#### 3.2 Duty-cycled Synchronized Communication

Once the nodes are synchronized, data-communication can take place between various nodes in a duty-cycled manner. Synchronization can be used to create timing boundaries (frame-boundary of rate  $T_{\text{frame}}$ ) with periodic exchange of the timing pulses (sync pulse) for the network. A PLL then can be used to divide this timing boundary ( $T_{\text{frame}}$ ) to  $N$  number of bins ( $T_{\text{bin}}$ ) (Fig.3.1). In these bins the sync pulse can be used to indicate timing information in the sync bin (aligned with the frame boundary), while data can be sent or received in designated bins decided by the central control block. A dynamic DLL can be used in the data bin and the sync bin to further facilitate power saving within the bins (Fig.3.1).

The large number of bins ( $N-1$ ) available for data communication gives flexibility to achieve data-communication in a number of ways. In the simplest form of

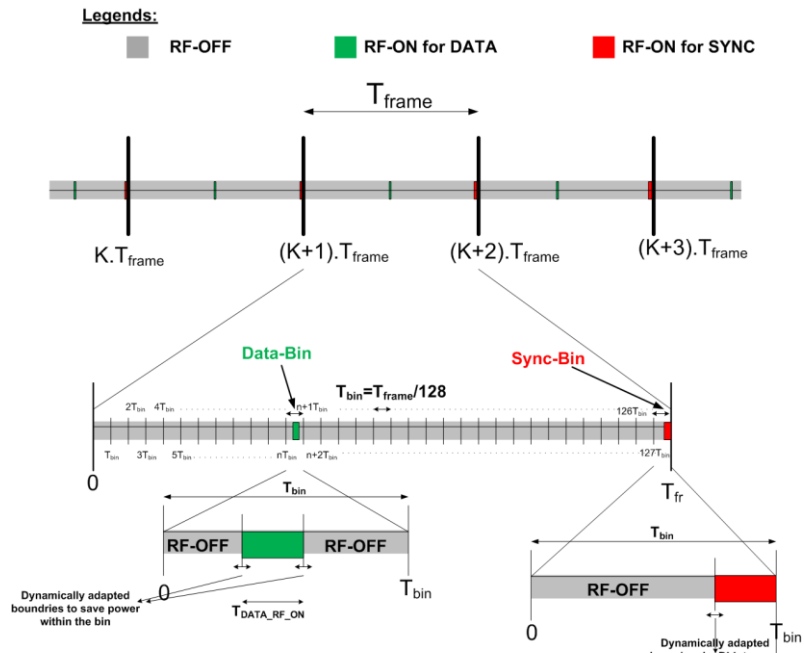


**Figure 3.1. Timing and data bin for exchange of information between different nodes.**

communication the information exchange between different nodes can happen on a fixed preconfigured data-bin. This method can provide communication between different nodes with a data rate corresponding to the frame-rate. This methodology is good for a decentralized mode (Fig.3.2.a) of communication, where nodes cannot be expected to have a pre-knowledge of where to look for the data-information. In

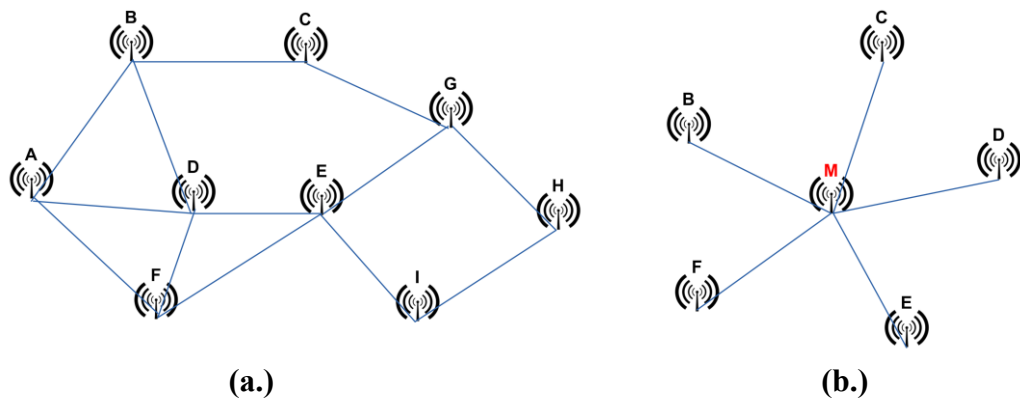


**Figure 3.2. (a.) Decentralized multi-hop and (b.) centralized cluster-head based network.**

comparison, for a centralized network with a cluster head (i.e. master node controlling communication in the network) (Fig.3.2.b), where all the sensor nodes are within the reach of the cluster-head, can configure their mode of communication to facilitate time-multiplexed dedicated channel originating between any two nodes.

Fig.3.3 shows one such timing scheme. In this type of configuration nodes in their immediate vicinity get local dedicated non-overlapping (time division multiple access) channels, on which communication can happen between the cluster-head and various nodes. This type of scheme can be very common for body-area-network where the central cluster head node (residing on a cell-phone/PDA) has to collect the various sensory information from different sensors embedded into different parts of the body. Since, the impulses are very short in time; the bin-boundaries facilitate dedicated channels. The central node however in this case has to consume higher power, as it

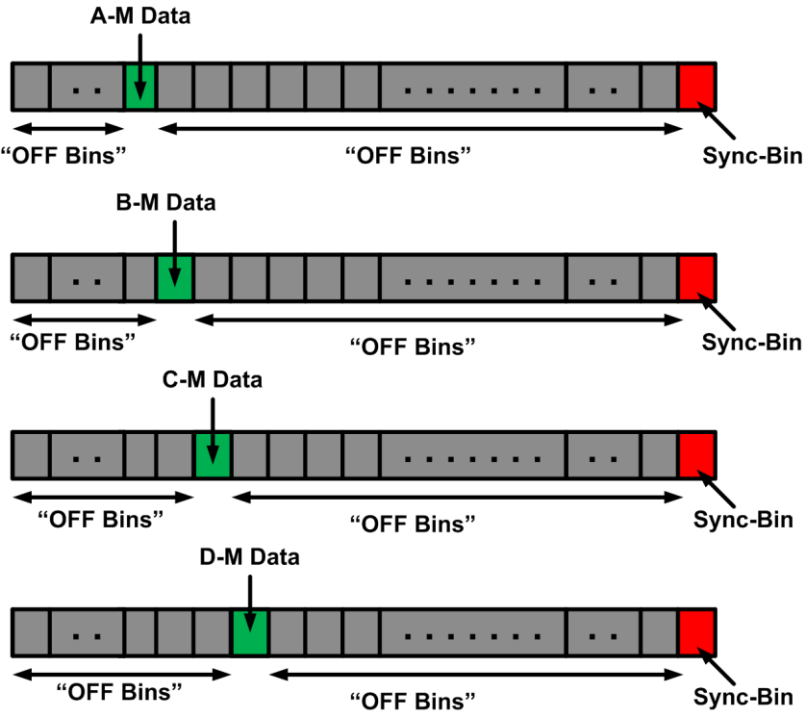


**Figure 3.3. Timing Scheme for a centralized Master-slave configuration, different bins can be utilized for dedicated communication between two nodes.**

needs to communicate to each of the nodes simultaneously with the ability to receive data every-bin, i.e. supporting a data rate of  $\sim 1/T_{bin}$ .

In decentralized communication, there can be situations with synchronized mode of operation, where a hidden terminal can corrupt an existing communication between two nodes. For example in a communication system, one can have a condition such that while node “A” transmits to “B”, the node “C” which can’t see the communication between node “A” and node “B”, starts communicating, thereby corrupting the existing communication between node “A” and node “B” (Fig.3.4). While, one can think of scheduling the communication between node “B” and node “C” in non-overlapping manner, by allocating different bin, in a decentralized communication it’s not possible within the low power framework of communication. There are existing methodologies, based on hand-shaking the “RTS” (Request to Send) and “CTS” (Clear to Send) packets that can reduce the chances of corruption of information due to hidden terminal. In this scheme, the node “B” before engaging into communication with node “A” can let its neighbors know that it will be

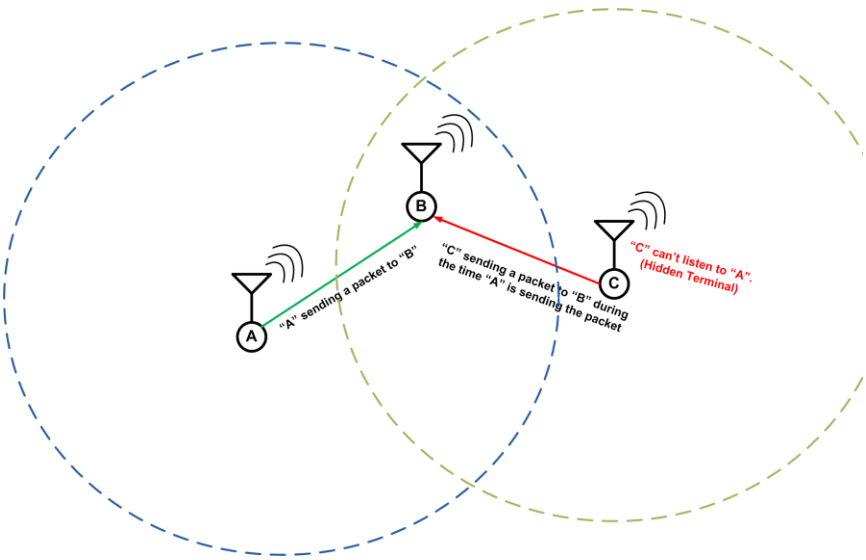


**Figure 3.4. Hidden Terminal problem, node “c” can create collision at node “B” disturbing the existing communication between node “A” and node “B”.**

communicating with node “A” by sending the “CTS” packet in response to the “RTS” packet sent by the node “A”. While node “A” sending the “RTS” packet also lets its other neighbor know of the communication in its neighborhood [51-52].

Though, “RTS”, “CTS” mode of communication can help solve the problem associated with the hidden terminal during actual communication, there are requirements for these packets to be small, as collision can occur during the exchange of the “RTS”, “CTS” packet itself [51-52]. To avoid collision, the information between nodes needs to be exchanged as fast as possible. In such type of system, while the average data rate of communication can be slow, instantaneous data rate of communication is required to be fast. This mode of communication can be achieved in conjunction with the synchronized communication by facilitating other bins to be dynamically open based on detection of a pulse in a particular bin. Duty-cycling and power saving still happens for all the nodes. A node when in idle mode listens into a fixed data bin (Fig.3.5). If no pulse (1) is detected in the fixed-data bin, it (the node) duty-cycles. A node turns itself “on” only for the “fixed-data-bin” and the “sync-bin”, when no activity is there in its neighborhood. When a “pulse” is detected in the fixed-data bin, it opens the rest of the subsequent bins to collect the data-packet. This ensures that the instantaneous data rate is  $\sim 1/T_{bin}$ , while the average data rate can be still very low. Since, communication of information happens fast, there is less chance of collision. This can also ensure that the effective latency for the data-packet transmission between node-node as well as in the network is kept low, even though the

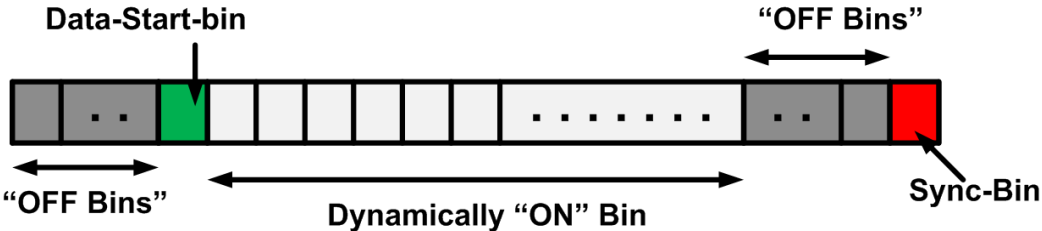


Figure 3.5. Simplified System Block, showing the Tx, Rx and the timing

exchange of data on average happens at a very low frequency.

From the physical design perspective this requires us to have an RF Front-end that can detect the signal very fast, and be able to resolve pulses separated by small amount of time. Detection of pulses separated by even  $\sim 1/T_{bin}$  is required to be supported in the design. Similarly the transmitter, though having a low average data rate, should be able to send instantaneously high data rate pulses. The RF Front End is also required to have the ability to duty-cycle i.e. fast turn-on characteristics and the ability to distinguish the timing and data pulses. With these requirements for the RF Front-end we set the framework for the preliminary design of the low power impulse transceiver.

**3.3 System Block Diagram:**

The Transceiver chain in our proposed system (Fig.3.6) consists of an antenna-driver, a monopole-antenna, duty-cycled amplifying stages and a non-coherent detector. This is followed by a pulse-classifier block that qualifies the pulse type as either a data pulse or a sync-pulse. Detected sync-pulses are sent to the pulse-coupled oscillator, advancing its phase, towards synchronization. Once synchronized, the

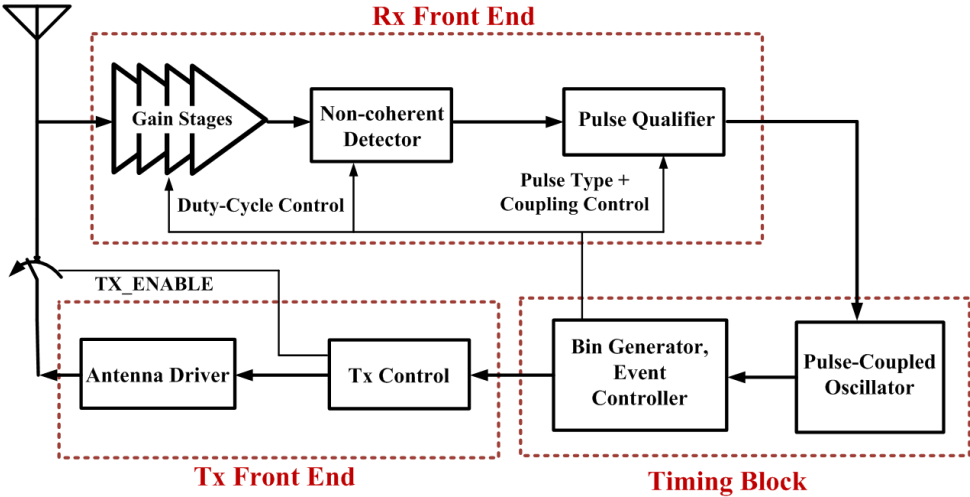


**Figure 3.6. Simplified System Block, showing the Tx, Rx, and The timing Block.**

timing block takes care of duty-cycling and creates the bin to support various data transmission protocols as discussed before.

### 3.4 H-bridge based Transmitter Design

We use an H-bridge antenna-drive scheme for pulse transmission proposed by Wang et al. [53] In this scheme the antenna is connected between two strong inverter pairs (Fig.3.7a) driven by tapered digital drivers with controlled timing sequence (Fig.3.7b). The key here is to inject a current into the antenna for radiation through its own LC-characteristics and then quench the radiation after a small time period (~500ps-1ns). A pulse transmission request by the transmit-control circuit controls the inverter pairs in a 3-step process. Fig.3.7c shows the current flow directions in case of

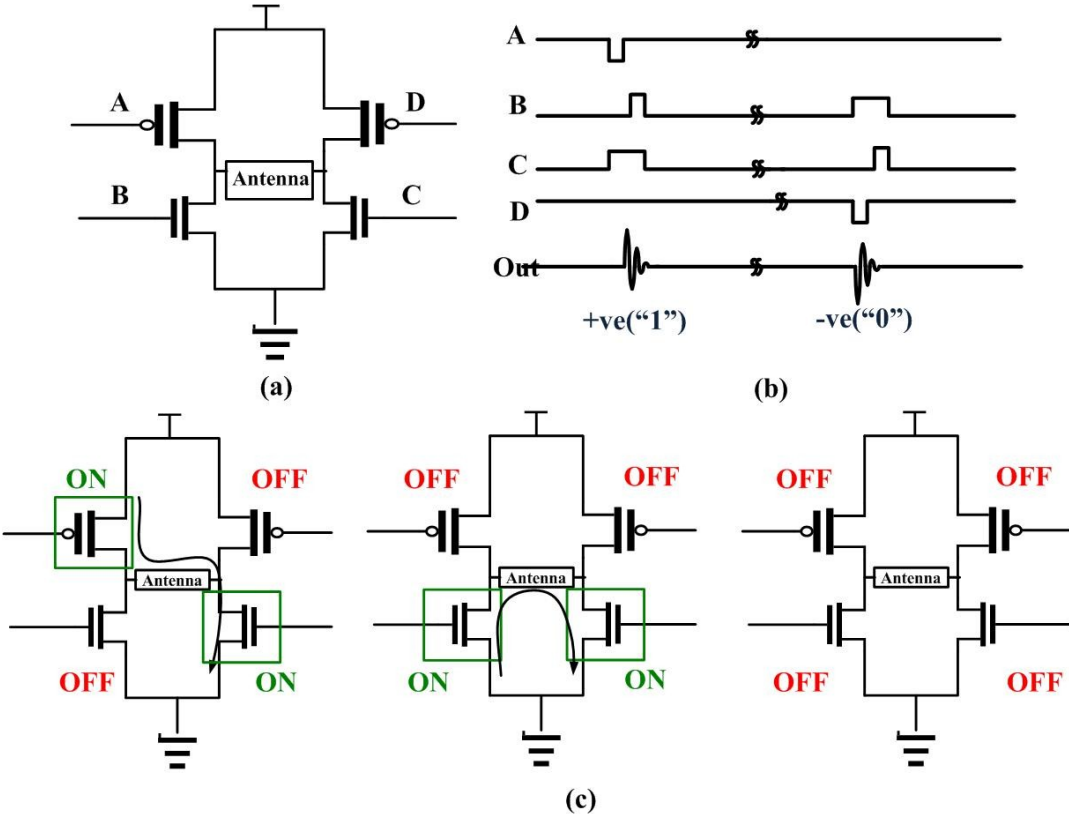
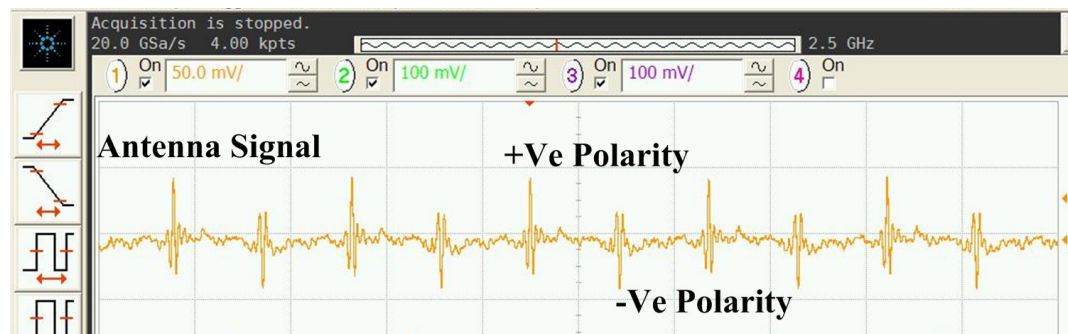


Figure 3.7. (a) Schematic of the antenna driver circuit, (b) timing diagram, (c) signal flow through antenna for a +Ve polarity ("1") signal.

the +Ve polarity signal. The radiation characteristics are dependent upon the strength of the current, the rising edge of the signal, as well as the pulse shaping characteristics of the antenna. The transistors are designed to be low in resistance when fully “on” to ensure large driving current. The large size of these transistors also requires tapered drivers. A 5-stage tapered drive is used to drive each of the transistors. This scheme allows BPSK as well as OOK transmission. The design operates at 1.2V supply and is digital in its driving characteristics. At 100kbps, the driver circuit was measured to have a total power consumption of only  $4.5\mu\text{W}$ , with a leakage power of  $1.5\mu\text{W}$ . The transmitter, though designed for low data rate communication, is also able to send pulses as fast as 200Mbps to enable bursty data communication.

### 3.4.1 Measured Bi-Podal (BPSK) Timing Pulses @ Transmitter

Fig.3.8 shows the measured bi-podal (BPSK) pulses at the receiver antenna using the H-bridge transmitter. The up-tick corresponds to a signal of +Ve polarity, while the down-tick corresponds to a signal of -Ve polarity. The bi-podal polarity in our scheme is used to convey the 1’s and 0’s. Alternatively, this signaling can be used for OOK, communication also, where the receiver doesn’t distinguish the polarity of the received signal, only the presence or absence of the signal in a bin dictates detection of 1’s and 0’s.



**Figure 3.8. (Measured) Bi-podal Signal generated by the transmitter @ a data rate of 50Mbps.**

### 3.5 Rx Gain Stage Design

The receiver design is implemented as a simple five-stage differential amplifier chain followed by a regenerative non-coherent peak polarity detector. Each duty-cycled amplifier stage is implemented as a common source amplifier with resistive feedback (Fig.3.9). Each stage provides 7 dB of gain. The gain stages are AC coupled to each other to guard against D.C. offsets and low-frequency noise. The gain stages are designed to have the same input and output biases, thereby ensuring the same voltage difference across the coupling capacitors, which aids in achieving a faster turn-on time. Care is also taken to suppress the supply transient by inserting a small resistor in the supply path as well as decoupling the biases and supply from ground. The amplifier stages were designed for an overall expected gain of 35dB, between 1-2GHz band. Fig.3.10 shows the measured gain of ~30dB for the design.

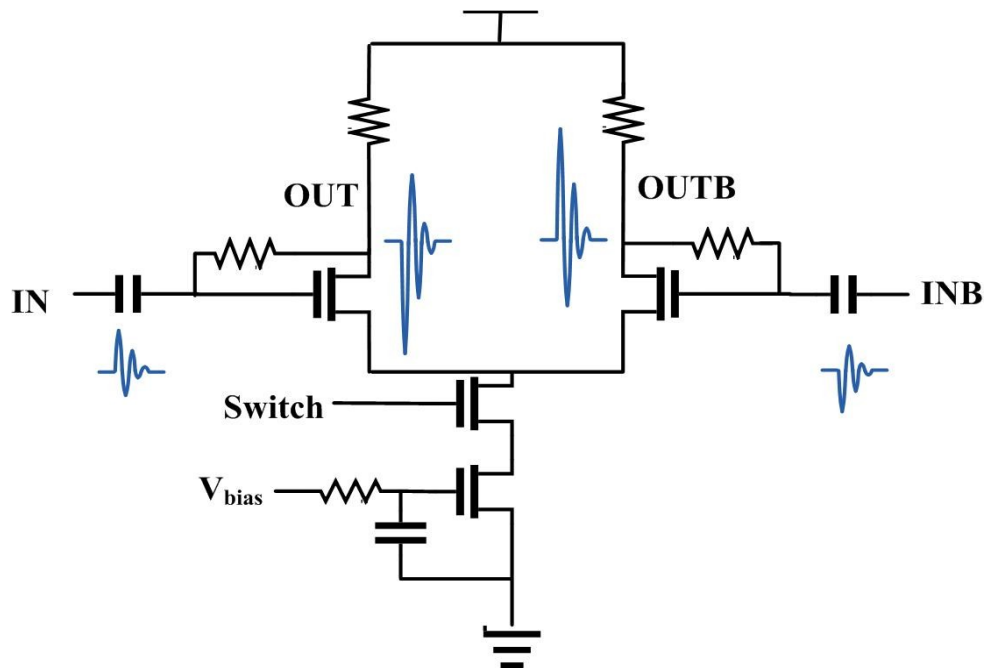


**Figure 3.9. Schematic Diagram of the gain stage of 5-stage differential amplifier chain, each providing ~7dB gain.**

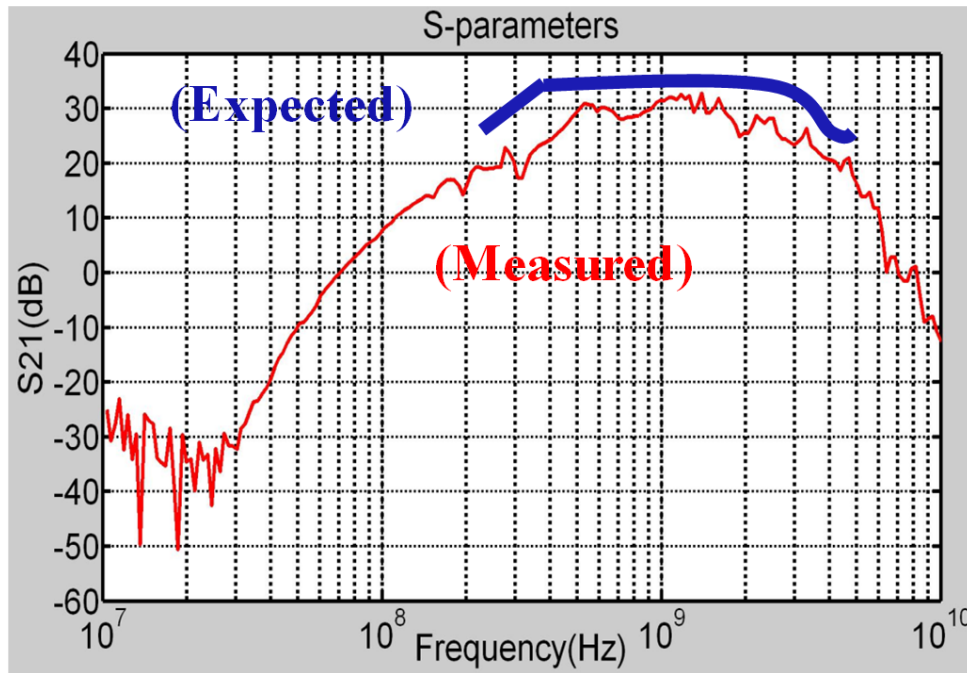


**Figure 3.10. Measured and Expected gain from the 5-stage gain amplifier.**

### 3.6 Non-Coherent Peak-Polarity Detector Design

After the gain stages, a peak polarity detector (Fig.3.11) is used to detect the reception of the pulse by the RF front end and effectively serves as an asynchronous self-timed one-bit ADC. The detection of pulses is done in a non-coherent manner in our scheme. Compared to coherent detection methodologies, where the time-alignment between the template signal and the receiver signal becomes very important, our scheme doesn't require perfect knowledge of the expected arrival of the pulses, and doesn't require any template signal generation either. Our scheme doesn't require any fast-sampling of the information either. The arrival and sampling of the signal is self-timed, thereby obviating the need of fast clocks in the design, resulting in power saving. The proposed circuit uses a regenerative latch and is biased such that  $MN_{6,7}$  are nominally in sub-threshold and that the positive feedback through inverter pairs  $MN_{3,4}$  and  $MP_{3,4}$  is suppressed by the presence of damping transistors  $MP_2$  and  $MP_5$ , thereby

providing a net negative feedback that holds both outputs close to VDD (Fig.3.11). However, in the presence of a pulsed signal, the total current through MN<sub>6,7</sub> rises exponentially, causing the positive feedback to increase and driving one of Vout+ or Vout- low, depending on the input polarity of the signal. In this case, the transistors MN<sub>6,7</sub> act as a self-mixing pair. After the pulse is detected, a delayed RST is triggered by the control circuit, driving the outputs near VDD and allowing this circuit to detect the next pulse. This circuit can also be duty-cycled using MN<sub>5</sub>. The nominal bias current of this circuit is 1  $\mu$ A when no signal is present and increases dynamically with the arrival of a signal, a highly desirable characteristic with sparse impulsive signals.

### 3.6.1 Detection of Pulses at low and high data rate (Measurement Results)

Fig.3.12 shows measured detection of signals of different polarities with this methodology, using an Omni-directional monopole antenna at a fast data rate of 50Mbps. While Fig.3.13, shows the detection of pulses at low data rate. Pulse detection could happen as fast as 200Mbps. This means that one can utilize the

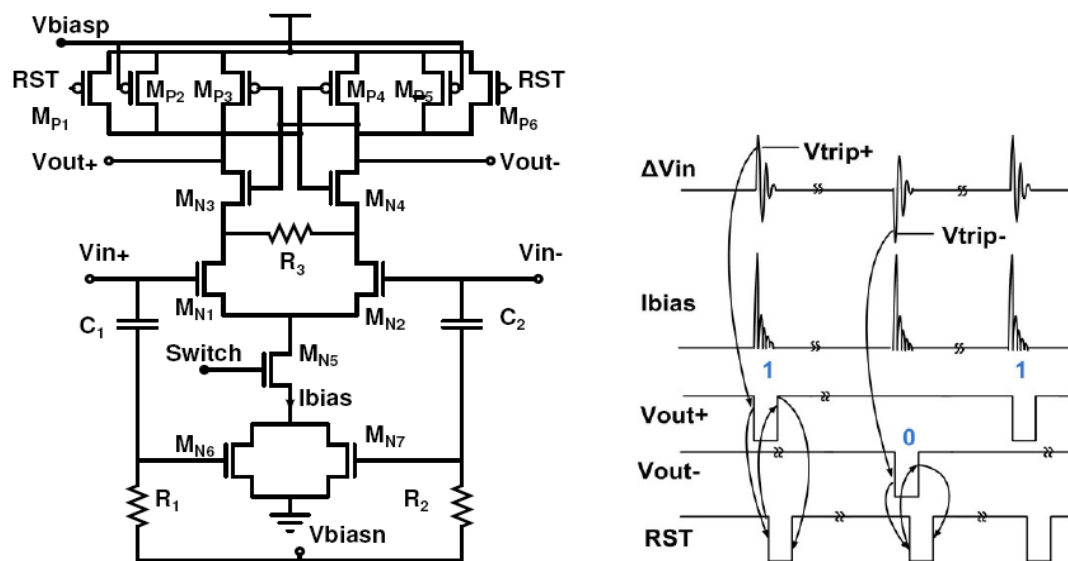
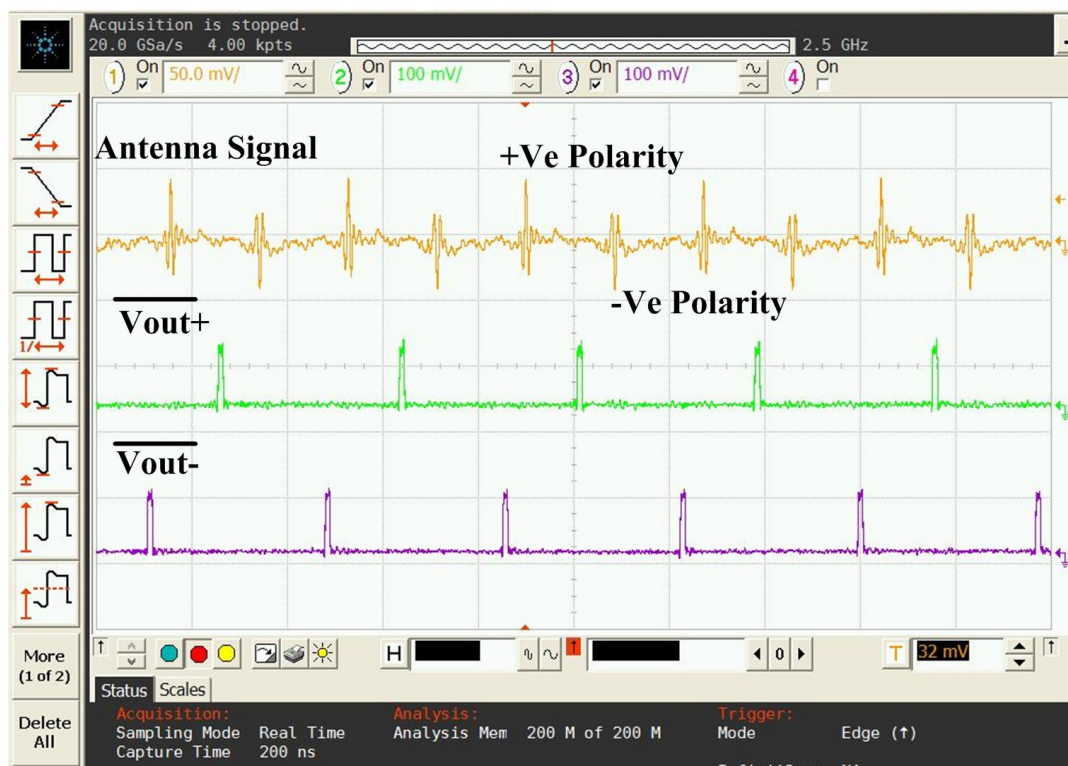


Figure 3.11. Schematic of the non-coherent pulse polarity detector and the corresponding timing.

receiver to support the bursty as well as low data rate communication. We also measured the required turn-on time for reliable detection (shown in Fig.3.14). Within a 10ns RF-On time window, the pulse was detected correctly at Vout+ with better than  $10^{-5}$  BER when the relative time of arrival of the pulse with respect to the RF-ON timing was controlled to as short as  $\sim 3$ ns (Fig.3.14). This means a timing margin of  $\sim 5$ ns is available for the synchronization uncertainty for the backend synchronizer during duty-cycling mode.

We also measured eye-diagrams of the pulse-detected signals relative to a periodic transmitter signal. Uncertainty of only 100ps (Fig.3.15) was measured. This low jitter



**Figure 3.12. (Measured) Waveform showing, transmission of positive as well as negative polarity signal and the corresponding detection on the Rx at a faster 50Mbps data rate.  $V_{out+}$  and  $V_{out-}$  go high corresponding to the polarity of the detected signal.**

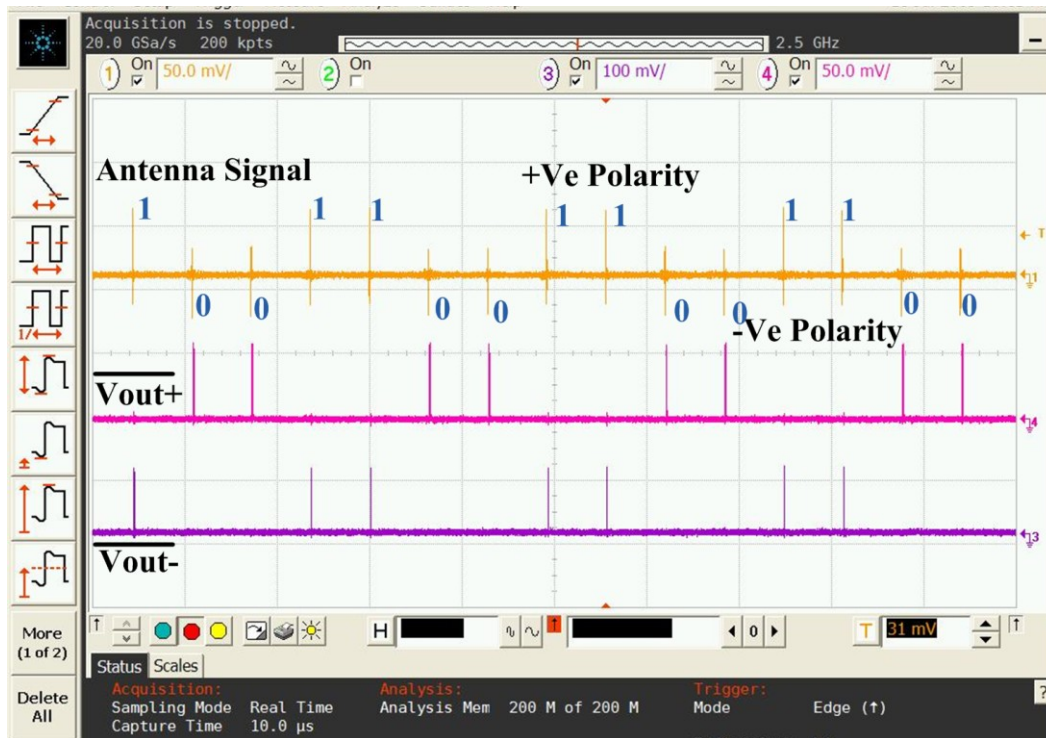


**Figure 3.13. (Measured) Waveform with the bi-podal signaling at low data rate with 1100 sequence and the corresponding detection of pulses in time.**

in the transceiver means that the uncertainty in synchronization will primarily be dependent upon the local time-keeper (i.e. the PLL) of the clocking circuit. The receiver was measured to consume 10.5mW in a 90nm process when fully “on”. However, this power is reduced by duty cycling when the Rx and Tx are synchronized. Accounting for synchronization accuracy (~5ns) the Rx needs to be “on” only for 10ns to detect a pulse ~1-2ns wide. At 100kbps this results in a measured power of 14.3 $\mu$ W, where measured leakage power for the receiver is 3.3 $\mu$ W.

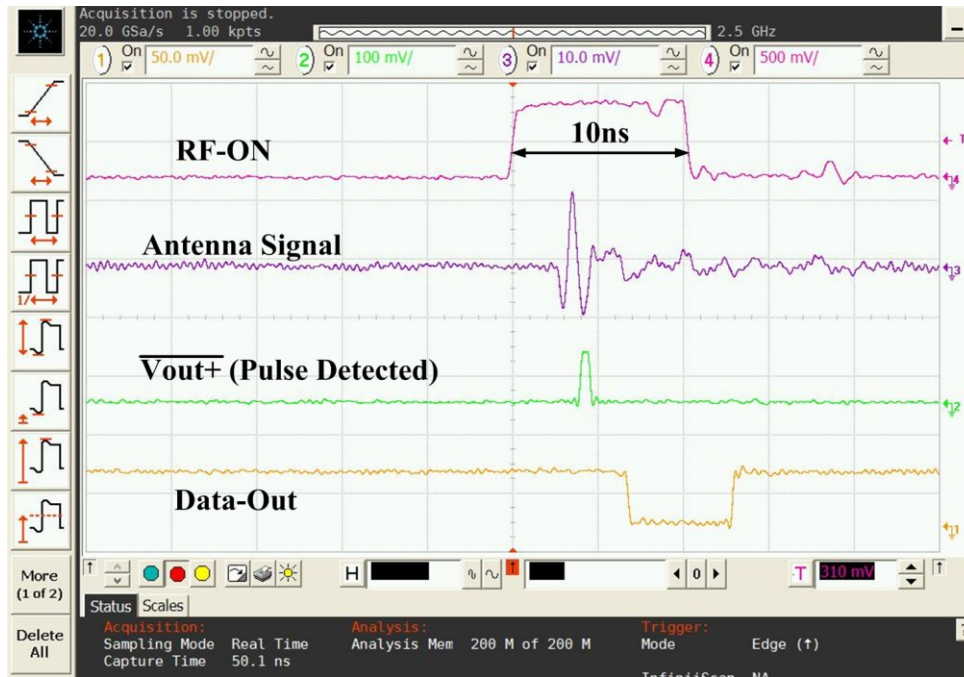


**Figure 3.14. (Measured) Pulse detection within a 10ns window of RF-ON, (Relative delays on the scope signals were controlled to correspond to the signal timing at the chip for this measurement).**

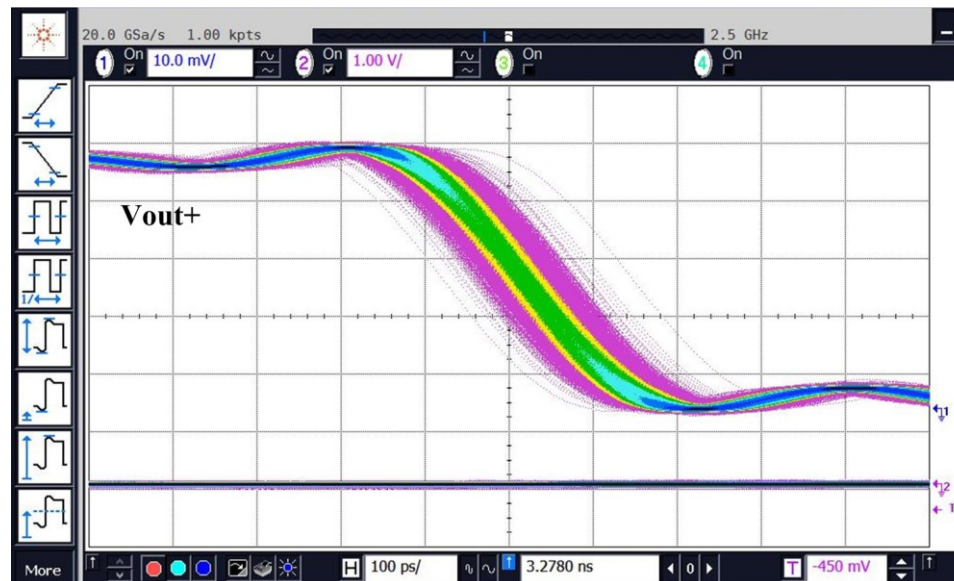


**Figure 3.15. (Measured) Eye-diagram of the falling edge (active edge), indicating received pulse arrival jitter as compared to the Tx-transmit request. Uncertainty is only ~100ps.**

### 3.7 Differentiating Timing and Data Pulses (A Pseudo-Coherent Self-Correlated Signature Detection and Generation mechanism)

Another challenge in UWB systems is classifying pulses as data or timing pulses. We propose a pseudo coherent self-correlated signature generation and detection method that may be enabled as part of this transceiver for further classification of a pulse into one of these types. In this scheme a pulse of type-1 (Normal Pulse) is encoded as a single pulse (Fig.3.16), while a pulse of type-2 (Signature Pulse) is encoded as a double pulse. For example, a type-1 pulse may be used for transmitting data while a type-2 pulse is used to generate timing and to synchronize the network across sync-beacons. At the transmitter, a double pulse can be generated from two trigger pulses to the transmitter separated in time ( $T_d = \sim 4\text{ns}$ ). At the receiver the timing pulse is decoded in a self-correlated manner. The onset of the first pulse creates

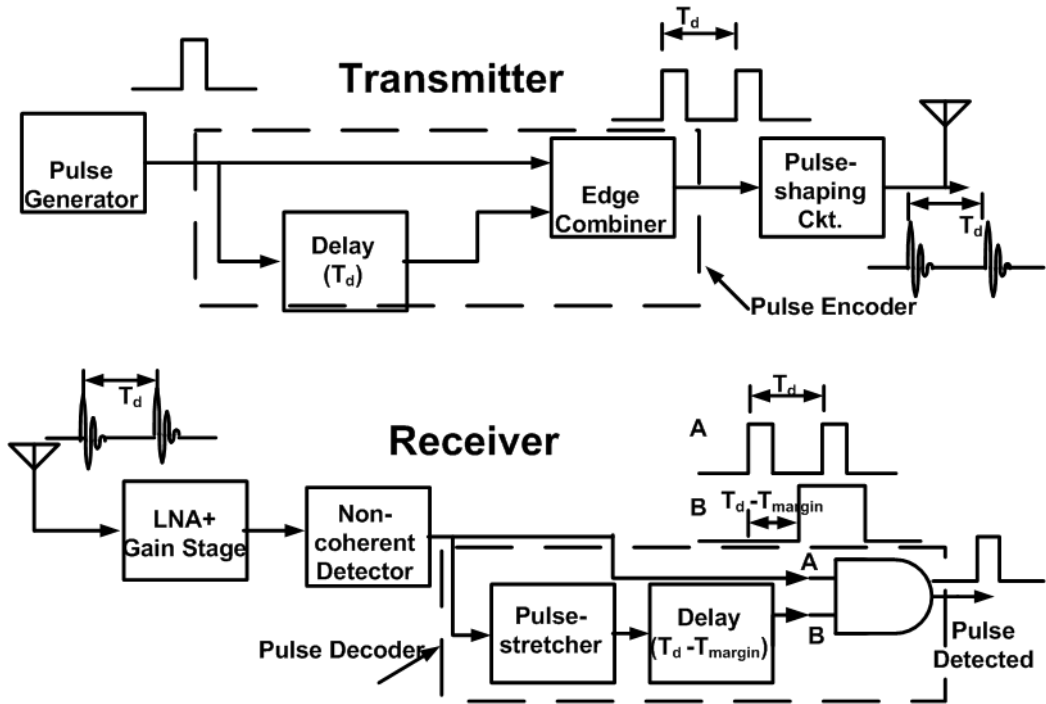
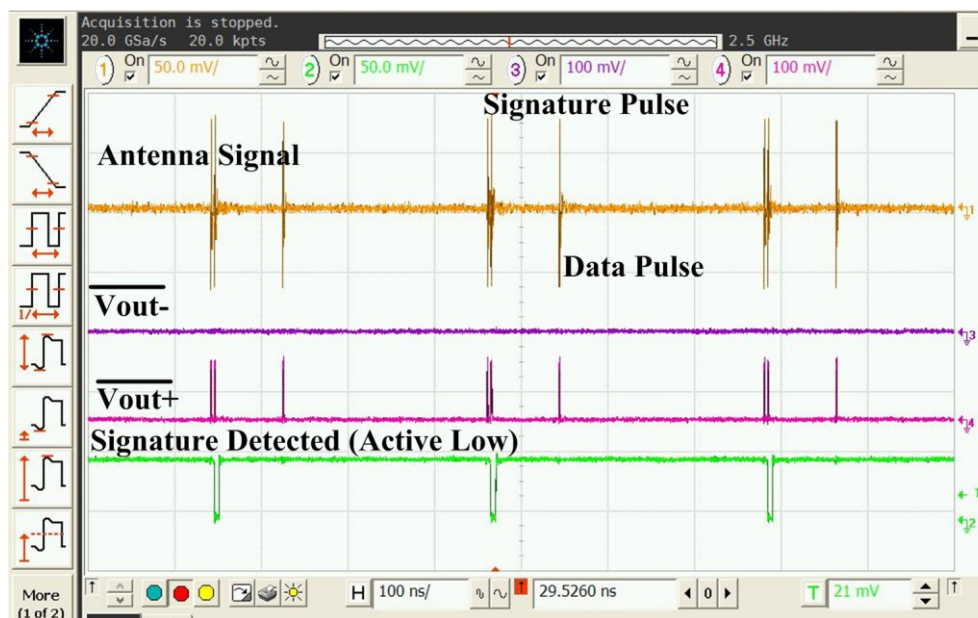


Figure 3.16. Schematic of Pseudo-Coherent self-correlated signature generation and detection mechanism.

a time window in which the circuit waits for the second pulse. If a second pulse is detected in this window, it is considered to be a type-2 pulse as shown in Fig.3.16. Margin is also given for process variations in the detection window of the 2nd pulse.

### 3.7.1 Measurement of the Pseudo-Coherent Self-Correlated Signature Detection

In Fig.3.17, we show measured pulse detection using this method on the same transceiver chip. The transmit power for the pseudo-coherent self-correlated scheme was measured to be  $7.5\mu\text{W}$ , while the Rx-power using a 16ns window is  $22\mu\text{W}$  @100kbps. The overall measured power for this scheme was  $29.5\mu\text{W}$ , indicating a power penalty of 50% when compared to single pulse based communication. This power penalty is a dependent function on the desired time-separation of the timing pulses. So, if larger than 5ns time-separation is required for the two pulses, then higher power will be consumed, for opening the Rx-window that much longer.



**Figure 3.17. (Measured) waveform showing detection of the signature pulse as well as the normal pulse.  $\overline{\text{Vout-}}$  and  $\overline{\text{Vout+}}$  go high corresponding to the polarity of the detected signal, while the signature detected signal (active low) is asserted only at detection of the signature pulses.**

### 3.8 BER Measurements

We used Omni-directional monopole antennas to also measure the BER while varying the distance between Tx and Rx. We measured a BER of better than  $10^{-5}$  up to a distance of 2.5m (Fig.3.18). An analysis of the BER sensitivity with the sub-threshold biasing voltage of the Peak polarity detector was also conducted. Fig.3.19 shows that error free operation is maintained over a large range of operating points for both normal as well as pseudo-coherent detection methodology. At lower bias voltage, the signal strength needs to be stronger, while at higher sub-threshold biases stronger positive feedback causes event detection even in the absence of a signal.

### 3.9 Performance summary

The design was fabricated in a 90nm CMOS process and occupies  $2.3\text{mm}^2$  of the silicon area. Table 3.1, summarizes the performance of our design and compares it to

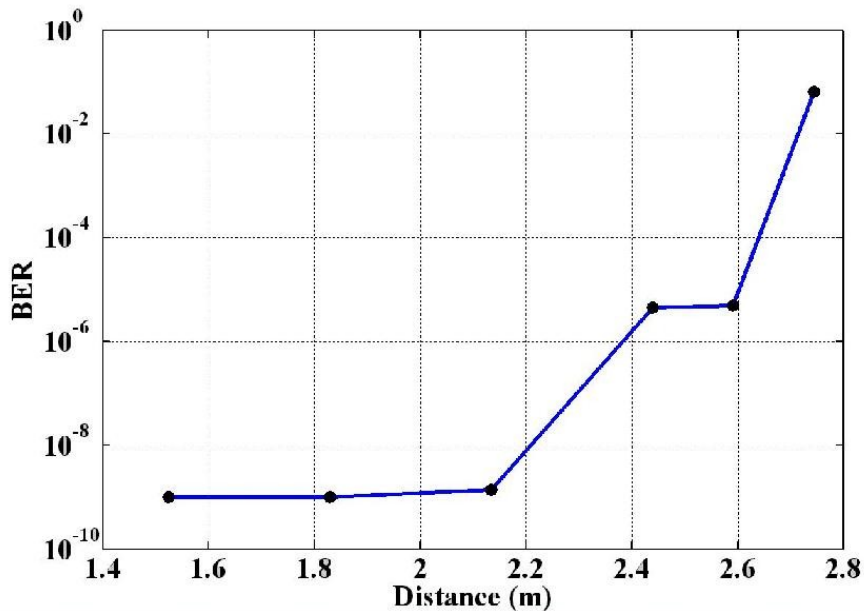


**Figure 3.18. ( Measured ) Variation of BER with separation between Rx and Tx antennas for single pulsing based communication.**

the current best state-of-the-art [54, 55]. Our transceiver consumes only  $19\mu\text{W}$ , compared to the previous best published  $350\mu\text{W}$  of power consumption. Both, the transmitters and receivers consume one order of magnitude lower power in our design.

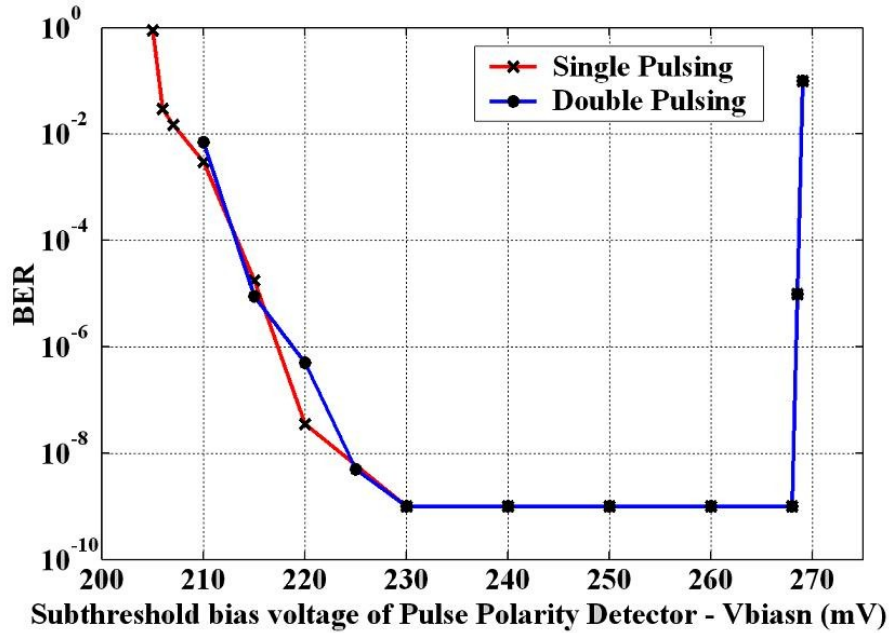


Figure 3.19. (Measured) Variation of BER with sub-threshold bias voltage of the peak detector for single and double pulsing based communication @ an average Rx received power of  $-75\text{dBm}$ .

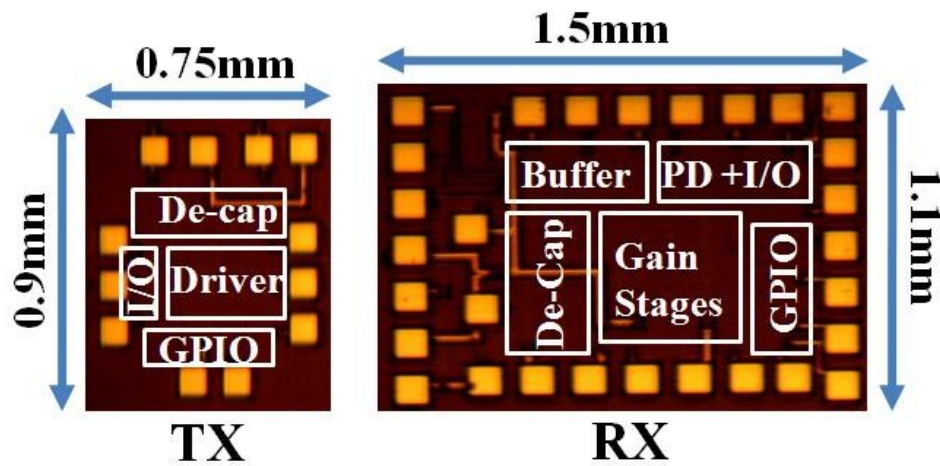


Figure 3.20. Die Photo of Tx/Rx Test-Chip in 90-nm CMOS process.

At  $19\mu\text{W}$ , this transceiver can be run continuously off a single AA battery for over five years, thereby making self powered, energy harvesting radios possible. The measured communication range of up to 2.5m at 100kbps makes it suitable for a variety of body area network applications as well as patient health tracking, automated drug-delivery, artificial cochlea, etc [56]. The reported total power consumption of

**Table 3.1 (Measured) Performance summary and comparison to the best UWB-IR state-of-the-art**

<b>Performance Parameters</b>	<b>Our Design</b>	<b>ISSCC'07 [53,54]</b>
<b>Technology</b>	<b>90nm CMOS</b>	<b>90nm CMOS</b>
<b>Rx- Leakage Power</b>	3.3 $\mu\text{W}$	3.5 $\mu\text{W}$
<b>Rx- Static Power</b>	10.5mW	35.8mW
<b>Rx- duty-cycled power @100kbps</b>	<b>14.3<math>\mu\text{W}</math>@1.1V</b>	250 $\mu\text{w}$ @ 0.65V
<b>Turn-on time</b>	~3ns	~2ns
<b>RX-sensitivity @<math>10^{-5}</math> BER @100kbps</b>	-81dBm	-98dBm
<b>Tx-Leakage power</b>	<b>1.5<math>\mu\text{W}</math></b>	96 $\mu\text{W}$
<b>Tx-dynamic power @100kbps</b>	<b>3<math>\mu\text{W}</math></b>	3.7 $\mu\text{W}$
<b>Tx-total Power @100kbps</b>	<b>4.5<math>\mu\text{W}</math>@1.2V</b>	99.7 $\mu\text{W}$ @1V
<b>Frequency spectrum</b>	1-2GHz	3-5GHz
<b>Total Tx-Rx power @100kbps</b>	<b>19<math>\mu\text{W}</math></b>	350 $\mu\text{W}$
<b>Distance</b>	2.5m	-
<b>Die Area (Tx+Rx)</b>	2.3mm <sup>2</sup> (Fig.3.20)	2.28mm <sup>2</sup>
<b>Total power for Psuedo-Coherent method</b>	29.5 $\mu\text{W}$	N/A
<b>Modulation</b>	OOK, BPSK	PPM

$\sim 19\mu\text{W}$  compares very favorably with the state-of-the-art lowest power continuous wave radio at  $\sim 900\mu\text{W}$  [56] as well as the state-of-the-art impulse radio at  $\sim 350\mu\text{W}$  [54, 55].

### 3.10 Problems and Required Improvements

Though, the designed impulse based radio consumes very low power, during the test process, we identified some problems associated with the detection methodology, spectrum utilization and interference as discussed below.

#### 3.10.1 Bi-Podal Signal Generation and Detection Methodology

Some problems associated with the generation and detection of the bi-podal signaling were identified while testing. The signal strength required for signal of one polarity was found to be higher than the strength required for the signal of the other polarity, due to offset and mismatch in transistors used in non-coherent detector, resulting in a signal of given polarity getting mis-detected as a pulse of different polarity at low signal levels. Similarly, on the generation side the signal strength for signal of one polarity was measured to be higher than the other polarity as can be seen in Fig.3.21. In the wake of this asymmetry the performance was limited by the lower limit of the signal strength. Also, since a “1” transmitted by one node can be treated as a “0” (due to uncertain phase accumulation) by another node depending upon the

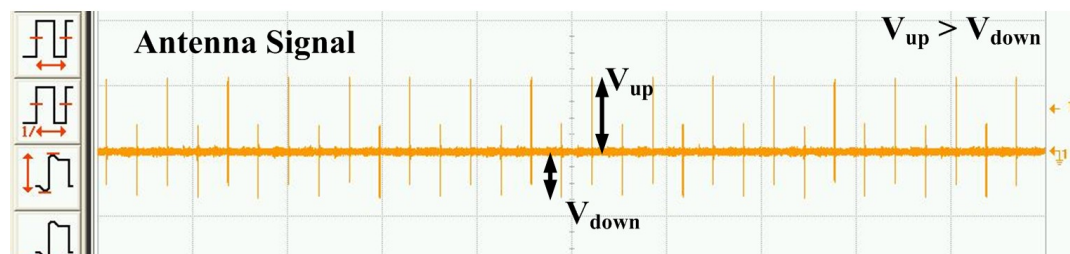


**Figure 3.21. ( Measured ) Assymetry in bipodal signal generation, the uptick is stronger than the down-tick.**

distance and the spatial orientation, it requires special coding and decoding for data structure to recover a transmitted “1” and “0” as such. In our next design discussed in chapter 4, we propose to use the OOK signaling as compared to the Bi-podal signaling in this design.

**3.10.2 Interference susceptibility**

Though the receiver was able to detect low strength signal, occasionally we saw high susceptibility to the environmental interference, particularly the strong interferer in the GSM-ISM band (Fig.3.22, 3.23). Periodic burst of strong TDMA packet signal

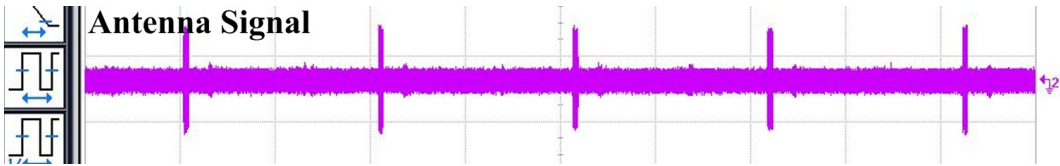


**Figure 3.22. ( Measured ) Periodic GSM signal, as received by the antenna.**

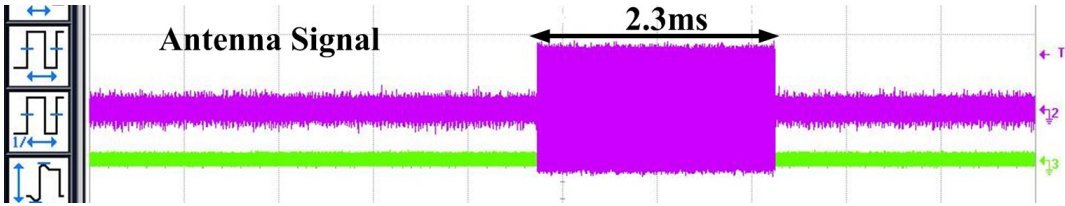


**Figure 3.23. ( Measured ) zoomed out version of the burst of periodic GSM signal, as received by the antenna.**

were received by the receiver, even when there was no transmission, requiring us to lower the sensitivity of the receiver and transmit a stronger impulse signal, thus contributing to lower performance.

**3.10.3 Unlicensed Spectrum Utilization**

In an impulse based low data rate transmission, average transmitted power is extremely low. This low average transmission power enables operation in unlicensed

spectrum. However, to operate at higher data-rate or range, operation in FCC mandated spectrum is required. FCC mandates UWB spectral range of 3.1-10.6GHz, which can be used for sending and receiving information, and so this gives us the opportunity to modify the design to make use of FCC mandated spectrum.

### 3.10.4 Double Pulsing Scheme and the Required Power

To distinguish between timing and data pulse, we utilized the double pulsing scheme. It was however noticed while taking measurements that in the presence of multi-path effect the data-pulse can impersonate itself as a timing pulse (double-pulse)

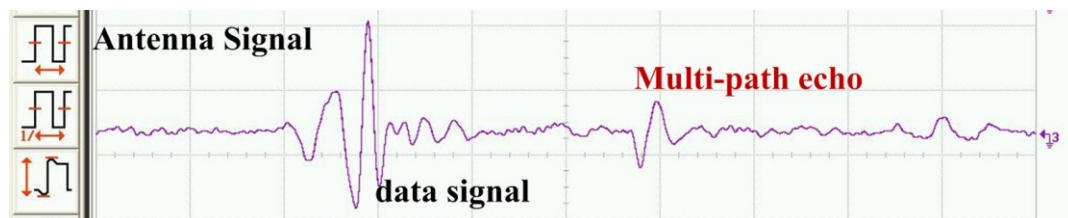


**Figure 3.24. (Measured) Data Signal, and the corresponding echo from a different reflected path (multi-path).**

at the receiver (Fig.3.24). To guard against this misdetection, one needs to separate the two pulses by a large amount depending upon the range of communication and the receiver sensitivity. Nevertheless, the larger separation for the signature pulses for timing means the receiver would be required to be “ON” for a longer duration, thereby consuming higher power at the receiver. Since the two pulses are required to be individually detected at the receiver to ascertain the signature, it doesn’t result into any processing gain at the receiver, while burning twice the power at the transmitter. To take into account this effect, in the next design discussed in chapter 4 we use time-multiplexed frequency bands for data and timing pulses, which saves power both at the receiver and transmitter.

### 3.11 Summary

In this chapter we presented different ways that a globally synchronized network can be used for exchange of information between sensor nodes, and the corresponding requirements for low data rate, as well as bursty fast pulse generation and detection. We also discussed the need for differentiating the timing and data pulses. Based on these requirements a preliminary design of impulse based duty-cycled, non-coherent transceiver in a 90nm CMOS process was presented. The measured results show only 19 $\mu$ W power consumption at a data-rate of 100kbps. The design was measured to give a BER of  $10^{-5}$  and works for a range of 2.5m at an average Rx-sensitivity of -81dBm, making it useful for low-power short-range wireless sensor networks. The transceiver was designed to enable bi-podal (BPSK) as well as OOK schemes and pseudo-coherent self-correlated signature detection and generation mechanism was also implemented to differentiate between data and timing pulses. While, order of magnitude better performance was achieved when compared to state-of-the-art designs, operating in unlicensed spectrum limited the performance of this design. Other problems such as larger time-window for the receiver to detect timing pulses in the presence of multi-path reflections, interference susceptibility and the asymmetry in bi-podal signaling require additional modifications in the design. In the next chapter we discuss the design of an FCC compliant OOK-modulation based UWB Impulse transceiver design that operates in unlicensed band. We also make use of time-multiplexed frequency bands to separate the timing and data pulses, thereby saving additional power associated with larger window sizing in the current design.

## **CHAPTER 4**

### **AN FCC COMPLIANT DUAL-BAND UWB IMPULSE RADIO DESIGN**

#### **4.1 Introduction**

Spectral allocation is one of the main concerns for any radio architecture. As shown in the previous chapter, a radio working on a given spectrum has to cope with unwanted but co-existing interferers. The radio design has to take into account the possibility of these interferers that can severely limit the communication performance. To enable efficient and effective utilization of sparse-spectrum government agencies across the world regulate the use of spectrum domestically and internationally. In the US, the Federal Communications Commission (FCC) designates different bands of spectrum for different applications while limiting radiation characteristics of radios operating in a specific band. While various commercial wireless communication systems such as GSM, CDMA etc. work on a licensed spectrum, FCC also provides various unlicensed spectral-bands, where one can design a radio by simply complying with the radiation emission mask. Since cost of operation is an important factor for wireless sensor network deployment, operating radios in the unlicensed band is also desired. In this chapter, we specifically look at FCC's UWB spectral mask, and provide design and measurement results of a multi-band radio that operates while complying with the spectral mask constraints placed by the FCC.

#### **4.2 UWB communication: A Primer**

Pulse based communication schemes require large bandwidth due to the duality between frequency and time. While for a continuous wave signal, the associated signal bandwidth for the signal is typically very low, and so a traditional continuous wave

signal is also called a narrowband signal communication. In pulse based communication, the signal occupies large bandwidth and so the communication scheme is called Ultra-Wide-Band (UWB) (Fig.4.1). According to FCC a signaling scheme has to occupy at least a 10-dB bandwidth of 500MHz or 20% of its central frequency, whichever is less, to be qualified as a UWB signal [57]. While for lower frequency bands of <2GHz, a signal can have less than 500MHz bandwidth, for higher frequency bands a signal needs to occupy at least 500MHz of bandwidth for it to be considered as UWB signal. These additional requirements thereby also help distinguish between spread-spectrum signaling and UWB signaling.

UWB has several advantages over narrowband radios. Due to impulsive nature of the pulses used in UWB communication, multi-path fading is almost negligible. These narrow pulses make precise localization possible in various applications. With higher bandwidth, UWB communication also offers the potential for high data rates and thereby is an important topic of research.

**4.3 FCC Spectral Mask for UWB communication**

FCC in February 2002 came up with the regulation guiding the emission spectral mask associated with the UWB mode of communication [57]. FCC allowed the unlicensed use of the spectrum in the 3.1GHz-10.6GHz range with constraints of

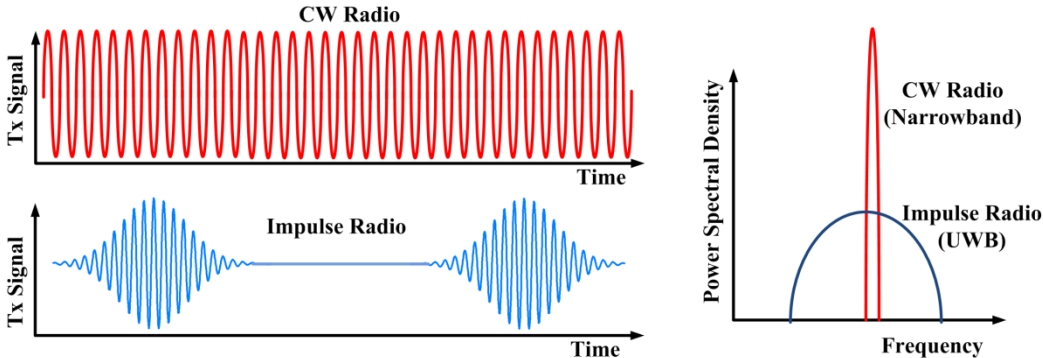


**Figure 4.1. Continuous Wave Vs Impulse based UWB Radio and signaling**

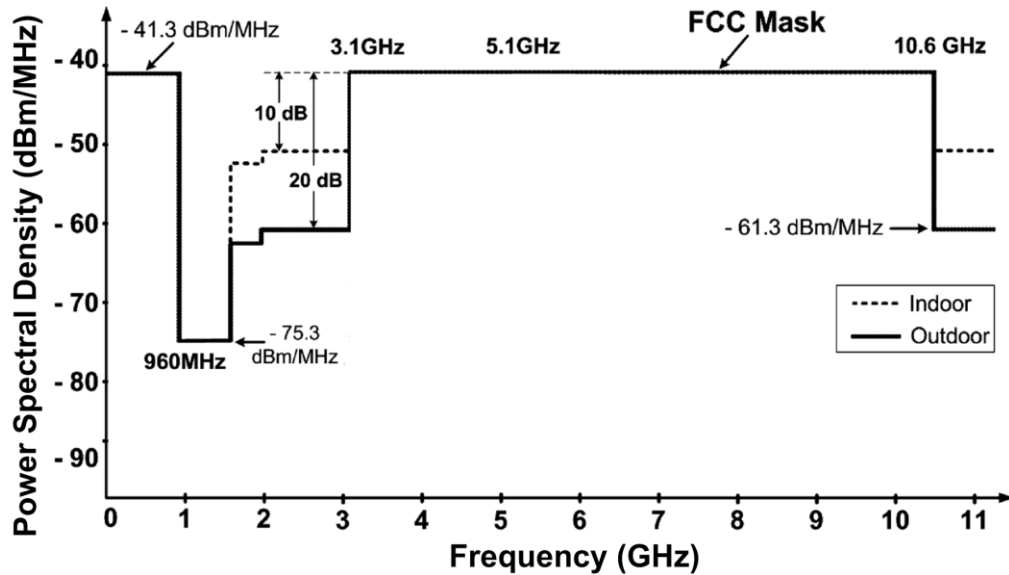


**Figure 4.2. FCC mask for UWB communication [55]**

maximum power level of  $-41.3\text{dBm/MHz}$  [55]. Department of Defense (DOD) was one of the earliest users of the UWB technology for military application and voiced concerns about the technology in commercial applications. FCC in its final guidelines took note of concerns regarding interference to the GPS devices as well as aircraft radar applications and cellular services. Initially FCC regulation for UWB catered to the emission limit of  $-41.3\text{dBm/MHz}$  for any frequency above 960MHz (Table 4.1). But due to interference concerns from UWB devices to other wireless services, a more conservative approach was followed. Higher sensitivities associated with GPS and PCS devices required a UWB device to radiate less energy in the corresponding bands of 1.2-1.6GHz and 1.9GHz respectively (Fig.4.2). FCC accommodated this by creating a deep notch at these frequency levels in the emission mask. They also put stricter requirements on the emission mask for outdoor/handheld devices as compared to devices for indoor applications.

The FCC mask has been divided into multiple regions. While a radiation limit of  $-41.3\text{dBm/MHz}$  is imposed for a device operating below 960MHz, between 960MHz-

**Table 4.1. FCC Spectral Emission Mask Limits for UWB Communication**

<b>Frequency Range</b>	<b>Indoor Emission Limit</b>	<b>Outdoor Emission Limit</b>
Below 960MHz	-41.3dBm/MHz	-41.3dBm/MHz
960MHz-1.61GHz	-75.3dBm/MHz	-75.3dBm/MHz
1.61GHz-1.99GHz	-53.3dBm/MHz	-63.3dBm/MHz
1.99GHz-3.1GHz	-51.3dBm/MHz	-61.3dBm/MHz
3.1GHz-10.6GHz	-41.3dBm/MHz	-41.3dBm/MHz
Above 10.6GHz	-51.3dBm/MHz	-61.3dBm/MHz

1.61GHz band the Outdoor limit of radiation is much tighter at -75.3dBm/MHz. This tight limit has been imposed to ensure that high sensitivity GPS devices operating between 1.2GHz-1.61GHz don't get impacted by UWB signals. Similarly, tighter limits are imposed up to 3.1GHz, while between 3.1-10.6GHz ranges -41.3dBm/MHz emission radiation is allowed. Table 4.1 shows the constraints imposed for radiation in different frequency band of operation by FCC.

#### **4.4 Different Ways one can utilize the UWB Spectrum:**

With the wide range of frequency over which one can operate a UWB device, there are various ways one can utilize the UWB spectrum. Two primary approaches are based on one with carrier and one without carrier based modulation. Since, in the allowed FCC mask there is a restriction on emission between 960MHz-3.1GHz spectral range, UWB signaling typically sits between either DC-960MHz or between 3.1-10.6GHz ranges. In a carrier-less signaling scheme, one relies on generating a pulse-shape that occupies completely the DC-960MHz frequency band or the 3.1-10.6GHz band. Typically a 4<sup>th</sup> order or 7<sup>th</sup> order Gaussian pulse is utilized to occupy the wide spectrum of 7.5GHz [58-60]. The pulse generation circuitry for these types of

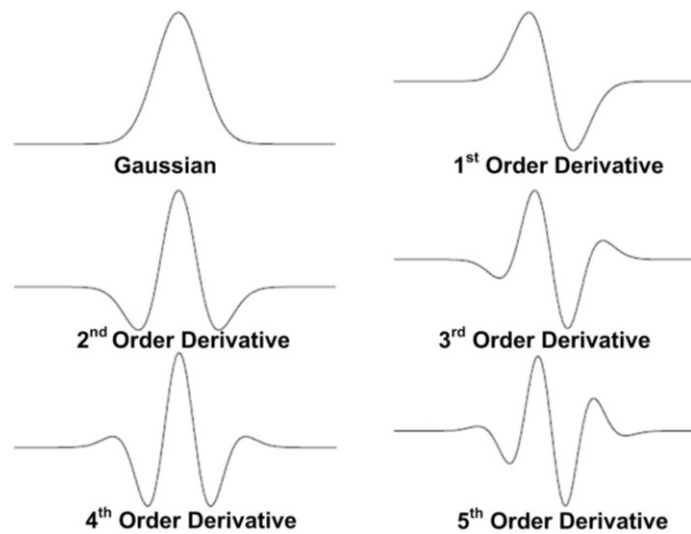


**Figure 4.3. Different types of Gaussian Wavelets utilized for impulse based communication. Higher order derivatives are also utilized.**

pulsing schemes typically generate a pulse that directly falls in the UWB band without requiring explicit frequency translation. In such schemes a baseband impulse is used to excite a filter that shapes the pulse in different shapes. Gaussian based pulse-shapes and their derivatives are utilized to occupy the whole spectrum. The key being the higher number of zero crossing with higher order derivatives (Fig.4.3). These zero-crossings effectively make the pulse look like a carrier modulated wavelet, but without any explicit carrier generation. There are various published designs in this space that generate the pulses utilizing filter response, occupying the whole UWB spectrum [61].

As can be seen in Fig.4.4, a Gaussian derivative of at least 4 is required for an impulse to occupy the UWB-band. Alternatively, in the 3.1-10.6GHz range one can operate a radio by dividing the spectrum in sub-bands of  $\sim 500$ MHz each. This approach requires signaling schemes that are based on generating a carrier signal. A carrier signal modulated with a pulse-wavelet which determines the center of the spectrum and the bandwidth (Fig.4.5, 4.6, 4.7). This scheme can facilitate various channels that can utilize different bands and can also enable multi-user

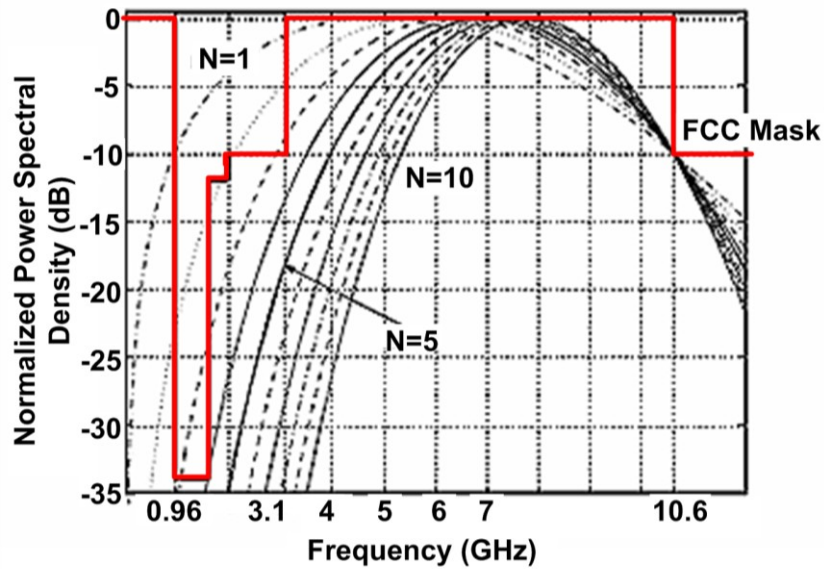


**Figure 4.4. The spectral radiation profile with different derivatives of the Gaussian pulses.**

communication. A pulse transmitter generate a pulse at baseband and up-convert it to a center frequency in the UWB band by mixing with a local oscillator.

#### **4.5 UWB Spectrum utilization for Low Data Rate Applications**

These are primarily the applications we are interested in this work. The applications for low data rate communication include wireless sensor networks and RFID tagging. Precise localization, faster startup time and relaxed constraints on frequency of operation associated with UWB signaling makes UWB impulse based communication an ideal choice for RFID tags. However, lower power emission of a UWB pulse constrained by FCC in the 3.1-10.6GHz band means these tags can't harvest as much power as they can by conventional narrowband operation in the 125KHz or 915MHz band. Thereby the low power application of wireless sensor networks is the most advantageous. The IEEE 802.15.4.a. standard committee has come up with a proposal that utilizes the 2.4GHz ISM sub-band, DC-960MHz UWB band as well as 3.1-10.6GHz UWB band. In this standard the 3.1-10.6GHz band is

sub-divided into a low band of frequency between 3-5GHz and another that sits between 6.3GHz-10.6GHz. This thereby avoids the known interferer between the 5.1-6GHz (Fig.4.8).

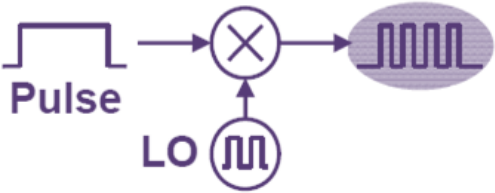


Figure 4.5. Carrier-based pulsing scheme for impulse generation in UWB Band

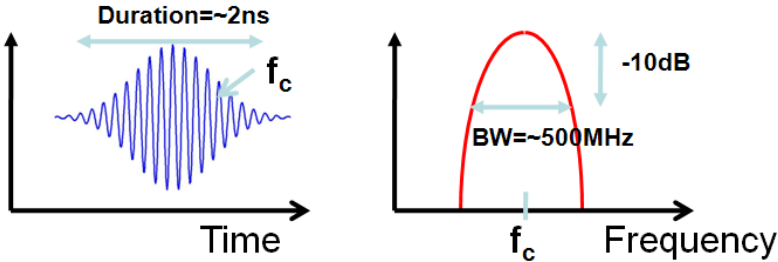


Figure 4.6. A carrier based impulse and indicative spectral profile.

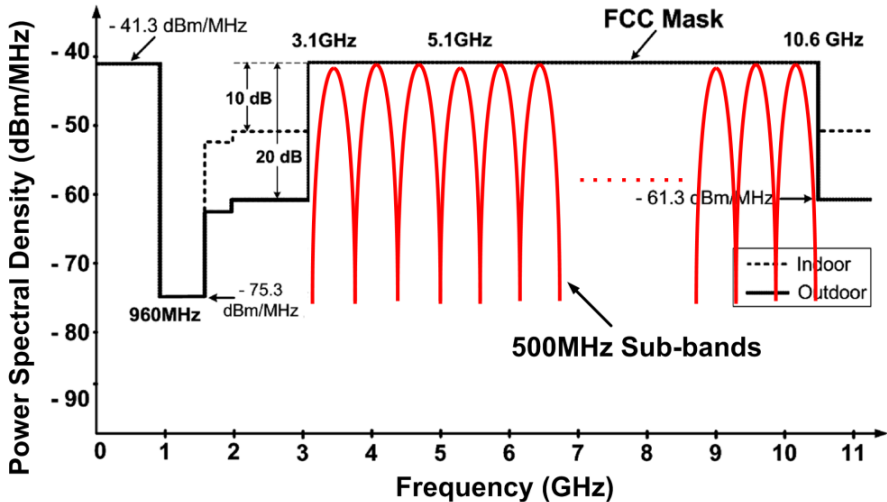


Figure 4.7. FCC mask and the corresponding utilization with the sub-bands of 500MHz each.

### 4.6 Towards Proposed Architecture

As seen from various implementations the wide-band of UWB spectrum can be utilized either fully or in a sub-banded structure. Utilizing the whole band will mean designing a receiver with huge bandwidth and will thereby have implications on the overall system power budget. The sub-banded structure in comparison offers more diversity and control over the frequency spectrum and has been the popular choice be it the DS-UWB, OFDM or 802.15.4.a standards. The sub-banded structure also provides one the means to selectively skip the part of the UWB spectrum where narrowband interferers such as WLAN/UNI can create problems for the communication channel. Thus in this work we propose to utilize the sub-banded structure to operate the radio in FCC mandated spectrum. As the path-loss increases with higher frequency, it makes sense to operate the radio in the lowest possible frequency band. With this we limit our usage of the FCC spectrum to the low-band between 3-5GHz.

One problem with the preliminary version of the radio was the differentiation

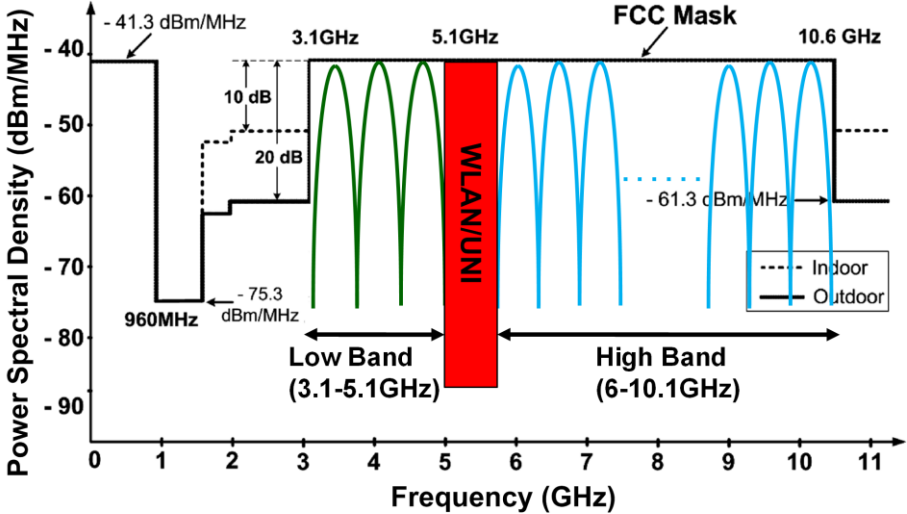
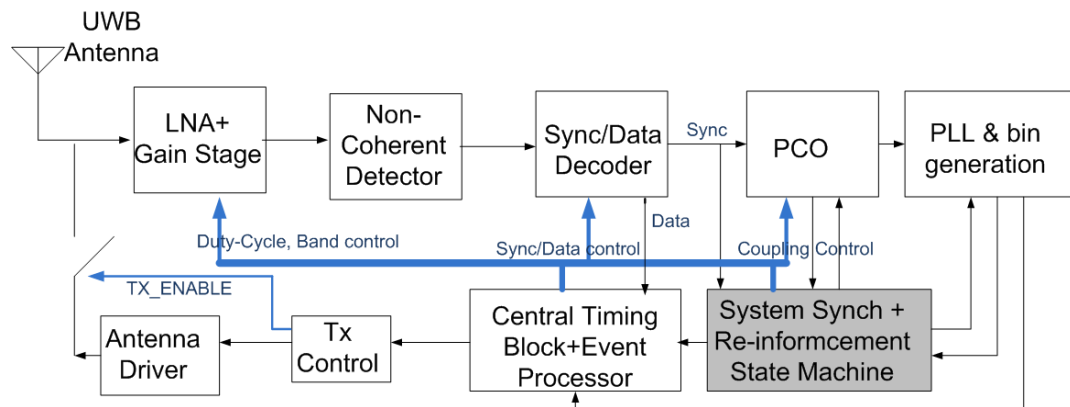


Figure 4.8. FCC mask and the corresponding utilization with the sub-bands of 500MHz each.

between the timing and the data pulses. Any time-based signature adaption on the timing pulse (i.e double pulsing scheme or time-referenced pulsing scheme) requires wide RF-ON window, thereby increasing the power budget for the whole system. It makes sense to utilize a scheme that can differentiate between the timing and the data pulse differently, without the extra burden of opening a wider RF-ON window to ascertain the pulses and their associated signature. We propose to utilize different sub-bands for the exchange of data and timing information between the sensor nodes. This requires us to have a transmitter and receiver which can send information on two different bands. Due to globally synchronized operation in our radio architecture, the timing and data are always guaranteed to be time-separated. A node if not synchronized will be interested in only timing pulses, while when synchronized it will send/receive the data and timing pulses at disjoint time-intervals. This means one can utilize the same transmitter and receiver with flexibility to change the band in time, i.e. time-multiplexed dual-band receiver and transmitter. Since, no signature needs to be coded (double pulsing) on the pulses in time, this means lower power both at the transmitter and receiver. One needs to design the transmitter and receivers such that there is sufficient isolation between the data-band and the timing-band, which will ensure that a data-pulse is not mistaken as a timing pulse and vice-versa. This is of importance for a multi-node communication synchronization scheme, where nodes can join and leave the network dynamically. This band-separation based differentiation between the timing and data pulses also takes care of the problem associated with the multi-path effect of earlier architecture, where a multi-path reflected signal can trick itself into a transmit-reference pulse, thereby making the data and timing pulses indistinguishable.

#### 4.7 Proposed Modified Radio Architecture & timing Scheme:

The Transceiver chain in the proposed system (Fig.4.9) consists of a UWB antenna, duty-cycle-able and/or band-tunable LNA and amplifying stages followed by some non-coherent detectors. This is followed by Sync/Data encoder block that qualifies the detected signal as either Sync or Data. The sync Pulse goes to the PCO that in conjunction with the PLL generates the bins. Every time the PCO fires, a sync pulse is generated, this way the sync pulse creates the timing boundaries for the (frame-boundary of rate  $T_{\text{frame}}$ ) for the network. The PLL divides the PCO rate ( $T_{\text{frame}}$ ) to  $N$  bins of length  $T_{\text{bin}}$  (Fig.4.10). In these bins the sync pulse is fired in the sync bin (aligned with the frame boundary), while data is sent or received in bins decided by the central control block. The system Sync State machine locally detects and maintains synchronization which enables data-communication between nodes. Once the nodes are synchronized as detected by the Sync-state machine, RF duty-cycling can start, thereby saving power for the system. Within a bin, the DLLs can further dynamically adapt the RF-ON window to do more aggressive duty-cycling, resulting in further power saving for the system. In this chapter we will focus on the transmitter and receiver design, while the timing circuit implementation/performance will be



**Figure 4.9. Modified System Architecture.**

**Legends:**

■ RF-OFF

■ RF-ON for DATA

■ RF-ON for SYNC

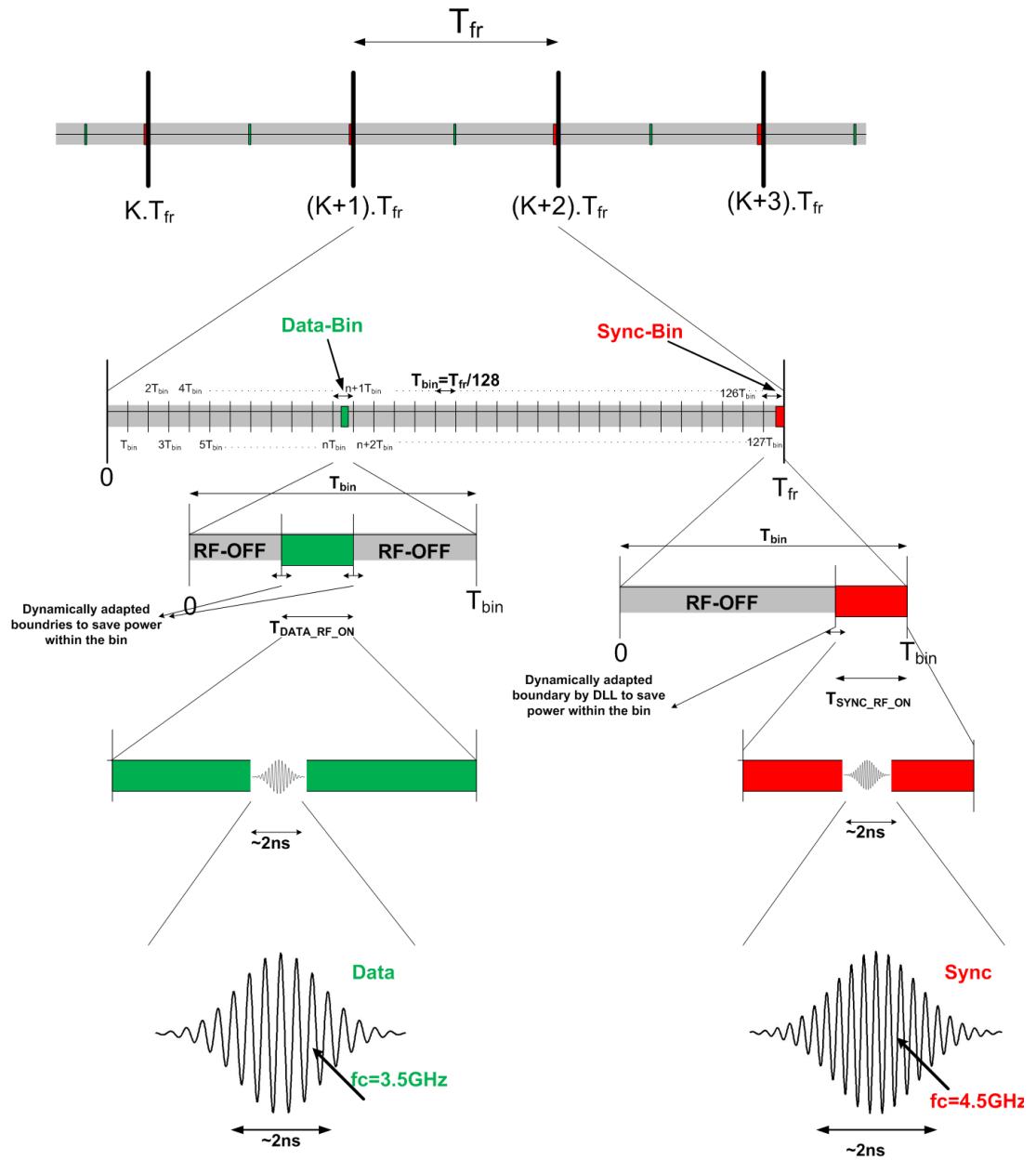


**Figure 4.10. Timing Scheme for the modified Architecture**

discussed in later chapter. Due to dual-band nature of the design, the transmitter and receiver both are designed with ability to tune the operating band. The band selected for data is centered at 3.5GHz, while the one for the timing pulses is at 4.5GHz. A 1GHz separation between the two bands was kept to ensure low cross-talk between the two channels.

### 4.8 Transmitter Design

As, noted earlier the transmitter in this architecture is required to generate carrier-based impulses to ensure signal transmission in FCC mandated spectrum. In its simplest form an impulse based transmitter design will involve an oscillator and a pulse-wavelet to modulate the information (Fig.4.11). The most popular modulation scheme for the transmitter designs are ON-OFF Keying (OOK), PPM (Pulse-Position Modulation) and BPSK (Binary-Phase-Shift-Keying). With the delay based BPSK scheme proposed by wentzolf et.al. [62], any impulse transmitter can support all these modulation schemes by simply controlling the timing of the pulse transmission (Fig.4.12). In our overall scheme we propose to use the OOK modulation, due to inherent simplicity of detection at the receiver. While designing the transmitter, there are a few things to consider. The low power design requirements require the architecture to be simple. As we need a transmitter that can transmit in the 3.5GHz and 4.5GHz bands, the design requirement would be to have a carrier based impulse



Figure 4.11. Simplest way of generating a wavelet based on carrier-wavelet modulation.

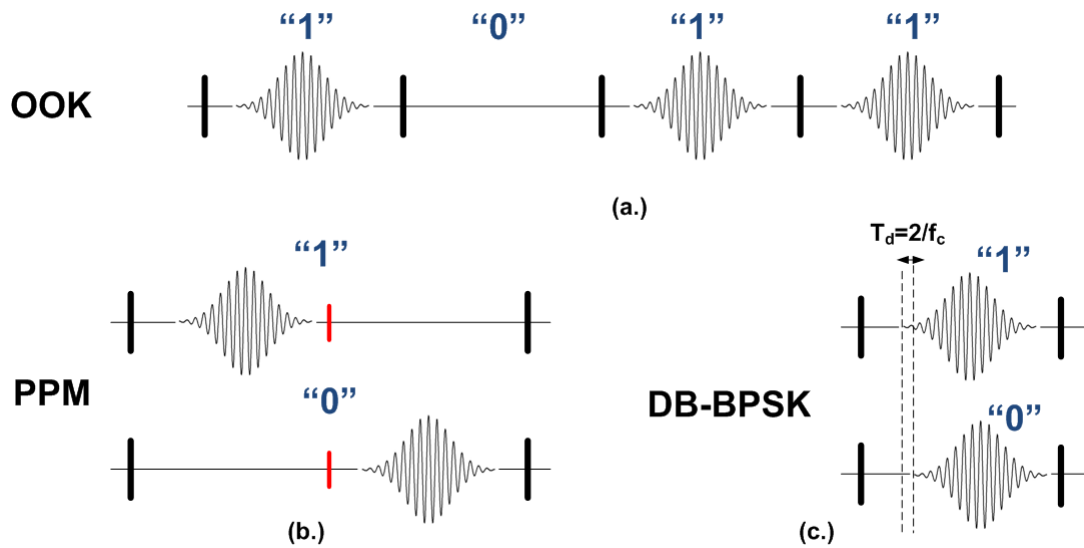


**Figure 4.12. Different Modulation schemes with impulse based UWB communication.**

transmitter. While the application space requires of very low-data-rates of  $\sim 100\text{Kbps}$  [63], maintaining energy efficiency (per bit) at these levels is important to keep the power budget as low as possible. At the same time, transmitter designs must meet the FCC spectral mask, which requires pulse-shaping to optimally utilize transmission in the mandated band. Due to on-board real-estate requirements, use of external filters to meet the FCC mask [62, 64, 65], is undesirable. Pulse-shaping can also be important for better inter-band isolation and side-lobe rejection as well as improved spectral efficiency. Thus, low power pulse-shaping techniques that avoid the use of external filters or baluns is an active area of research [66].

#### 4.8.1 Pulse-Shaping Requirements

For an impulse transmitter other than complying with FCC mask some other performance matrices are also important. They are namely: Spectral Efficiency, Out-of-band emission and side-lob rejection.

##### 4.8.1.1 Spectral efficiency

The spectral efficiency of a pulse is an important performance parameter. This

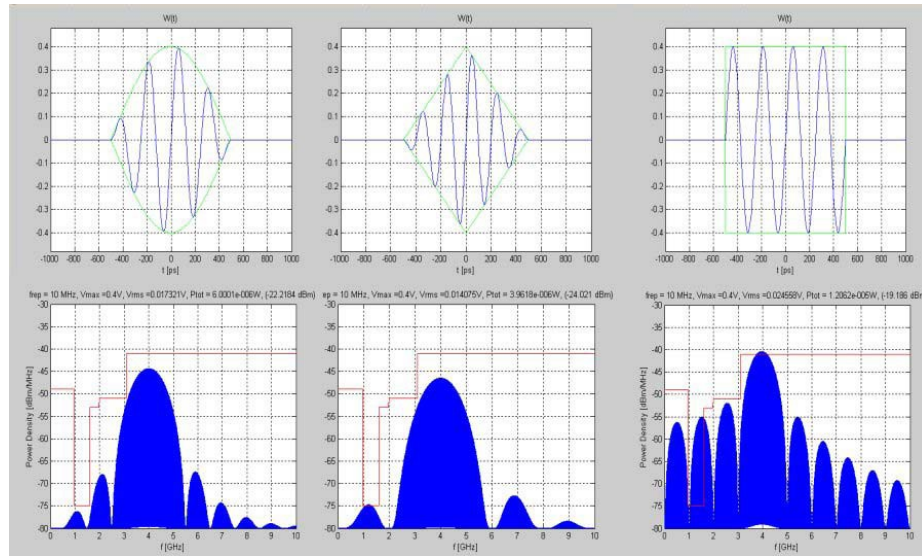


**Figure 4.13. Different pulse wavelets and the corresponding spectral profiles (figure taken from ref. [67]).**

indicates how well the available spectrum is utilized by the pulse. For a non-coherent energy based detection scheme this is an important parameter, as the link performance is dependent upon the total power received by the receiver. One needs to design a pulse-shape that fits the available spectrum as tightly as possible for a given average power limit and -10dB channel bandwidth. This is important for realizing higher range of communication, by optimally utilizing the FCC power limit. Different pulse shaping functions have different spectral profile (Fig.4.13), for example, while a sinc pulse-wavelet can give a 100% spectral efficiency due to rectangular spectral profile, a rectangular wavelet can provide a spectral efficiency of only 58% (Table 4.2).

#### 4.8.1.2 Out-of-Band Emission

Out-of-band emission is also an important performance metric for various pulse-shapes. For an ideal channel one would like to limit out-of-band emission to as close to null as possible to limit possible interference into adjacent channels. While a sinc pulse-wavelet has only 0% out-of-band emission, a square wavelet can have 16% out-of-band, while a Gaussian wavelet will have only 3% out-of-band emission, indicating

**Table 4.2 Wave-shapes and the corresponding spectral efficiencies**

Wavelet Type	Spectral Efficiency	Out-of-Band Power Emission	Side-Band Rejection
Sinc	100%	0%	None
Square	60%(-2.2dB)	12.8% (-8.9dB)	-13dB
Gaussian/Tanh	56.5%(-2.5dB)	3.3%(-14.9dB)	None
Triangular	57%(-2.5dB)	3%(-15dB)	-30dB

trade-offs associated with this metric.

#### 4.8.1.3 Side-Lob Rejection

Though out-of-band emission is an important performance metric, side-lobe rejection captures the essence of interference to adjacent channel a bit better, and hence is also an important performance parameter. While a Gaussian pulse doesn't have any side-lobe, the side-lobe associated with a square pulse-shape is 13dB. In comparison the side-lobe associated with a square pulse is  $\sim$ -13dB.

Based on these performance metrics one might be tempted to design a pulse-shape that looks like a sinc. But because of long time-duration associated with a sinc-pulse-shape, it's almost impossible to generate a pulse with a sinc wavelet, thus a Gaussian

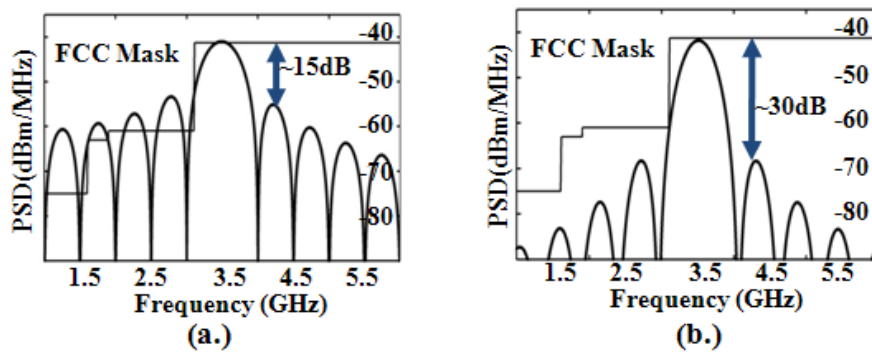


**Figure 4.14. MATLAB simulation of the output spectrum with (a) rectangular, and (b) triangular pulse shapes.**

pulse-wavelet looks to be a promising pulse-shape with no side-band rejection. But due to relative ease of generation a triangular pulse-shape is utilized. A triangular pulse-shape also has acceptable side-band rejection (Fig.4.14).

## 4.9 Transmitter System Architecture

Fig.4.15 shows the block diagram of the impulse transmitter, which consists of a timing block, a current-starved duty-cycled ring oscillator, a triangular-pulse shaping circuit, and an antenna driver stage. In idle mode between data transmission-request, all the blocks are off, thereby consuming only sub-threshold leakage power. The absence of large computation or memory storage in this simplified design enables very low leakage power.

### 4.9.1 Timing Circuit

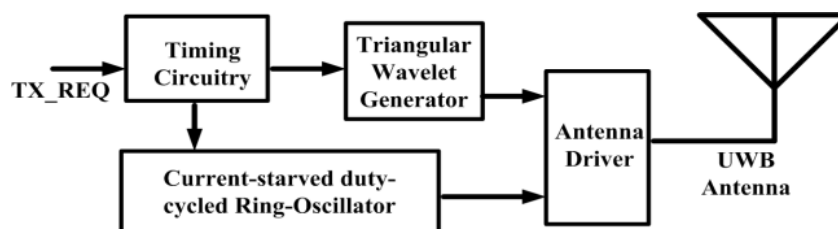


**Figure 4.15. Impulse radio transmitter architecture.**

The timing circuit at the advent of TX\_REQ pulse, generates appropriate timing pulses for various blocks, providing an enable signal OSC\_EN to the oscillator, and a rectangular pulse to the pulse-shaping circuit. Since this circuit is designed with logic gates and delay blocks, it consumes negligible dynamic and static power.

### 4.9.2 Current-Starved Ring Oscillator

This design utilizes a three-stage current-starved-ring-oscillator topology, such as the one shown in Fig.4.16, due to its low power, wide tune-ability and fast turn-on

characteristics. The two disadvantages usually associated with ring-oscillators of phase-noise and process variability are not of great concern here as most UWB-IR receivers are designed for wide-bandwidth and utilize non-coherent energy detection [68] with 4-5% frequency tolerance. Low variation methodologies [69] or other calibration circuits [66] can also be utilized for variation robustness.

As shown in Fig.4.16, the Pbias and Nbias biasing voltages control the current during transitions. The frequency can be tuned up to 6GHz, thereby providing flexibility to tune the bands. The transistors were sized for the same rise and fall times as well as to reduce process variability. The OSC\_EN signal also provides a large initial excitation for the oscillator, thereby reducing the startup time to less than 0.5ns. Aided by the fast startup and low duration of the transmitted pulse, the oscillator is typically “on” for only a ~4ns duration, thus contributing only a small amount of dynamic power.

### 4.9.3 Triangular Wavelet Generator

The triangular wavelet generating circuit is realized with a simple charge-pump scheme, as shown in Fig.4.17. A rectangular pulse gives rise to a triangular wavelet at the output due to the current-limiting RampP and RampN biasing voltages, which in this case, were both set to  $V_{DD}/2$ . The design consumes power only when a pulse

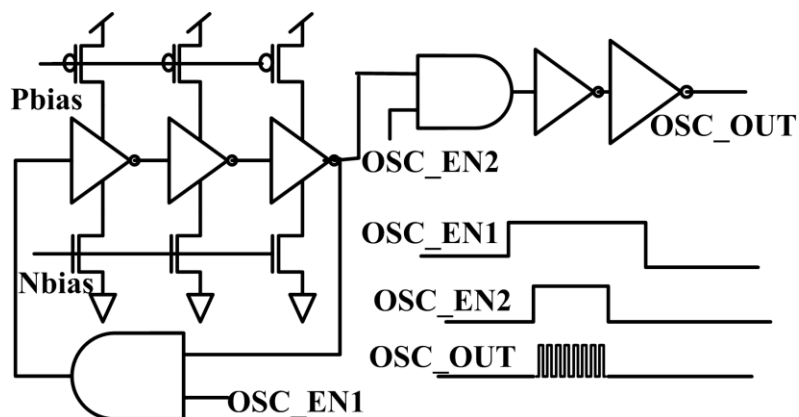
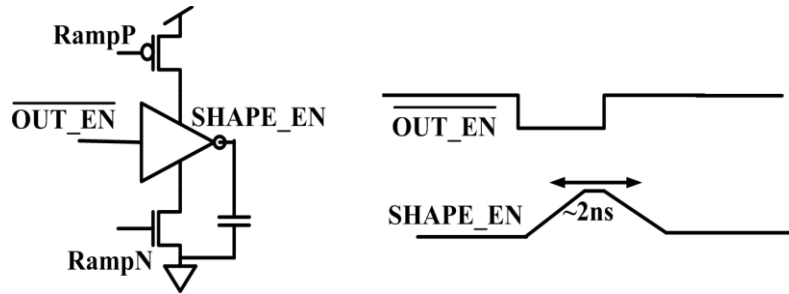


Figure 4.16. Three-stage current-starved ring-oscillator.



**Figure 4.17. Rectangular-to-triangular wavelet generator.**

arrives at the input. Compared to other complex analog [70] or complex digital pulse-approximation techniques [66, 71] this design is extremely simple and low power.

#### 4.9.4 Antenna Driver Circuit

Multiple designs were explored for low power antenna drivers. While the inverter based driver shown Fig.4.18a gives a rectangular wavelet, the design with triangular modulation of the inverter driver shown in Fig.4.18b can provide the desired triangular

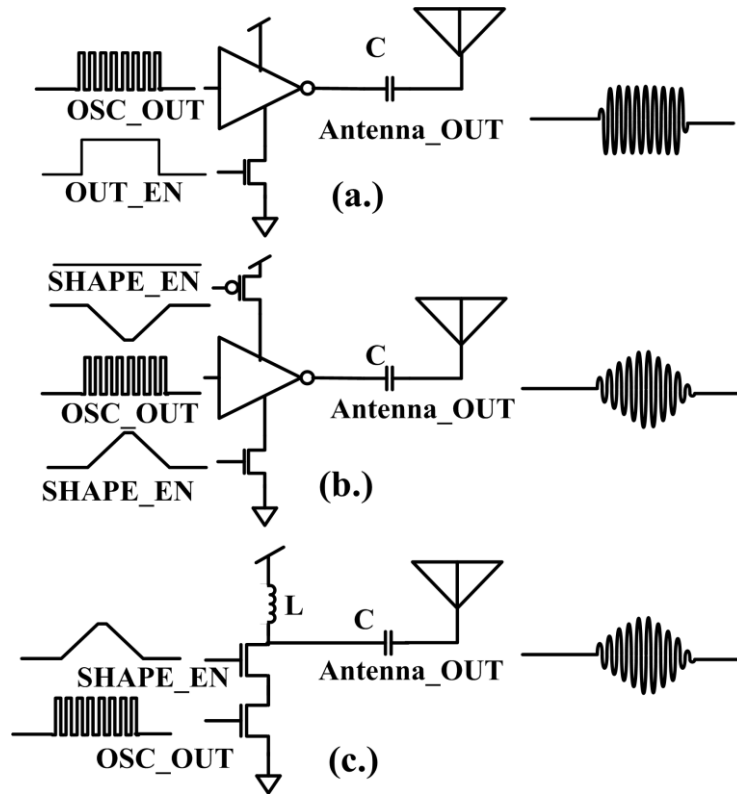


**Figure 4.18. Simple inverter, (b) modulated inverter, and (c) class-C antenna driver circuits.**

pulse-shape. However, this modulated inverter requires differential triangular pulse-shapes. However, the class-C driver based design shown in Fig.4.18c requires only one triangular pulse-shape, thereby reducing both power consumption and complexity. The output power efficiency of the transmitter was simulated to be  $\sim 40\%$ . When not transmitting a pulse, the two NMOS transistors are connected to GND to eliminate any static bias power consumption. Pulse shape output due to process variation can cause the signal to deviate from a triangular pulse shape, but such deviations don't change the inter-band isolation by more than 5dB.

#### 4.10 Measurement Results

The design was fabricated in a 90nm CMOS process, as shown in Fig.4.19, with both the inverter based driver (Fig. 4.18a), as well as the triangular-pulse shaping class-C driver (Fig.4.18c). Fig.4.20 shows the measured time domain pulse-shape for the two designs. While the simple inverter based driver gives a rectangular pulse, the pulse with the pulse-shaping circuit is triangular. As illustrated in Fig.4.21, the spectrum for the three different frequency bands was also measured for both designs operating at 5Mbps with non-random periodic pulsing. Note that design is FCC compliant only when triangular pulse shaping was enabled. The circuit was measured to consume only  $5.7\mu\text{W}$  of power, with  $2.8\mu\text{W}$  due to leakage power, and  $2.9\mu\text{W}$  at

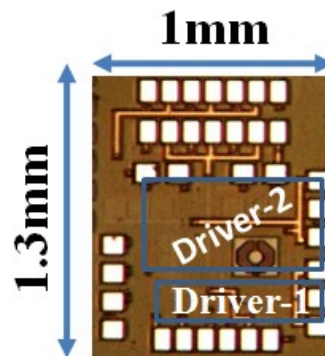
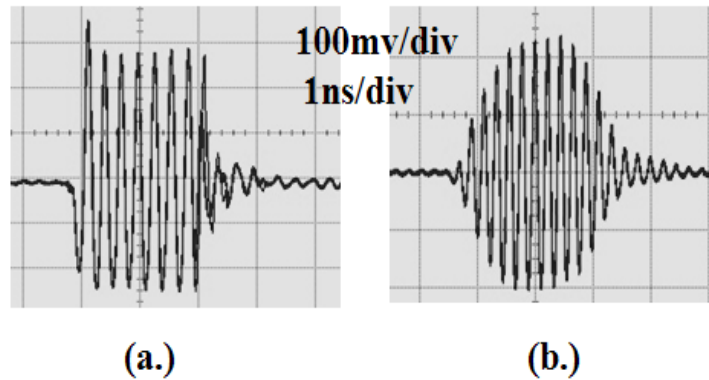


Figure 4.19. Die photo of the chip with the two driver circuits.

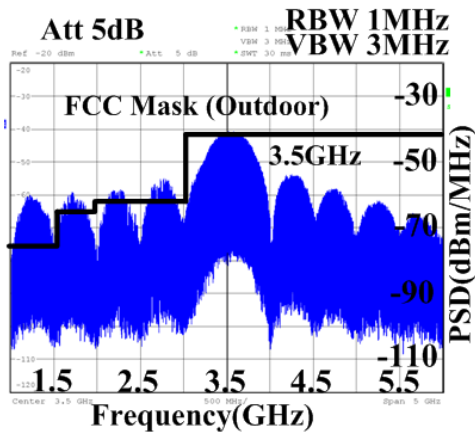
100Kbps due to dynamic power at a 0.9V supply. The energy/pulse at 5Mbps was measured to be only  $\sim 29\text{pJ/pulse}$  with an output voltage swing of 450-500mV across a 50-ohm load (Table 4.3).



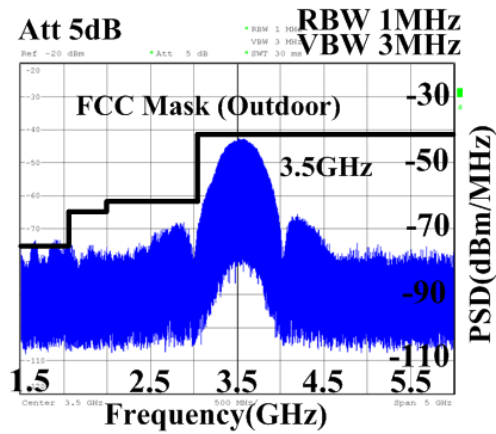
**Figure 4.20. Measured output (a) without pulse-shaping, and (b) with pulse-shaping.**

**Table 4.3 Measured Overall Power performance comparison to other UWB-IR Transmitters**

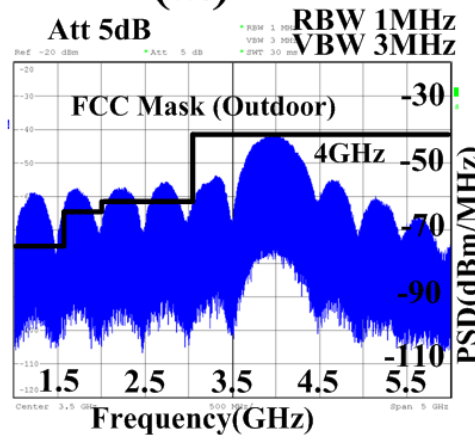
TECHNOLOGY	90nm CMOS
Active Area	0.3x0.3mm <sup>2</sup>
Modulation	OOK, PPM
Supply	1V
Static Power	2.9 $\mu$ W
Active E-Pulse	28pj/pulse
Total Power @100Kpulses/sec	5.7 $\mu$ W
Output Voltage Swing	$\sim$ 500mV
Pulse Repetition frequency Range	Up to 10MHz
Frequency Band	3-5GHz (Low UWB Band)
Spectral Range	3-5GHz Band
Energy/bit Range	57pj/pulse-29pj/pulse
Side-lob rejection	-28dB



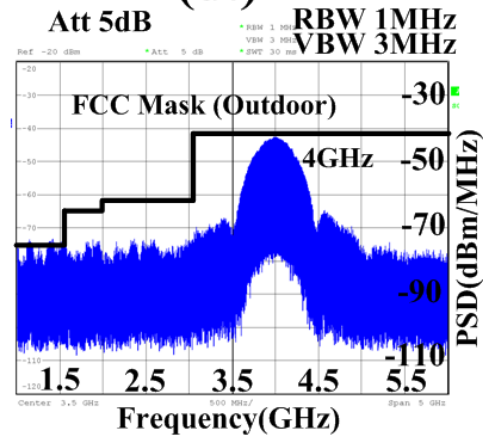
(a.)



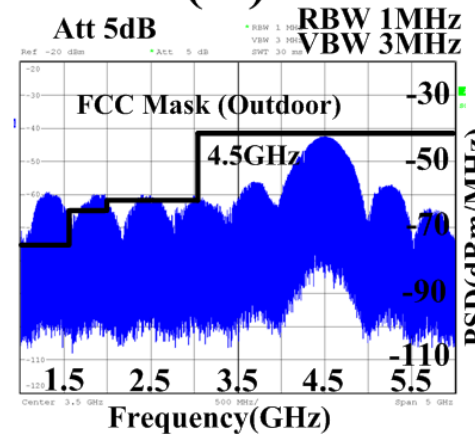
(d.)



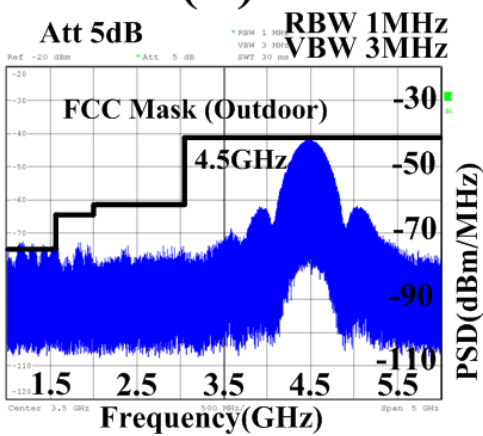
(b.)



(e.)



(c.)



(f.)

Figure 4.21. Measured output spectrum with (a, b, c) rectangular pulse shape, and (d, e, f) triangular pulse shape at 5Mbps for the 3 different frequency bands.

#### 4.11. Performance Comparison of the Transmitter

Table 4.4 compares the design performance with some of the recently published work. Comparison is done along the line of dynamic power, leakage power, and output voltage swing. In some of the designs the leakage power is obscured by operating in burst mode, thereby having a high effective pulse rate [66, 72, 73]. While comparing such designs we have taken care to use equivalent pulse rates. As can be seen from the table, this design provides one of the best performances for UWB-IR transmitters, particularly at low data-rates. At high data rates, 29pJ/bit energy efficiency is also comparable to the best.

Taking into consideration the output voltage swing of only 165mV and 160mV in [66] and [74] respectively, at high data rates, we can argue that our design performance is comparable even at higher data rates. As an example, at a data rate of

**Table 4.4 Measured Overall Power performance comparison to other UWB-IR Transmitters**

	Power at 100Kbps or Minimum Reported Power		Output swing	Energy Per Pulse	
	Static and Leakage	Total		@ 100Kbps	@High Rate
<b>This Work</b>	<b>2.8<math>\mu</math>W</b>	<b>5.7<math>\mu</math>W</b>	<b>0.5V</b>	<b>57pJ</b>	29.2pJ
[62]	96 $\mu$ W	99.7 $\mu$ W	0.65V	997pJ	47pJ
[66] <sup>†</sup>	123 $\mu$ W	125 $\mu$ W	0.17-0.7V	1.25nJ	17.5pJ <sup>§</sup>
[74]	2.5mW	2.5mW	0.16V	25nJ	16.8pJ*
[75]	10mW	10mW	0.35V	100nJ	62.5pJ
[71]	29.7mW	29.7mW	1.28V	297nJ	825pJ
[72] <sup>†</sup>	~800 $\mu$ W	805 $\mu$ W	0.2V	8.05nJ	50pJ
[73] <sup>†</sup>	N/A	650 $\mu$ W	0.2V	N/A	40pJ
[70]	31.3mW	31.3mW	0.25V	313nJ	313pJ

\*- Ref. [74], Doesn't account for antenna driver power at high rate.

§- Ref. [66], Reduces output swing to ~165mV at high data rates.

†- Symbol rate converted to equivalent pulse rates for power estimation.

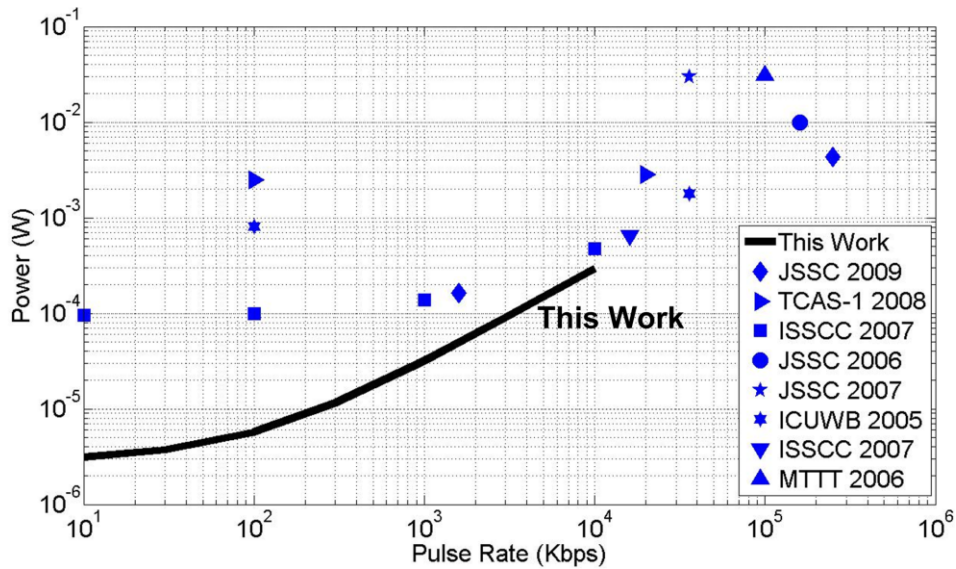


**Figure 4.22. Power Vs Data Rate of different published schemes and comparison to our work. (ref. are [66, 74, 62, 75, 71, 72, 73, 70] in order).**

1Mbps, our design consumes a total of only  $\sim 32\mu\text{W}$ , which still is the lowest power number among state-of-the-art designs. Simplified design architecture, where none of the blocks have any static power consumption, results in these improved performance numbers. It should be noted that most sensing network applications require only low data rate ( $\sim 100\text{Kbps}$ ) operation. At these operating rates, while all other designs consume in excess of  $100\mu\text{W}$  of total power, our design only consumes  $\sim 6\mu\text{W}$  total power, enabling the longest battery lifetime (Fig.4.22). While there are designs [66, 74] that can claim better energy/bit numbers at very high data rates, they don't have equally good energy/bit numbers for low data rate applications (Fig.4.23). Also, while comparing the energy/bit one should also take into account the radiation energy as a figure of merit. When taken in to account the radiation energy, and normalizing the energy/bit requirement for the equivalent radiated power as this design, we see that our performance even at high data rate is better than other published results (Fig.4.24).

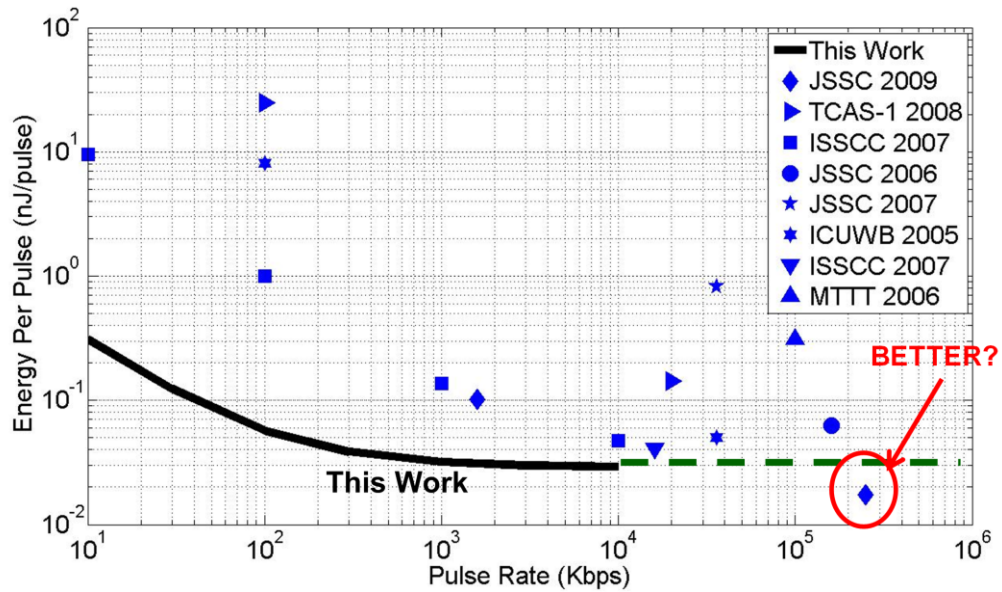


Figure 4.23. Energy/bit Vs Data Rate of different published schemes and comparison to our work (ref. are [66, 74, 62, 75, 71, 72, 73, 70] in order).

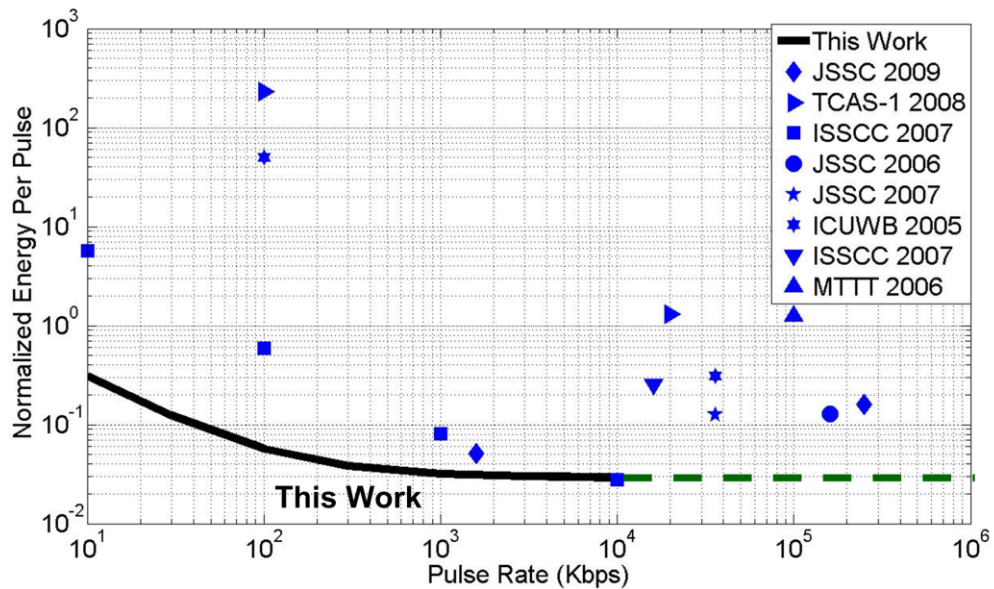


Figure 4.24. Normalized Energy/bit Vs Data Rate of different published schemes and comparison to our work (ref. are [66, 74, 62, 75, 71, 72, 73, 70] in order).

### 4.12 Study of the effect of Non-Idealities

Non-idealities, particularly associated with process-variation, can change the timing as well as spectral characteristics of the transmitted pulse and so warrant study.

#### 4.12.1 Effect of Pulse-width variation

Pulse-width of the impulse wavelet controls the 10-dB bandwidth of the transmission spectrum. Since FCC requires an impulse to have a 10-dB bandwidth of at least 500MHz. One needs to provide design tolerances such that the variation doesn't make this bandwidth to go below 500MHz. A higher bandwidth than 500MHz

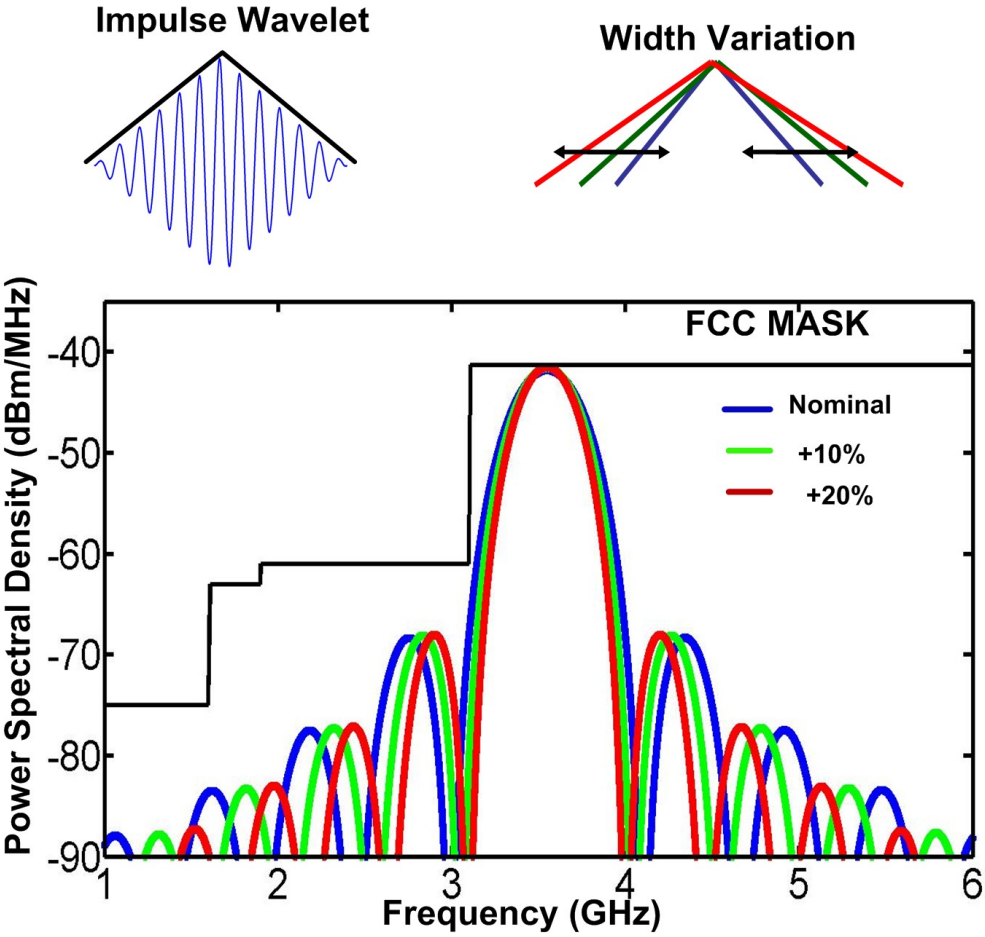
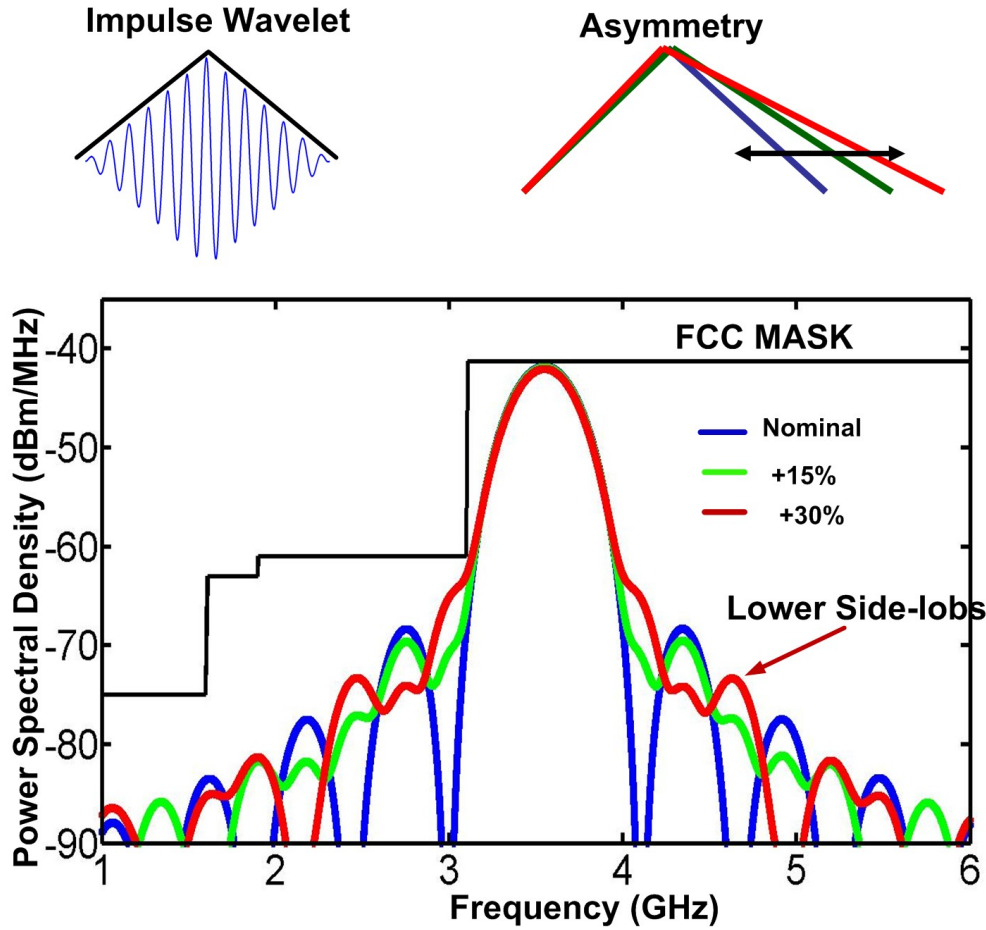


Figure 4.25. Spectral profile impact with Impulse wavelet width variations

can have the potential to increase the out-of-band losses and can potentially create cross-talk in adjacent channel. A Matlab simulation incorporating the pulse width variation however shows that the out-of-band losses and cross-talk are not significant even for a delay variation of up to 20% (Fig.4.25). Particularly, for our architecture with a 1GHz separation between the bands the cross-talk between channels remains mostly constant.

**4.12.2 Effect of Asymmetry in the Triangular wavelet**

Due to mismatch in the pfet and nfet current sources in the charge-pump circuit



**Figure 4.26. Spectral profile impact with asymmetric Impulse wavelet rise and fall time.**

that generates the triangular pulse-shape, there may be asymmetry in the pulse wavelet in the wake of process variation. A matlab simulation incorporating this asymmetry however shows negligible impact on the spectrum. The side-lobes are in-fact lower with higher asymmetry, as the nulls and the peaks in the side-band gets spread out. Even with 30% asymmetry no appreciable impact on the spectral profile was noticed (Fig.4.26).

#### 4.12.3 Effect of non-linearity in the Triangular wavelet

Due to non-linearity in the output driver & triangular pulse generator circuitry the pulse-shape is not expected to be exactly triangular. A matlab simulation of the pulse-

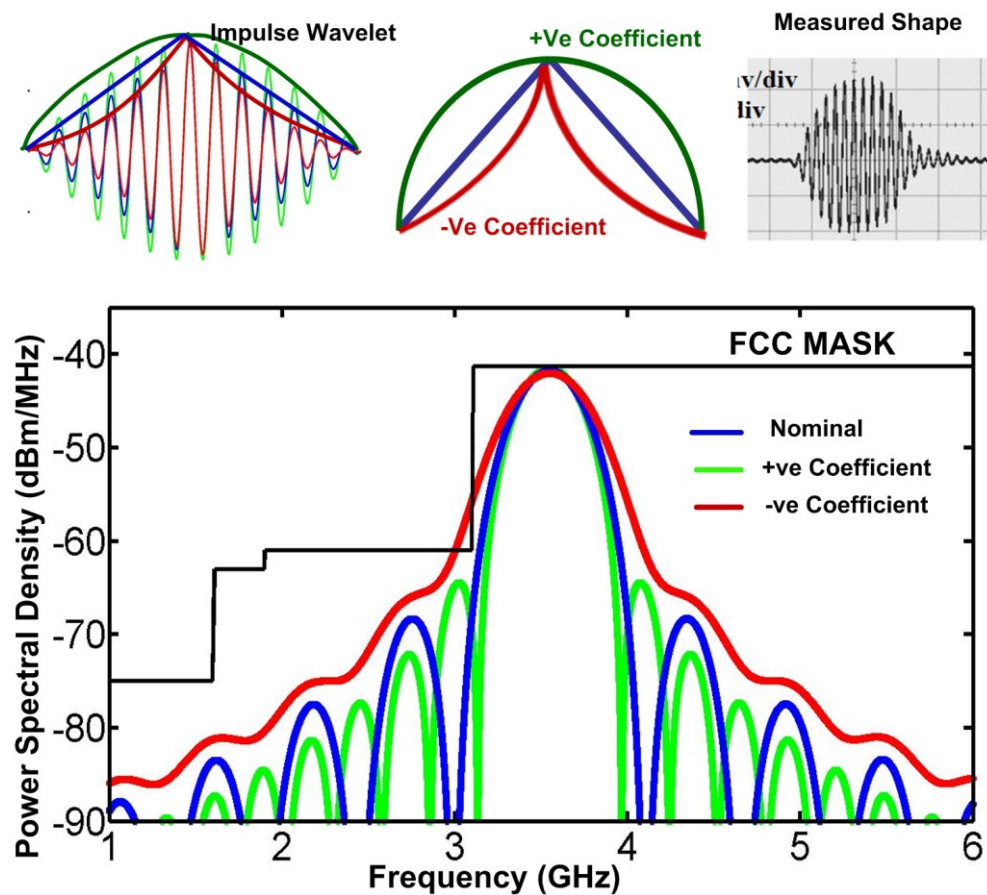


Figure 4.27. Spectral profile impact with non-linearity in the circuit.

shape with  $-ve$  and  $+ve$  second order non-linear terms suggest that while  $-ve$  non-linearity can increase the bandwidth (due to lower effective pulse-width) and thereby potentially violate the FCC spectral mask, with  $+ve$  coefficient the pulse-shape appears similar to raised cosine pulse-shape, and is not much of a concern. It does add extra side-lobes though; however for our purpose for a channel sitting at 4.5GHz the side-lobe strength it is lower than normal, thereby having improved cross-talk performance (Fig.4.27). Our measured results also indicate that the non-linearity was of  $+ve$  coefficient type.

#### 4.12.4 Effect of Frequency Mismatch

Ring oscillators are prone to frequency-variation due to process, temperature and voltage. Unlike the traditional continuous wave radios precise frequency synchronization between the transmitter and receiver is not required for UWB impulse based communication. This is primarily due to use of non-coherent energy detection based architecture, commonly used in receiver front-end. Even if the frequency

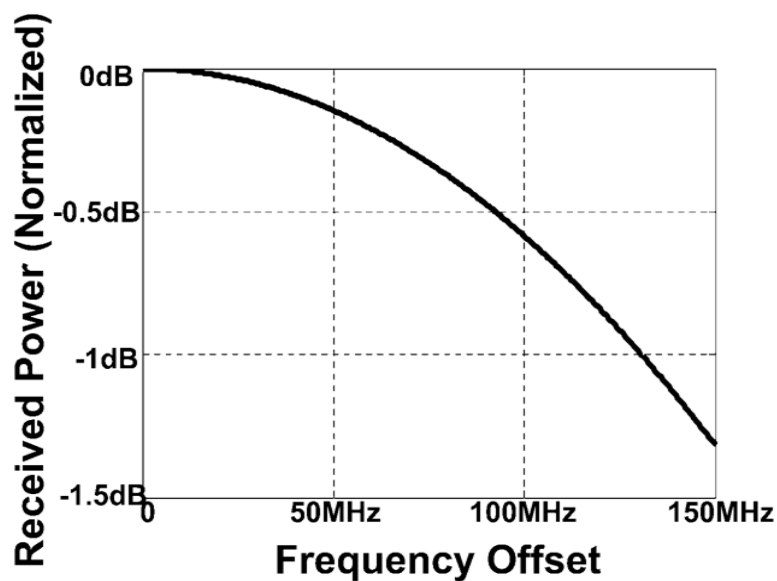
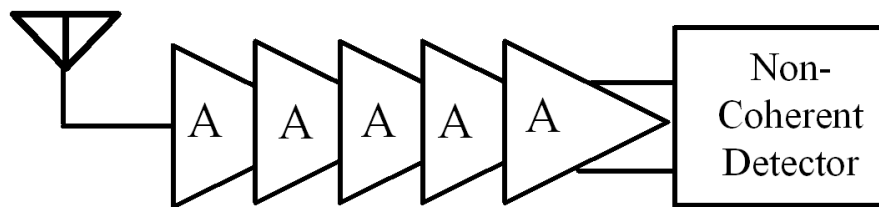


Figure 4.28. Effect of frequency mismatch between the receiver and the transmitter.[68]

mismatch between the receiver and the transmitter is of the order of 150MHz (@3.5GHz band, i.e. ~5%), the power loss is still close to ~-1dB (Fig.4.28), having very low impact on the overall performance of the system. For higher variation calibration circuitry can also be easily implemented. As only one time or opportunistic calibration will be required, overhead associated with the calibration circuitry can be kept to very low. Due to inherent tolerance to frequency variation between the transmitter and receiver circuits, the calibration circuit doesn't need to be very precise either. Furthermore, a digital calibration is also possible with the ring-oscillator based design.

Thus study of the non-idealities associated with the triangular wavelet shape and frequency variation indicates that the design is robust and can be used without much adverse impact on the performance of the system.

#### 4.13 RX-Design: Front End Design



**Figure 4.29. Receiver Front-End design, consisting of 5 gain stages followed by a non-coherent detector**

The receiver Front-End Circuit, with a resistive 50-ohm termination at the input stage, consists of multiple gain stages followed by a non-coherent detector. The design was implemented in a 90nm CMOS process (Fig.4.29). Due to the system requirement of supporting two bands the receiver circuit was designed with band-selectivity. Fast turn-on, high receiver sensitivity, asynchronous detection, and high narrowband

interference rejection were some of the design parameters that were focused on for this design.

#### 4.13.1 Gain Stage design & Measurement Results

The gain stage circuit, which is composed of a five-stage tunable wide-band amplifier, is illustrated in Fig.4.30. Each stage uses a differential common-source amplifier with tunable LC load, optimized for switching transients of  $\sim 1\text{ns}$ . The gain stages were designed for a total combined gain of 39dB, a center frequency tuning

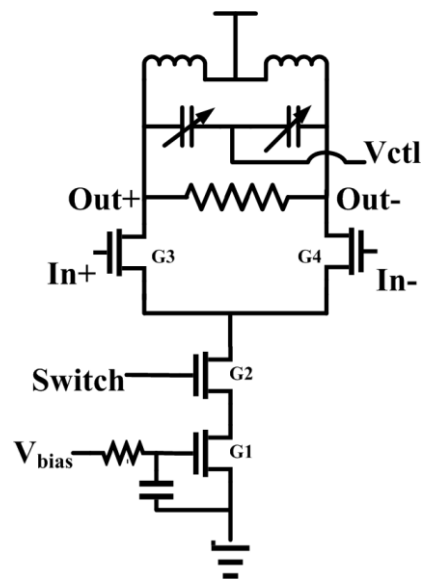


**Figure 4.30. Single stage of the 5-stage band-tunable duty-cycleable gain stage.**

range of 3.5-4.6GHz, and a steady state power consumption of 7.5mW in a 90nm IBM process. The choice of 5-gain stages was made based on the trade-off between power consumption, Rx-sensitivity, tunability, and bandwidth. Since power increases roughly quadratically with gain in a single stage, use of 5-cascaded lower gain stages enables us to reduce the power, while achieving our gain and bandwidth specifications. To achieve faster turn-on times, the gain stages were designed to have the same input and output biases, eliminating the need for inter-stage AC-coupling. AC coupling requires

capacitor charge-up, increasing the turn-on time. Care was also taken to suppress the supply transient when duty-cycling by inserting a small resistor in the supply path as well as decoupling the supply and biases from ground.

Fig.4.31 shows the S11 characteristics of the designed amplifier chain. In Fig.4.32, we show measured gain of the proposed scheme at different Vctl voltages. At a Vctl of 0V, the band-center sits at 4.5GHz, while at 1V, the center is at 3.5GHz. The inter-band isolation is 35dB.

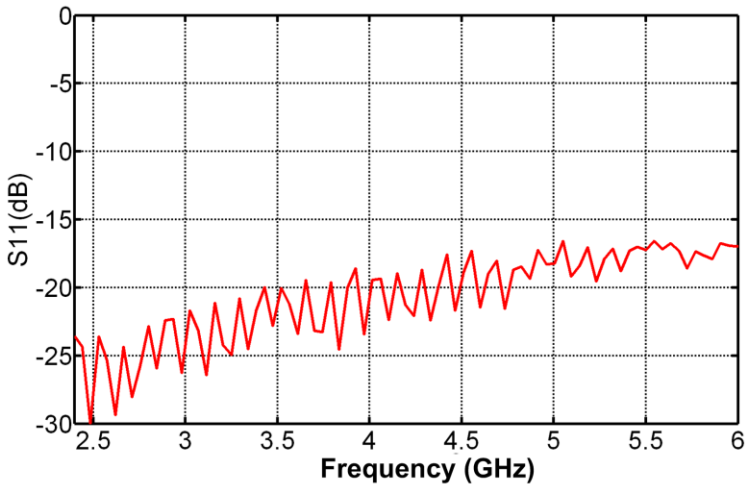


Figure 4.31. S11 measurement of the die at various frequencies.

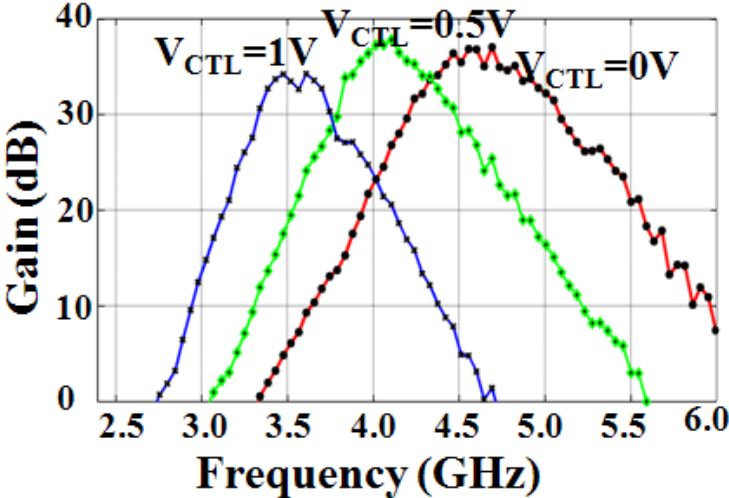
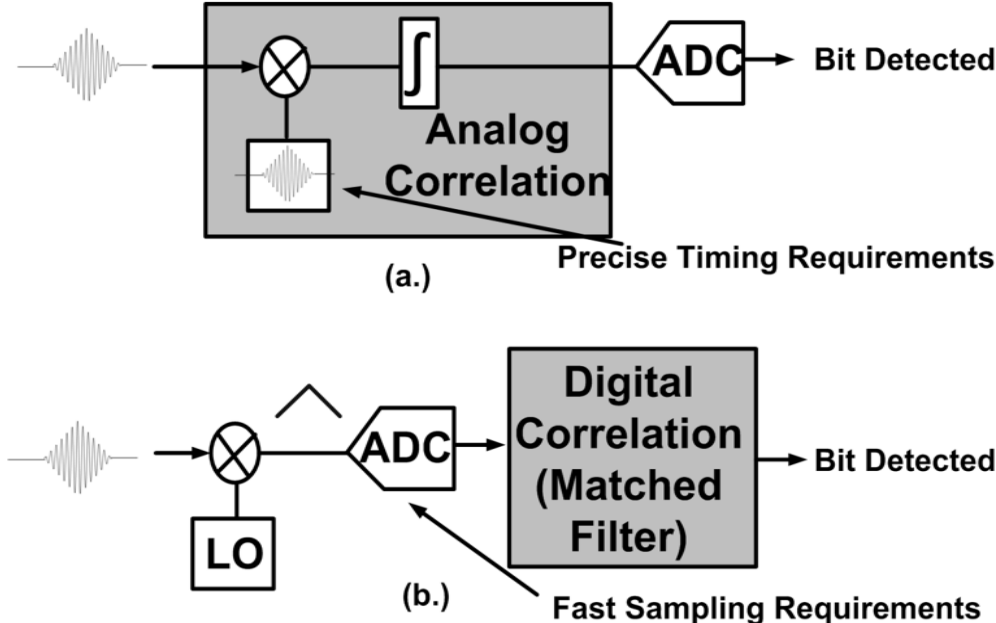


Figure 4.32. Measured gain of 5-stage gain circuit at different control voltages (Vctl).

### 4.13.2 Pulse-detection Mechanism

There are various existing methodologies to detect pulses in time [68, 76-79]. But most of these existing methods can be classified primarily into two categories, a non-coherent pulse detection method and coherent-pulse detection method. In a coherent detection methodology, the detection works similar to the traditional continuous wave signal. The signal is compared with a local template signal and time-alignment between the two signals becomes very important (Fig.4.33). The precise timing requirement in these cases (of the order of 50-100ps) warrants the use of faster clock circuitry and makes the scheme mostly very power hungry. Similarly schemes exist that rely on down-conversion and then high speed sampling of the signal to look for pulse. Due to high sampling rate requirements in these scheme of the order of close to 1-2Gbps, the scheme tends to again consume high power. For pulse detection, non-



**Figure 4.33. Most common pulse detection methodologies, such as analog correlation as well as digital correlation techniques both consume high power either due to very precise timing requirements (~50-100ps) or high sampling rate (~2Gbps).**

coherent detection based schemes are usually considered for low power applications. A comparison between non-coherent and coherent detection based scheme published recently in top conferences indicates low power capabilities of the non-coherent detection schemes (Fig.4.34). While some non-coherent schemes require the incoming signal to be mixed with a local oscillator signal, and then from I & Q generated components the energy of the received signal is measured. Some other schemes

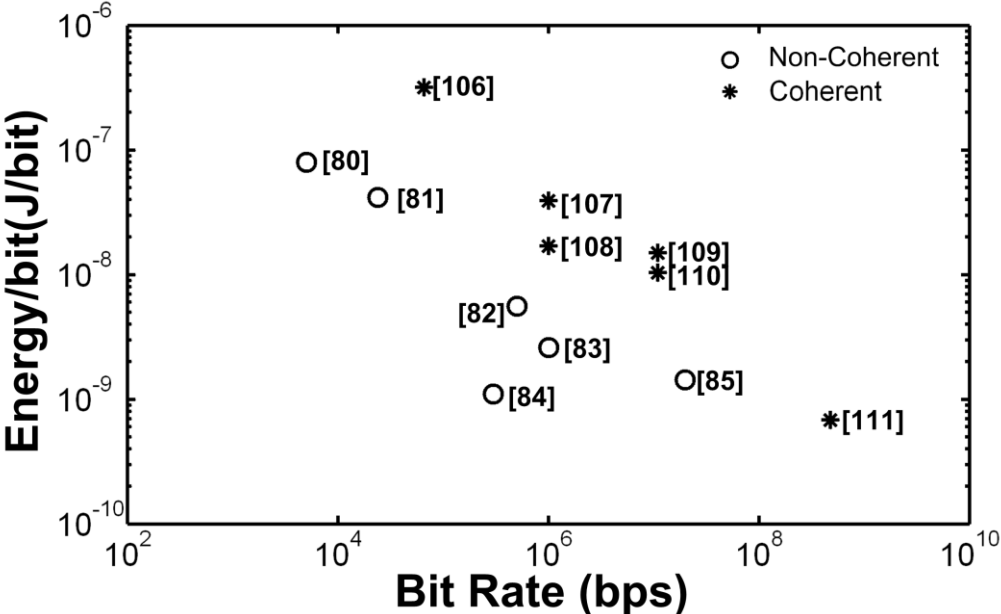


**Figure 4.34. A survey of non-coherent and coherent receiver design papers. Non-coherent detection schemes tend to be lower power [112].**

directly rectify the signal and then look for the energy over some timing window by integrating the received energy [68]. These designs still consume high power due to sampling of the signal. In comparison we utilize a peak-detection based low power asynchronous detection scheme.

**4.13.3 Peak-detection based self-timed pulse-detection**

5-stage gain amplifier in our RF-Frontend feeds a peak detector (Fig.4.35), which detects the arrival of the pulse, effectively serving as an asynchronous self-timed one-

bit ADC. The detector uses a regenerative latch and is biased such that  $M_{1,2}$  are nominally in sub-threshold and that the positive feedback through inverter pairs  $M_{9,10}$  and  $M_{11,12}$  is suppressed by the presence of damping transistors  $M_{7,8}$ , providing a net negative feedback that holds both outputs close to the supply voltage  $V_{DD}$ . However, in the presence of a pulsed signal, the total current through  $M_{1,2}$  rises exponentially, causing positive feedback to increase and driving either the  $PD\_Out+$  or  $PD\_Out-$  outputs low. Resistor  $R1$  maintains the source potential of  $M_{9,10}$  to be equal. While, transistors  $M_{1,2}$  act as a self-mixing pair. Once the pulse is detected, the control circuit generates a delayed reset signal  $RST$  that drives the outputs back to  $V_{DD}$ , allowing detection of the next pulse. The nominal bias current of this duty cycled circuit is  $10\mu A$  when no signal is present and increases upon arrival of a signal.

Short transient decay times allow the receiver to be duty cycled to less than 0.1% (10ns in a 10us period), yielding an average power consumption of  $\sim 12\mu W$ , including

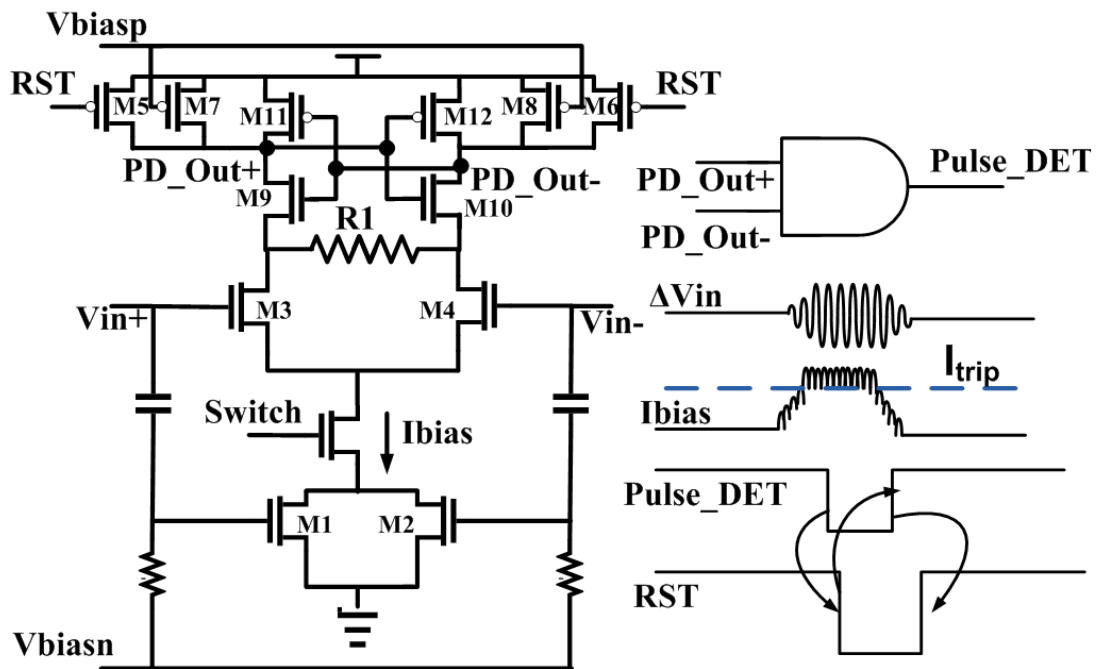


Figure 4.35. Schematic of non-coherent detection scheme

leakage.

#### 4.13.4 Time Domain Measurement Results

In Fig.4.36, we show the measured detected signals in time domain using the proposed receiver scheme. The receiver could detect pulses separated in time by as little as 10ns with low BER. This means the data-rate can be scaled from 100Kbps to even 100Mbps, using the same transceiver, albeit at the cost of increased power consumption. Using an omni-directional monopole antenna we also measured the timing uncertainty of detection. As shown in Fig.4.37, at a 1.5m distance the measured timing uncertainty due to noise in pulse-detection is only  $\pm 250$ ps peak-peak (Fig.4.38). This indicates that while duty-cycling the receiver, the detection circuit

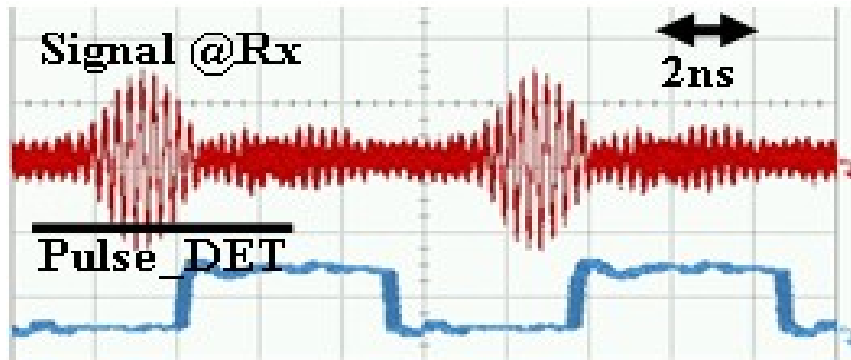


Figure 4.36. Time-domain Detection of the signal by the receiver

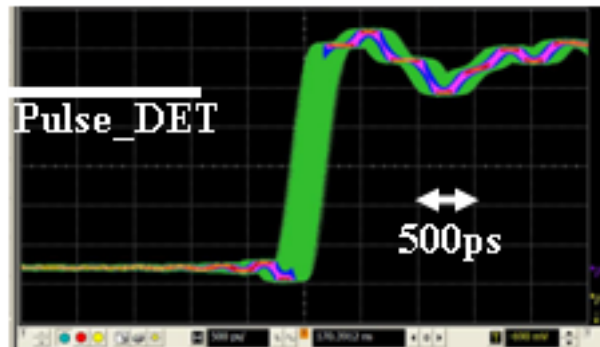


Figure 4.37. The eye-diagram of the pulse\_det signal

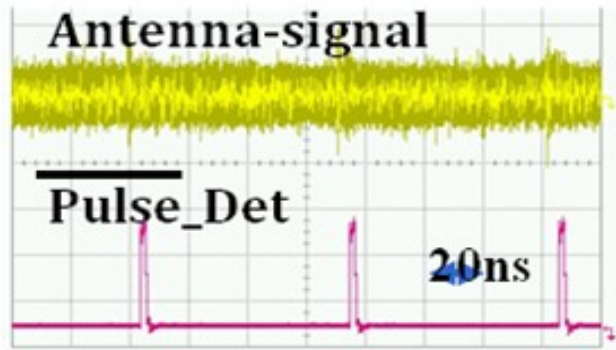


Figure 4.38. Antenna received signal and corresponding pulse\_det signal at an antenna separation of 1.5m.

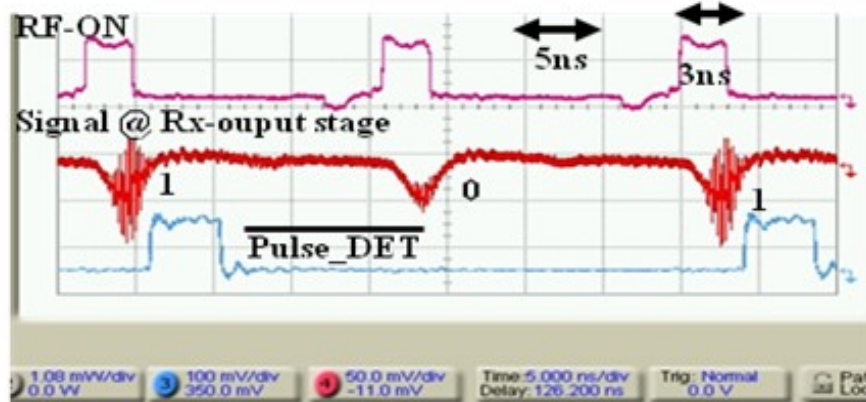


Figure 4.39. Measured OOK detection, while duty-cycling. (With RF-ON, the output stage shows a small dip due to turn-on transients.)

does not add any significant timing uncertainty.

In Fig.4.39 we show the measured detected signals in time while duty-cycling the RF. A correct signal transmission sequence of 1-0-1 was detected even when the RF-ON window was reduced to as low as 3ns. This means the Rx can detect impulses within a 3ns window. However to accommodate synchronization uncertainties, we propose and measure the power numbers with a 10ns RF-ON window.

#### 4.13.5 BER Measurement Setup & Methodology

An FPGA based scheme was utilized for testing the BER at various data rates for the receiver test block (Fig.4.40). The essence of this scheme is as given below. A pattern generator/Tx or an impulse generator is used to send pulses at a given data

rate. The receiver is duty-cycled externally, while opening the pulse-detection window for a small time. The error counter which was implemented in an FPGA counts the error and so the error-rate. Alternatively ANRITSU Bit-error Tester was also utilized for getting the BER directly from the instrument with a 1-0-1-0 pattern, without using FPGA.

#### 4.13.6 RX-Sensitivity and Frequency Selectivity Measurements

Fig.4.41 shows the measured Rx-sensitivity of the receiver at the two designated bands. The sensitivity at the 3.5GHz band is slightly lower than that at the 4.5GHz due to the lower gain in the 3.5GHz band. At the receiver a signal of  $\sim 1\text{mV}$  instantaneous amplitude can be detected. With a  $\sim 500\text{mV}$  peak-peak signal from the

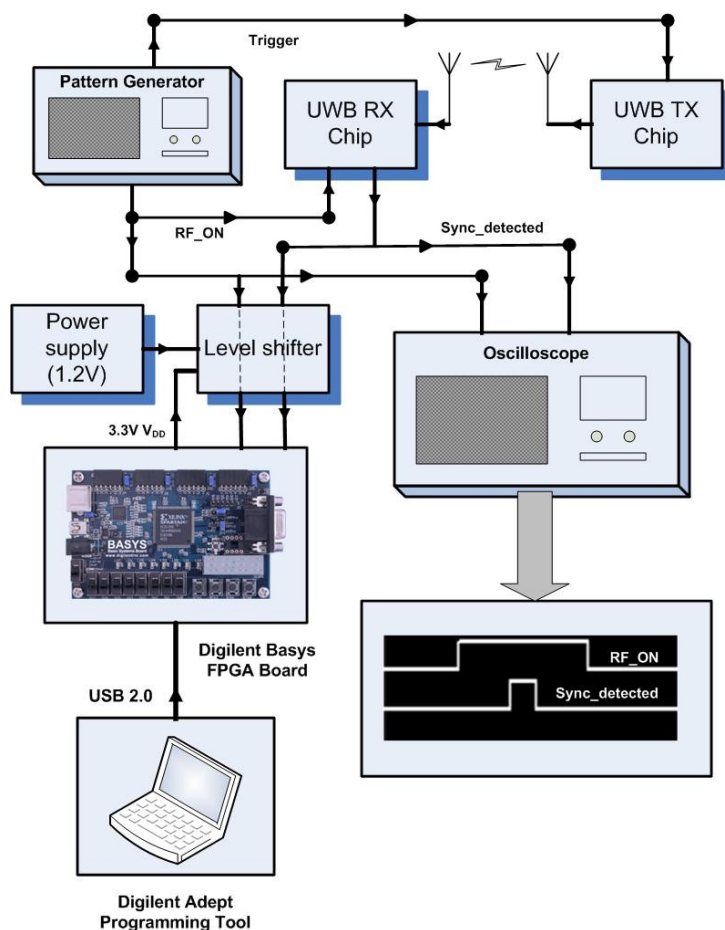
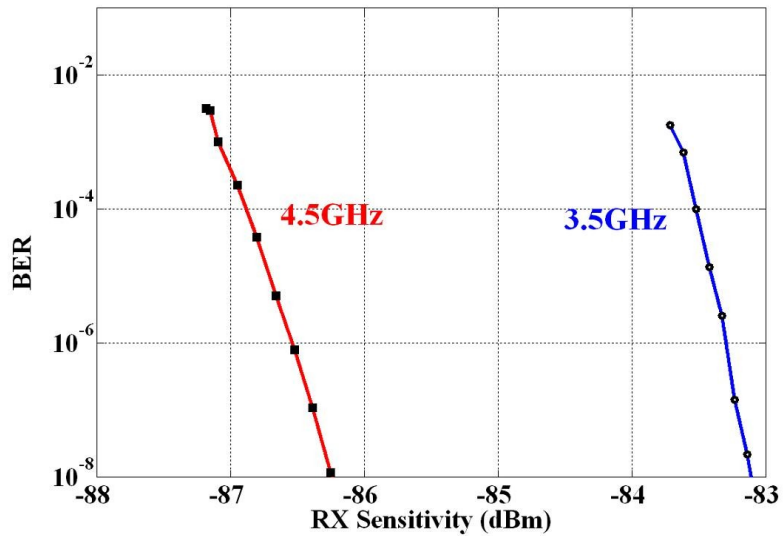


Figure 4.40. BER Measurement Setup for the receiver test-chip



**Figure 4.41. Measured Rx-sensitivity @100kbs for the two bands.**

transmitter, and channel loss as defined by the formula  $-40-20*\log_{10}(d)$ , where  $d$  is the distance in meters. We can use this transceiver for a range of  $\sim 2.5m$ , sufficient for most of the body-area applications. For longer range the Tx power can be increased, as we are still operating below the FCC-mandated power levels at the 100Kbps data rate.

In Fig.4.42 we present the BER sensitivity for the two bands while changing the central frequency of the input impulse. For a BER of  $10^{-3}$  the allowable central frequency variability of input impulse is  $\sim 250MHz$  @4.5GHz band at  $-86.2dBm$ , while it is measured to be  $\sim 125MHz$  @3.5GHz band at  $-82.7dBm$ . This provides some robustness against process variations affecting the transmitter's oscillation frequency. However for larger process variations a calibration scheme will be required.

#### 4.13.7 Effect of Narrowband Interferer

Fig.4.43 illustrates the instantaneous signal-to-interference ratio (SIR) for the two bands for a BER of  $10^{-3}$ . The measurement was done by setting the signal strength 1dB higher than the minimum required sensitivity. As expected, the SIR is high at out-of-band signals, with more than 50dB of isolation for a most common narrowband

interferer signal at 2.4GHz. This means only a continuous wave signal of +4dBm (Rx-Sensitivity + signal\_Duty\_Cycling - SIR = -83+ 37 + 50 = +4dBm) or higher at 2.4GHz at the receiver can create appreciable errors in detection. Another common narrow-band interferer is normally at 5.1GHz, and a notch filter will be required to

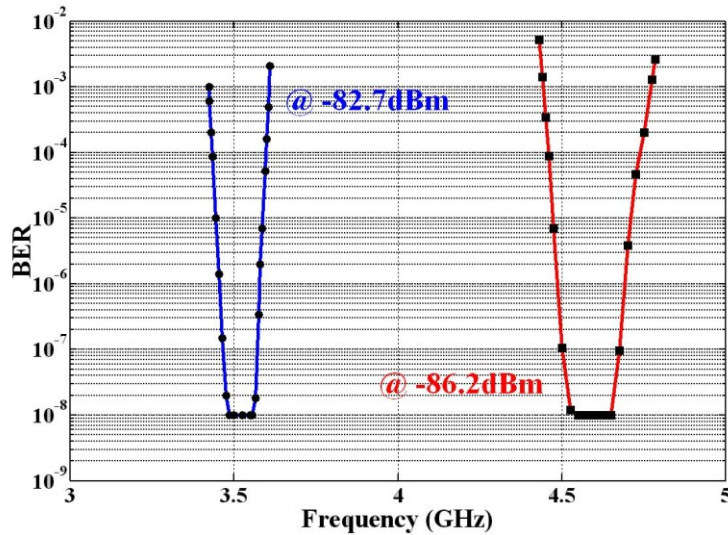


Figure 4.42. Measured BER Vs Carrier frequency of the input impulse of fixed strength, with channel tuned to the 3.5GHz and 4.5GHz bands respectively.

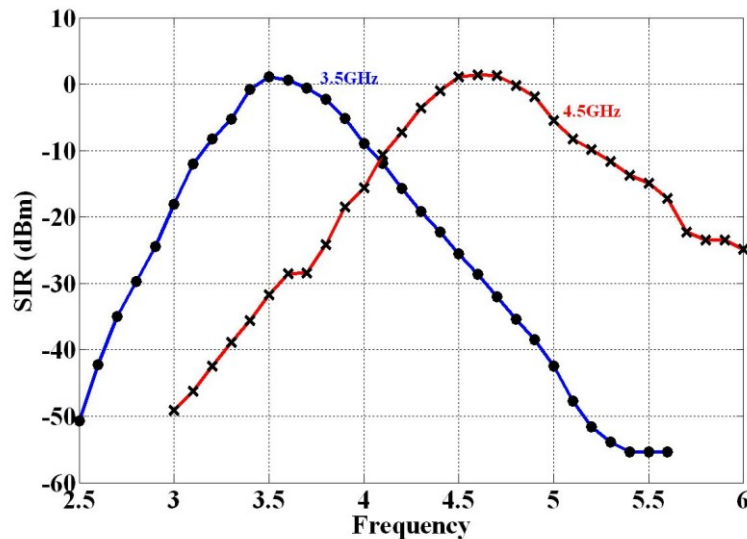
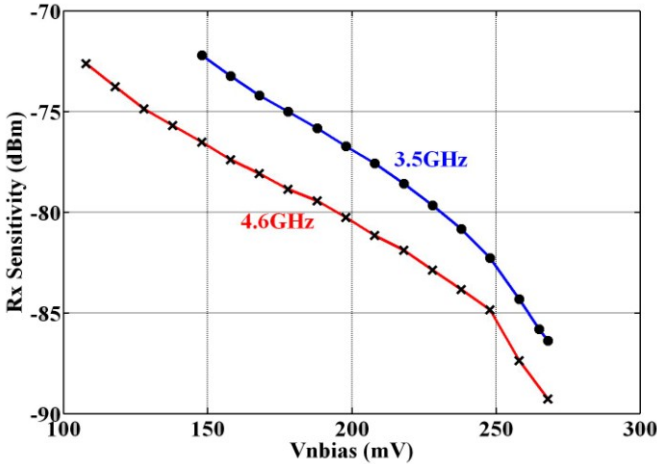


Figure 4.43. Measured Signal to narrow-band Interference power ratio (SIR), (instantaneous power) at different frequencies, when the receiver is configured to listen into one of the two bands.

avoid misdetections in presence of strong narrowband signal at 5.1GHz. Omnidirectional monopole antennas with notch-characteristics [86] can also be utilized to avoid misdetections due to the 5.1GHz narrowband interferer.

**4.13.8 Rx-sensitivity Control**

Since, the non-coherent detector in our scheme is based on regenerative positive feedback; by changing the  $V_{biasn}$  (controlling positive feedback) and  $V_{biasp}$



**Figure 4.44. Measured Rx-sensitivity at BER of  $10^{-5}$  while varying the  $V_{biasn}$  for both 3.5GHz and 4.5GHz bands**

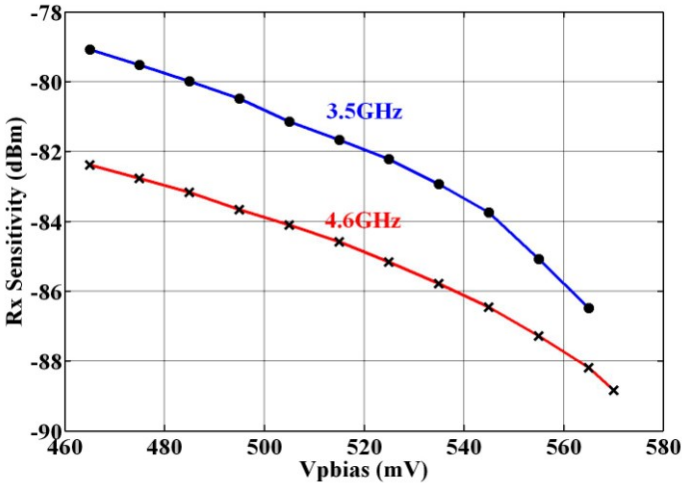


**Figure 4.45. Measured Rx-sensitivity at BER of  $10^{-5}$  while varying the  $V_{biasp}$  for both 3.5GHz and 4.5GHz bands**

(controlling negative feedback) one can change the receiver sensitivity (Fig.4.35). In Fig.4.44, 4.45, we show measured results of how  $V_{biasn}$  and  $V_{biasp}$  change the Rx-sensitivity for a BER of  $10^{-5}$ . As expected a lower  $V_{biasn}$  requires a stronger signal, due to reduced positive feedback. Similarly, a higher  $VDD-V_{biasp}$  requires a stronger signal due to increased negative feedback. This shows that with even a 10% variation in  $V_{biasp}$  and  $V_{biasn}$ , the sensitivity stays better than -80dBm.

#### 4.14 Performance Summary

Table 4.5 summarizes the overall performance of our receiver design. Overall the Rx Frontend is expected to consume only 20 $\mu$ W of power when operating at 100Kbps. This is the lowest reported power for a receiver working at the comparable data rate.

**Table 4.5 Performance summary and comparison to the state-of-the-art design**

TECHNOLOGY	90nm CMOS	ISSCC'07 [62,68]
Active Area	1.8x0.8mm <sup>2</sup> (Fig.4.46)	2*1mm <sup>2</sup>
Modulation	OOK	PPM
Supply	0.75V, 1V	0.65V
Rx Leakage Power	3.0 $\mu$ W	3.5 $\mu$ W
Rx static-Power	7.5mW	35.8mW
Rx Duty-cycled Power	<b>12 <math>\mu</math>W</b>	250 $\mu$ W
Turn-On time	~1-2ns	2ns
Average Rx-Sensitivity @ $10^{-5}$ BER @4.5GHz	-87dBm	-98dBm
Spectral Range	3-5GHz Band	3-5GHz Band
$P_{interferers}$ @2.4GHz for $10^{-3}$ BER	<b>+4dBm</b>	-20dB
In-band SIR for $10^{-3}$ BER	<b>0 dB</b>	-15dB

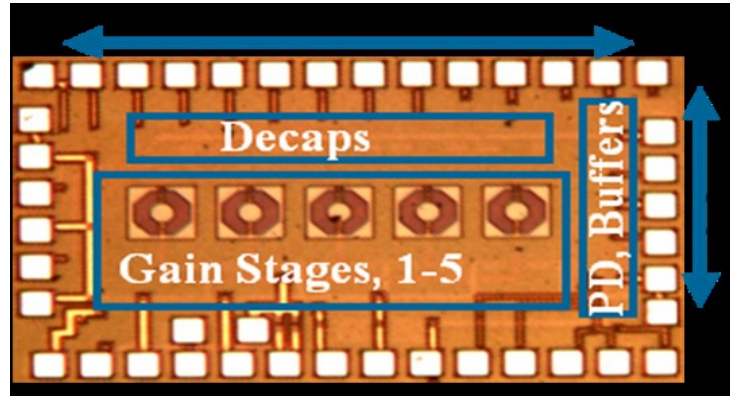


**Figure 4.46. Die Photo of the Rx test chip fabricated in a 90nm CMOS process.**

We also compare our results to a state-of-the-art non-coherent-detection-based architecture operating in the same band. Our total power consumption of  $20\mu\text{W}$  compares favorably to the best published impulse radio at  $350\mu\text{W}$  [62, 68] as well as the best published continuous wave radio at  $\sim 1\text{mW}$  [56]. The measured static, duty-cycled, and leakage powers are significantly lower for both the Tx as well as the Rx blocks in our case at the same data rate. We note that a PPM-modulated signal requires observing 2 time-integrals within a bit-detection period. As a result, our use of OOK modulation requires only half the RF-ON time, thereby half the power, of the PPM scheme reported by Lee et.al [62]. Our receiver design is also more power efficient due to use of simple, asynchronous circuits for pulse detection and power-gain optimized amplification. Finally, design of a simplified pulse-shaping transmitter provides further power saving due to a reduced number of components.

Our interference tolerance performance is also better than the time-integration-based detection scheme proposed by Lee et.al [62] in which the interferer energy is integrated over the whole RF-ON window ( $T_{\text{RF-ON}}$ ). In our scheme the interference tolerance is independent of the  $T_{\text{RF-ON}}$ . The inter-band isolation in our case was measured to be around 30dB at both the Tx as well as Rx, enabling time-multiplexed band-switching.

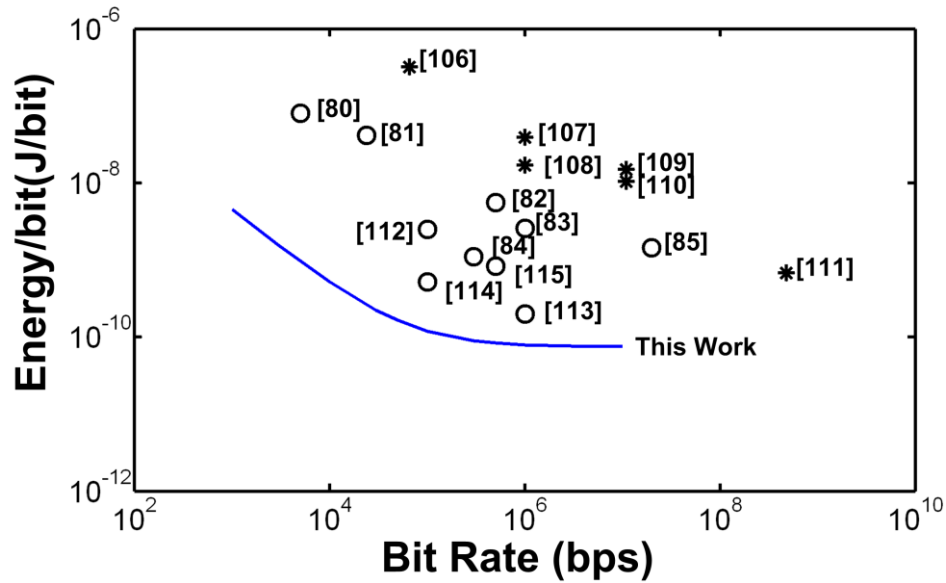


**Figure 4.47. Energy/bit comparison of the receiver with other recently published results, (figure adapted from ref. [112]).**

We also compare the energy/bit performance for our receiver to other designs. This result is summarized in figure as below (Fig.4.47). The energy/bit requirement for this receiver is much lower than any other published design, with a 120pJ/bit at low data rate of 100Kbps.

#### 4.15 Summary

The receiver and transmitter circuit described above can be used to implement an ultra-low-power impulse radio optimized for duty-cycled operation of the power-hungry RF circuits. The measured power consumption for the transceiver was found to be 20 $\mu$ W at 100Kbps while using external timing controller. Lower power at <100kbps data rates can be achieved, though static leakage power eventually can mitigate further benefits. To the best of our knowledge, these operating power levels are far below any other published to date for these data rates, and would enable years of continuous communication with standard batteries or integration with scavenging power supplies.

With ultra-low stand-alone transceiver power, we can now go back to the system design around this transceiver and calculate how much would be the power requirement for the whole system and what type of range of communication we can expect this system to work at. The next chapter will look at the system aspect of the design based on this transceiver design.

## **CHAPTER 5**

### **OTHER SYSTEM REQUIREMENTS AND OVERALL SYSTEM PERFORMANCE**

#### **5.1 Introduction**

The previous chapters have talked about the need of synchronization, the methodology to achieve global synchronization and the design and performance of the FCC compliant duty-cycle-able RF front-end as building component for the system. In this chapter we present in brief the performance achieved for the overall system with the timing circuitry designed in our lab (by project-mate X. Wang). We talk about the timing and power performance of the timing circuits and how they stack up in deciding the overall system performance. We then move to the design & measured performance of some of the wide-band omni-directional antennas required for our application. After the antenna design, we focus on path losses and the expected range of achievable communication by the designed transceiver circuitries. We also discuss how one can increase the range of communication further by increasing the transmitted power due to available margin in the FCC-mask. We then look at scalability of the system for even lower data rate communication and the peak power limit on the transmission power therein which constrains average power at low data rates due to peak-average power ratio (PAPR) constraints.

#### **5.2 Timing Circuitry Requirements & Measured Overall System Performance**

Timing is critical for the overall performance of the system, as it determines how aggressively one can duty-cycle the power hungry RF-Frontend of the radio system.

The Pulse-Coupled Oscillator, the PLL, and the bin-generation blocks are the main timing circuitry in the system. Each one of these circuits is required to be low in timing-jitter and is expected to consume low power as well.

In our lab we built a low frequency PCO operating at 150 KHz (6.5 $\mu$ s period,  $T_{fr}$ ), with a very low timing jitter ( $\sigma_{PCO}$ ) of  $\sim$ 1ns. For the PLL the design achieved a very low timing jitter of  $\sim$ 2ns ( $\sigma_{PLL}$ ), while using a divide-by 128 divider (128-bins), thereby providing a bin size of  $\sim$ 52ns ( $T_{bin}$ ) (Fig.5.1). The Delay-Locked-Loops (DLLs) were used in the design to further control the bin-opening window within the bin to dynamically adapt it to a lower value, enabling duty-cycling within the bin. The overall power consumption of these timing circuitry was measured to be 25 $\mu$ W @ 1V supply in a 90nm CMOS process. The overall timing uncertainty ( $\sigma_{SYS}$ ) with the PCO

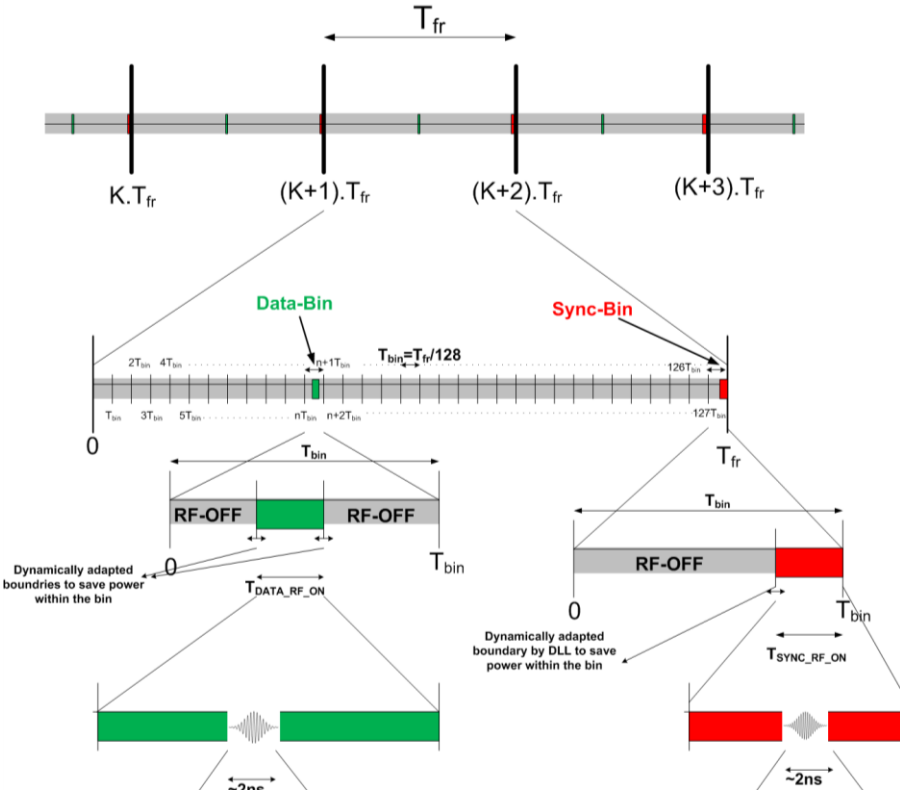


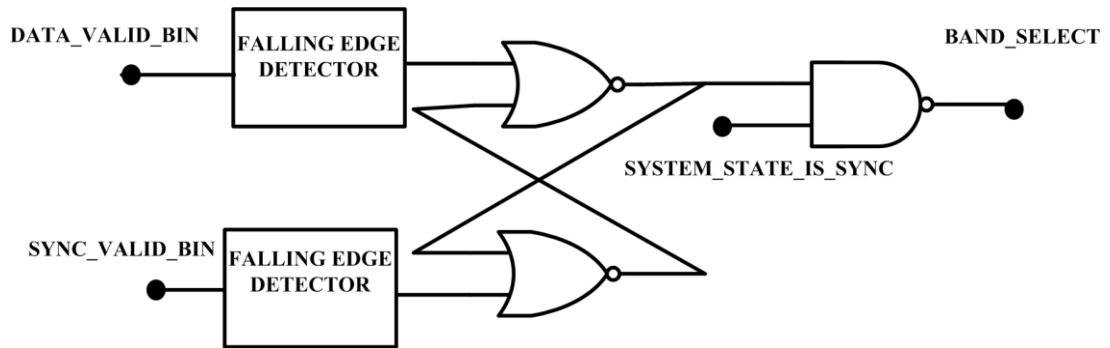
**Figure 5.1. Timing Scheme of the system, the “red” and “green” colored time instances are the ones where the RF is “ON”, during the duty-cycling mode.**

and PLL was measured to be  $\sim 3\text{ns}$ . For a measured pulse-error rate of  $10^{-5}$ , the timing window ( $T_{\text{RF-ON}}$ ) requirement for the receiver was found to be  $\sim 20\text{ns}$ , which takes into account the timing jitter ( $5\sigma_{\text{SYS}} = 15\text{ns}$ ), receiver turn-on time ( $\sim 2\text{ns}$ ) and signal pulse-width ( $\sim 2\text{ns}$ ) in the system configuration.

The band-switching for the receiver and transmitter was enabled by simple set-reset latch based scheme, as shown in Fig.5.2. At the end of the data-bin, the band-selection logic is set to the “sync” bin while at the end of the sync-bin it changes to the “data” bin. In tests it was found that a separation of at least 1-bin between the data and sync bin is required for correct-operation of the band-switching circuitry.

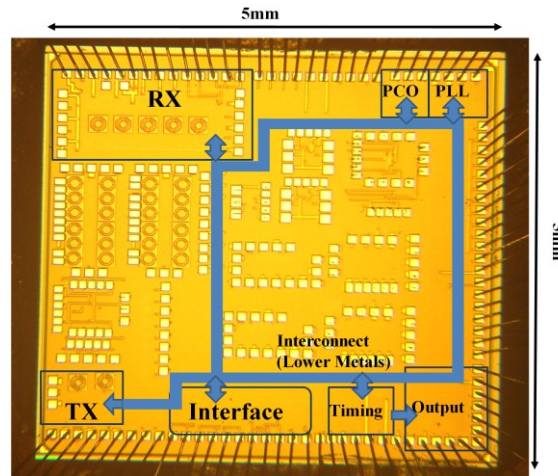
Overall, since in the system configuration the receiver needs to be turned-on twice per frame cycle (Fig.5.1) once for “sync” and once for “data”, the amount of achieved duty-cycling at the receiver with this system was measured to be  $40\text{ns}/6.5\mu\text{s} = 0.6\%$ , which is a very low value.

Table 5.1 provides the overall measured performance of this system at 150Kbps with a design fabricated in a 90nm CMOS process (Fig.5.3) and compares it to the



**Figure 5.2. A simple set-reset latch controlling the band-select logic for the receiver and transmitter. At the end of the data-bin the band is set to the “sync”, while at the end of the “sync” bin the band is set to “data”. The band-switching time was simulated to and measured to be 50ns ( $\sim 1$ -bin) duration, requiring the data-bin and the sync-bin to be apart by at least 1-bin for correct operation of the scheme.**

state-of-the-art IR UWB designs. Fig.5.4 shows the board design encapsulating the radio chip with extra peripheral circuitry, and the antenna.



**Figure 5.3. Die Photo of the system chip with different blocks involved in the design, in a 5mmX5mm die, the actual area occupied by the required circuit blocks was 5mmX2mm.**

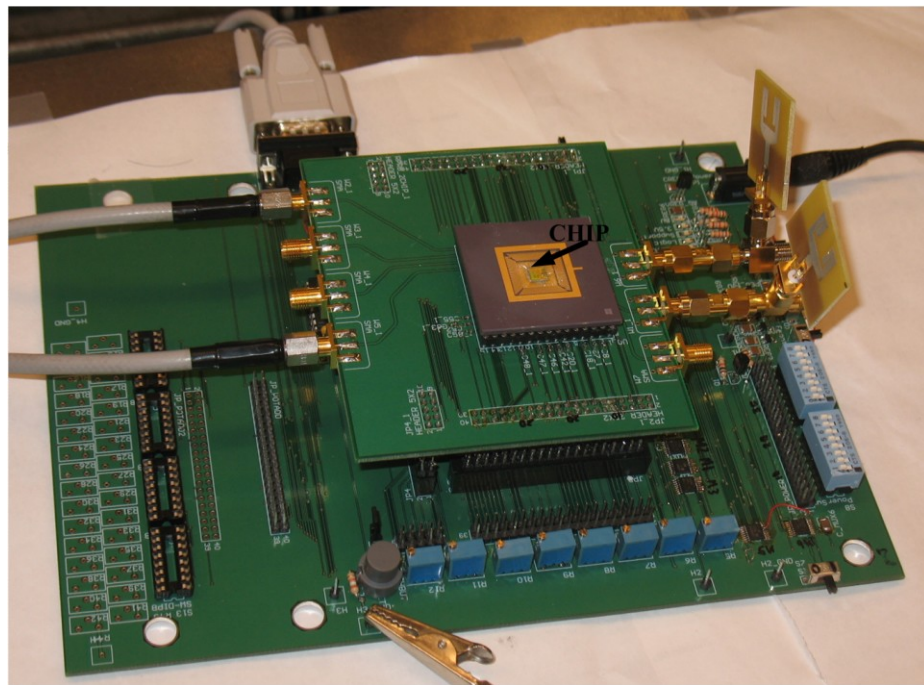


**Figure 5.4. System board with the system chip for system testing.**

**Table 5.1 Performance Summary of the system and comparison with the state-of-the-art IR-UWB design.**

<b>Transceiver Parameters</b>	<b>Our Design</b>	<b>ISSCC 2007<sup>[62][68]</sup></b>	<b>ISSCC 2010<sup>[113]</sup></b>
Process	90nm	90nm	90nm
Modulation	OOK	PPM	OOK
Crystal Requirement	<b>None</b>	40 ppm	None
Scalable Synchronization	<b>Yes</b>	No	No
Receiver Frequency Range	3.5 – 4.5GHz	3.5 – 5GHz	3.6 – 4.3GHz
RX-sensitivity @ $10^{-3}$ BER	-87dBm @ 150Kbps	-98dBm @ 100Kbps	-65dBm @ 1Mbps
Rx- static On power	7.5mw	35.8mw	4.1mw
Rx-duty cycled power at $10^{-3}$ BER	<b>52<math>\mu</math>w @ 150Kbps</b>	250 $\mu$ w @ 100Kbps	1.64 mW @ 1Mbps
RX Energy / bit	<b>0.4 nJ</b>	2.5 nJ	1.64 nJ
2.4 GHz NBI Tolerance at $10^{-3}$ BER	<b>4 dBm</b>	-20 dBm	-8 dBm
Relative In-band SIR for $10^{-3}$ BER	<b>-1dB</b>	-15dB	N/R
Tx-Frequency Range	<b>3.5 – 4.5 GHz</b>	2.1-5.7GHz	2.9 – 3.8GHz
Tx Output Swing	600 mV	700 mV	610mV
Tx-static power	<b>5<math>\mu</math>w</b>	96 $\mu$ w	184 $\mu$ w
Tx power	<b>8.8<math>\mu</math>w @ 150Kbps</b>	99.7 $\mu$ w @ 100Kbps	251 $\mu$ w @ 1Mbps
Timing and Control Power	<b>25<math>\mu</math>w</b>	-	200 $\mu$ w
Total Power	<b>86<math>\mu</math>w @ 150 Kbps</b>	350 $\mu$ w @ 100Kbps	2mW @ 1Mbps

As, can be seen from the table, the design consumes an overall power of  $\sim 85 \mu\text{W}$ , at 150Kbps, that includes the power consumed in the timing circuitry. The numbers for the receiver and transmitter in the overall design are higher due to larger RF-ON window opening at the receiver (20ns as compared to 10ns, 2X), higher data rate requirements (150Kbps Vs 100Kbps, 1.5X), and the fact that the receiver and

**Table 5.2 Measured Timing Performance Parameter of the PCO and PLL**

<b>Timing Parameter</b>	<b>Performance @ 150Kbps</b>
Synched PCO Period Jitter	1.1ns
PLL Clock Period Jitter	1.7ns
Locked PLL Offset from PCO	3ns
PLL to PCO Jitter	2.1ns
Synched PCO to PCO Jitter	0.1ns

**Table 5.3 Measured Power Performance Summary**

<b>Block</b>	<b>Power (uW) 150Kbps</b>
RX	51.8
TX	8.8
PLL	7.9
Timing	10.5
PCO	6.8
<b>Total</b>	<b>85.9</b>

transmitter need to be switched on twice per frame (2X), thereby contributing to increment in the power consumption of the receiver and the transmitter circuitries from a combined  $20\mu\text{W}$  as stated earlier to  $61\mu\text{W}$  in the system configuration at 150Kbps. In addition with the  $25\mu\text{W}$  power consumption in timing circuitries this puts the overall measured power requirement for the system at  $86\mu\text{W}$  (Table 5.1). Table 5.2 shows the timing performance summary of the PCO and the PLL blocks designed in our lab by project-mate X. Wang, while Table 5.3 gives the summary of the measured power of various blocks in our system.

As can be seen from the comparison of the design, our design not only provides a crystal-less synchronization but also results in to the best power numbers of all the recently published results in IR-UWB design space.

### **5.3 Ultra-Wide-Band Antenna Requirements for the System**

With the ultra-wideband nature of pulsing involved in our system, we require antennas that can radiate electromagnetic energy in the environment over a large range of frequencies. For a wireless sensor network application, these antennas are also required to be omni-directional. Monopole antennas in literature have been found to

provide wide-band matching [86-89], and in this section we talk about the measured results of some of the antennas that we designed in this project that meet the requirement of the system.

Fig.5.5 shows a monopole antenna, that we used for initial testing of the system, the simulated radiation profile was omni-directional, while wide-band matching between 1.6GHz-10GHz was simulated using HFSS. Fig.5.6 shows the measured S11 and S21 performance of the same antenna, as can be seen even though the simulated performance of the antenna indicates a wide-band match between 1.6GHz-10.5GHz, in measurement matching was found to be only between 1.6-4.1GHz. This was due to

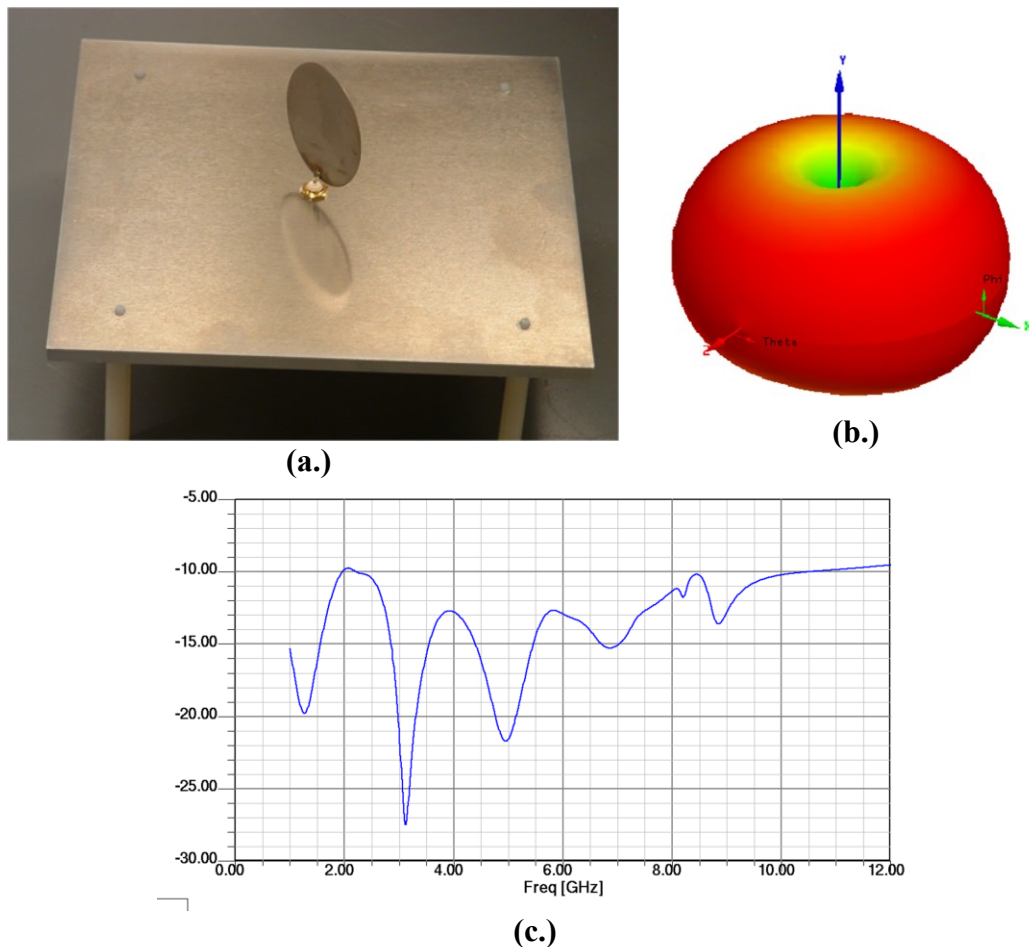


**Figure 5.5. (a.) Designed vertical monopole antenna with a radius of 2.5cm (b.) radiation profile and the (c.) performance simulation using HFSS**

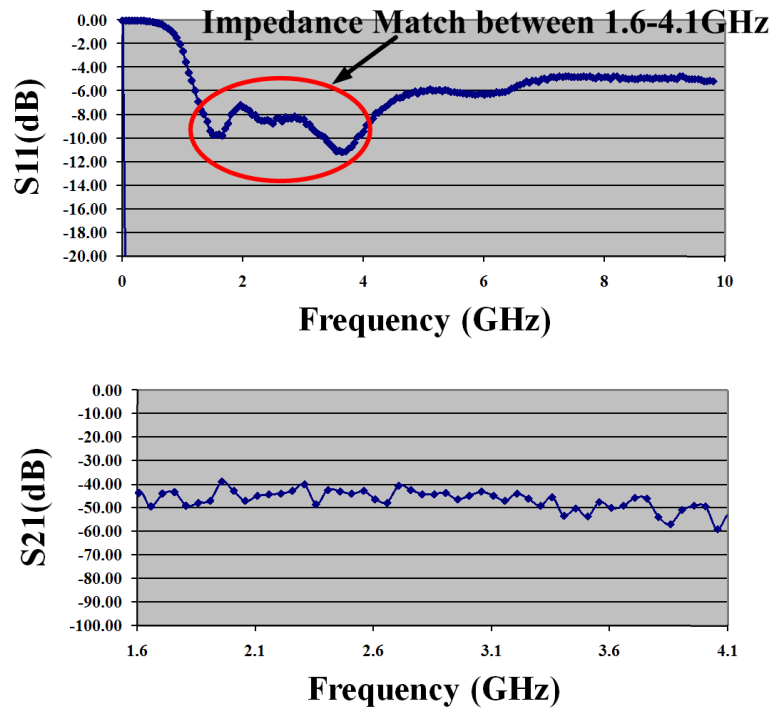
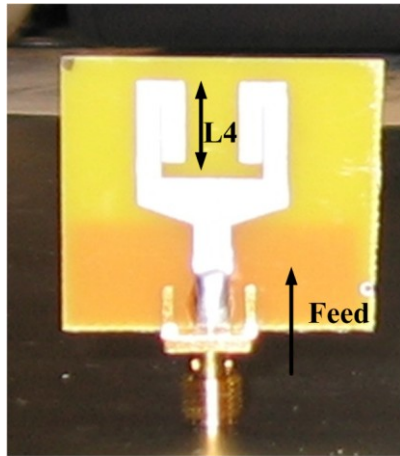


**Figure 5.6. S11 measurement showing wide-band matching, and the path loss (S21) over 1.2m distance with elliptical monopole antenna.**

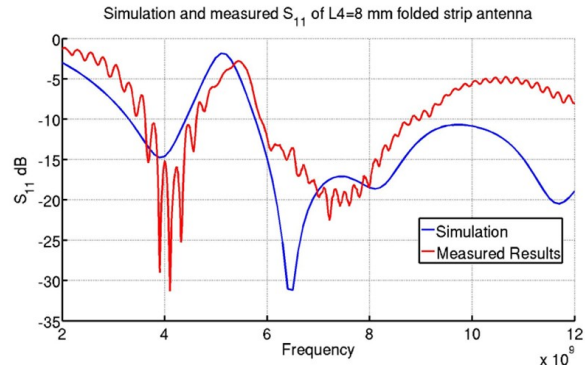
the antenna impedance dependence on the vertical air-gap. The path loss over 1.2m range was measured to be only 45dB. The dependence of the radiation profile based on air-gap can pose system integration problems, and so we instead propose to use planar monopole antenna designs, which are easier to fabricate on standard PCB.

Fig.5.7 shows the design and measured results of a folded-strip monopole planar antenna based on work done by [90]. These antennas were designed to operate between 3.5-4.5GHz, while providing a notch at WLAN frequencies by controlling the dimension of the antenna. Good agreement between the simulation and measurement was found using these antennas, compared to the vertical antenna. More details about the working principle behind these antennas can be found in ref. [90].

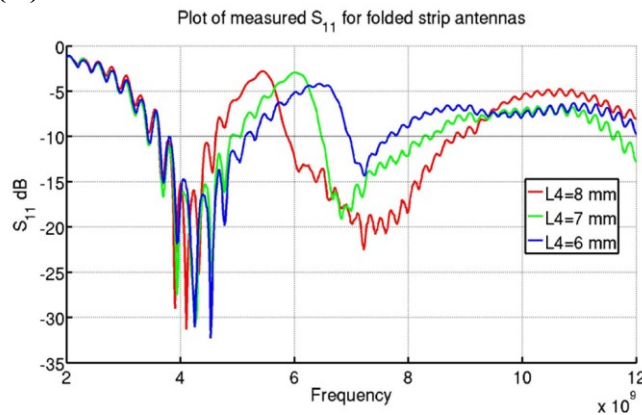
While, we used some of these antennas for our system in initial testing, there are multiple monopole antennas now commercially available in very small size that



(a.)



(b.)



(c.)

**Figure 5.7. (a.) A folded-strip monopole UWB antenna. (b.) S11 matching measured Vs simulation (c.) Measured S11 for different dimensions of the antennas.**

provide omni-directional radiation profiles as well as wide-band impedance matching and efficient radiation characteristics over the frequency range of 3.1GHz-10.6GHz.

Due to availability of these well-characterized small-size wide-band commercial antennas, the system requirement of a bandwidth of 3.1-5GHz can be easily achieved. Also, as shown in Fig.5.7 one can shape the antenna geometry to provide rejection to interference at desired frequency, which in our case can be utilized to reject the WLAN narrow-band interferes at 5.1-6GHz band.

## 5.4 Range of Communication

The path loss associated with the impulse based communication scheme is given as in equation (1), below, where  $d$  is the distance in meters.

$$\text{Path Loss } (M) = -40 - 20 \log_{10}(d) \quad (1)$$

In our design transmitter transmits with peak-peak amplitude of  $\sim 500\text{mV}$ , while the receiver can detect a signal of peak-peak amplitude of  $2\text{mV}$ . The path loss margin associated with the channel would be  $-47.9\text{dB}$ . At this channel margin using equation (1) above we get a range of communication of  $2.5\text{m}$ . Using the designed omnidirectional antennas we achieved a measured range of  $1.6\text{m}$ . The lower than expected range can be attributed to losses associated with the long cable and radiation inefficiency of the antenna.

To further increase the range of communication, one can increase the signal amplitude at the transmitter. Though with a  $1\text{V}$  CMOS process, we were limited to a

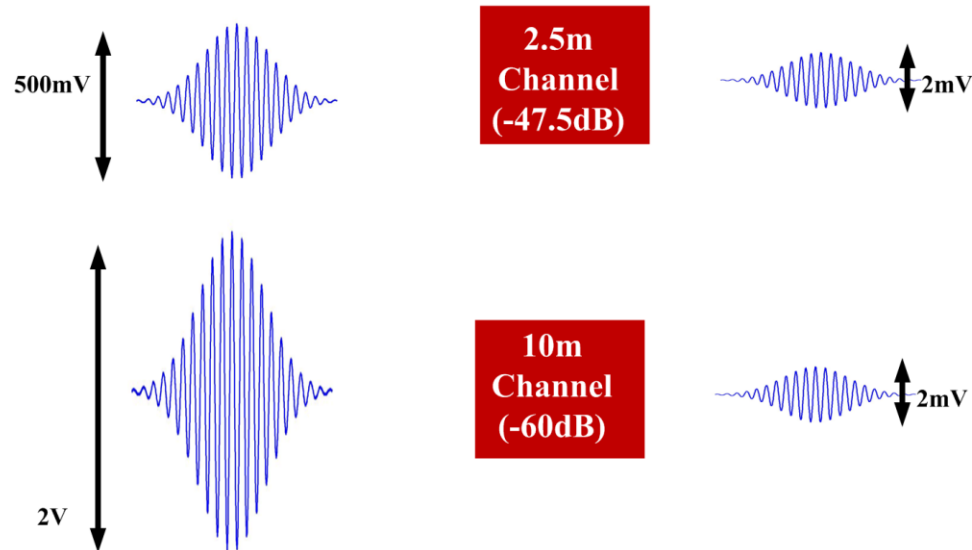


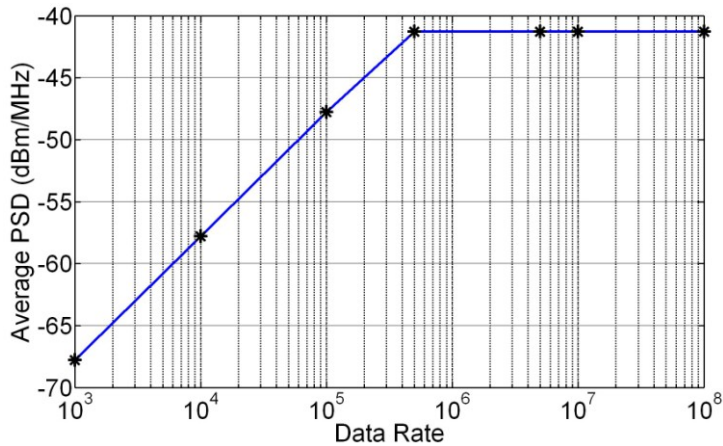
**Figure 5.8. Channel loss and received signal amplitude for different transmit signal amplitude showing the range of communication possible.**

swing of  $\sim 500\text{mV}$ - $550\text{mV}$ . Higher voltage output stages can provide larger swing. As shown in Fig.5.8, by increasing the swing to 2V peak-peak one can increase the range of communication to 10m. This increased range of communication however comes with a 16X increase in the transmitter radiated power as well as increased data-window size requirement of 80ns, which will mean the total system power requirement of  $\sim 230\mu\text{W}$  for our design. This number is still better than more than 10mW power consumption with a Bluetooth based design for same range of communication [91, 92].

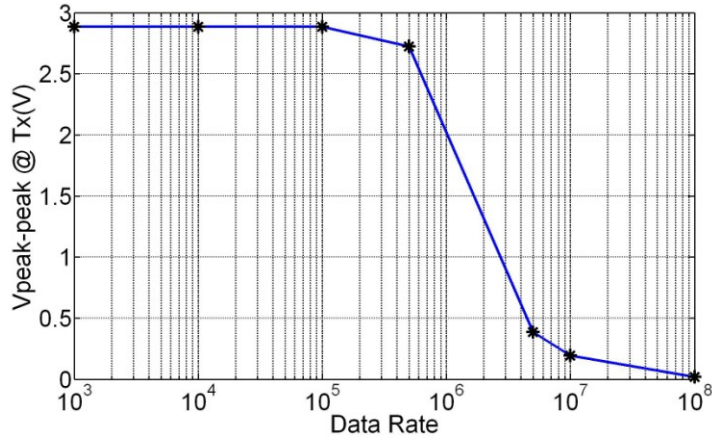
### **5.5 Limits on Range of communication**

As discussed in previous section, using larger transmit signals one can potentially increase the range of communication, albeit at a cost of increased power budget. The increased transmitted signal not only increases the power budget for the system, but may also violate FCC transmission constraints. In this section we determine the range of communication one can expect at a given data rate based on FCC mask constraints and a given Rx-sensitivity. As the FCC mask constraints are on average radiation profile, one can expect higher range of communication at lower data rate. If scaled to very low data rate, that can mean communication range of 100's of m or km, due to increased instantaneous signal amplitude that one can have while maintain the same average radiation profile. This however is not the case, FCC, while providing average radiation profile, also provides a peak power profile and is limited to 0dBm/50MHz and is measured using the spectrum analyzer in the peak-hold mode.

An extensive formulation of this limit was done by Wentzolf et.al, and the corresponding details can be found in ref. [70]. The outcome of this is that at lower data rate, one can't really increase the range of communication due to peak-power limit given by FCC which limits the average power radiated at low data rate to very



(a.)



(b.)

**Figure 5.9. a.) Average power limit at various pulse-repetition rates, and (b.) the corresponding impulse peak-peak swing limit.**

low value. We use the formulae given by Wentzlf et.al in ref. [70] to evaluate these limits.

Fig.5.9.a shows the average power limit at different pulse repetition rates, and the corresponding peak-peak amplitude limitations on the transmitted signal. While at higher data rate one can utilize the full limit of -41.3dbm/MHz, at low pulse-repetition rates, the average PSD is required to be lower due to the peak-average power ration constraints imposed by FCC. This means the maximum peak to peak voltage of the impulse is limited to ~2.9V, and one can't expect to use these impulse based radios for

extremely high range of communication (Fig.5.9.b). An improvement in the receiver sensitivity only can then give higher range of communication.

Fig.5.10 shows the range of communication one can achieve using an impulse radio at different pulse-repetition rates based on channel loss model (1) and the FCC-regulated peak as well as average power constraints. Higher range at high pulse repetition rate (average-power limited range of communication) can be achieved by using different frequency-bands. Since in the 3.1-10.6GHz UWB range one can have up to 14 channels, these channels can be utilized for increased range by frequency-hopping, thereby reducing average power in a frequency band. Though, in the peak-power limited range of pulse-repetition rates, one can't increase the range of communication even with frequency hopping. Increased receiver sensitivity or processing gain used by frequency-coding schemes (using multiple bands

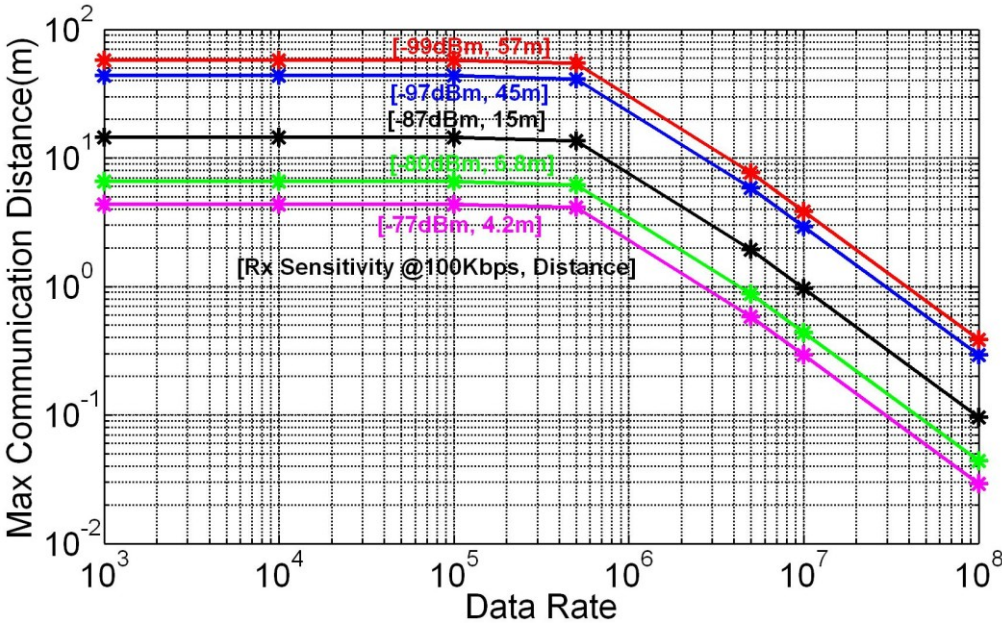


**Figure 5.10. Pulse Repetition rate Vs. maximum communication distance achievable using the FCC constraints on the radio. While at high data rates, the range of communication is limited due to average power requirements, at lower data rate the range of communication gets saturated due to peak power radiation constraints.**

simultaneously) are the only ways one can improve the range of communication.

## 5.6 Chapter Summary

In this chapter we presented the overall system performance, while considering the timing circuitry performance in the system. At 150 KHz repetition rate, the overall system power was measured to be  $86\mu\text{W}$ . Our designed system, while providing scalable crystal-less synchronization scheme, is also 5X lower power compared to other state-of-the-art impulse radio designs.

We also designed monopole antennas which were simulated to have omnidirectional radiation profile, and were measured for wide-band matching and radiation that provided a communication range of 1.6m. With more efficient commercial antennas, and smaller cable length one can increase the range to  $\sim 2.5\text{m}$ . Range can be increased by increasing the transmitted power. For example an increase of 16X radiated power at the transmitter, giving 2V peak-peak can provide a range of 10m for an expected overall power requirement of less than  $230\mu\text{W}$  system power. An analysis of the maximum achievable range of communication was also presented at various data rates, based on FCC's peak as well as average power constraints. It was found that with various practical receiver sensitivities one can achieve range of up to 50m, albeit at higher power consumption, without violating the FCC mask. Since, in most of the wireless sensor networks the communication-range requirements are in the 1m-30m range, designs operating in the FCC-mandated 3.1-10.6GHz range can be utilized for unlicensed wireless communication.

## CHAPTER 6

### SYNCHRONIZATION DETECTION AND RETENTION METHODOLOGY

#### 6.1 Introduction

While the proposed PCO based global synchronization scheme creates a common time-base for various nodes in a network, duty-cycling also requires that the nodes know if and when they are synchronized to the rest of the network. This chapter covers localized detection of system synchronization in a pulse-coupled oscillator based system. The proposed methodology enables localized per-node detection of synchronization and does not rely on any packet based communication or other hand-shaking signals for this purpose. The proposed synchronization consists of a state-machine that tracks the advent of synchronization based on timing correlation of two signals on a per node basis. These two signals are the detection of external sync pulses “sync (detected)” and the signal that indicates the internal firing of the PCO, “PCOout”. Duty-cycling is controlled by this synchronization state-machine. Since, in a realistic network errors in detection pulses can also occur, a scheme is required to maintain synchronization in the event of occasional misdetection of these pulses. In this work we propose an algorithm that helps locally detect synchrony and provides features that enable the system to maintain synchrony even in the presence of misdetections. While synchronized, a self-reinforcement methodology enables retention of synchronized state, while allowing occasional “sync” pulse detection failure at a node. For the scalability of the network the proposed synchronization-state-machine also enables nodes joining and leaving and actively changing in the network, i.e. a dynamic network configuration and organization.

## **6.2 Synchronization Detection**

PCO synchronization can provide a global synchronization in a multi-hop network of randomly distributed nodes starting from an initial desynchronized state. The nodes can synchronize in typically 5-20 cycles, where the exact time taken for synchronization is dependent upon the initial state of the system. While, this synchronization time is of some importance and provides a means to study the dynamics of the synchronization process, for any realistically deployed network, one can think of achieving synchronization as a dynamically evolving process. The nodes in the network cannot be expected to be switched “on” simultaneously, and so any mechanism to sense the advent of synchronization has to be dynamic in nature. Ideally a network will evolve from a single node in the network, and then grow/evolve as new nodes join in the network. In this case, the synchronization and loss of synchronization will be a dynamic process, and a mechanism is required to facilitate this dynamic process in the network.

### **6.2.1 The Methodology for Sync Detection**

In this section we examine the advent of synchronization at any node in the network by taking in to account the relative timing of the external sync-detected (“sync”) pulse and internal PCO firing pulses (“PCOOut”). Looking at the PCO synchronization process and the inherent dynamics therein, one can see various possible network scenarios that can exist in a synchronized state. One such scenario would be a node finding itself isolated in the network, i.e. no node in its own neighborhood. In this case, the node will not get any external coupling from any neighboring node. Such an isolated node in the network can identify itself as such, as the node between its successive firing will not detect any “sync” pulses from the external environment (Fig.6.1). Different configurations can exist in the presence of

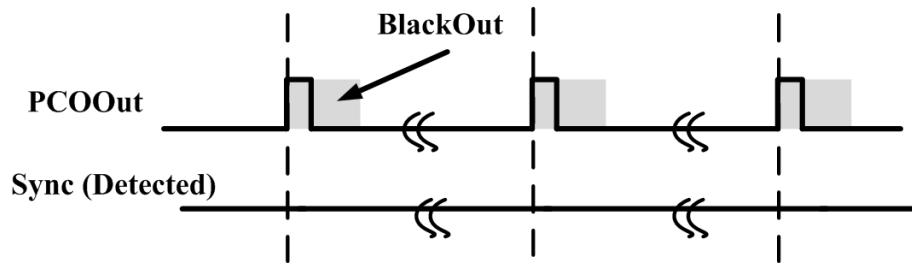


**Figure 6.1. PCOOut and the Sync(detected) timing in the case of a single isolated node in the network**

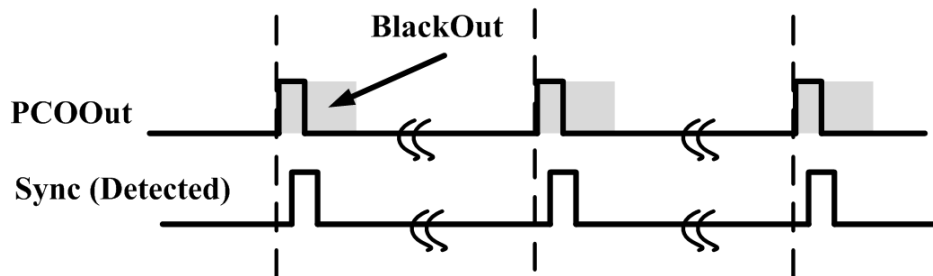


**Figure 6.2. PCOOut and the Sync (detected) timing at a master node in the network. The sync detected pulse is during the phase of the blackout, thereby effectively not resulting into any coupling at the node.**

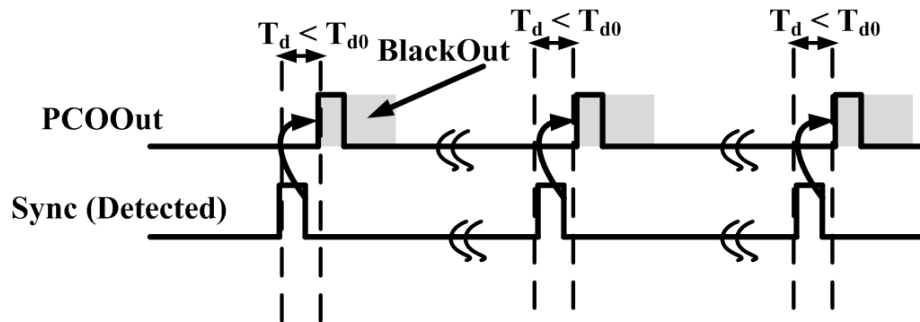


**Figure 6.3. PCOOut and the Sync (detected) timing at a slave node in the network, the time-correlation between the two event is lower than the circuit delays ( $T_{d0}$ ).**

other nodes in the neighborhood of a node. As discussed in chapter 2 before, the PCO dynamics in presence of more than one node in the network always contain a master node, i.e. a node that fires first, before any other node fires. Thus very clearly in a network configuration, with more than one node, some node is supposed to be a

master node, while all other nodes are expected to be dependent nodes, i.e. they fire after they receive a pulse (sync) from the network. A master node in the network, doesn't receive any coupling, due to it always being the first to fire. The master node receives the external sync-pulses only during the phase of the blackout, thus the sync detected pulses effectively get masked (Fig.6.2), from providing any coupling at the node. If a node does not fire based on any external coupling then it can be made to understand as a master node in the network. The slave nodes, i.e. dependent nodes, that are dependent upon the external sync firing before they themselves fire, will have a timing correlation between their sync ("sync") detected pulses and PCO firing ("PCOOut") pulses, i.e. within a small time-window after sync pulse is detected, the PCO fires in the presence of synchronization. This time-correlation can be detected using the time-correlation window, and can be easily implemented by stretching the sync-detected signal by a small amount and seeing if the PCO fired in that window by doing a logical "ANDing" of the stretched "sync" detected pulse and the PCOOut pulse (Fig.6.3).

Since, in a PCO scheme, a node always sends out a "sync" pulse, after the internal PCO fires, it may result into self-detection of the sync-pulse if the receiver is not "turned-off" during the transmission. This self-detection of the "sync" pulse means however that a "master node" cannot distinguish itself from an "isolated node" in such cases and vice-versa. However, this is not a problem as an isolated node in the network can be effectively considered as the "master node" in its own neighborhood. The only limitation is that a "master node" in network will not effectively be aware if other nodes exist in the system or it's the isolated ("only") node in the network. However, the node can find out the presence of other nodes if packet communication happens.

As explained before, a node in the network is always either a “master” or a “slave” or an “isolated” node. And there exists relative timing between sync-detected pulses and PCOout pulses at the time of synchronization that can be exploited to establish the advent of synchronization at a per-node basis. While, this relative timing of the pulses can help us establish synchronization, one needs to have a state-machine that tracks and counts the number of time these time-correlated events were found, to enable setting the system state to “synchronized” only after these correlations have occurred continuously for some preset number of time.

Other cases of timing can also exist at a node in the network during the process of becoming synchronized. These need to be tracked to understand non-synchronized state. Conditions like two or more “sync” pulse detections before successive firing of

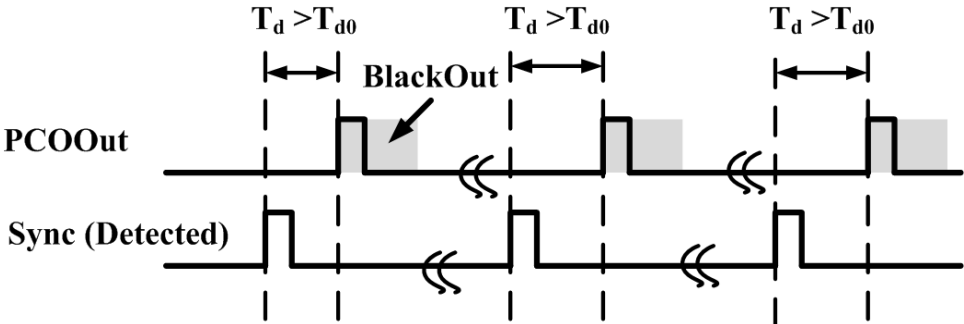


**Figure 6.4.** PCOOut and the Sync(detected) timing, unsynchronized state, as the correlated delay between the two signal is large.

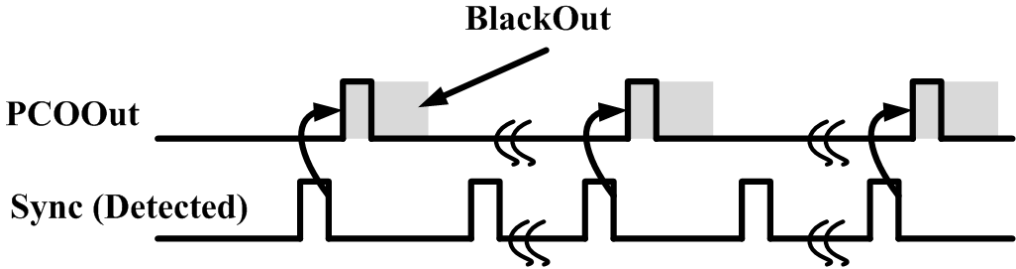


**Figure 6.5.** PCOOut and the Sync (detected) timing, unsynchronized state as more than one sync-detected pulses were detected between consecutive firings of the PCO.

the PCO, will mean the coupling occurred twice or more, and is not the condition for synchronization (Fig.6.4). Similarly if only one “sync” pulse is detected between successive pulse firings, but the time-delay between the two was large, then also it shouldn't be counted towards synchronization detection, as the two pulses don't occur in the small time-window of correlation (Fig.6.5). Based on the relative timing of these two pulses one can design a state-machine that follows the synchronization detection algorithm to detect the advent of synchronization and can help maintain different synchronization states.

### **6.2.2 Synchronization Retention and facilitating node joining and leaving the network**

Once in a given network a node is identified as a master or isolated node, it's the node's responsibility to look for changes in the network. For example in the case of an isolated node, it's the node's responsibility to look for new node joining in the network, thereby facilitating synchronization with the new node. Similarly for a master node, if a new node joins the network, it needs to facilitate the switchover role if required. So, the synchronization state-machine which will be required for the system has to take into consideration this aspect of the system. Similarly for a slave node, a scheme is required to facilitate retention of synchronization i.e. even if occasional sync pulse misdetections happen, it should not result into the loss of synchronization. Based on frequent and consecutive misdetections the node should also be able to dynamically move to an unsynchronized state, where it will open the whole timing window i.e. non-duty-cycled state.

### **6.2.3 Sync State Detection Algorithm**

Overall, based on the discussion in previous sections, an algorithm was devised to help enable the detection of synchronization. The central algorithm for proposed

system sync detection is dependent upon these three basic events.

1.) A sync detection event: A sync event is registered whenever a sync-pulse is detected at the receiver.

2.) A PCO firing event (PCOOut): A PCO firing event is registered whenever the PCO is fired.

3.) A SYNC\_PCO\_OVERLAP event: An event signal which looks at the relative timing between the sync event and the PCO firing event (PCOOut), this event is registered whenever the sync-detection event is followed by a PCO firing event within some small programmable timing window decided by the circuit delays, which establishes the time-correlation of the two.

Various counters can keep track of the number of sync detection per PCO-cycle as shown in Fig.6.6. Out of these basic events the two fundamental events are created (Fig.6.6). An Event-1 is registered whenever SYNC\_PCO\_OVERLAP event happens subject to the condition that the number of sync detections during successive firing of the PCO is less than or equal to 1. An Event-2 is registered whenever the PCO firing happens without detecting any sync event during successive firings of the PCO.

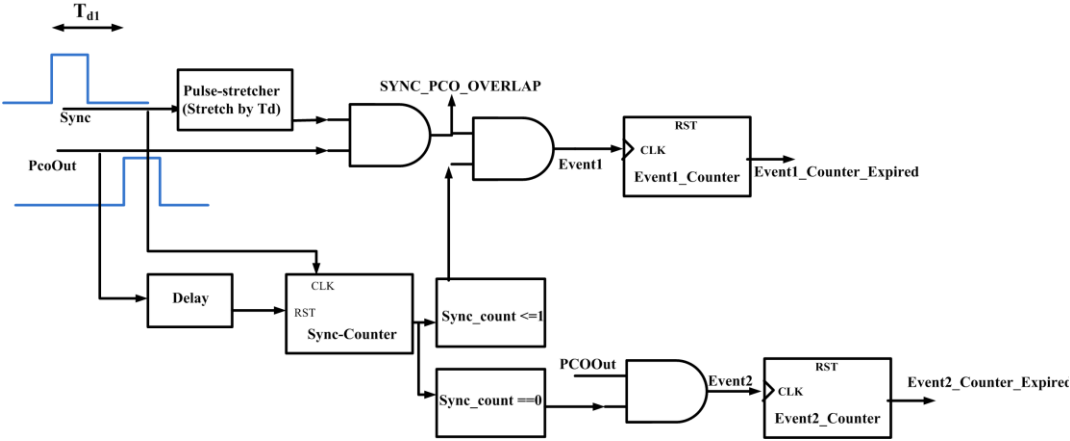


**Figure 6.6. Event Generation and detection circuits. These events control the system synchronization state machine.**

(Fig.6.6). these two events are important inputs to the state-machine that are used to control and detect the system synchronization. Continuous detection of Event-1 means the node is synchronized in a slave-configuration. While the detection of Event-2 means either the node is alone in the network or is the master, i.e., either way duty cycling can happen. Note, the slave and master configuration for a node is self determined and is dynamic. A Slave configuration means the node fires after detecting sync, i.e. a slave configuration means the node needs coupling from other nodes in the network during synchronized state. While a master configuration means the node is the first to fire and that it doesn't need coupling from other nodes. The PCO firing by other neighboring nodes (if available) in this case gets buried in the blackout window and hence doesn't impact the PCO of the master node.

The programmable counters in the system help keep the count for event-1 and event-2 thereby helping the state-machine to transition from a non-synchronized state to synchronized-state. Provision is also made for a reinforcement counter in the system that keeps track of the number of times the self-reinforcement has happened, thereby detecting potential loss of synchronization and helps the state machine transition back to non-synchronized state. Similarly there is a lookout counter that facilitates a node in the master configuration to go out and open the window to see if any new nodes have joined the network occasionally, which are not in synchronized state or if there is a requirement for the node to switch roles. The lookout counter gets triggered whenever a pre-programmed lookout counter expires and is masked when data-communication is happening in the system.

#### **6.2.4 System Synchronization State Machine**

The state machine (Fig.6.7) works on tracking these two main events (Event-1, Event-2) and is clocked with the PCO-firing events.

*Step1:* Start with `system_synch_state=0`;

*Step2:* Wait for either the event-1 or event-2 counters to expire, if event-1 counter expires, that means the system has synchronized in the slave configuration, while if the Event-2 counter expires that means the system is in master configuration. The state machine transitions to a new state indicating node synchronization. `SYNCH_TYPE` “S1” or “S2” keeps track of which event type forced the system into the synchronized state. Either event allows the duty-cycling of the receiver.

*Step3:* In the `SYNCH_TYPE` “S1”, the system keeps track of event-1, if event-1 is missed, the reinforcement state machine (explained later) keeps track and if it finds that the reinforcement count has been exceeded, then it helps the state-machine transition first to an intermediate step, before transitioning to a non-synchronized state. From the intermediate state `SYNCH_TYPE` “S3” the system can make a transition back to “S1” if it detects Event-1 else it transitions back to completely non-synchronized state as in step-1. This scheme helps the system to maintain synchronization with Reinforcement as well as helps detect the loss of synchronization.

*Step4:* In the `SYNCH_TYPE` “S2”, the system keeps track of lookout counter, and if the lookout counter gets expired, the system goes into an intermediate state `SYNCH_TYPE` “S4” and opens the RF window completely to see if it still detects an Event-2. If it doesn't detect Event-2, then the node goes back to unsynchronized state as in step-1. But if the system sees an Event-2 it goes back to `SYNCH_TYPE` “S2” state. The intermediate state “S4” in this case helps the node to go out and open the window while looking at possibly any new nodes joining the network or a change of role for the node from master to slave.

This intermediate state also helps the node to quickly change back to `SYNCH_TYPE` “S2” in case the network condition hasn't changed. This step ensures,

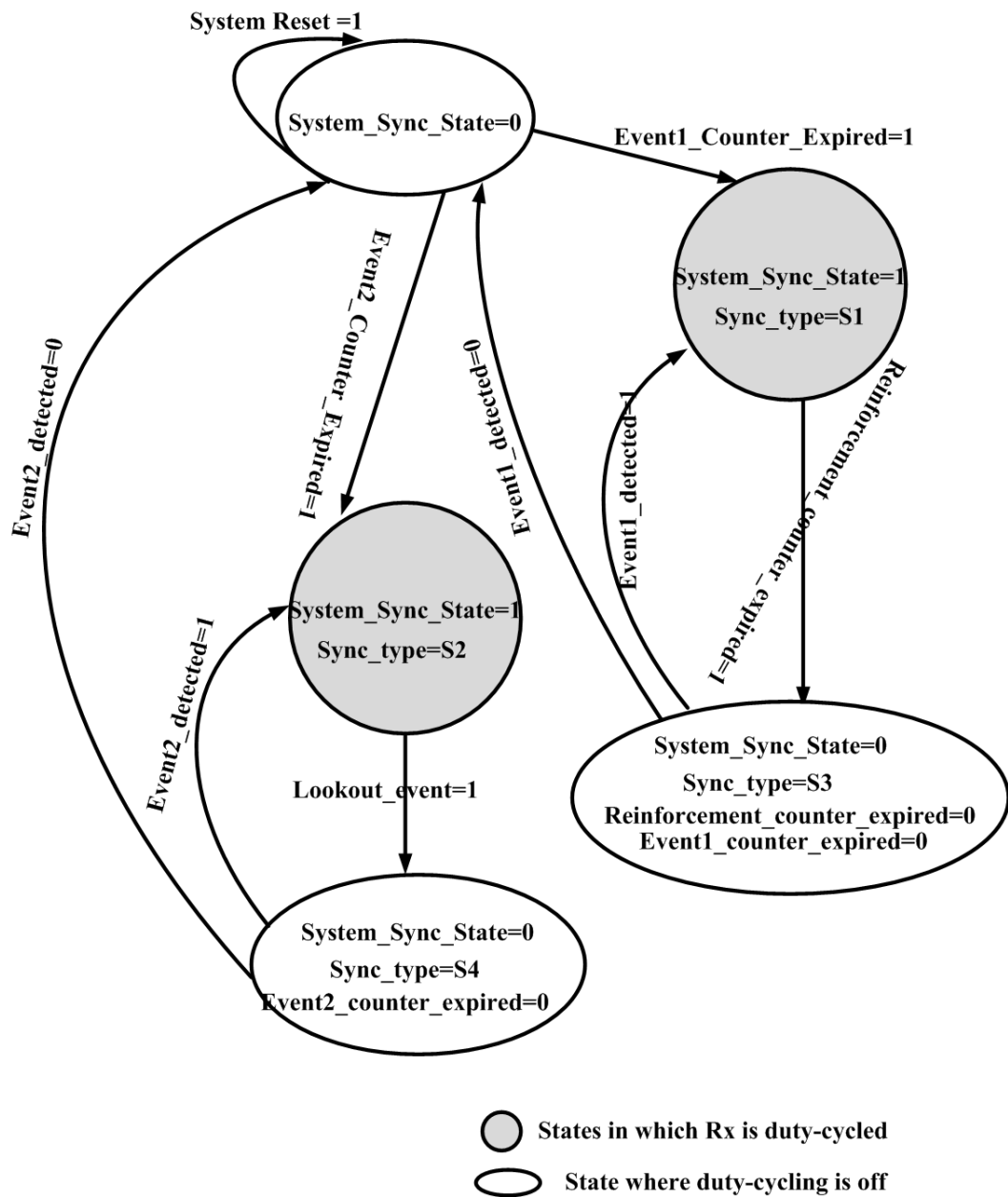


**Figure 6.7. System Synchronization State Machine.**

that if someone joins the network after the network is built-up or if two nodes which were otherwise not connected come closer, then they can have a chance to get synchronized based on the changes in the spatial distribution of the nodes in a dynamic system. It also takes care of the cases where a master node might have to

change itself to a slave node, due to a faster node joining the network. The duty cycling of the RF is “off” when the `system_sync_state` is set to “0”. Whenever the `system_sync_state` is “1”, the duty-cycling of the RF is enabled.

### 6.3 Self-Reinforcement

When a node goes into a synchronized state as a slave node, it might still be a master node to some other set of nodes in its own neighborhood for a large multi-hop network. In such scenarios, in a synchronized state if this type of node somehow misses detection of a “sync” event, then letting the node fire according to its own PCO state-function may result in a significant timing problem for the node itself as well as

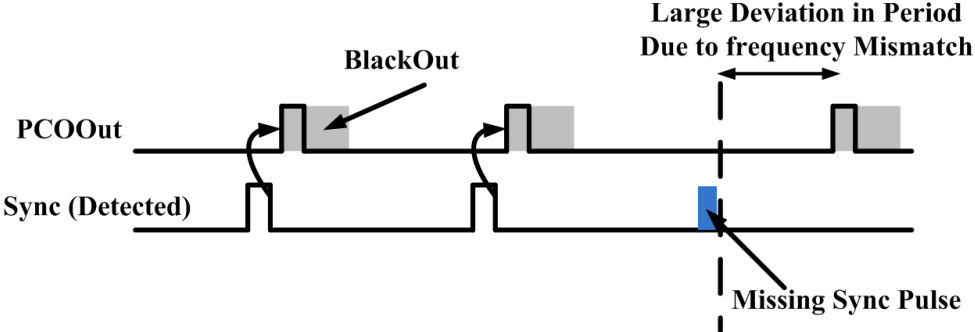


**Figure 6.8.** PCOOut and the Sync(detected) timing, in case of missed sync pulses, that results in to large deviation in period.

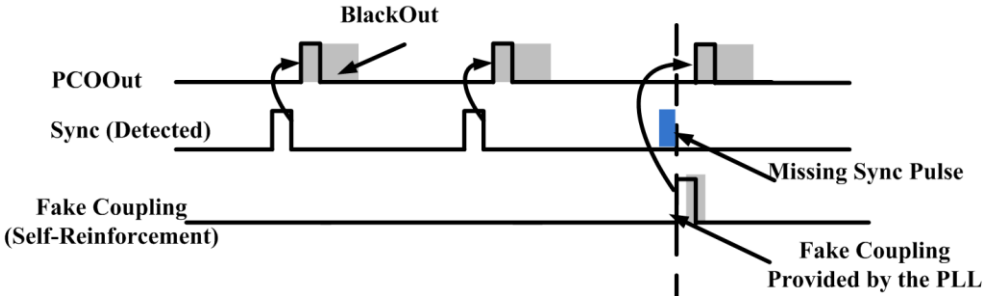


**Figure 6.9.** PCOOut and the Sync (detected) timing in case of missed sync pulses, with the incorporation of the fake coupling provided by the PLL, at the expected time of the sync-detection pulse.

the network due to process mismatch in the PCO frequency (Fig.6.8). This is where the self-reinforcement comes into the picture. In the self-reinforcement scheme, we take advantage of the PLL in our transceiver chain which is synchronized to the PCO firing event (PCOOut). Since, in a system synchronized state, the PLL is expected to be synchronized to the PCO, in case of missing a “sync” event, the PLL will still be able to guide the node about the relative expectation per the timing of sync-event occasionally (based on prior history of the pulses). The PLL, by generating a fake coupling signal in the event of missing the sync event (Fig.6.9), can help maintain synchrony in the presence of errors.

The implementation of this scheme (Fig.6.10) is straightforward. In a system synchronized state a node enables the self-coupling to the PCO, by the PLL’s clock-edge which is synchronized to the PCO’s firing event. To avoid a race condition between detection of Event-1 and PLL’s clockout, a small delay is provided before the PLL clock self-couples to the PCO. This delay also helps in registering an event-1 “miss” for the node. Which is important for the node to keep track of its synchronized state in conjunction with the system synchronized state machine and the reinforcement state machine (explained below).

### 6.3.1 Self-Reinforcement State Machine

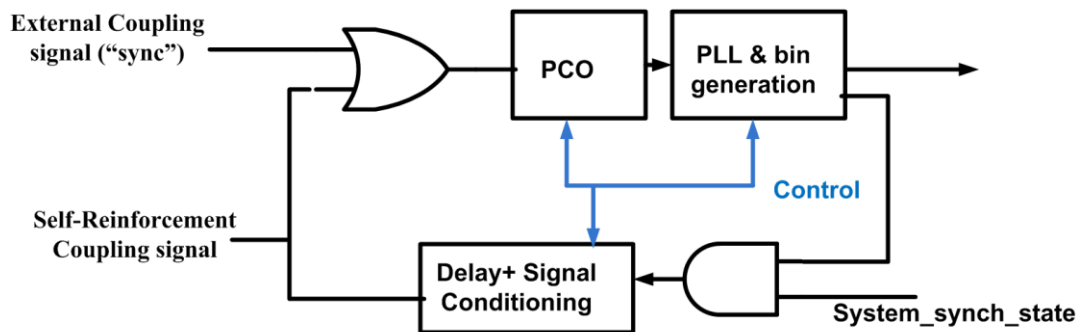


**Figure 6.10. Reinforcement implementation scheme (simplified block diagram).**

The reinforcement state machine (Fig.6.11) keeps track of the reinforcement count and is required only if the node goes into the synchronized state as a slave node, i.e. SYNCH\_TYPE= "S1". If self-reinforcement is enabled the PLL locked to the PCO will provide the reinforcement to the PCO which will ensure that the pulse coupled oscillator system doesn't lose synchronization and that the other nodes in the network waiting on the PCO firing at the expected time do not fail. Even though the implementation of the self-reinforcement is done in a decentralized manner, the state machine will come to know that the self-reinforcement has happened as it will detect a non occurrence of event-1. Based on the knowledge of missing the event-1, the state machine increases the reinforcement count, till the count expires based on pre-programmed value.

This reinforcement thus helps in maintaining the synchronization as well as detection of loss of synchronization and can be implemented using standard logic gates. Reinforcement for some network might also be disabled based on the internal PLL drift and the synchronization accuracy requirements of the system. For most of the system though, one or two cycles of continuous reinforcement would be reasonable.

#### **6.4. Modification while incorporating the PLL locking signal**

Since, the duty-cycling of the RF block is finally controlled by the bin generation logic dictated by the PLL, it's important to ensure that the PLL has also locked before the duty-cycling of the RF is enabled. While, delaying the duty-cycling for 5-10 cycles (the worst case lock time of the PLL) even after the state-machine has detected synchronization can ensure that the PLL has locked to PLL, process variation can cause this lock time to vary, a safer approach in that case would be to detect the synchronization of the PLL to the PCO, which can again be implemented by the local

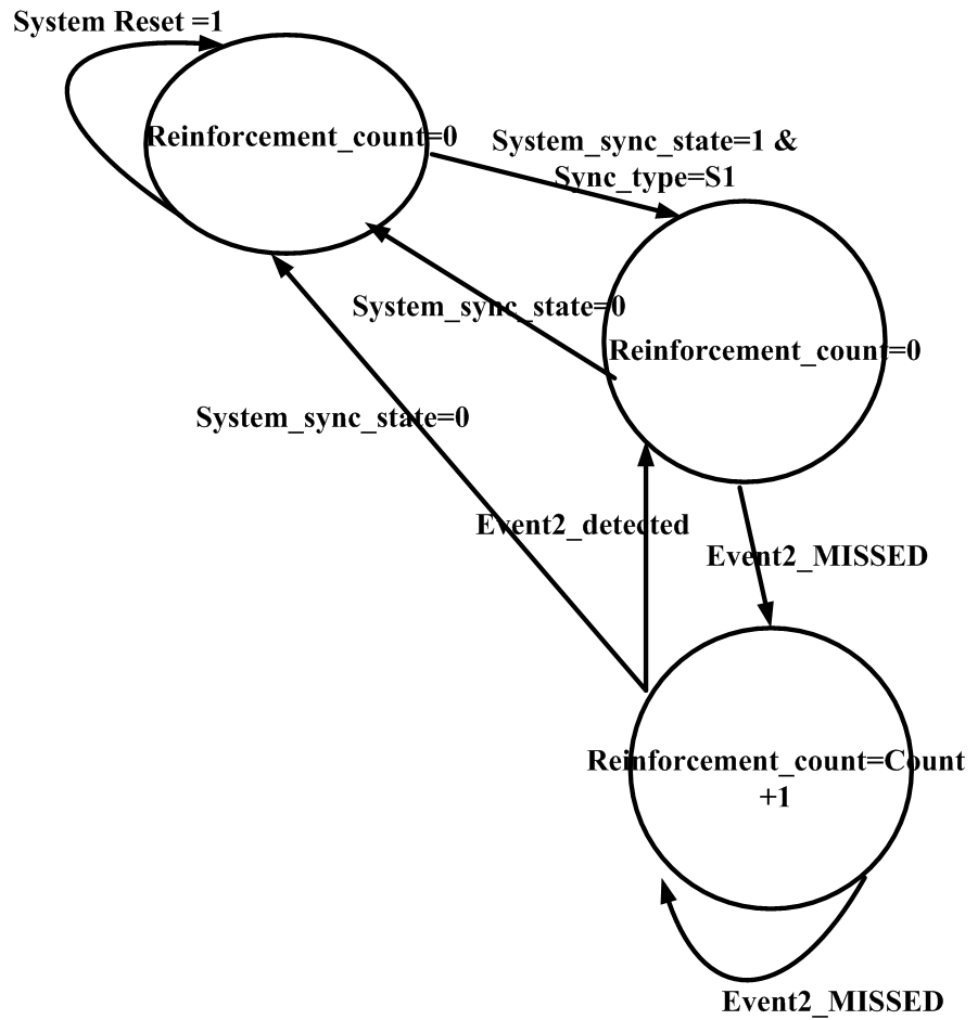


**Figure 6.11. Reinforcement State Machine keeps track of Reinforcements also helps in detecting the loss of synchronization in conjunction with the system synchronization state machine.**

correlation of the pco and pll signal for both the +ve time offset as well as -ve time offset as shown in Fig.6.12. In this case the PCO\_PLL\_OVERLAP Signal which measures the correlated advent of the PCO and PLL edges within a small time window help determine the PLL locking to the PCO and can be easily implemented with simple logic and counters.

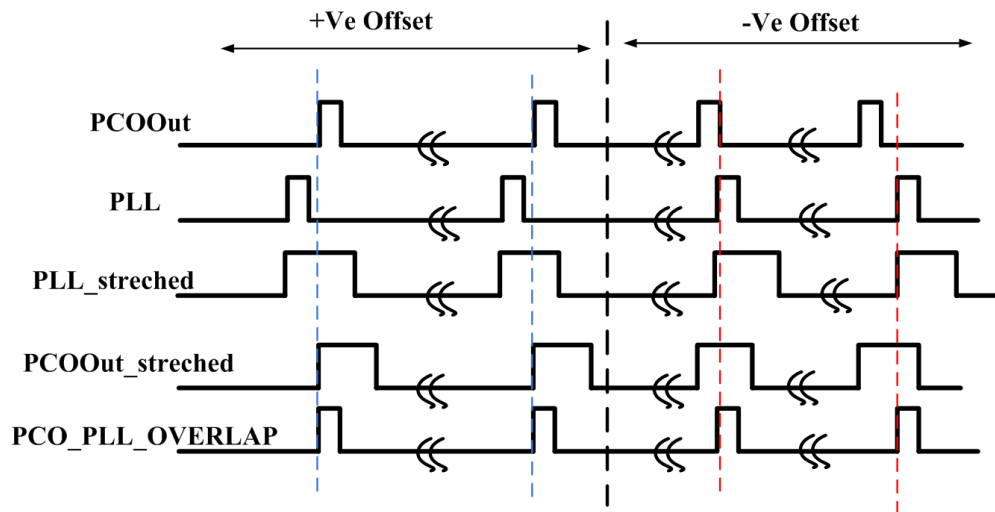


**Figure 6.12. PCOOut and PLL correlation to generate the PLL-Lock signal**

### 6.5 Matlab Simulation of Synchronization state machine

A Matlab simulation was done to verify functionality of the proposed scheme. The basic structure of the simulation for the PCO was kept the same as the one elaborated in chapter-2. Event based simulation helped in saving the simulation time, as the information for detection of synchronization are still dependent upon the PCO firing and the sync detections (i.e. coupling).

The scheme was found to be working as expected, with the nodes individually being able to determine when they are synchronized to the rest of the network (Fig.6.13). Errors were also injected to see the behavior of the network dynamics. Fig. 13 shows the phase of different nodes in a network configuration. Initially the nodes start with unsynchronized state (red), while slowly they get synchronized (green or black). As can be seen one node identified itself as synchronized as the master node (black) while all other nodes identified themselves as synchronized as 'slave node'(green). Later on as we inject errors (i.e. misdetections) at different nodes at random times, the nodes lose synchronization. In this simulation the self-

reinforcement was disabled.

We also did the simulation while enabling the self-reinforcement feature. As shown in Fig.6.14, the node again starts from unsynchronized state (red) before getting synchronized. In this case, unlike the previous case, when the errors are injected, the nodes stay in synchronized state, due to self-reinforcement feature.

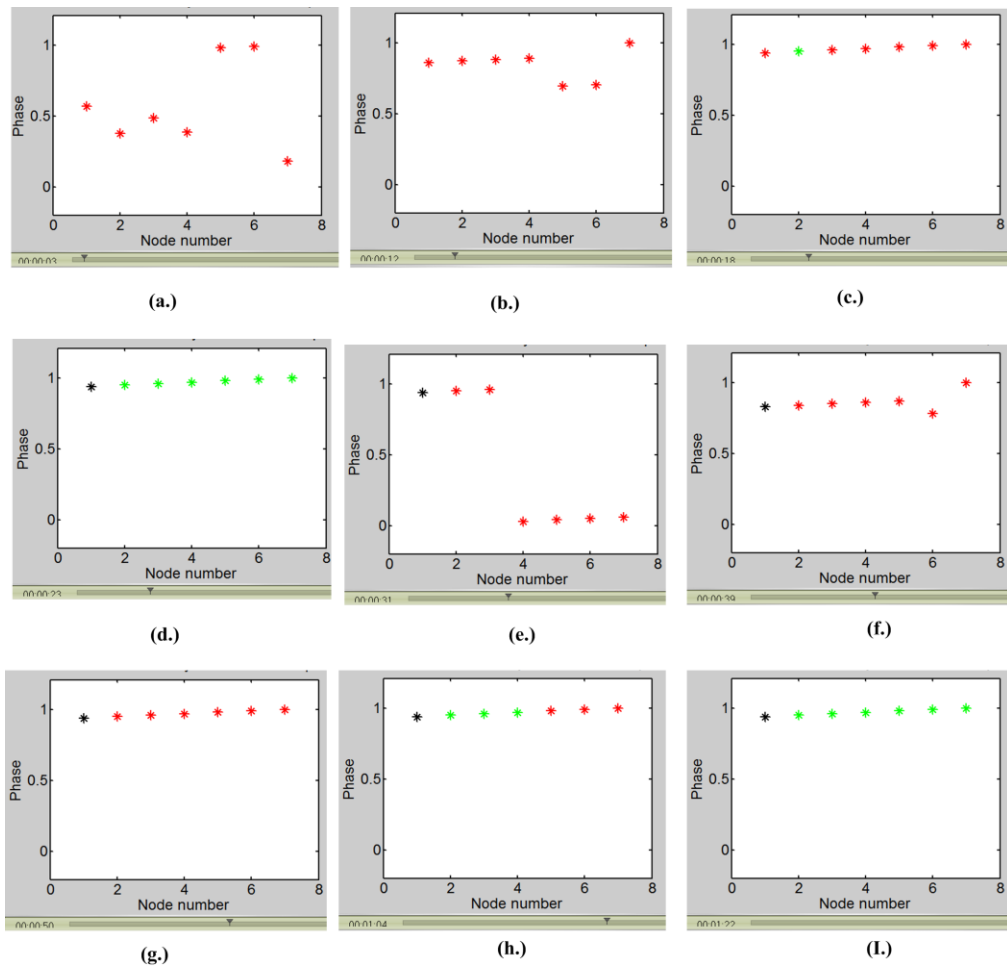


**Figure 6.13. Time evolution of the phase of different nodes (a total of 7 in this case) at different instances of time without reinforcement. Red indicates unsynchronized state, green- synchronized in slave, and black- synchronized in master mode. Nodes start from unsynchronized state, then get synchronized, while losing synchronization due to misdetection, but able to regain synchronization.**

In Fig.6.15 & Fig.6.16 we show the time evolution of the nodes in the network with random error injection at different nodes in the network, with and without the self-reinforcement feature. As can be easily seen, in the case where the self-reinforcement feature is disabled (Fig.6.15), the misdetections result into large deviation of the successive period for each oscillator in the network, this is due to large frequency variations between different oscillators.

While, with the self-reinforcement feature enabled no such frequency period deviations are there even in the presence of misdetections, as the PLL in this case gives an exact estimation of where the pulse was expected to arrive, and forces the circuitry to self-reinforce. The PLL was assumed to provide an exact estimation of

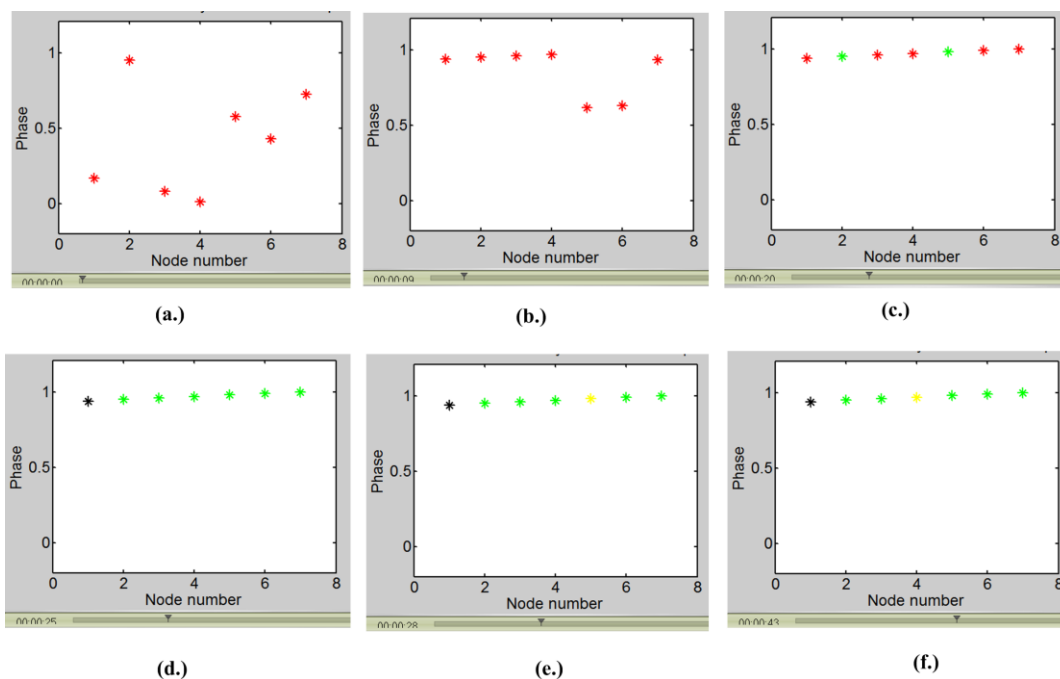


**Figure 6.14. Time evolution of the phase of different nodes (a total of 7 in this case) at different instances of time without reinforcement. Red indicates unsynchronized state, green- synchronized in slave, black- synchronized in master mode, yellow- means self-reinforcement was applied (synchronized state). Nodes start from unsynchronized state, then get synchronized, while still maintain synchronization even during misdetections due to self-reinforcement feature.**

where the pulse is expected to arrive. In non-ideal case, the PLL can't provide an exact estimation of where the pulse is expected to arrive, thus an error in detection of the pulse, will still create little bit of frequency variations, though such variations are expected to be small ( $<10\text{ns}$ ) while in comparison the frequency variations are expected to be of the order of 10% of the period ( $\sim 10\mu\text{s}$ ), i.e.  $1\mu\text{s}$ .

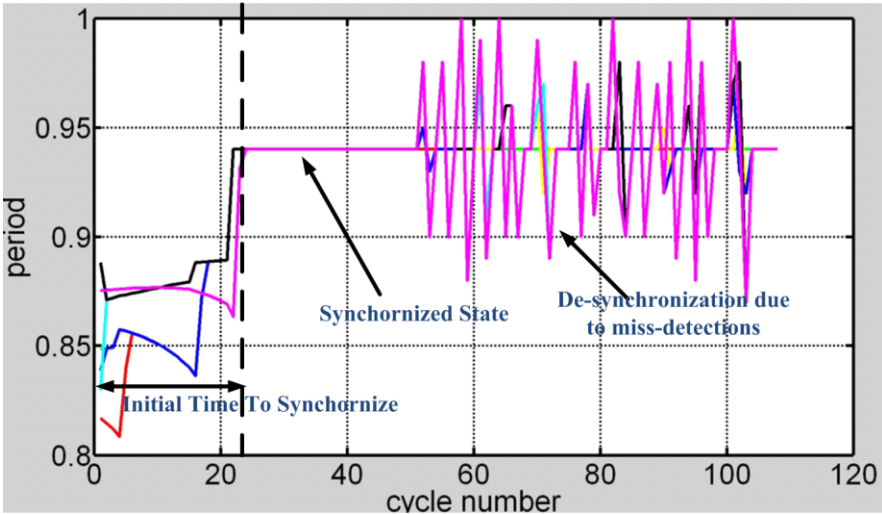


**Figure 6.15. Time Evolution of the period for different nodes in the network, in presence of error injection without the self-reinforcement feature.**

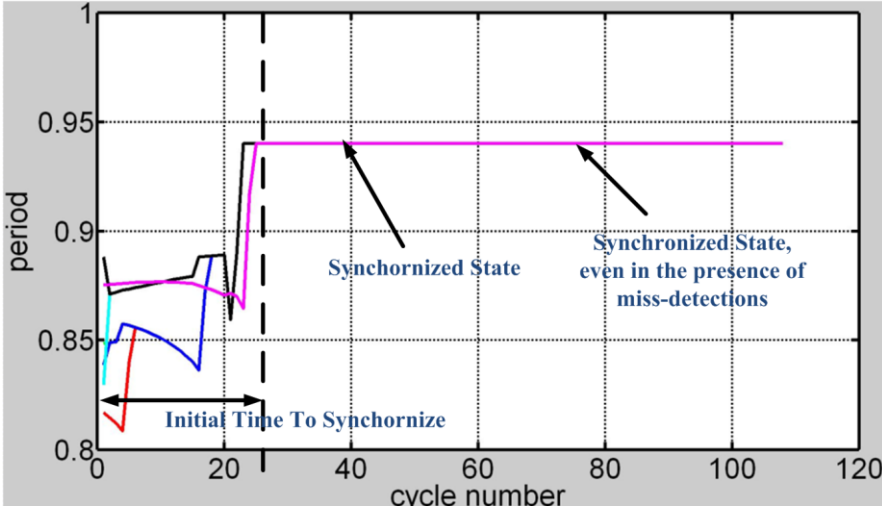


**Figure 6.16. Time Evolution of the period for different nodes in the network, in presence of error injection with the self-reinforcement feature enabled.**

## 6.6 Discrete PCO and FPGA Simulations

To verify the properties of the synchronization detection and reinforcement scheme, the state-machine was also implemented in an FPGA. To enable simulations within the FPGA environment we could design a discrete version of the PCO by implementing the state function as a linear counter. Coupling was implemented by incorporating discrete jumps in the counter value. However, The PCO dynamics for global synchronization per Mirrollo and Strogatz [35] require a non-linear convex down state-function. A closer look though on the requirement of this non-linear convex down state-function reveals that it is required just to ensure that the coupling is non-constant and increases depending upon the phase of the oscillator. Thus, alternatively one can have a linear state-function, but one need to ensure non-constant increasing phase jump along the state-curve. This was ensured in the discrete FPGA implementation by ensuring that the external coupling, implemented in terms of

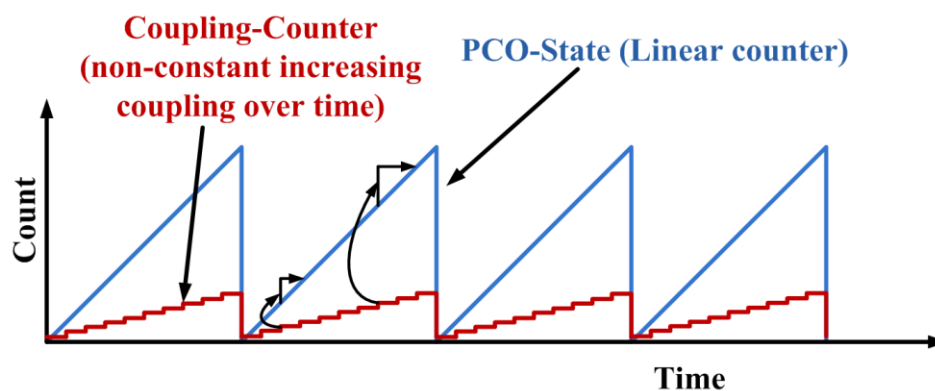


**Figure 6.17. PCO-counter based implementation concept. Instead of non-linear state-function, a linear, counter based PCO-state function is implemented. While the amount of coupling is tracked by another counter, which increases the coupling count value (the amount of discrete jump in the count value if a pulse is detected) over time, thereby keeping the essence of the PCO dynamics intact for simulation in an FPGA environment (note: no coupling was applied in the actual pco-state diagram above, coupling count shows how much coupling will be applied, if there was a sync pulse detected at a given point of time.**

discrete counter jumps is non constant and increasing.

We could very easily implement this by using another set of counter that dictates coupling, where the value was changed discretely again. For example, a PCO full cycle that takes say, 1000 cycle of the clock, can be implemented by a count to 1000 counter. The coupling counter starts at the start of the PCO cycle with a value of 1, but every 10-counts of the PCO-counter, it increases its count by 1, thereby ensuring non-

```

assign reset = reset_pco | (count_pco >= period_pco) | reset_ext ;

always @ (posedge clk)
  if (reset) begin
    overlap_pco <= 0;
    count_pco = 0;
    couple <= couple_init;
  end else begin
    if (sync_pco | sync_pco_self) begin
      count_pco = count_pco + 1 + couple;
      if (count_pco >= period_pco)
        overlap_pco <= 1 & sync_pco ;
    end else begin
      count_pco = count_pco + 1;
      if ((count_pco % thresh_mod == 0) && (count_pco > 0))
        couple <= couple + 1;
    end
  end
end

```

Initial Value for Coupling Counter

Coupling applied only when sync is detected, or a self-reinforcement pulse is generated

PCO Counter (linear increment)

Coupling Counter (linear increment discretely at a much lower rate determined by thres\_mod)

**Figure 6.18.** A small snapshot of the discrete PCO implementation program in Verilog. The detailed program is given in the appendix. count\_pco is the pco state function implemented using a counter. While, the couple is also a counter, but increments it's value from an initial value (couple\_init) and in discrete jumps dictated by thres\_mod parameter value.

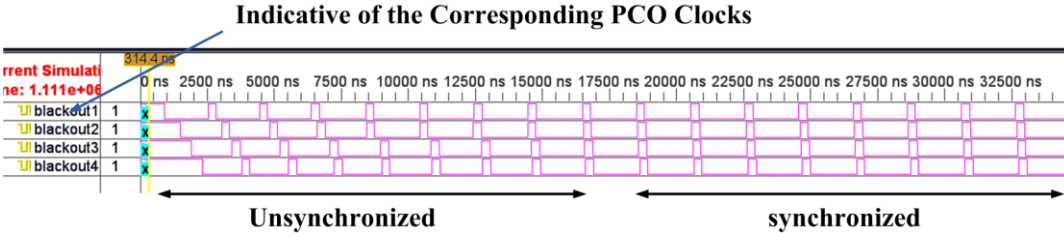


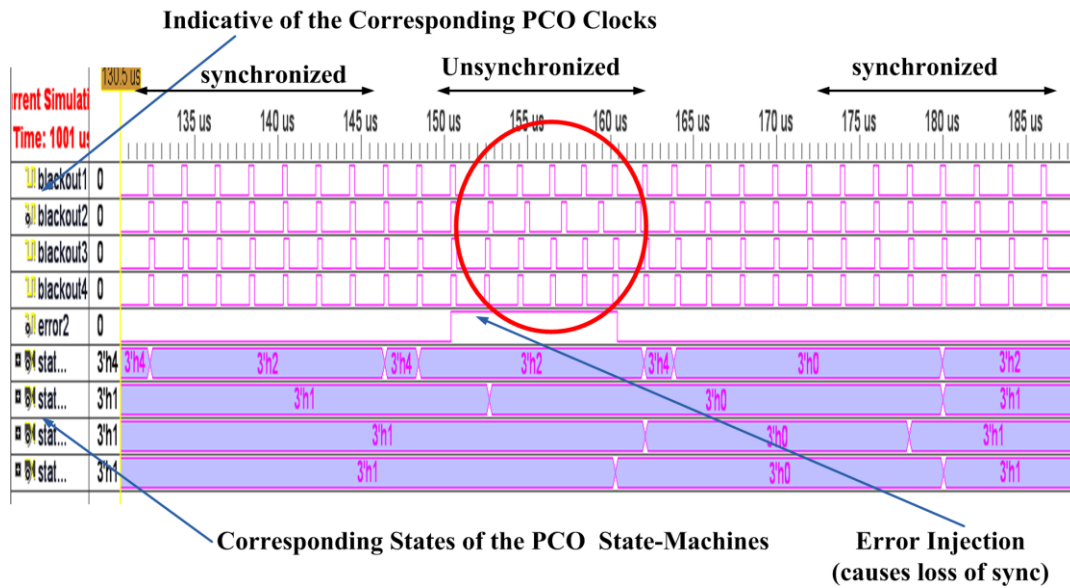
**Figure 6.19.** ISIM simulation of the discrete-PCO implementation. Note, the 4-PCOs signal starting from a random unsynchronized state move to a synchronized state, following the PCO dynamics as elaborated above in the discrete FPGA implementation. The 4 PCOs had mismatch in their nominal frequency.

constant increasing coupling, if a signal has to couple on the PCO(Fig.6.17). Similarly, the PLL was implemented on the FPGA by setting another counter that tracks the PCO time between successive firing and thus can keep the history of the PCO edges and can be used to predict the expected occurrence of sync detection (i.e. coupling) as well as misdetection.

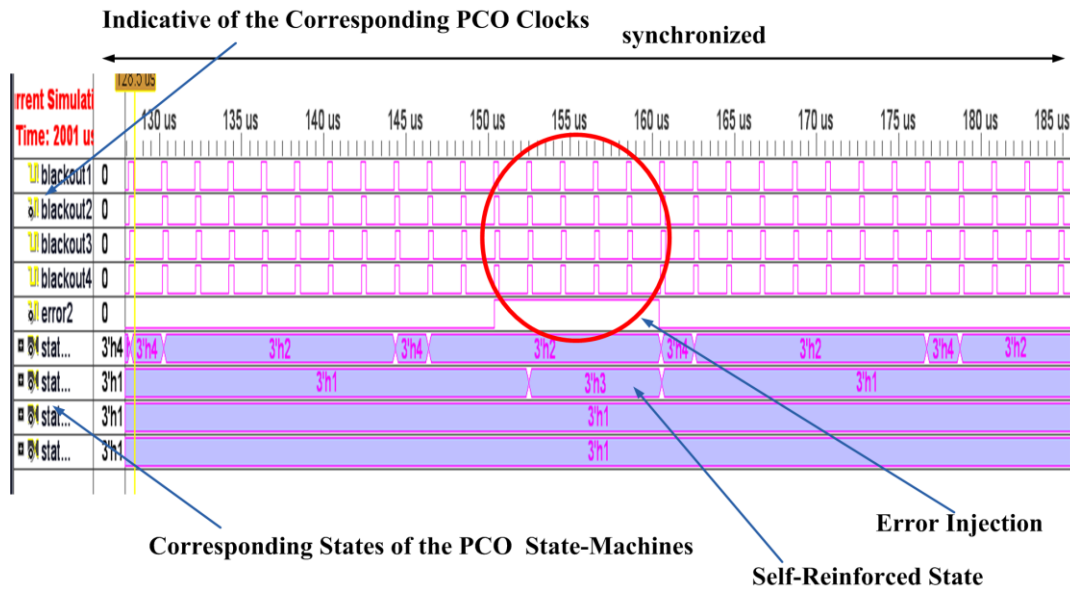
A small snapshot of the FPGA program written to synthesize the scheme is as shown in Fig.6.18. While the Fig.6.19 shows the Verilog simulation of the discrete-PCO design for simulation of the PCO concept.

Fig.6.20 & Fig.6.21 shows the ISIM simulation of the verilog code for the discrete-PCO implementation. The PCO timing and the states of the PCOs are shown in the presence of errors. As expected without self-reinforcement the PCO-clocks drift away, resulting into the loss of synchronization (Fig.6.20). But with the self-reinforcement enabled, the clocks don't drift, and the PCOs are able to maintain synchronization (Fig.6.21).

Fig.6.22 shows the synthesized simulation on the FPGA with 4-PCO implemented on a single FPGA board. The displays show the status of the 4-PCOs. The different PCOs start with a 0-state (unsynchronized state) and then finally get into the synchronized state. A state of 1 means the node is synchronized as a slave, while a state of 2 means the node is synchronized as master. A master node occasionally has to go out and look for new nodes joining the network, and that state is shown in the display as state-4. We also inject errors at different node selectively, that results into a node getting back to desynchronized state (0) in the absence of self-reinforcement. While in the presence of self-reinforcement the nodes were found to have tolerance to these errors, as the node moves to intermediate state (3), detecting self-reinforcement, as expected.



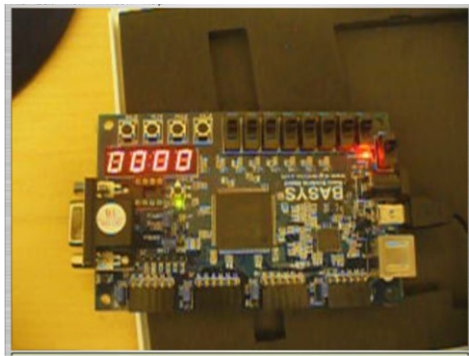
**Figure 6.20. ISIM Simulation: States of the various pco-clocks and their pco-firing instances, showing error injection and recovery (loss of synchronization to synchronized mode of operation), in case of no self-reinforcement.**



**Figure 6.21. ISIM Simulation: States of the various pco-clocks and their pco-firing instances, showing error injection, not resulting into any loss of synchronization, due to self-reinforcement that happens locally at the node. See the change of states at the node that correspond to the dynamics here.**

## **6.7 Impact of self-reinforcement for a global network scalability and sync error rate**

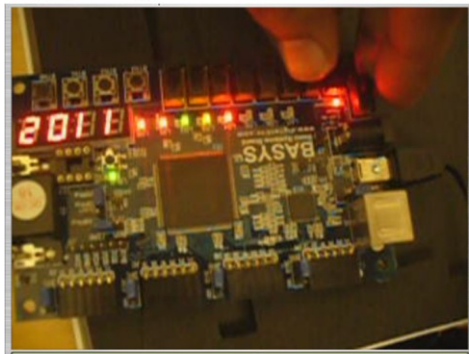
The self-reinforcement scheme is important for the scalability of the network. As, in the absence of it, a remote fault at a distant node in the network, due to dependent nature of synchronization scheme can show up as a fault locally detected at a node. For example, in a network consisting of 4 nodes A, B, C & D if they are linearly connected, with “A” being the master node in the network, error in sync pulse detection at “B” will automatically create an error in “C” and “D” as well. Thus even though “C” and “D” may have no misdetections, the misdetections at “B” will create errors, thus self-reinforcement is important to keep the effective error count in check for a large network. Even for small networks, for any given link margin pulse-detection errors can occur (typically  $10^{-3}$  or  $10^{-5}$  order). With reinforcement feature effectively these errors can be made very low. For example with a self-reinforcement detection errors can occur (typically  $10^{-3}$  or  $10^{-5}$  order). With reinforcement feature effectively these errors can be made very low. For example with a self-reinforcement threshold (number of times consecutive self-reinforcement is allowed) of only one a sync error rate of  $10^{-5}$  at a node can be effectively reduced to  $10^{-10}$ . Higher self-reinforcement threshold value can make this number even lower. Though, to achieve higher self-reinforcement threshold one need to look at the PLL drift too. If the PLL is designed with low loop-bandwidth then one can have higher self-reinforcement threshold. A low loop bandwidth however means slower locking dynamics between the PCO and the PLL and might not have adverse impact in networks, where the node configuration changes more often. Though for mostly static network configuration one can have low loop-bandwidth. Low loop-bandwidth for PLL can also however limit



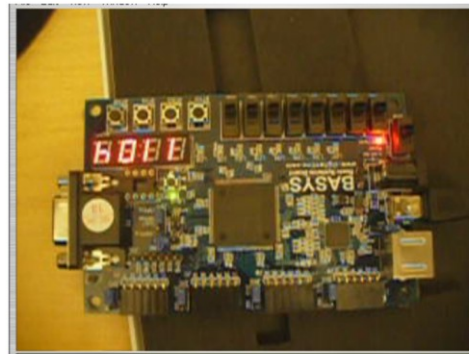
(a.) Unsynchronized (0, 0, 0, 0)



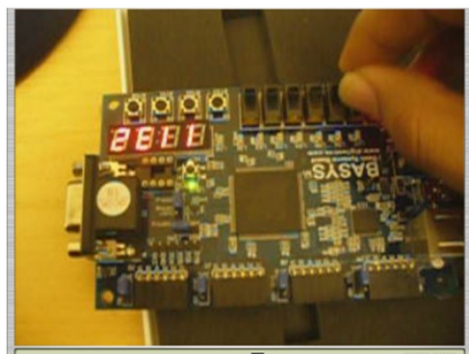
(b.)- synchronized (2, 1, 1, 1)



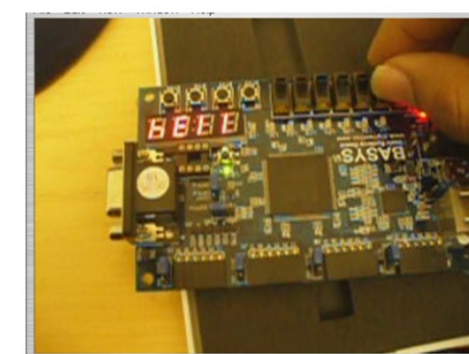
(c.)- Unsynchronized (2, 0, 1, 1)



(d.)- unsynchronized (4, 0, 1, 1)



(f.)- Synchronized (2, 3, 1, 1)



(g.) -Synchronized (4, 3, 1, 1)

**Figure 6.22. FPGA simulation depiction of the state-machine with discrete PCO with 4 difrerent PCOs. The displays show the states of each pco in different time. State-0 unsynchronized, state-1-synchronized in slave mode, state-2 synchronized in master mmode, state-4, synchronized in master (but on lookout for new nodes) and state-3 means reinforcement. Plot c and d are without reinforcement enabled, while the ploclf and g. are with reinforcement enabled.**

the locking range of the PCO and PLL frequency mismatch. A PLL with dynamically adaptable loop-bandwidth will be desired in that case, to ensure faster dynamics and larger locking range while in the locking mode, while ensuring small loop-bandwidth at locked mode, and can be implemented.

## **6.8 Summary**

In this chapter, we proposed a methodology to locally detect the advent of synchronization at a node. The synchronization detection state machine enables the detection of synchronization as well as helps maintain synchronization in combination with the self-reinforcement feature. The self-reinforcement methodology proposed uses the time history of the sync-pulses to enable the synch state machine to maintain the synchronization in the event of missing sync pulses. The state-machine was simulated with Matlab as well as FPGA. FPGA was used to have a hardware implementation of the scheme and was also used to implement a discrete PCO and a discrete PLL to enable simulation of the whole system. The scheme was found to be correctly working for the synchronization detection in conjunction with the self-reinforcement scheme even in the presence of missing pulses.

## CHAPTER 7

### EVENT BROADCASTING APPLICATIONS USING PCO BASED SYNCHRONIZATION

#### 7.1 Introduction

We have seen that Impulse Radios within communication networks using Pulse Coupled Oscillator (PCO) global synchronization can be efficiently duty cycled for significant power savings. In this chapter we utilize the emergent dynamical behavior in the PCO network to enable some of the novel applications particular to this type of network.

A wireless sensor network is often designed with the intention to collect/sense physical information (such as temperature, pressure etc.) from the environment in a distributed manner [93]. For many applications, such as in intrusion detection, temperature exception detection, pressure exception detection, gas leak detection etc., this information is simple and sparse. In these types of applications one is primarily interested in knowing if an exception (or an event) occurred at any node [94]. The goal in these applications is to broadcast the occurrence of an event to the entire network in the simplest and fastest way possible. In some applications localization of the event in space is also of importance [94-97]. In this chapter we propose two different methodologies that rest on the unique properties of the PCO based global synchronization scheme. The first proposed scheme enables structure-less communication of event information to all the nodes in the network without the need of any packet formation. The second scheme can be used in conjunction with any globally synchronized network, and enables not only event propagation, but also localization, neighborhood validation, and fault detection. The scheme makes use of

dynamic duty-cycling of the timing-bins as well, thereby facilitating low power communication. We also propose how to use the method while facilitating packet type communication as well as for very low latency routing of the packet to data-collector node in a bucket-passing type of algorithm.

## **7.2 Structure-less Communication of Event Based on PCO Synchronization**

In this section we show how one can utilize the inherent synchronization dynamics of PCO nodes in passive communication of detection of events such as, intrusion detection, gas leak, fire, smoke detection, metal detection, etc. In this proposed methodology, events sensed locally by a node can be broadcasted to far away nodes in a passive manner, without having to utilize any data/packet structure. The simple method proposed here can be used for event classification in case of different types of events as well as event prioritization. The methodology proposed here makes the task of propagating the event/exception seen at any node very simple. The proposed methodology uses the intrinsic properties of PCO-synchronization to create an event-to-frequency map that excites a change of the global pulse repetition rate of the entire network, based on event detection at any node. The communication methodology is based on emergent dynamic behavior in a PCO network that allows development of a leader node in the network. In this section we will discuss these dynamics in detail and show how the proposed communication scheme can be utilized.

### **7.2.1 The Development of a Leader Node in the Network**

In a group of PCO sensor nodes operating in the strong coupling regime it has been observed in simulation and experiments that the fastest node sets the frequency of the network clock in synchronized state, thereby becoming the leader for the network (Chapter 2). This means the network frequency is the same as the frequency

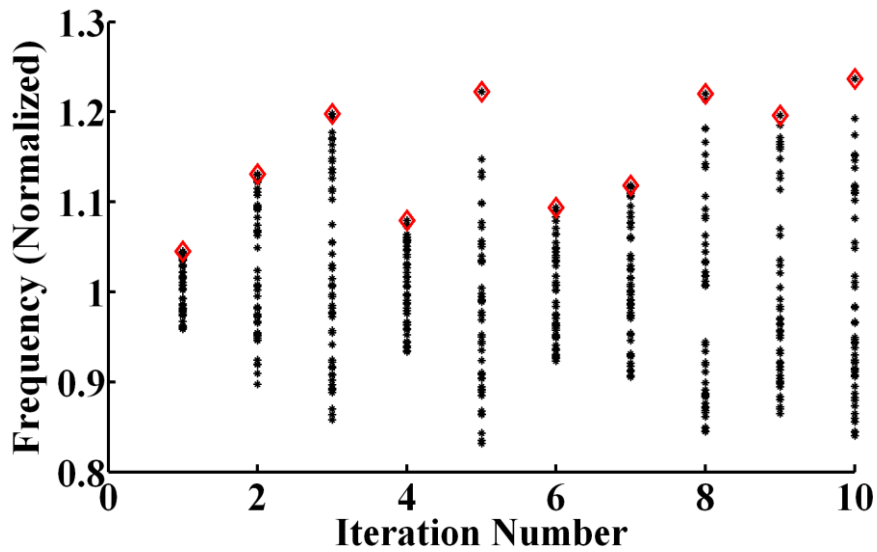


**Figure 7.1. Simulation results showing the randomly distributed frequency of the various nodes (when no coupling is there) for different frequency variations across different runs (iterations) and the corresponding frequency (in red diamond shape) of the network in the synched state after the coupling is enabled. Note the frequency of the synchronized network corresponds to the highest frequency node.**

of the fastest node in the network. Fig.7.1 shows ten separate simulations done with randomly distributed node nominal frequencies (without coupling) and the synchronized frequency of the network (once the coupling is enabled), for each iteration in red diamond shape. One can see the network frequency in the synchronized state corresponds to the highest frequency node in the network. We utilized this development of the leader node in the network characteristics for structure-less communication of events in the network.

### 7.2.2 The Scheme for Event Detection

For a group of connected nodes, each with a nominal frequency between  $f_0 + \Delta f$  and  $f_0 - \Delta f$ , the network frequency will be  $f_0 + \Delta f$ . Upon detection of an event, the node that senses the event can set its frequency to  $f_1$  such that  $f_1 > f_0 + \Delta f$  (Fig.7.2), thereby becoming the new leader for the network. For an analog PCO this can be done by

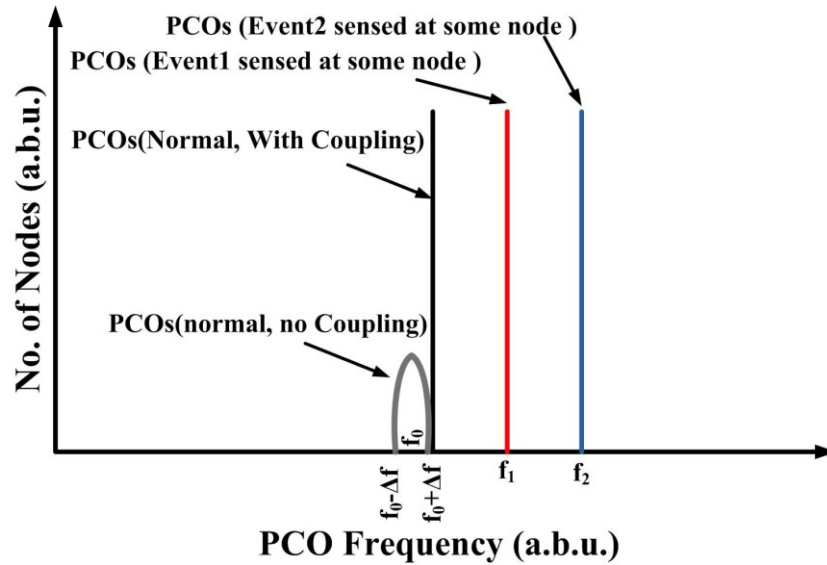


**Figure 7.2. Depiction of frequency distribution in case of the passive communication of events. Nominally frequencies are centered at  $f_0 + \Delta f$ , but on the advent of an event the PCO frequencies become  $f_1$  or  $f_2$  depending upon the type of event sensed.**

changing the voltage trip point from  $V_{trip0}$  to a lower value  $V_{trip1}$  (Fig.7.3). Due to this change of rate, the global network frequency becomes  $f_1$ , which can be locally sensed by all the nodes in the network (Fig.7.3). In this case, due to the event to frequency map and the resultant change in frequency of the network, information about the occurrence of the event is passively communicated to all the nodes, without forming any data packets. Moreover, this network frequency change can occur virtually instantaneously if the nodes are set up to expect this change by opening their listening windows slightly earlier.

### 7.2.3 Event Classification

Event classification can be accomplished using event to frequency maps. For example an event of type 1 sensed at a node causes the PCO to set its frequency to  $f_1$ , while an event of type 2 sensed at a node causes a frequency transition to  $f_2$  (Fig.7.2, Fig.7.3). The number of different event classifications that can be supported by this

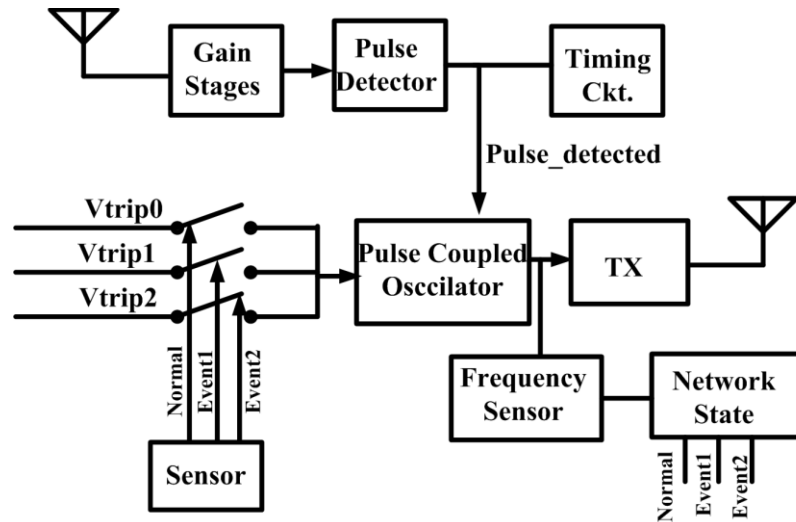


**Figure 7.3. A simplified schematic of possible implementation of the passive event communication methodology.**

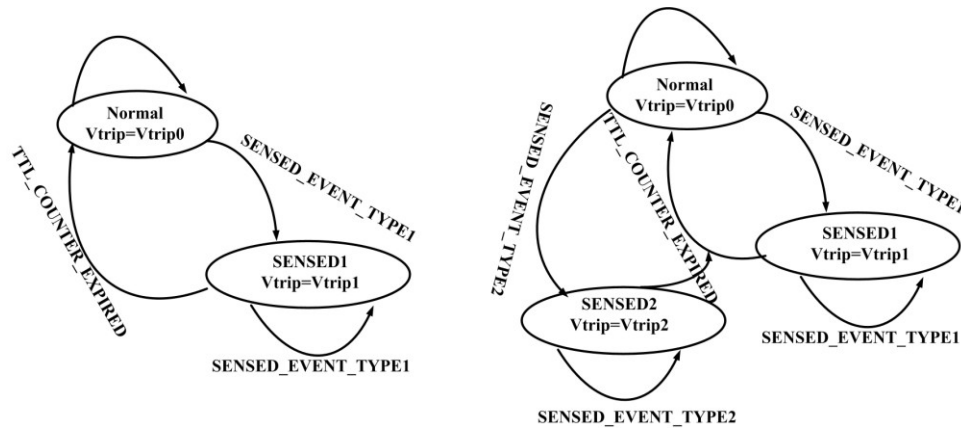


**Figure 7.4. State Representation of the Passive Event communication.**

mechanism will depend upon the frequency variation tolerance of individual nodes, as well as frequency sensing capability. Depending upon the type of usage, one can provision for a “Time To Live” (TTL) parameter, where the node that changed its frequency to a faster value, can return back to its normal value after some time (Fig.7.4). Alternatively, the node will return back to its original frequency only if the sensed event has been cleared.

#### 7.2.4 Event Prioritization

Priority between different events occurring at various nodes can also be easily provisioned. Since the network frequency is dictated by the fastest node, a higher priority event mapping to higher frequency can ensure that an event of higher priority will be broadcast to the nodes in the network, in the case where two nodes sense different types of events simultaneously.

#### 7.2.5 Network Simulation Results

We verified the functionality of this scheme through network simulation. Our simulated network consisted of fifty nodes with a maximum single-hop spacing of 20 meters. The simulation space was made large enough that nodes separated at its extreme ends were connected by 10-15 hops through intermediate nodes. The nodes were simulated with 5% random distribution in their nominal frequencies of 100 KHz.

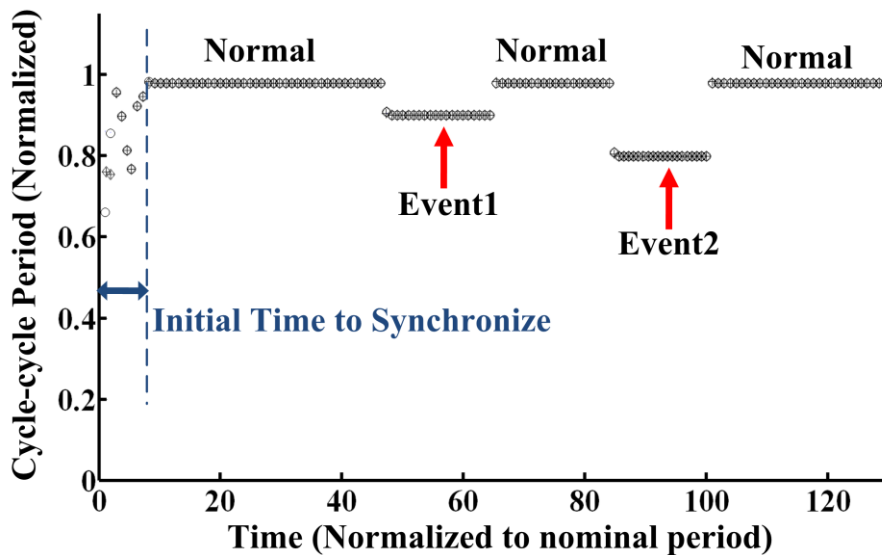


**Figure 7.5. Matlab simulation of the global period in case of event transition and event recovery. Initially the nodes are all un-synchronized, and so the nominal global period is low. Once synchronized, the node period is nominally ~1, when an event happens at any node, the global period goes low, while on recovery it sets itself back to the nominal value.**

A representative example of the network dynamics under our proposed scheme is shown in Fig.7.5. Starting from a random desynchronized phase, the system converges to synchrony, at which point the cycle-cycle period is same for all the nodes. A randomly selected node at some time detects an “Event1”, and transitions it’s frequency to a higher frequency (lower cycle-cycle period). Other nodes in the network almost immediately respond to this change in frequency and resynchronize to the new cycle-cycle period. Subsequently the sensing node goes back to normal period, and so do all the nodes in the network. Sometime later, an "Event2" transition happens at another node, which corresponds to higher frequency (lower cycle-cycle period). The figure shows the nodes again respond to the dynamics of the node that detected the event in the same cycle. Please note, in the figure the cycle-to-cycle periods of all the nodes are put together. Due to the synchronized mode of operation all the nodes show the same period, making it hard to distinguish between them.

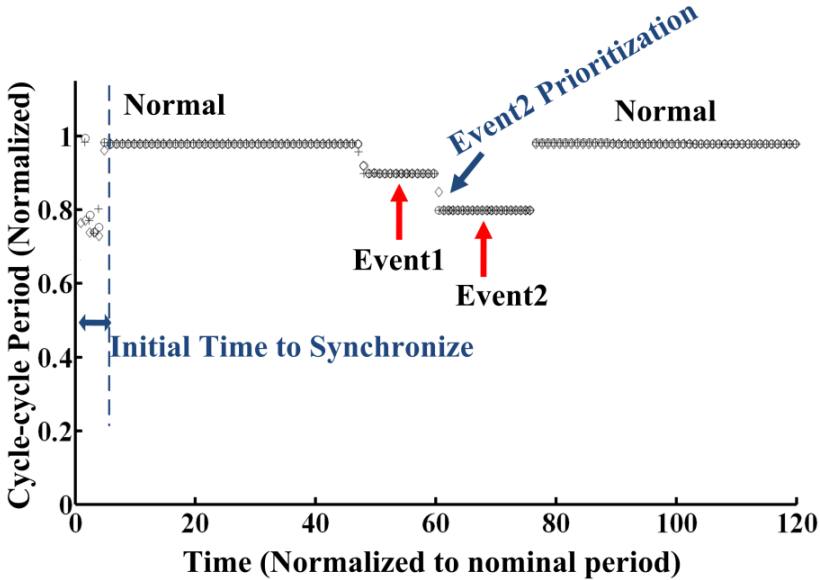


**Figure 7.6. Matlab simulation of the global period (of all the nodes) in case of event transition and event recovery. Also shown is the case of event 1 and event 2 happening simultaneously (shows event2 prioritization).**

Fig.7.6 shows a similar situation to Fig.7.5, except Event2 and Event1 are concurrent. This shows the ability of the proposed scheme to establish event prioritization, when another node detects an “Event2”, the cycle-cycle period of all the nodes in the network corresponds to the “Event2” and not “Event1”. This happens as the frequency map for “Event2” is higher compared to “Event1”, thereby giving higher priority to “Event2”.

We also demonstrate the scalability of the proposed scheme to six different event classifications (Fig.7.7), along with a possible failure mode. In this case, the coupling in the network was insufficient to offset the large shift in the oscillator’s period corresponding to event 7. However, the network is still able to recover to its synchronized state upon the conclusion of the invalid event, for which the nodes couldn’t synchronize to a common cycle-cycle period (i.e. frequency).

The event detection scheme is compatible with duty cycled impulse radio systems. To be able to capture each type of event in the network instantaneously, the nodes are

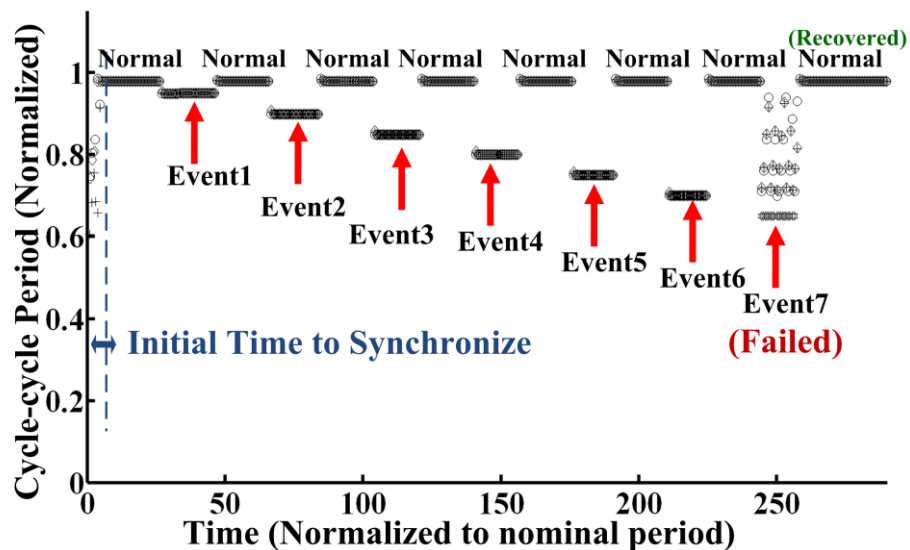


**Figure 7.7. Shows the scalability of the scheme to more than 2 events. Also, shows a failure mode, in this case for event-7, the network doesn’t synchronize, as the coupling wasn’t sufficient to counter the increased frequency mismatch.**

setup to open the listening window slightly earlier than the expected arrival time of the highest priority event (the event mapped to the highest frequency). The spacing of  $\Delta f_{\text{EVENT}}$  is limited by the frequency mismatch of the network's oscillators. If the worst case mismatch of two oscillators in the network is 5%, then  $1/\Delta f_{\text{EVENT}}$  is set to 10% of the nominal period, which gives some additional margin against random factors such as period jitter.

Fig.7.8 shows the power saving capability at the receiver of this scheme based on various frequency mismatches. Although, the greatest power savings can be achieved through the use of Xtal oscillators, the scheme still works well with practical integrated silicon-based oscillators with realistic frequency mismatch. The fact that nodes immediately synchronize and recover ensures that the event information at any node propagates through the network at the speed of light plus the latency of each node's PCO circuitry each hop (4-5ns). This is in contrast to other broadcasting

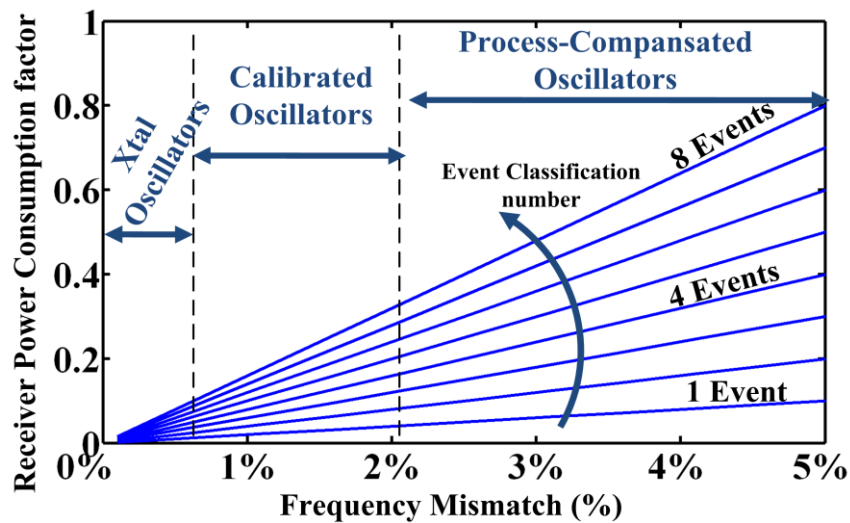


**Figure 7.8. Matlab simulation of power saving at different number of events classification and frequency mismatch for single cycle event transition and recovery. Higher the number of event classification support, lesser is the amount of power saving one can achieve at the receiver. With calibrated oscillators, while supporting 8 different types of events one can still save close to 80-90% of the RF power by duty-cycling the receiver.**

schemes that exhibit significant latency down the link due to the reliance on complex packet structures. One can save more power by doing adaptive duty-cycling, but that will incur increased cost of synchronization and resynchronization ( $\sim 10$ - $100$  cycles). In this scheme the nodes are required to implement a synchronization state machine, which can track the loss of synchronization, thereby adaptively opening the bigger time window to help resynchronize. This scheme can be utilized as a trade-off between increased duty-cycling and latency in communication.

For the transmitter in these types of network a node has to send only 1 pulse ( $\sim 2$ ns duration) per cycle ( $\sim 10$ us), and hence is inherently duty-cycled. Thus the power saving is there both at the transmitter and receiver.

### **7.3 Event Broadcasting in Synchronized Environment**

In contrast to the structure-less event communication scheme described earlier, in this section we propose a methodology that can be used with any globally synchronized network in conjunction with impulse based UWB communication. We assume an impulse radio scheme based upon time division multiplexing is used for communication of the events. The proposed methodology facilitates event localization using hop-counting as a measure of distance in such a system. Simplified local neighborhood validation is also proposed to make event propagation conditional on local event correlation, avoiding false triggers. The proposed methodology can work in conjunction with dynamic duty-cycling, thereby enabling low power consumption when there is no communication as well as during the communication of events. The scheme also ensures fairness to all the nodes in the network.

The proposed methodologies have significant advantages over existing packet based communication schemes. Existing broadcast packet-based communication schemes need to implement very detailed and complex MAC and routing protocols

[94-97], requiring significant overhead of power and chip area. In comparison, the proposed method is very simple. The information propagates without any complex protocol for medium access, while the routing of the information is self-determined. The method also enables dynamic duty-cycling at every node, thereby allowing nodes to save power even when communicating. Localization information is conveyed in a decentralized manner, thereby making the information available to any node in the network. The added simple methodology of neighborhood validation avoids false-triggers and can additionally be used for self-healing of a failing sensor node.

### 7.3.1 Event Detection, Propagation, and Localization

The method proposed here utilizes the bin-structure as defined in Chapter 4 to communicate the occurrence of an event. While a sync pulse is fired in the sync bin (aligned with the frame boundary), other bins are utilized to convey messages about the event as well as localization information. Fig.7.9 shows one illustrative bin arrangement for this scheme. Event communication proceeds as follows. One can begin by using bin#0 as the event bin, while other bins are utilized to convey the hop-count (localization) information (Fig.7.9). Every node, when synchronized, keeps its receiver “ON” only in “Bin#0” and the “Sync bin”. The sync bin is required for the timing pulse in order for the node to maintain synchronization to the rest of the network. The “Bin#0” is used to convey the start of the message. Any node intending

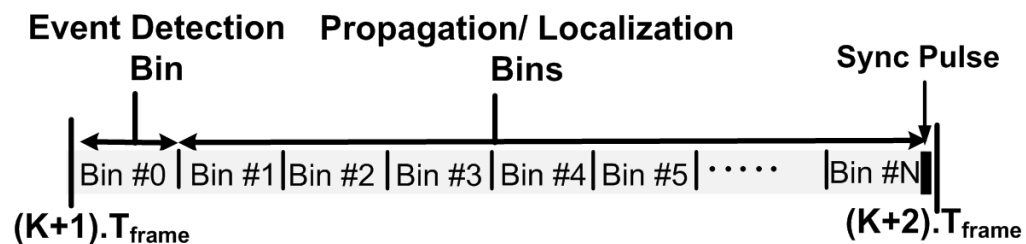


**Figure 7.9. Illustration of the bin structure for event detection and localization.**

to communicate any information transmits a “1” in Bin#0, signaling to the other nodes to dynamically open other bins. This ensures duty-cycling of the power hungry receiver in normal mode of operation. Other bins are dynamically opened based on our proposed algorithm.

The algorithm we propose when implemented at every node ensures that whenever an event is sensed at any node, the other nodes can learn the “hop-count” distance of the node where the event occurred in a decentralized cooperative manner. The algorithm ensures that other nodes will know the shortest direct hop-count from the node where the event occurred. This hop-count information can be utilized at each node to estimate the distance based on communication range of the radio. The algorithm is as follows.

**1):** Every Node listens to Event bin (bin#0), if no “1” is detected, they duty-cycle, i.e. turn the receiver and transmitter off for the rest of the frame.

**2):** A node sensing an event puts a “1” in the Event bin (bin#0), indicating the event.

**3):** The node where the event happens also transmits a “1” in bin#1 (localization bin), indicating its own hop-count.

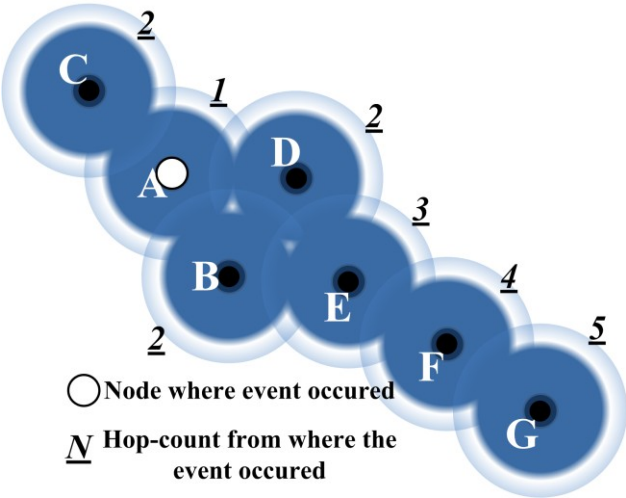
- 4):** Any node in the neighborhood that finds a “1” in Event bin (bin#0),
- looks for the first localization bin where a “1” is found
  - In the next frame cycle, it replicates a “1” in bin#0
  - It also puts a “1” after the bin where the first “1” was found, other than bin#0.
  - Beyond that bin, they duty-cycle again.

**5):** The hop-distance from any node in this case will be the timing bin# in which they transmitted a “1”.

**6):** After a node has forwarded the event, and a waiting period has elapsed (after 2-3 frame cycle), it goes into inactive mode for a duration equivalent to the worst case

event reflection in the network or neighborhood; this ensures the network broadcast also dies outward from the point where it was first detected. The worst case event reflection time will be dependent upon the maximum hop-count to avoid message looping back.

Fig.7.10 shows one illustration of this methodology. Node “A” is the node where an event was detected, it sends (1, 1). In the Node “A’s” neighborhood node “B”, “C” & “D” receives (1, 1), thereby learning that an event occurred and that they are a hop-count of “1” away. Since they receive (1, 1), they transmit (1, 0, 1). The node “E” will receive (1, 0, 1), thereby learning that it is at a hop-count of “2” away, and it transmits



Bin#	Node-A		Node-B		Node-C		Node-D		Node-E		Node-F		Node-G					
	Rx	Tx	Rx	Tx	Rx	Tx	Rx	Tx	Rx	Tx	Rx	Tx	Rx	Tx				
0		1	1	1	1	1	1	1	1	1	1	1	1	1				
1		1	1		1		1		0		0		0					
2				1		1		1	1		0		0					
3			<b>INACTIVE</b>							1	1		0					
4															1	1		
5																		1

**Figure 7.10. Example depiction of 1-node event initiation and the automated hop-count realization for all the nodes in the network. (The shaded area in the Rx, Tx column, means the corresponding circuit is switched “off”).**

a (1, 0, 0, 1) as shown in the table in Fig.7.10. This way all the nodes in the network record the occurrence of the event as well as their hop-count distance from the event-node. Note that when the node E transmits (1, 0, 0, 1), the node B, and D in the neighborhood still get only (1, 1) from Node “A” due to logical “ORing” of the bits in the bins, and so there is no ambiguity problem. Also, the OOK modulation scheme in conjunction with energy detection for pulse detection ensures that there is no collision of information in the neighborhood of a node.

Fig.7.11 depicts the meaning of the information transmitted by a node as well as the meaning of information received at a node for additional clarity.

The methodology can also be extended to include additional event classification bins, following the event bin, to classify types of events sensed at a node. In that case every node must replicate the event classification bin information in addition to the event bin while propagating the event information.

<b>Bin Structure at the Transmit Side</b>							
<b>Meaning</b>		<b>Event Bin</b>	<b>Propagation / Localization Bins</b>				
No event occurred		X	X	X	X	X	.... X
Event locally sensed		1	1	X	X	X	.... X
Event sensed in an immediate neighbor (1 hop away)		1	0	1	X	X	.... X
Event sensed 2 hops away		1	0	0	1	X	.... X

<b>Bin Structure at the Receive Side</b>							
<b>Event Bin</b>	<b>Propagation / Localization Bins</b>						<b>Meaning</b>
0	X	X	X	X	....	X	No event occurred
1	1	X	X	X	....	X	Event occurred in an immediate neighbor (1 hop away)
1	0	1	X	X	....	X	Event occurred 2 hops away
1	0	0	1	X	....	X	Event occurred 3 hops away

**Figure 7.11. Figure illustrating the meaning of information received and information transmitted in the case of event propagation and localization methodology as described in the section above.**

### 7.3.2 Neighborhood Validation

The methodology discussed in the previous section enables communication of an event with location information. In this section we also propose a novel method for localized neighborhood validation, which can be utilized to prevent false-detection. The localized neighborhood validation method proposed in this section requires an event sensed by a node to be validated by at least one of its immediate neighbors. In the absence of neighborhood validation, the event propagation is locally terminated. This prevents propagation of a false-detection, and is good for systems where information sensed by a node should be correlated with its immediate neighborhood for it to be useful for the whole network.

The algorithm in this case is a slightly modified version of the one in the previous section. Fig. 7.12 shows an illustrative frame boundary and its corresponding bin structure. In this case one can have bin#0 as the event bin and utilize bin#1 for event validation, while using the rest of the bins to convey the hop-count (localization) information (Fig.7.12). The algorithm is as follows:

**1):** Every node listens to bin#0, if no “1” is detected, they duty-cycle, i.e. turn the receiver and transmitter off for the rest of the frame.

**2):** A node detecting an event puts a “1” in bin#0, indicating the event.

-note: In this case it just puts a one indicating an event occurred, without putting

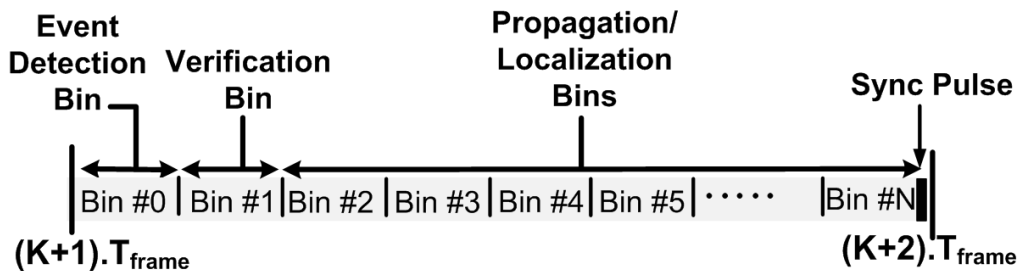


**Figure 7.12. One example definition of the bin structure for event detection, localization methodology with immediate neighborhood validation.**

anything on the next immediate bin, thereby becoming the event-initiator.

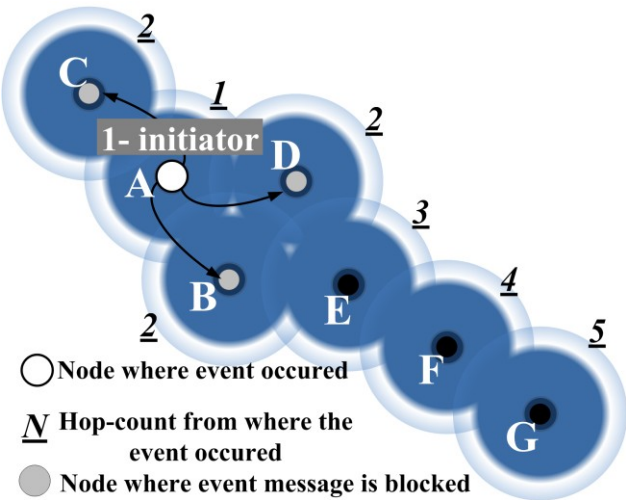
**3):** If a node sees a “{1, 0}” in bin#0, bin#1, then it sends out “{1, 1}” in the {bin#0, bin#1} only if it has also sensed the event, thereby verifying by local correlation of the event in this case before sending out the information.

- Else it drops out, without even replicating anything.

Thus {bin#0, bin#1} = {1, 0} => event detected but not validated yet.

{bin#0, bin#1} = {1, 1} => event detected and validated by at least one node in the neighborhood.

- It also puts a “1” in bin#2, thereby indicating the hop-count of the event-initiator



Bin #	Node-A		Node-B		Node-C		Node-D		Node-E		Node-F		Node-G	
	Rx	Tx	Rx	Tx	Rx	Tx	Rx	Tx	Rx	Tx	Rx	Tx	Rx	Tx
0		1	1		1		1							
1	0													
2														
3														
4					<b>INACTIVE</b>									
5														

**Figure 7.13.** Example depiction of 1-node event initiation but no neighborhood validator and the corresponding activity at various nodes, showing the event message getting locally dropped. (Shaded region in the Rx, Tx table means the receiver or the transmitter in that particular bin was “turned off”).

to be “1”.

**4):** If any node in the neighborhood finds a “1” in bin#0 and a “1” in bin#1.

-Then if event was locally sensed too, it just sends “1,1,1” in {bin#0, bin#1, bin#2}, thereby just sending already verified event forward, with a hop-count of “1”.

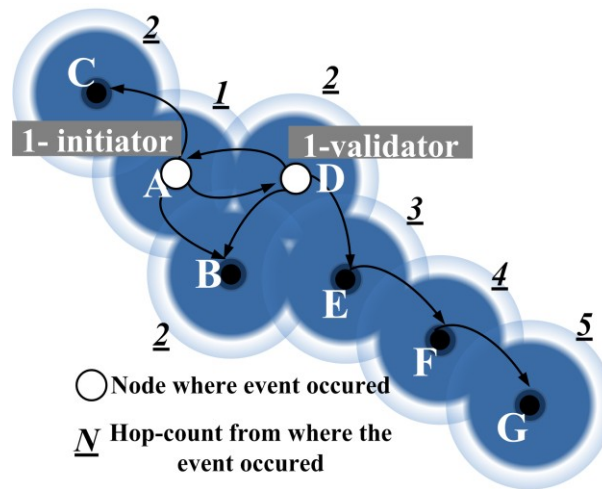
-Else, it looks for the immediate next bin if a “1” is found

- In the next cycle, it replicates a “1” in bin#0, bin#1

- it also puts a “1” after the bin where the first “1” was found, other than bin#0 & bin#1.

- Beyond that bin, they duty-cycle again.

**5):** The hop-distance for any node in this case will be the “bin# -1” in which they



Bin #	Node-A		Node-B		Node-C		Node-D		Node-E		Node-F		Node-G	
	Rx	Tx	Rx	Tx	Rx	Tx	Rx	Tx	Rx	Tx	Rx	Tx	Rx	Tx
0		1	1	1	1	1	1	1	1	1	1	1	1	1
1	1	1	1	1	1	1		1	1	1	1	1	1	1
2		1	1		1			1	1		0		0	
3				1		1				1	1		0	
4	<b>INACTIVE</b>													
5														1

**Figure 7.14. Example Depiction of 1-node event initiation and one validator and the corresponding activity at various nodes, showing the event message getting propagated in the network and the automated hop-count realization for all the nodes in the network. (Shaded region in the Rx, Tx table means the receiver or the transmitter in that particular bin was “turned off”).**

had to put a “1”

**6):** Once a node has forwarded the event, it goes into sleep mode, after sometime for a duration equivalent to the worst case event reflection in the network; this ensures the network broadcast also dies outward from the point where it was first detected.

Fig.7.13 shows one illustration of this methodology. Node “A” is the node where an event was detected; it sends a “1” in bin#0. In this case none of the immediate neighbors could validate the event. Thus none of them take any action on it and as expected the event does not propagate. Since, Node “A” does not receive a “1” in bin#1, it understands that the message did not propagate.

Fig.7.14 shows the illustration of the same methodology, where in Node “A’s” neighborhood the node “D” could validate the event and hence the message propagates further down the network. Fig.7.15 additionally depicts the meaning of the information transmitted by a node as well as the meaning of information received at a

<b><i>Bin Structure at the Transmit Side with Validation Bin</i></b>								
<i>Meaning</i>		<i>Event Bin</i>	<i>Valid- ation</i>	<i>Propagation / Localization Bins</i>				
No event occurred		X	X	X	X	X	X	... X
Event locally sensed but not verified		1	X	X	X	X	X	... X
Event sensed locally and a validator was found		1	1	1	X	X	X	... X
Event sensed in neighborhood (1 hop away)		1	1	0	1	X	X	... X
Event sensed in neighborhood (2 hops away)		1	1	0	0	1	X	... X

<b><i>Bin Structure at the Receive Side with Validation Bin</i></b>								
<i>Event Bin</i>	<i>Valid- ation</i>	<i>Propagation / Localization Bins</i>						<i>Meaning</i>
0	X	X	X	X	X	...	X	No event occurred
1	0	X	X	X	X	...	X	Event without validator
1	1	1	X	X	X	...	X	Event validated
1	1	0	1	X	X	...	X	Validated event occurred (2 hops away)
1	1	1	0	1	X	...	X	Validated event occurred (3 hops away)

**Figure 7.15. Table illustrating the meaning of information received and information transmitted in the case of Event propagation, localization and immediate neighborhood validation methodology as described in section above.**

node for more clarity in the case of neighborhood validator.

### 7.3.3 Simulation Results

We verified the effectiveness of the proposed algorithm using a Matlab simulation with randomly distributed nodes in a sensor-network while limiting the range of direct-communication for any node in the network. As expected, the nodes in the network could correctly establish their hop-count from the event-location (Fig.7.16a, b). Fig.7.17 shows the distance versus hop-count relationship of various nodes in the network. As expected, a direct linear relationship exists between the hop-count and distance-distribution of the other nodes from the event-node in the network. The maximum error-bound in distance estimation of a node in a well connected network was found to be only 1-hop-count. This means the accuracy of the distance-estimation in this scheme is limited to  $\pm 0.5*d$ , where  $d$  is the direct communication reach

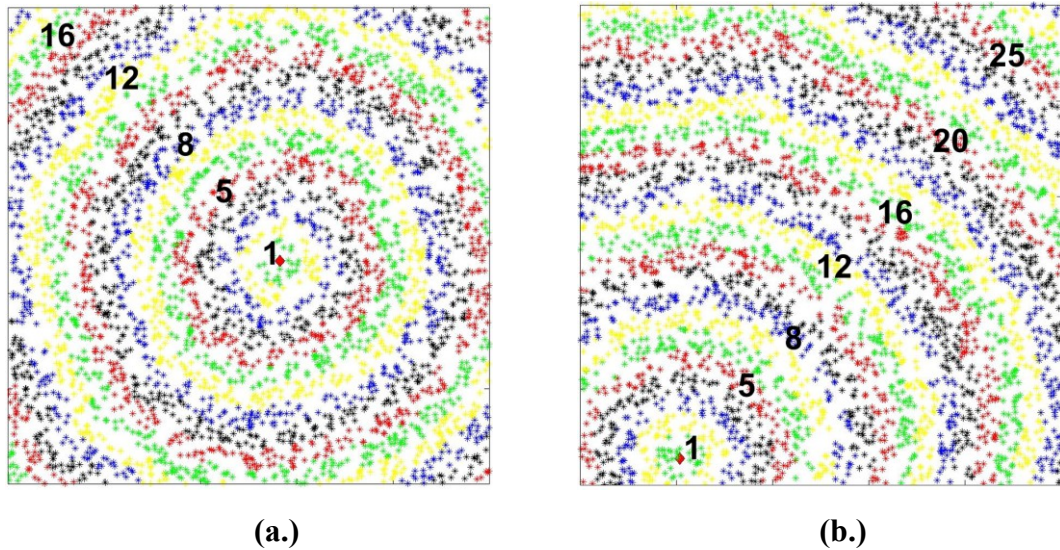


**Figure 7.16. Example simulation of events and the corresponding hop-count estimation from the event-node using the algorithm in a sensor network: (a.) event-node (red diamond shape) at the close to center of the network (b.) event-node at the bottom right-edge. Nodes at various hop-counts are shown in different colors, while reusing the color combination after 5-hop-counts. There is a radial symmetry of nodes (shown as dots) locatted at the same hop-count away from the event-node.**

distance of a node in the network.

We ran a second set of simulation to determine the effectiveness of this localization scheme (Fig.7.18a, b.) with the assumption that base-station nodes, which can share the hop-count information amongst themselves, exist at the periphery of the network. This information then can be individually utilized by each one of the base-station nodes to triangulate the exact location of the event-node. Fig.18a, b shows a Matlab simulation of this estimation. Based on the hop-count distance each base-station can find out a boundary of possible locations within which the event-node is situated. Since the base-stations know the physical locations of all the other base-stations, the intersection points of these boundary locations can be calculated. Note that while determining the intersection points, the base-stations in the immediate neighborhood only are considered. The intersection points from the base-stations diagonally apart are ignored. This gives us 4-possible intersection points (A, B, C and

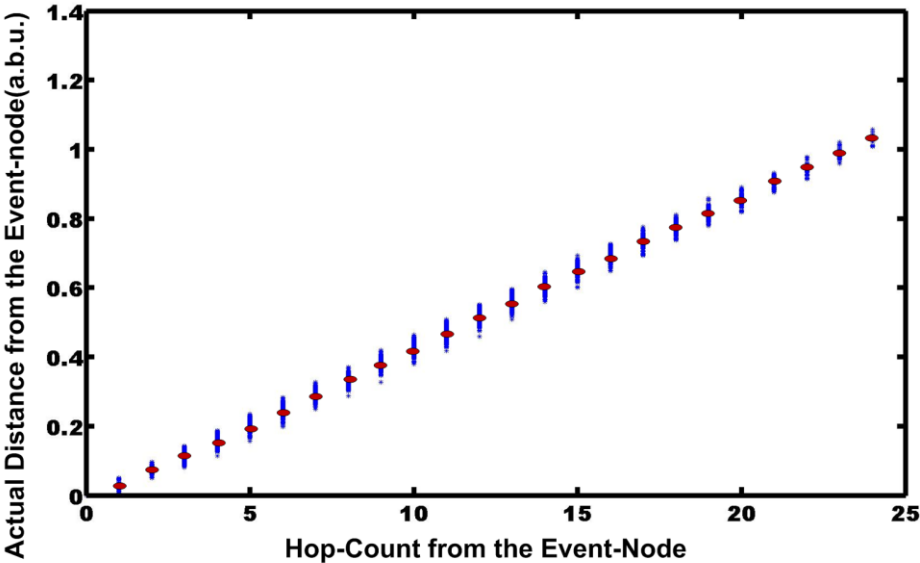
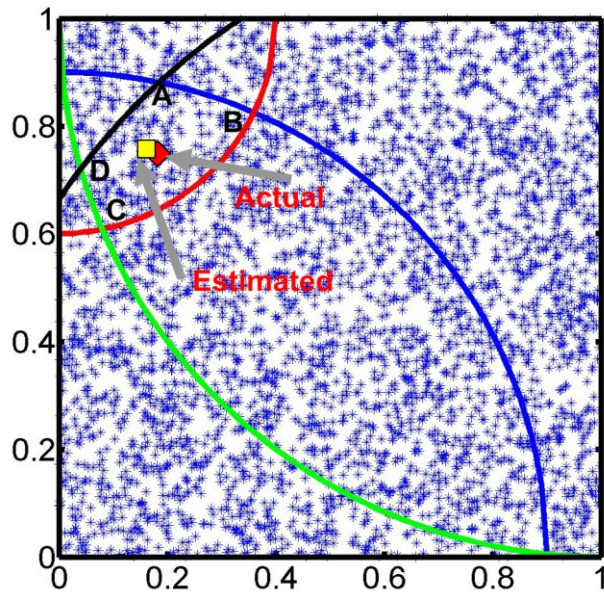
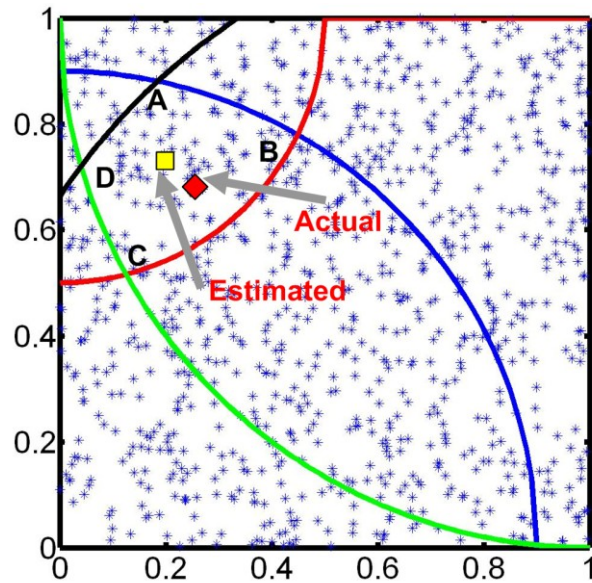


**Figure 7.17. Hop-count Vs actual distance distribution of the nodes from the event-node. As can be seen there is a linear relationship between the hop-count and actual distance of the node with very small error distribution due to discreteness of the hop-count.**



(a.)



(b.)

**Figure 7.18. Simulation of localization point based on base-stations at the corner of the rectangular sensor network field. Red-diamond shape is the event-node, while the yellow rectangular box shows the estimated value. a.) simulation with dense network (b.) simulation with a less dense network. Sensor nodes are marked as blue asterisk points.**

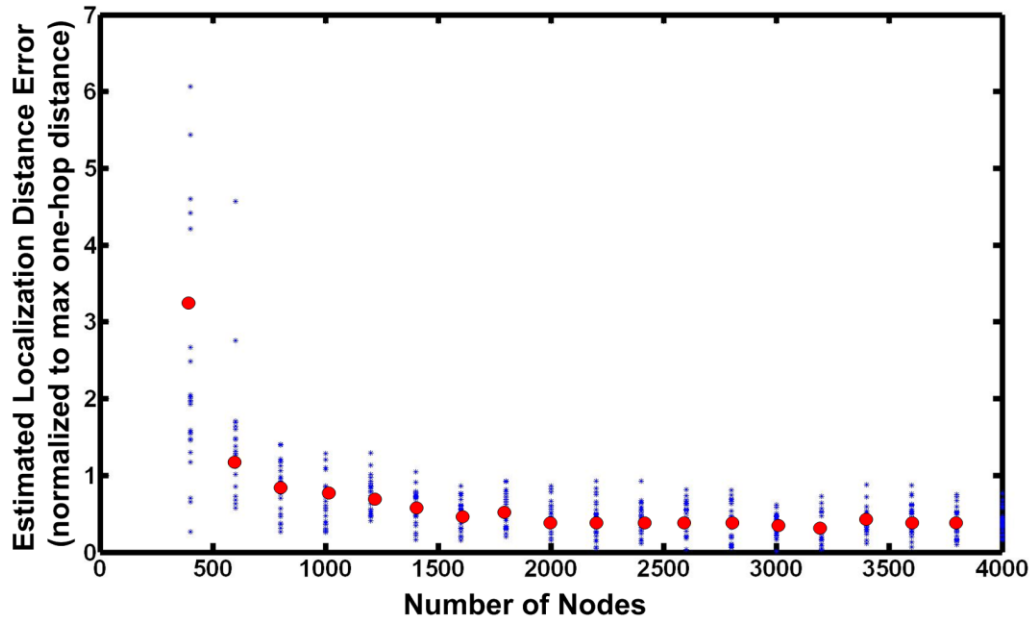


**Figure 7.19. Simulation of maximum errors for various iterations (blue), while varying the node density. The average errors numbers are marked with red-circles for each node density. For sufficient node density the localization error can be reduced to less than max one-hop distance.**

D). Each base-station takes the average of these 4 locations to give an average expected location of the event-node. In Fig.7.18, the yellow rectangular point indicates estimated location of the event-node while the red diamond shape corresponds to the actual location of the event-node.

A further simulation was performed to calculate the error in localization estimation using this scheme as a function of the density of the sensor nodes. At sufficient node densities, the estimation error is limited to less than the one-hop-count distance (Fig.7.19). With low density of nodes in the network the error is high due to breakdown of the connectivity of the network. For randomly distributed nodes in the network of area  $A$  and communication range  $d$  the node density required is approximately  $10 \cdot A/d^2$ .

### **7.3.4 Other Conditions and Analysis**

#### **7.3.4.1 Condition when the event initiator is in the same neighborhood for two nodes**

This race condition can be controlled by having random fall-back and reinitiating the event-circulation if the event wasn't validated. Since, in the algorithm the event initiators know that the event wasn't validated; they can reinitiate the event transactions again after random-fallback. Irrespective of which node becomes the initiator in a neighborhood, the event-hop count distance remains the same for any other node, where the event didn't happen. If two events happen at different locations in the network at the same time, then the event will still propagate, with the nodes hop-count for any node corresponding to the nearest event location.

#### **7.3.4.2 Condition when the event initiator is in the same neighborhood for two nodes**

Continuous blocking of events at a node (self-healing and self-validating): If an event-initiator finds that its event is not getting forwarded most of the time, it may mark its sensor as faulty and take corrective healing actions. Alternatively, it can also self-elevate/self-validate the events, depending upon the confidence level it has on the accuracy of its own sensor.

#### **7.3.4.3 Addition of Event Classification Feature**

One can add an event classification feature by adding some bins before the event-localization bins. Fig.7.20 shows one illustrative arrangement of the bin structure in this case. With the event classification, every propagating node has to replicate the message that they see in event-classification bin in addition to the event bin and validation bins.

Alternatively, the classification feature can also be utilized for a node to enable a normal packet based communication. For a normal packet based communication, the

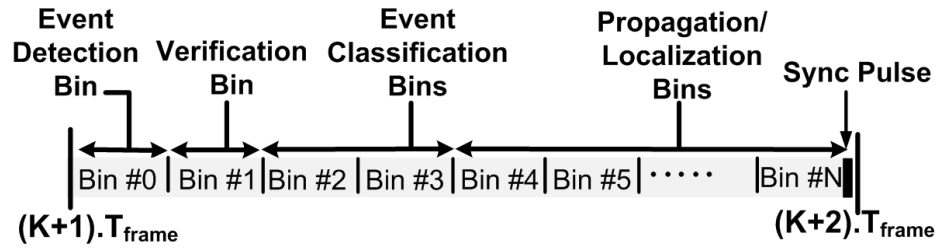


**Figure 7.20. One example definition of the bin structure for event detection, localization methodology with immediate neighborhood validation as discussed in section.**

classification bin information can be treated as message classification and the rest of the bins can be utilized for packet payload and header information. This ensures that the whole infrastructure is not built just for event communication but can be utilized for normal packet communication between any two nodes as well.

#### **7.3.4.4 Multiple pulses in the same bin**

The proposed algorithm is dependent upon the receiver based on energy detection. Any number of pulses within a bin is still treated as just one pulse (“1”). While the absence of a pulse in a bin means a (“0”). This also ensures logical “ORing” of the information within a bin.

#### **7.3.4.5 Network Size Limitation**

The network size in our implementation will be limited to approximately number of bins. For 128 bins and a node-node separation of 10m, this will mean a coverage area of  $\sim 1\text{km}^2$ . Further coverage can be increased by incorporating cellular structure based network designs, where neighboring cells can operate in a different spectral-frequency band.

### 7.3.4.6 Power Saving for Different Activity factor

An analysis of power saving at the receiver shows that the receiver can be duty-cycled to approximately 2% (Fig.7.21), while supporting high level of activity in the network. The receiver is normally switched “on” only for the “Event bin” and the “sync bin”, while other bins are dynamically opened only when an event happens. Similarly, the transmitter (based on OOK) needs to be sending only an average of ~1-2 pulses (of ~2ns duration each) per frame (~10us duration), and hence will consume very low power.

### 7.4 Routing Using the Synchronized Event-broadcasting Mechanism

The proposed synchronized event-broadcasting mechanism in conjunction with event-classification can also be used for routing data-packets, which can be particularly useful in a data-collection type of network. In such a system the data-collector node can initiate an event transaction, thereby letting all the nodes in the network establish their hop-count from the data-collector node, by the methodology proposed earlier. After establishing the hop-count for each node in the network, a node

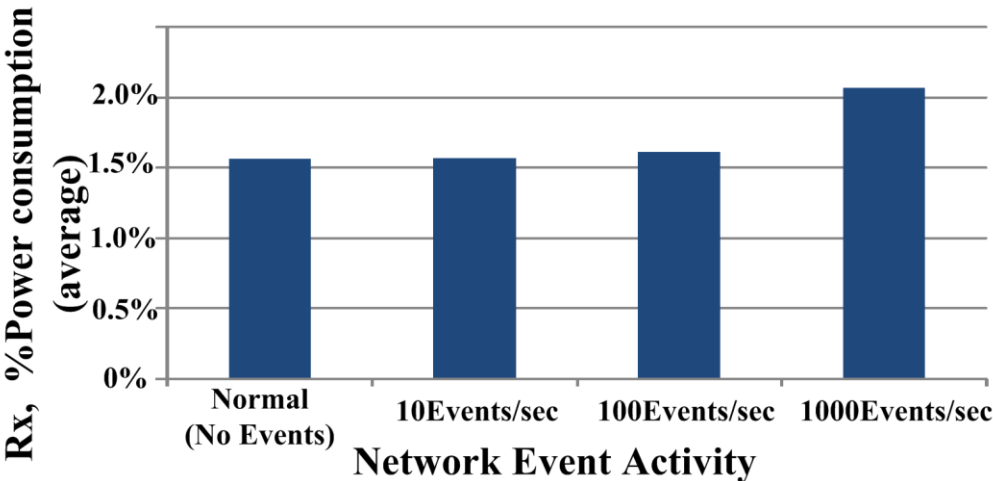
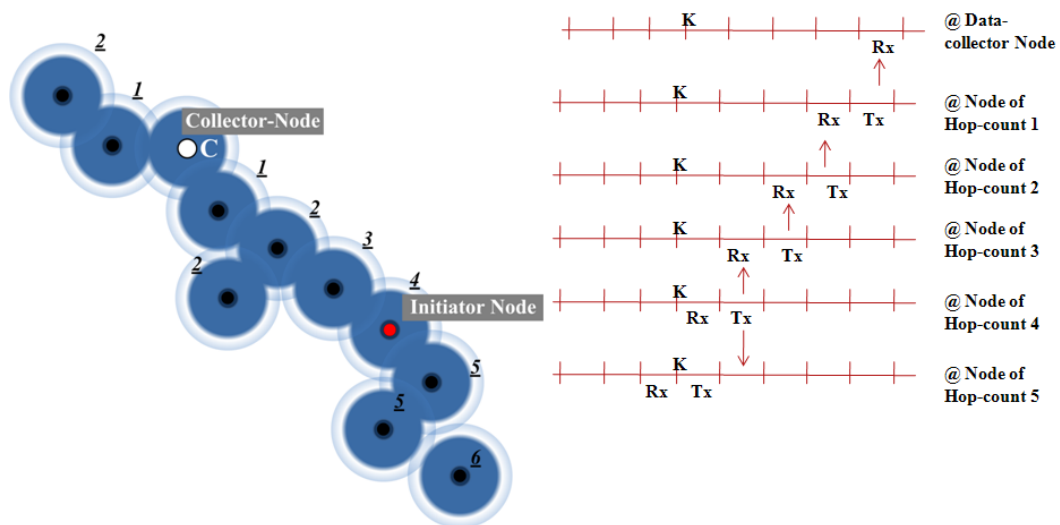


Figure 7.21. Network Event Activity and per node power consumption as % of “fully on” power.

at a hop-count of “n” can be constrained to send the packet at bin number “n-1”, while listening for the packet in the bin number “n”. This thus can ensure that the message passes to the data-collector node in a directed manner, while still ensuring the duty-cycling at all the nodes in the network. The information moves from anywhere in the network, through the least potential hop-count to the central data-collector node and is similar to bucket-passing. Alternatively, one can also have a node at a hop-count of “n” send the information at “N-n” bin (where N is total number of bins available for sending data) while listening into the “N-n-1” bin (Fig.7.22). This can ensure not just the directed way of sending information, but also a very fast way of sending it, as a node that receives the information in a particular bin, can directly send the information in the immediate next bin, ensuring faster communication of the information, instead of waiting for the next frame to send the information out. For example, a node at a hop-count of “4”, where N=8, will send the information in bin number 4, which will be listened in by a node at a hop-count of “3”, which will send the information in bin number 5, getting listened by the nodes only at a hop-count of “2” and similarly



**Figure 7.22. Bucket Passing type of packet routing scheme.**

finally to the root node (i.e. data-collector node). In cases where the information has to always reach the data-collector node, the scheme proposed adds significant advantage compared to the simple broadcasting based schemes, as only nodes in the direct-common path towards the data-collector node participate in sending the information, while the rest of the nodes do not have to send any information. The information from end-to-end also reaches very fast with latency of only one frame cycle due to true bucket-passing type of scheme in this case. The scheme works well due to the nodes partitioning the frame-duration in small bins according to their spatial/physical distance (i.e. hop-count) to the central-node.

## **7.5 Summary**

In this chapter we presented two different new methodologies for event broadcasting in a wireless sensor network. While the first methodology presented provided a means of sending information in a structure-less manner without the use of any data-packet structures, it nevertheless was limited to a small number of distinguishable messages. In the second methodology we presented a simple algorithm, which can be implemented in conjunction with UWB impulse radios to broadcast the occurrence of an event to all the nodes in the network. The hop-count of a node where the event was sensed gets transmitted through the network telling every node approximately how far away an event happened. We also show that with the use of base-station nodes and exchange of the hop-count information between them a more exact localization can be done. The proposed method supports dynamic as well as opportunistic duty-cycling of the RF circuits at every node during ongoing communication. This helps reduce the node power at all the nodes and is fair. Event verification can also be utilized to allow neighborhood correlation of the event to check the event propagation. This method enables self-healing of the sensor nodes and

can also be used for self-validation of higher priority events. Furthermore, with the addition of event-classification, different type of events can be propagated. The classification bins can also act as message classifier, giving one the opportunity to use the scheme for normal packet-based communication between any two nodes as well. With the successes in designing ultra low power impulse radio designs [98-100], as well as implementation success in high accuracy synchronization scheme [101-102] one can see the usefulness of this scheme for low power wireless sensor networks.

## CHAPTER 8

### SUMMARY AND FUTURE WORKS

#### 8.1 Dissertation Summary

The fast emerging field of wireless sensor networks holds a lot of promise for future applications ranging from healthcare, agriculture, and military to hazard and border protection etc. Low power communication is the key to the large scale deployment of these sensory networks.

In this dissertation work, we did link-margin optimization based analysis to show that with traditional narrowband radio approach, one cannot achieve the low power required of these sensor radio nodes, and identified duty-cycled radio architecture as the architecture of choice. However, in order to save power, these duty-cycled radio architectures require synchronization. We identified the pulse-coupled oscillator based synchronization scheme for realizing global synchronization. A study of the robustness of this synchronization scheme was conducted using event based simulator to see the impact of the frequency-mismatch, delay or jitter on the network.

After, verifying the robustness of these synchronization schemes, we designed a low power transceiver operating at  $19\mu\text{W}$  system power as an initial proof of concept design, and show it to be working over 2.5m range. We then identified certain limitations of the design that required us to move to FCC-mandated 3.1-10.6GHz band. A  $20\mu\text{W}$  100Kbps FCC compliant transceiver was designed and fabricated in a 90nm CMOS process that compares very favorably with the state-of-the-art designs at similar data rates. In collaboration with other project-mates we designed the whole radio system, including the timing circuitry that was measured to consume  $86\mu\text{W}$  at 150Kbps. The design could operate up to 2.5m, with a demonstrated range of 1.6m.

By increasing the transmitted power and fully utilizing the FCC mask, the design can be extended to 15m range.

In this work, we also devised a scheme for localized, per node synchronization detection that controls the duty-cycling of the radio. A self-reinforcement based scheme was also designed to help maintain synchronization in the wake of misdetections thereby improving the robustness of the synchronization scheme.

We also proposed some novel applications around the globally synchronized wireless network. A structure-less event-communication scheme based on interesting properties of the PCO synchronization scheme can be used for event-broadcasting for events such as fire or gas hazards. Another event-broadcasting scheme was also devised, that facilitates localization, event classification, as well as neighborhood validation while facilitating dynamic duty-cycling.

## **8.2 Future Works**

In the rest of this chapter, we discuss various challenges that we came across while designing and analyzing the system. Degenerate cases associated with the proposed global synchronization scheme can lead to some of the system problems such as symbol self-interference, offset spread, in-band narrowband interference etc. These problems can have significant potential for performance degradation of the system scalability, and are discussed in that context in this chapter. We also propose some solutions that can be pursued to tackle each one of the challenges.

### **8.2.1 Offset-spread due to Distance-delay**

While, distance-delay in the Pulse-coupled oscillator network does not create problems for synchronization, it does degrade the quality of synchronization by creating phase-offset between nodes. In a network of randomly arranged nodes, the

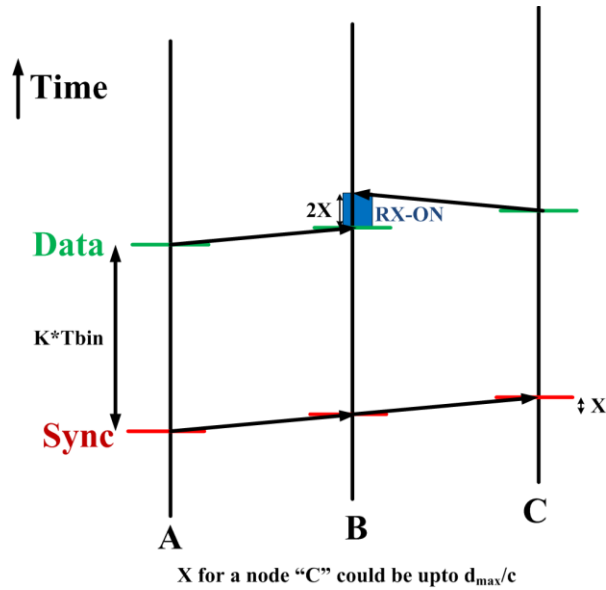


**Figure 8.1. Showing the offset expectation, in the neighborhood of a node “B” in the simple pulsing scheme. Based on different values of “x” for “B” to be able to receive the signal from both “A” and “C” has to open the window for “2x” duration in the data-bin.**

phase-offsets are a function of inter-node distances. Since, a node in any given location communicates to only the neighboring nodes, the phase-offsets uncertainty can result into an uncertainty in expecting the data signal of  $\pm T_d$ . Where  $T_d$  can be calculated as maximum distance-delay based on maximum range of communication between two neighboring nodes. For example for a 1m range of communication  $T_d$  will be 3ns ( $d/c$ , where  $d$ =distance,  $c$ =speed of light), while for a 10m communication it will be 30ns, giving an uncertainty in the expectation of pulses, of 6ns and 60ns respectively.

Since, in the duty-cycled mode of communication, a node doesn't know which node may want to initiate communication with it; all nodes have to be prepared to be able to listen to any of the neighbors in their neighborhood during the data-bin. The pulse-arrival uncertainties will require the node to open the timing window for longer duration to be able to intercept the pulses from any node in the neighborhood, thereby

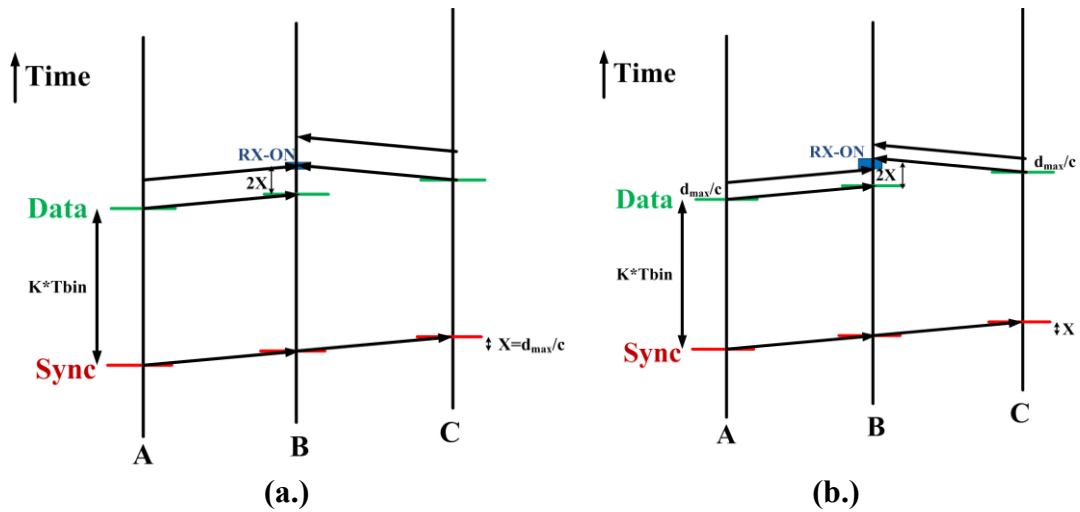


**Figure 8.2. (a.) RX-ON window opening requirement with “X” known , using double pulsing (b.) RX-ON window opening requirement with “X” unknown, using double pulsing. Both result into power saving for the receiver, due to lower window opening requirements.**

requiring higher power consumption at the receiver (Fig.8.1).

While, a node can expect to learn these offsets in its neighborhood, for a static network, they cannot still utilize this knowledge, unless a node knows a-priori which other node wants to talk to it and thus the narrowing of the data-window is applicable only during the data-communication phase, or alternatively in a 2-node system. For a large number of randomly distributed nodes, a node has to open the RF-ON window taking into account all possible pulse arrival timings, thereby increasing the power budget of the receiver.

### 8.2.1.1 Solution Direction

Since, the  $X$  can be  $d_{max}/c$  (Fig.8.1) (where  $d_{max}$  is maximum one-hop communication range and  $c$  is the speed of light), one can think of sending two pulses apart by  $d_{max}/c$  to ensure an overlap of at least one pulses in time at a receiving node “B” in the network, over a small time-window from any node in its neighborhood (“A” or “C”). This thereby removes the RX-ON window constraints based on timing offset (Fig.8.2.a). This is however true if the nodes are uniformly distributed with a

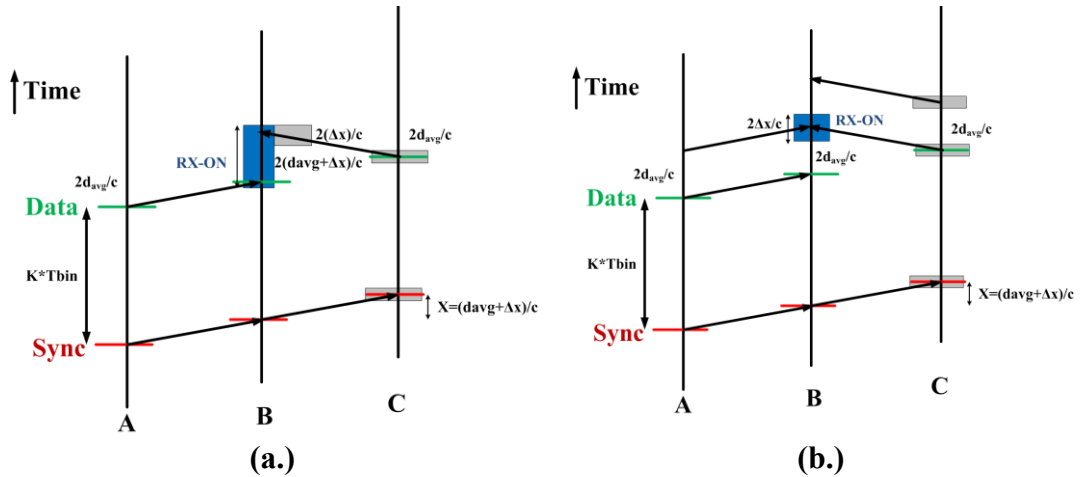


**Figure 8.3. (a.) RX-ON window opening requirement with  $x=d_{avg}+ \Delta x$ , in case of single pulsing, (b.) the Rx-On opening requirement with double pulsing in the same situation.**

fixed inter-node distance between them. In a sensor network, however nodes might be distributed randomly, thus  $X$  is not pre-known. For example  $X$  for a node “C” (Fig.8.2.b) could be anything between 0 to  $d_{max}/c$ , and “B” won’t know about the exact value of “ $X$ ”, in this case, the double pulsing will still need a window to be open, but instead of  $2*d_{max}/c$  (Fig.8.1), the window will be required to be opened only for  $d_{max}/c$ , as shown in Fig.8.2.b. This will mean a  $2x$  power saving at the receiver but  $2x$  power consumption at the transmitter, and thus the scheme would be useful only if the transmitter power consumption overhead outweighs the receiver power saving.

An alternate situation in a sensor network can exist, where the nodes are deployed pseudo-randomly, meaning the nodes are distributed in any neighborhood with a distance distribution of  $(d_{avg}+\Delta X)$ , in this configuration double pulsing scheme will require the window to be opened for only  $2\Delta X/c$  (Fig.8.3.b.), as compared to  $2(d_{avg}+\Delta X)/c$  (Fig.8.3.a) for the nominal case, and can result in lot of power saving. For example, for a 10m communication, with distance uncertainty of  $\pm 2m$ , this results in a saving of  $24/4 = 6$  times @ Rx.

Delay offset can also happen in the network of pulse-coupled oscillators due to delays associated with the circuits for pulse-detection, coupling and firing of up to  $\sim 10$ ns. All these delays can contribute to the fixed offset, even without any distance uncertainties. The proposed solution will perform in the presence of circuit delays as well and can result in more than twice the improvement even for completely random distribution of the nodes in the network.

### **8.2.2 A node-at the threshold of pulse detection-range**

In a network of pulse-coupled oscillators, the dynamics were studied based on a hard-threshold of detection, which implies a hard-threshold on the range of communication. In a practical network these hard-threshold or hard-boundaries do not exist and there is a region of uncertainty, where the pulses will be occasionally missed. While, the synchronization retention mechanism is expected to take care of occasional misses at a node, higher miss rates can create problems for the whole network. One can easily envision a situation, where a node has high pulse-miss rates in such cases, and thus can create large amount of large error injections (due to frequency mismatch) into the network, which will be detrimental for maintaining the synchronization in the whole network.

#### **8.2.2.1 Solution Direction**

The problem however can be tackled, using dense-network, ensuring that any such node in the network always have a more guaranteed route of pulse arrival, albeit with an extra hop-count, i.e. delayed path. In such cases, the miss-rate induced timing errors will be limited to only the extra delay from the more assured path, and so will reduce the severity of the problem for the network.

### **8.2.3 Two nodes destructively interfering at another node**

Inherent in the proposed scheme of global synchronization is the expectation that

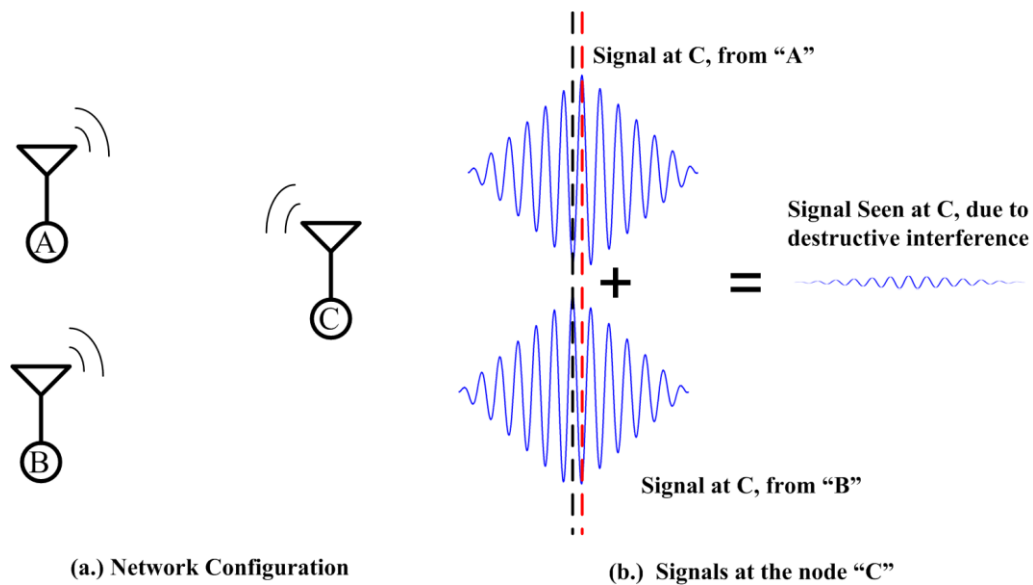


**Figure 8.4. Showing an example network configuration and how a node "C" can have destructive interference from the signal emitted from node "A" and node "B", making it blind to node "A" and node "B" even though it's there in the neighborhood of the two nodes.**

along the sync-boundaries all the nodes fire together. Even though there are delay offsets in firing of pulses by various nodes in the network, one can always envision a situation where two "sync" pulses from two nodes in the neighborhood of another node arrive with a phase-offset that creates a completely destructive interference of the signal at the receiving node (Fig.8.4). In this case, even though the node was in the receiving range of both nodes, it still gets blinded due to destructive interference of the pulse-wavelet, resulting in a loss of connectivity for the network, i.e. making this node blind to the other two nodes.

Though, in a randomly deployed network, there is very low probability of this happening; one still needs to take care of this effect. A node becoming blind to other nodes in its neighborhood is akin to being a non-cooperative node in the network, and since synchronization is co-operative in the pulse-coupled oscillator based scheme it

can create complications for the whole network.

### **8.2.3.1 Solution Direction**

This problem can be solved by using antenna diversity at the receiver for any node. For example at node “C” if there are two antennas separated by  $c/2f_0$ , where “c” is the speed of light and  $f_0$ , the carrier frequency inside the wavelet, then if the signals at one antenna destructively interfere, then the signals at the other antenna will constructively interfere, thereby always ensuring a signal detection at node “C”. The signal energy from the two antennas can be combined together and processed to take care of the destructive interference problem in such situations, though it will add to the complexity of the receiver design.

### **8.2.4 Asymmetric communication**

In our network analysis in chapter-2, we considered symmetric communication, i.e. if a node “A” can reach a node “E” directly, then the node “E” can also reach the node “A” directly, which meant the connectivity was always bi-directional.

In a real network, however, the communication is not always symmetric, due to transmit power variation or the receiver power sensitivity variations, the two nodes in the immediate neighborhood are not guaranteed to be able to reach other and an asymmetric link may exist between two nodes in the same neighborhood, where one node can receive the signal from other node, but is not able to transmit/reach back directly.

When this effect was included in the network, for sparsely connected network of pulse-coupled oscillator it was found that sometimes the network will not synchronize, or will settle to an unstable synchronization mode. A further debug of the failure mode in such cases was found to be due to delayed path/link that can exist for a node in such network. (Fig.8.5). For example, as shown in Fig.8.5, the echo from node “A” can get

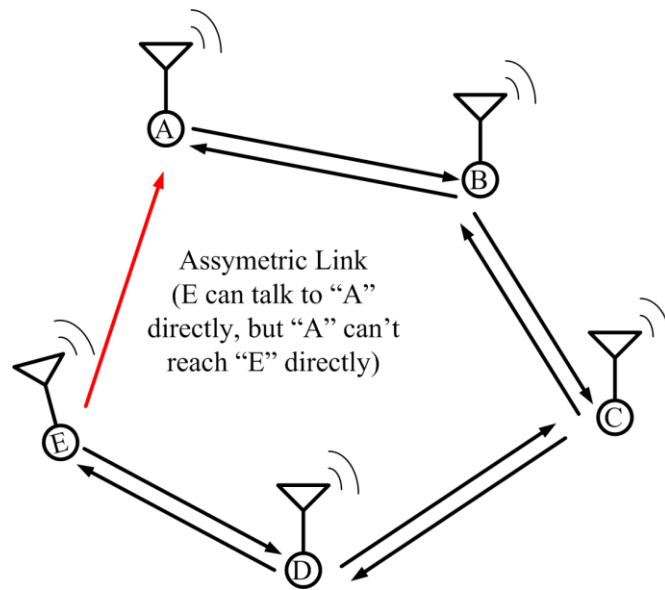


**Figure 8.5. An Assymmetric network configuration, “A” can receive the signal from “E” directly but “E” can’t receive the signal from “A” directly.**

repeated by a chain of nodes in this case, after a 4-hop count delay during the synchronized state. This makes the node “E” effectively reachable to “A”, but through a long distance, that creates the synchronization problem. In this particular case, the blackout window of “A” needs to be increased to take care of this worst case delay in the network to achieve synchronization. In a large network, this delay can be high (> nominal frame rate) and thus can result in failure of synchronization.

#### **8.2.4.1 Solution Direction**

As suggested above, increasing the blackout window to take care of the worst case round-trip delay forces synchronization; however, it also limits the scalability of the network. An alternate approach can be to make the network dense, which can effectively reduce the worst case round-trip delay between any such nodes that has an asymmetric link, without causing any impact on the scalability of the network. Though, higher density will certainly mean a greater cost of deployment of such networks.

### **8.2.5 Synchronization in the presence of an un-cooperating node (node failures)**

In a large network of pulse-coupled oscillators a node due to its internal faults may become un-cooperative i.e. doesn't follow the pulse-coupling phenomenon. One such type of fault could be where the receiver circuitry can't detect any pulses, while the transmitter circuit continues to transmit. Since, the pulse-coupled oscillator based synchronization scheme is dependent upon co-operation between nodes. It has been found that in presence of such uncooperative nodes in the network can lead to failure of the whole network.

#### **8.2.5.1. Solution Direction**

Since, the synchronization in a large network of oscillators is co-operative, one can think of isolating the non-cooperating node, by providing the ability for every node to find the non-cooperative node. Now, since there is no unique signature on a per-node basis assigned to each node in the impulse based signaling, it's impossible for any node in the network to know which node is non-cooperating. In the shared wireless medium that all nodes in the network share, a pulse sent by a non-cooperating node is as good as any pulse from a cooperating node and making it difficult to isolate the faulty node from the network.

Since, in a co-operative network, all the nodes cooperating in the network have the tendency to get into the global order (i.e. synchronized), while the non-cooperating node doesn't have such global order purpose requirement, an alternate selective coupling based methodology, originally proposed by Strogatz et. al. [103] for PLL locking can be thought of in the pulse-coupled system. In this scheme, each pulse-coupled oscillator node first evaluates the amount of coupling (phase-advancement) that it has to apply based on the "sync" pulse detection, but delays this coupling till it's closer to firing (Twait) as shown in Fig.8.6. The PCO after Twait, applies the coupling signal that corresponded to the closest "sync" pulse that it detected. In the limit where

$T_{wait}$  is closer to  $T_0$  (nominal firing time of the PCO) (Fig.8.6), this system can achieve good quality synchronization. This happens, as the nodes cooperating to each other will eventually fire at the same time as other nodes, while the faulty non-cooperating node signal will fall “out of sync”.

The pulse from non-cooperating node signals, though “out of sync” can still sometimes fall in the window between  $T_{wait}$  and  $T_0$ , and thus can create a coupling for the nodes in the network. This can create a timing uncertainty of “ $T_0 - T_{wait}$ ”, degrading the synchronization performance for the network. In this case, one will be required to have “ $T_0 - T_{wait}$ ” as small as possible, though in the case of frequency mismatch the “ $T_0 - T_{wait}$ ” has to compensate the period mismatch, and so can’t really be zero. That means the system will have similar % timing performance uncertainties as the % frequency mismatch, which could be ~20% for the network, thereby severely degrading the performance of the network, while adding significant complexity.

An alternate approach could be to create a self-diagnostic circuit that checks for

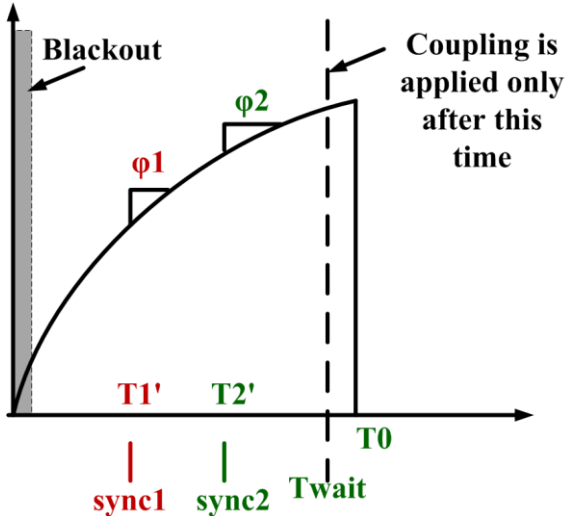


**Figure 8.6. Concept of selective coupling, based on “sync” detected at various instances, a node evaluates the phase-change required, but applies the coupling only after  $T_{wait}$ , and applies the coupling corresponding to the closest signal that was received, thereby effectively ignoring the coupling from “sync1” in this case.**

such failures of the design (receiver not working), and thereby shuts off the transmitter in field. For example the receiver not working can be easily checked if the design doesn't receive any pulses, or if the localized state-machine detects non-advent of synchronization after multiple efforts, thereby forcing the node to shut-off its own transmitter.

### **8.2.6 Security problem: an unwanted jammer in the network**

While a faulty node can be expected to self-isolate itself due to the presence of fault-detection circuitries, some time a non-cooperating node can exist in the system, due to the presence of a jammer that wants the synchronization to fail, thereby bringing down the network. In this case, the jammer has to just send pulses periodically or periodically in the “sync” channel and the whole network can be brought down imposing serious threats for the large scale deployment of the network.

#### **8.2.6.1. Solution Direction**

Most of the existing networks come around these security problems by employing some type of “coding”, that the jammer network must break to bring down the whole network. Due to simultaneous transmission of the “sync” pulse in synchronized mode of operation by various nodes, a time-signature of code is not possible. Nodes can however use orthogonal frequency codes to identify the “sync” pulse, which can be coded over multiple frequency-bands, where the frequency-coded “sync” signature can be simultaneously transmitted over various bands. Since, 14-UWB bands can exist between 3.1-10.6 GHz; one can have 14-bit code by utilizing all the bands simultaneously. This however can create significant overhead for the design of the receiver and transmitter circuitries, and are still prone to jammer, as the jammer can easily get to know the code, as it is shared by all the nodes in the network in the shared medium. A band-hopping code sequence of the “sync” pulses can also work, but again

it's open to jammer to learn. This however, is not an uncommon problem in wireless communication; an intelligent jammer of this kind has to be removed by a network manager and it will require some type of manual intervention for the system to work in the presence of intelligent jammers.

### **8.2.7 High frequency mismatch & susceptibility of the system to misdetections**

In chapter-2 we discussed how frequency mismatch can be negated by increased coupling. At increased coupling however, the system also becomes very sensitive to misdetection of pulses, where every misdetection of a pulse can necessitate a resynchronization, and thus can be bad for the scalability of the system unless some amount of tolerance can be provided. While in chapter-6 we talked about robustness against missing pulses, in this case, the robustness is required against detecting pulses, where there wasn't originally supposed to be a pulse.

#### **8.2.7.1 Solution Direction**

A node can potentially implement selective coupling rules once, synchronized, to see which pulse might be a valid pulse, based on its relative location compared to existing pulses. Alternatively, one can lower the sensitivity of the receiver to ensure very low probability of detecting a pulse, where none exists.

### **8.2.8 Susceptibility to narrow-band in-band interferers**

Impulse based radio with their ultra-wide-band characteristics is prone to narrow-band interferers. While out-of-band narrowband interferers can be easily rejected using the band-select filters, and to that end good design performance was achieved by the receiver. The in-band narrowband interferers can still create problem with impulse-detection, thereby operability of the sensor network. Since, UWB communication system has to co-exist with various narrowband interferers in the same band, schemes are required to reject the narrowband interferers in the same-band. For

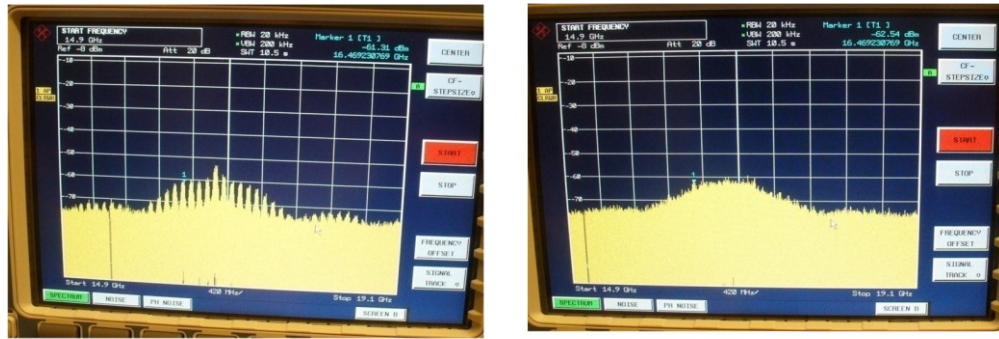
example for our band of interest a WI-MAX narrowband interferer at 3.5GHZ can create problem for the system, where it can effectively act as a jammer, bringing down the network.

#### **8.2.8.1 Solution Direction**

Various narrow-band rejection schemes exist in literature, simplest being the notch-filter based design. However a notch filter based solution is not desired for in-band interfere rejection, as it requires the pre-knowledge of the interferer frequency. Some adaptive notch-filtering schemes that don't require pre-knowledge of the interferer frequency are also not good, as by putting the notch filter, they also take significant part of the signal power due to low Q of such filters. In recent time non-linear operations such as squaring and T-K energy operator based designs [104] have come up in the UWB impulse radio space, where a narrowband interferer, is translated to close to DC irrespective of the frequency, while the UWB impulse translates to a wider band of signal. A high pass filter with a cut-off of ~10MHz, then can remove the narrowband interferer completely without losing much of the signal power. A T-K operator based design was demonstrated in our lab by project-mate Wacek Godycki, which could reject the in-band narrowband interferers very effectively [105]. Further improvement on these designs is however required to make the rejection circuitry duty-cycle-able. Rejection of two or more simultaneous in-band interferers though is still an open question for these systems.

#### **8.2.9 Scaling to higher data rates and optimizing the FCC-mandated power spectrum**

The periodic pulse transmission of the “sync” pulse along a fixed frame-boundary can create frequency spikes in the measured spectrum of the signal (Fig.8.7 a) , this at low data rate of 100KHz results into periodic spike every 100KHz, and are typically



(a.)

(b.)

**Figure 8.7. (a.) spectrum without frequency dithering. (b.) spectrum with frequency dithering.**

not a concern as the FCC spectral mask is measured with an RBW of 1MHz. However, if one were to utilize the pulse-coupled oscillator based synchronization at a higher rate, these spikes may result into inefficient utilization of the FCC’s UWB mask, and depending upon the rate requirement, the underutilization could be as much as 6dB.

### 8.2.9.1 Solution Direction

A spread-spectrum based carrier-frequency dithering can be done to effectively redistribute these spikes around resulting into efficient use (Fig.8.7.b) of the average power limit set by FCC, a measured result of the spectrum without frequency dithering and with dithering is shown as in Fig.8.7.

### 8.2.10 Summary of Challenges/Future Work

Most of the challenges as discussed in this chapter, can however only limit the scalability of the solution in a randomly deployed sensor network, but can be very easily managed by manual intervention, and are not of much significance in a managed sensor network. For randomly deployed sensor network, however the challenges discussed in this chapter can limit the performance of the network and so requires further investigations along the line of suggested solution directions.

## REFERENCES

- [1] T. H. Lee, "The Design of CMOS Radio-Frequency Integrated Circuits", Cambridge, U.K. Cambridge Univ. Press, 1998.
- [2] Pinel, S.; Sarkar, S.; Sen, P.; Perumana, B.; Yeh, D.; Dawn, D.; Laskar, J.; , "A 90nm CMOS 60GHz Radio," Solid-State Circuits Conference, 2008. ISSCC 2008. Digest of Technical Papers. IEEE International , vol., no., pp.130-601, 3-7 Feb. 2008.
- [3] B. Chi, et.al., "Low-Power Transceiver Analog Front-End Circuits for Bidirectional High Data Rate Wireless Telemetry in Medical Endoscopy Applications," Biomedical Engineering, IEEE Transactions on , vol.54, no.7, pp.1291-1299, July 2007.
- [4] H. Sari, G. Karam, and I. Jeanclaude,"Transmission techniques for digital terrestrial TV broadcasting," Communications Magazine, IEEE , vol.33, no.2, pp.100-109, Feb 1995.
- [5] Dr. Khaled Elleithy, Mobile communications CpE481 course slide, Mobile Communication: introduction, Chapter-01, <http://www1bpt.bridgeport.edu/sed/fcourses/cpe481/Lectures/C01-Introduction.ppt>, school of engineering at the University of Bridgeport.
- [6] Shaw, M.; Ziglioli, F.; Combi, C.; Baldo, L.; , "Package design of pressure sensors for high volume consumer applications," Electronic Components and Technology Conference, 2008. ECTC 2008. 58th , vol., no., pp.834-840, 27-30 May 2008.
- [7] Zhou Shenghua; Wu Nanjian; , "A novel ultra low power temperature sensor for UHF RFID tag chip," Solid-State Circuits Conference, 2007. ASSCC '07. IEEE Asian , vol., no., pp.464-467, 12-14 Nov. 2007.
- [8] He, C.; Arora, A.; Kiziroglou, M.E.; Yates, D.C.; O'Hare, D.; Yeatman, E.M.; , "MEMS Energy Harvesting Powered Wireless Biometric Sensor," Wearable and Implantable Body Sensor Networks, 2009. BSN 2009. Sixth International Workshop on , vol., no., pp.207-212, 3-5 June 2009.
- [9] Sang-hyeok Yang; Kyoung-bum Kim; Eung-ju Kim; Kwang-hyun Baek; Suki Kim; , "An ultra low power CMOS motion detector," Consumer Electronics, IEEE Transactions on , vol.55, no.4, pp.2425-2430, November 2009.

- [10] Haibing Hu; Gang Wang; Qixing Zhang; Jinjun Wang; Jun Fang; Yongming Zhang; , "Design wireless multi-sensor fire detection and alarm system based on ARM," *Electronic Measurement & Instruments*, 2009. ICEMI '09. 9th International Conference on , vol., no., pp.3-285-3-288, 16-19 Aug. 2009.
- [11] Erden, Fatih; Soyer, E. Birey; Toreyin, B. Ugur; Cetin, A. Enis; , "VOC gas leak detection using Pyro-electric Infrared sensors," *Acoustics Speech and Signal Processing (ICASSP)*, 2010 IEEE International Conference on , vol., no., pp.1682-1685, 14-19 March 2010.
- [12] A. Bharathidasan and V. A. Sai Pondura, "Sensor Networks: An Overview," Department of ECE, University of California, Davis, Technical Report, May 2003, [www.csif.cs.ucdavis.edu/~bharathi/sensor/survey.pdf](http://www.csif.cs.ucdavis.edu/~bharathi/sensor/survey.pdf).
- [13] J. Ryckaert, "Ultra-wideband communication technology for sensor network applications", presentation slides, session 9, April 1-4, 2008, IMEC, <http://www.unithertechnologyconference.com/downloads/SESSION9/RYCKAERT.ppt> , 1st Annual Uniter Nanomedical & Telemedical Technology Conference.
- [14] J. M. Rabaey, J. Ammer, B. Otis, F. Burghardt, Y.H. Chee, N. Pletcher, M. Sheets, and H. Qin, "Ultra-low-power design," *IEEE Circuits and Devices Magazine*, Vol. 22, No. 4, July 2006.
- [15] B. Otis and J. Rabaey, "Ultra-Low Power Wireless Technologies for Sensor Networks", Springer, US, 2007.
- [16] S. Roundy, "Energy scavenging for wireless sensor nodes with a focus on vibration to electricity conversion", PhD thesis, University of California, Berkeley, May 2003.
- [17] V. Ekanayake, C. Kelly IV, and R. Manohar, "An Ultra Low-Power Processor for Sensor Networks". In proceedings of International Conference on Architectural Support for Programming Languages and OS (ASPLOS), 2004.
- [18] Nazhandali, L.; Zhai, B.; Olson, A.; Reeves, A.; Minuth, M.; Helfand, R.; Sanjay Pant; Austin, T.; Blaauw, D.; , "Energy optimization of subthreshold-voltage sensor network processors," *Computer Architecture*, 2005. ISCA '05. Proceedings. 32nd International Symposium on , vol., no., pp. 197- 207, 4-8 June 2005.

- [19] L. Nazhandali, M. Minuth, B. Zhai, J. Olson, T. Austin, and D. Blaauw, "A second-generation sensor network processor with application-driven memory optimizations and out-of-order execution," in Proc. Int. Conf. Compilers, Architecture Synthesis, Embedded Systems, 2005, pp. 249–256.
- [20] J.R. Long, W. Wu, Y. Dong, Y. Zhao, M.A.T. Sanduleanu, J.F.M. Gerrits, and G.V. Veenendaal, "Energy-efficient wireless front-end concepts for ultra lower power radio," IEEE Custom Integrated Circuits Conference. vol., no., pp.587-590, 21-24 Sept. 2008.
- [21] B. W. Cook, A. Berny, A. Molnar, S. Lanzisera, K. S. J. Pister, "Low-Power 2.4-GHz Transceiver With Passive RX Front-End and 400-mV Supply", IEEE Journal of Solid State Circuits (JSSC), December 2006.
- [22] A. Molnar, B. Lu, S. Lanzisera, B.W. Cook, and K.S.J. Pister, "An ultra-low power 900 MHz RF transceiver for wireless sensor networks," Custom Integrated Circuits Conference, 2004. Proceedings of the IEEE 2004 , vol., no., pp. 401- 404, 3-6 Oct. 2004.
- [23] W. Wu; M.A.T. Sanduleanu, X. Li, and J. R. Long , "17GHz RF Front-Ends for Low-Power Wireless Sensor Networks," Bipolar/BiCMOS Circuits and Technology Meeting, 2007. BCTM '07. IEEE , vol., no., pp.164-167, Sept. 30 2007-Oct. 2 2007.
- [24] A. Medi, and W. Namgoong, "A High Data-Rate Energy-Efficient Interference-Tolerant Fully Integrated CMOS Frequency Channelized UWB Transceiver for Impulse Radio," Solid-State Circuits, IEEE Journal of , vol.43, no.4, pp.974-980, April 2008.
- [25] A.C.W. Wong, G. Kathiresan, C.K.T. Chan, O. Eljamaly, and A.J. Burdett, "A 1V wireless transceiver for an ultra low power SoC for biotelemetry applications," Solid State Circuits Conference, 2007. ESSCIRC 2007. 33rd European , vol., no., pp.127-130, 11-13 Sept. 2007.
- [26] B. Cook, "Low Energy RF Transceiver Design", PhD report, EECS Department, University of California, Berkeley, 2007.
- [27] G. Gramegna, M. Paparo, P. G. Erratico, and P. D. Vita, "A sub-1-dBm  $\pm$ 2.3-kV ESD-protected 900-MHz CMOS LNA," IEEE J. Solid-State Circuits, vol. 36, no. 7, pp. 1010–1017, Jul. 2001.

- [28] D. Linten, S. Thijs, M.I. Natarajan, P. Wambacq, W. Jeamsaksiri, J. Ramos, A. Mercha, S. Jenei, S. Donnay, and S. Decoutere, "A 5-GHz fully integrated ESD-protected low-noise amplifier in 90-nm RF CMOS," *Solid-State Circuits, IEEE Journal of*, vol.40, no.7, pp. 1434- 1442, July 2005.
- [29] B.W. Cook, A. Molnar, and K.S.J. Pister, "Low power RF design for sensor networks," *Radio Frequency integrated Circuits (RFIC) Symposium, 2005. Digest of Papers. 2005 IEEE*, vol., no., pp. 357- 360, 12-14 June 2005.
- [30] N.M. Pletcher, S. Gambini, and J. Rabaey, "A 52  $\mu$ W Wake-Up Receiver With -72 dBm Sensitivity Using an Uncertain-IF Architecture," *Solid-State Circuits, IEEE Journal of*, vol.44, no.1, pp.269-280, Jan. 2009.
- [31] S. Drago, D.M.W. Leenaerts, F. Sebastiano, L.J. Breems, K.A.A. Makinwa, and B. Nauta, "A 2.4GHz 830pJ/bit duty-cycled wake-up receiver with -82dBm sensitivity for crystal-less wireless sensor nodes," *Solid-State Circuits Conference Digest of Technical Papers (ISSCC), 2010 IEEE International*, vol., no., pp.224-225, 7-11 Feb. 2010.
- [32] C. Andrews, and A.C. Molnar, "A passive-mixer-first receiver with baseband-controlled RF impedance matching,  $\ll$  6dB NF, and  $\gg$  27dBm wideband IIP3," *Solid-State Circuits Conference Digest of Technical Papers (ISSCC), 2010 IEEE International*, vol., no., pp.46-47, 7-11 Feb. 2010.
- [33] F. S. Lee and A. P. Chandrakasan, "A 2.5nJ/b 0.65V 3-to-5GHz subbanded UWB receiver in 90nm CMOS," *ISSCC 2007, Feb. 2007*.
- [34] Ryckaert, J.; Badaroglu, M.; De Heyn, V.; Van der Plas, G.; Nuzzo, P.; Baschiroto, A.; D'Amico, S.; Desset, C.; Suys, H.; Libois, M.; Van Poucke, B.; Wambacq, P.; Gyselinckx, B.; , "A 16mA UWB 3-to-5GHz 20Mpulses/s Quadrature Analog Correlation Receiver in 0.18/spl mu/m CMOS," *Solid-State Circuits Conference, 2006. ISSCC 2006. Digest of Technical Papers. IEEE International*, vol., no., pp.368-377, 6-9 Feb. 2006.
- [35] R. E. Mirollo and S. H. Strogatz, "Synchronization of pulse-coupled biological oscillators," *SIAM J. Appl. Math.*, vol. 50, no. 6, pp. 1645–1662, Dec. 1990.

- [36] J. Buck, Synchronous rhythmic flashing of fireflies. II, *Quart. Rev. Biol.*, 63 (1988), pp. 265-289.
- [37] J. Buck, and E. Buck Synchronous fireflies, *Scientific American*, 234 (1976), pp. 74-85.
- [38] F. E. Hanson, "Comparative studies of firefly pacemakers, *Fed. Proc.*, 37 (1978), pp. 2158-2164.
- [39] H. M. Smith, " Synchronous flashing of fireflies", *Science*, 82 (1935), p. 151.
- [40] A. T. Winfree, "The Geometry of Biological Time", Springer-Verlag, New York, 1980.
- [41] G. Ermentrout, and J. Rinzel "Beyond a pacemaker's entrainment limit: phase walk-through," *American Journal of Physiol*, vol. 246, pp. R102-R106, 1984.
- [42] Peskin, *Mathematical aspects of heart physiology*, Courant Institute of Mathematical Sciences, New York University, New York, 1975, pp. 268-278.
- [43] Y. Kuramoto, "Collective Synchronization of pulse-coupled oscillators and excitable units", *Physica D: Nonlinear Phenomena* , vol. 50 Issue 1, May, 1991.
- [44] Y. W. Hong and A. Scaglione, "A scalable synchronization protocol for large scale sensor networks and its applications," in *IEEE J. Sel. Areas Commun.*, pp. 1085-1099, May 2005.
- [45] M. Timme, "Collective Dynamics in Networks of Pulse-Coupled Oscillators," Ph. D. dissertation, Max Planck Institute, Gottingen, Netherlands, 2002.
- [46] W. Gerstner, "Rapid phase locking in systems of pulse-coupled oscillators with delays," in *Phys. Rev. E* vol. 76, pp. 1755-1758, Mar. 1996.
- [47] L. Abbott and C. van Vreeswijk, "Asynchronous states in networks of pulse-coupled oscillators," in *Phys. Rev. E* vol. 48, pp. 1483-1490, Aug. 1993.
- [48] U. Ernst, K. Pawelzik, and T. Geisel, "Delay-Induced multistable synchronization of biological oscillators," in *Phys. Rev. E* vol. 57, pp. 2150- 2162, Feb. 1998.

- [49] M. Zeitler, A. Daffertshofer, and C. C. A. M. Gielen, "Asymmetry in pulse-coupled oscillators with delay," in *Phys. Rev. E* vol. 79, 065203-1- 4(R), Jun. 2009.
- [50] X. Wang, R. Dokania, Y. Zhuang, C. Dorta-Quinones, W. Godycki, M. Lyons, A. Apsel, "A Self-Synchronized, Crystal-Less, 86uW, Dual-Band Impulse Radio for Ad-Hoc Wireless Networks", submitted to ISSCC 2011.
- [51] Qayyum, A.; Saleem, M.U.; Tauseef-Ul-Islam; Ahmad, M.; Khan, M.A.; , "Performance increase in CSMA/CA with RTS-CTS," Multi Topic Conference, 2003. INMIC 2003. 7th International , vol., no., pp.182-185, 9-9 Dec. 2003.
- [52] Baek, W.; Kuo, C.-C.J.; Wei, D.S.L.; , "CSMA/CA MAC Protocol Design for Topology Controlled Ad Hoc Networks: A Cross Layer Approach," *Computer Science and Information Engineering*, 2009 WRI World Congress on , vol.1, no., pp.413-417, March 31 2009-April 2 2009.
- [53] S. B. T. Wang, "Design of Ultra-Wideband RF Front-End," Ph. D. dissertation, University of California at Berkeley, Berkeley, CA, 2005.
- [54] F. S. Lee and A. P. Chandrakasan, "A 2.5nJ/b 0.65V 3-to-5GHz subbanded UWB receiver in 90nm CMOS," ISSCC 2007, Feb. 2007.
- [55] D. D. Wentzloff and A. P. Chandrakasan, "A 47pJ/pulse 3.1-to-5GHz All-Digital UWB Transmitter in 90nm CMOS"; ISSCC 2007, Feb. 2007.
- [56] B. W. Cook, A. Berny, A. Molnar, S. Lanzisera, K. S. J. Pister, "Low-Power 2.4-GHz Transceiver With Passive RX Front-End and 400-mV Supply", *IEEE Journal of Solid State Circuits (JSSC)*, December 2006.
- [57] "Revision of Part 15 the Commission's rules regarding ultra-wideband transmission systems," FCC, ET Docket 98-153, 2002.
- [58] Salehi-Abari, O.; Plett, C.; , "A differential 5th derivative Gaussian pulse generator for UWB transceivers," *Circuits and Systems (ISCAS)*, Proceedings of 2010 IEEE International Symposium on , vol., no., pp.1089-1092, May 30 2010-June 2 2010.
- [59] Haolu Xie; Xin Wang; Wang, A.; Bin Zhao; Yumei Zhou; Bo Qin; Hongyi Chen; Zhihua Wang; , "A varying pulse width 5th-derivative gaussian pulse generator for UWB transceivers in CMOS," *Radio and Wireless Symposium*, 2008 IEEE , vol., no., pp.171-174, 22-24 Jan. 2008.

- [60] Tuan-Anh Phan; Krizhanovskii, V.; Seok-Kyun Han; Sang-Gug Lee; Hyun-seo Oh; Nae-Soo Kim; , "4.7pJ/pulse 7th Derivative Gaussian Pulse Generator for Impulse Radio UWB," Circuits and Systems, 2007. ISCAS 2007. IEEE International Symposium on , vol., no., pp.3043-3046, 27-30 May 2007.
- [61] Yunliang Zhu; Zuegel, J.D.; Marciante, J.R.; Hui Wu; , "Distributed Waveform Generator: A New Circuit Technique for Ultra-Wideband Pulse Generation, Shaping and Modulation," Solid-State Circuits, IEEE Journal of , vol.44, no.3, pp.808-823, March 2009.
- [62] D. D. Wentzloff and A. P. Chandrakasan, "A 47pJ/pulse 3.1-to-5GHz All-Digital UWB Transmitter in 90nm CMOS"; ISSCC 2007, Feb. 2007.
- [63] J. L. Hill and D. E. Culler 2003. System Architecture for Wireless Sensor Networks. 2003, PhD thesis, University of California, Berkely.
- [64] Norimatsu, T.; Fujiwara, R.; Kokubo, M.; Miyazaki, M.; Maeki, A.; Ogata, Y.; Kobayashi, S.; Koshizuka, N.; Sakamura, K.; , "A UWB-IR Transmitter With Digitally Controlled Pulse Generator," Solid-State Circuits, IEEE Journal of , vol.42, no.6, pp.1300-1309, June 2007.
- [65] Chen, X.; Kiaei, S.; , "Pulse generation scheme for low-power low-complexity impulse ultra-wideband," Electronics Letters , vol.43, no.1, pp.44-45, Jan. 4 2007.
- [66] Mercier, P.P.; Daly, D.C.; Chandrakasan, A.P.; , "An Energy-Efficient All-Digital UWB Transmitter Employing Dual Capacitively-Coupled Pulse-Shaping Drivers," Solid-State Circuits, IEEE Journal of , vol.44, no.6, pp.1679-1688, June 2009.
- [67] J. Ayadi, J. Gerrits, Q. Xu, A. Hutter, P. Eggers, and I. Kovacs, "Design and Performance Analysis of UWB Communication System for Low Data Rate WPAN Applications", Report, IST PACWOMAN – Power aware communications for wireless optimised personal area networks, <http://www.imec.be/pacwoman/Welcome.shtml>.
- [68] F. S. Lee, and A. P. Chandrakasan 2007. A 2.5nJ/b 0.65V 3-to-5GHz Subbanded UWB receiver in 90nm CMOS. ISSCC 2007, 11-15 Feb. 2007.

- [69] X. Zhang, R. Dokania, M. Mukadam, and A. Apsel, "A Successive Approximation Based Process-Invariant Ring Oscillator", IEEE International Symposium on Circuits and Systems, June 2010, Paris, France.
- [70] D.D. Wentzloff and A.P. Chandrakasan 2006. Gaussian pulse generators for subbanded ultrawideband transmitters. IEEE Trans. Microw. Theory Tech., vol. 54, pp. 1647–1655, Jun. 2006.
- [71] T. Norimatsu, et. al. 2007. A UWB-IR transmitter with digitally controlled pulse generator. IEEE J. Solid-State Circuits, vol. 42, pp. 1300–1309, June 2007.
- [72] J. Ryckaert, et. al. 2005. Carrier-based UWB impulse radio: Simplicity, flexibility, and pulser implementation in 0.18-micron CMOS. in Proc. IEEE Int Conf. Ultra-Wideband, Sep. 2005, pp. 432–437.
- [73] J. Ryckaert, et al. 2007. A 0.65-to-1.4nJ/burst 3-to-10GHz UWB Digital TX in 90nm CMOS for IEEE 802.15.4a. ISSCC. Dig. Tech. Papers, Feb. 2007, pp. 120-121.
- [74] A. T. Phan, J. Lee, V. Krizhanovskii, Q. Le, S. Han, and S. Lee 2008. Energy-Efficient Low-Complexity CMOS Pulse Generator for Multiband UWB Impulse Radio. IEEE TCAS- I, Vol.55, No.11, December 2008.
- [75] L. Smaini, et. al. 2006. Single-Chip CMOS Pulse Generator for UWB Systems. IEEE J. Solid-State Circuits, Vol 41, 2006, pp. 1551-1561.
- [76] J. Ryckaert, M. Badaroglu, V. De Heyn et al., "A 16mA UWB 3-to-5GHz 20Mpulses/s Quadrature Analog Correlation Receiver in 0.18 $\mu$ m CMOS", ISSCC 2006, Feb. 2006.
- [77] I. D. O'Donnell, S. W. Chen, S. B. T. Wang, and R. W. Brodersen, "An integrated, low power, ultra-wideband transceiver architecture for lowrate, indoor wireless systems," Proc. IEEE CAS Workshop Wireless Communications and Networking, Sep. 2002.
- [78] F. Zhang, A. Jha, R. Gharpurey and P. Kinget, "An Agile, Ultra-wideband Pulse Radio Transceiver with Discrete-Time Wideband-IF," IEEE Journal of Solid-State Circuits (JSSC), May 2009.

- [79] T. Terada, S. Yoshizimi, M. Musqsith, Y. Sanada, and T. Kuroda, "A CMOS Ultra-Wideband Impulse Radio Transceiver for 1-Mb/s Data Communications and +/-2.5-cm Range Finding," *IEEE Journal of Solid-State Circuits*, Vol. 41, No. 4, Apr. 2006.
- [80] B. P. Otis, Y. H. Chee, and J. Rabaey, "A 400  $\mu$ W-RX, 1.6mW-TX Superregenerative Transceiver for Wireless Sensor Networks," in *IEEE Int. Solid-State Circuits Conf. Dig. Tech. Papers*, February 2005.
- [81] A. Porret, T. Melly, D. Python, C. C. Enz, and E. A. Vittoz, "An Ultralow-Power UHF Transceiver Integrated in a Standard Digital CMOS Process: Architecture and Receiver," *IEEE Journal of Solid-State Circuits*, vol. 36, pp. 452–466, 2001.
- [82] J. Jarvinen, J. Kaukovouri, J. Ryyanen, J. Jussila, K. Kivekas, M. Honkanen, and K. Halonen, "2.4GHz Receiver for Sensor Applications," *IEEE Journal of Solid-State Circuits*, vol. 40, no. 7, pp. 1426–1433, July 2005.
- [83] Y.-H. Chen, C.-W. Wang, C.-F. Lee, T.-Y. Yang, C.-F. Liao, G.-K. Ma, and S.-I. Liu, "A 0.18 $\mu$ m CMOS Receiver for 3.1 to 10.6 GHz MB-OFDM UWB Communication Systems," in *IEEE Proceedings of the Radio Frequency Integrated Circuits Symposium*, 2006.
- [84] B. Cook, A. Berny, A. Molnar, S. Lanzisera, and J. Pister, "An Ultra-Low Power 2.4GHz RF Transceiver for Wireless Sensor Networks in 0.13 $\mu$ m CMOS with 400mV Supply and an Integrated Passive RX Front-End," in *IEEE Int. Solid-State Circuits Conf. Dig. Tech. Papers*, 2006.
- [85] J. Ryckaert, M. Badaroglu, V. D. Heyn, G. V. der Plas, P. Nuzzo, A. Baschiroto, S. D' Amico, C. Desset, H. Suys, M. Libois, B. V. Poucke, P. Wambacq, and B. Gyselinckx, "A 16mA UWB 3-to-5GHz 20Mpulses/s Quadrature Analog Correlation Receiver in 0.18 $\mu$ m CMOS," in *IEEE Int. Solid-State Circuits Conf. Dig. Tech. Papers*, February 2006.
- [86] Y. J. Cho, K. H. Kim, D.H. Choi, S.S. Lee and S. Park "A Miniature UWB Planar Monopole Antenna With 5-GHz Band-Rejection Filter and the Time-Domain Characteristics", *IEEE Transactions on Antennas and propagation* , Vol. 54, No. 5, May 2006.
- [87] Alipour, A.; Hassani, H.R.; , "A Novel Omni-Directional UWB Monopole Antenna," *Antennas and Propagation*, *IEEE Transactions on* , vol.56, no.12, pp.3854-3857, Dec. 2008.

- [88] Qi Wu; Ronghong Jin; Junping Geng; Min Ding; , "Printed Omni-Directional UWB Monopole Antenna With Very Compact Size," *Antennas and Propagation, IEEE Transactions on* , vol.56, no.3, pp.896-899, March 2008.
- [89] Cemin Zhang; Fathy, A.E.; , "Development of an ultra-wideband elliptical disc planar monopole antenna with improved omni-directional performance using a modified ground," *Antennas and Propagation Society International Symposium 2006, IEEE* , vol., no., pp.1689-1692, 9-14 July 2006.
- [90] Tzyh-Ghuang Ma; Sung-Jung Wu; , "Ultrawideband Band-Notched Folded Strip Monopole Antenna," *Antennas and Propagation, IEEE Transactions on* , vol.55, no.9, pp.2473-2479, Sept. 2007.
- [91] van Zeijl, P.; Eikenbroek, J.-W.T.; Vervoort, P.-P.; Setty, S.; Tangenherg, J.; Shipton, G.; Kooistra, E.; Keekstra, I.C.; Belot, D.; Visser, K.; Bosma, E.; Blaakmeer, S.C.; , "A Bluetooth radio in 0.18- $\mu$ m CMOS," *Solid-State Circuits, IEEE Journal of* , vol.37, no.12, pp. 1679- 1687, Dec 2002.
- [92] Si, W.W.; Weber, D.; Abdollahi-Alibeik, S.; MeeLan Lee; Chang, R.; Dogan, H.; Haitao Gan; Rajavi, Y.; Luschas, S.; Ozgur, S.; Husted, P.; Zargari, M.; , "A Single-Chip CMOS Bluetooth v2.1 Radio SoC," *Solid-State Circuits, IEEE Journal of* , vol.43, no.12, pp.2896-2904, Dec. 2008.
- [93] I.F. Akyildiz, Weilian Su, Y. Sankarasubramaniam and E. Cayirci, "A Survey on Sensor Networks" *IEEE Communication Magazine*, Vol. 40, Issue 8, August 2002.
- [94] Thanigaivelu, K.; Murugan, K., "Reduced energy dissipation using Beacon Based Data Collection algorithm for mobile sink in wireless sensor networks," *First International Conference on Advanced Computing*. pp.112-115, 13-15 Dec. 2009.
- [95] Haque, Md. Rakibul; Naznin, Mahmuda; Asaduzzaman, Md.; Ahmed, Rakib Uddin; , "STP: In-network aggregation through proximity queries in a Sensor Network," *12th International Conference on Computers and Information Technology, ICCIT '09.*, Dec. 2009.
- [96] Chugh, S.; Dharia, S.; Agrawal, D.P., "An energy efficient collaborative framework for event notification in wireless sensor networks," *Proceedings. 28th Annual IEEE International Conference on Local Computer Networks, LCN '03* , 20-24 Oct. 2003.

- [97] Vu, C.T.; Beyah, R.A.; Yingshu Li; , "Composite Event Detection in Wireless Sensor Networks," Performance, Computing, and Communications Conference, 2007. IPCCC 2007. April 2007.
- [98] Chandrakasan, A.P.; Lee, F.S.; Wentzloff, D.D.; Sze, V.; Ginsburg, B.P.; Mercier, P.P.; Daly, D.C.; Blazquez, R.; , "Low-Power Impulse UWB Architectures and Circuits," Proceedings of the IEEE , vol.97, no.2, pp.332-352, Feb. 2009.
- [99] R. Dokania, X. Wang, S. Tallur, A. Apsel, "A 19uW, 100Kbps Impulse Radio Transceiver for Body-Area-Networks", International Symposium on Circuits and Systems, Paris, France, 30May-2June 2010.
- [100] R. Dokania, X. Wang, S. Tallur, C. Dorta-Quinones, A. Apsel, "An Ultralow-Power Dual-Band UWB Impulse Radio", Transactions on Circuits and Systems - II, Volume-57, Issue-7, July 2010 .
- [101] P. P. Mercier, M. Bhardwaj, D. C. Daly, A. P. Chandrakasan, "A 0.55V 16Mb/s 1.6mW Non-Coherent IR-UWB Digital Baseband with +-1ns Synchronization Accuracy," IEEE International Solid-State Circuits Conference (ISSCC), pp. 252-253, February 2009.
- [102] X. Wang, R. Dokania, A. Apsel, "PCO Based Synchronization for Ad-Hoc Duty-Cycled Impulse Radio Sensor Networks" , Accepted in special issue on cognitive sensor networks of IEEE Sensors Journal. Early access version can be found at IEEE Sensors Journal website. <http://ieeexplore.ieee.org/stamp/stamp.jsp?tp=&arnumber=5483153&tag=1>.
- [103] O. Simeone, U. Spagnolini, Y. Bar-Ness and S. Strogatz, "Distributed synchronization in wireless networks", IEEE Signal Processing Magazine, Vol.25. Issue 5, September 2008.
- [104] Ozdemir, O.; Sahinoglu, Z.; Jinyun Zhang; , "Narrowband Interference Resilient Receiver Design for Unknown UWB Signal Detection," Communications, 2008. ICC '08. IEEE International Conference on , vol., no., pp.785-789, 19-23 May 2008.
- [105] W. Godycki, R. Dokania, X. Wang, A. Apsel,"A High-Speed On-chip Implementation of Teager Kaiser Operator for In-Band Interference Rejection" Asian Solid State Circuit Conference 2010, November 8-10, 2010, Beijing, China.

- [106] P. Choi, H. Park, I. Nam, K. Kang, Y. Ku, S. Shin, S. Park, T. Kim, H. Choi, S. Kim, S. Park, M. Kim, S. Park, and K. Lee, "An Experimental Coin-sized Radio for Extremely Low Power WPAN (IEEE802.15.4) Application at 2.4GHz," in IEEE Int. Solid-State Circuits Conf. Dig. Tech. Papers, 2003.
- [107] C. Cojocaru, T. Pamir, F. Balteanu, A. Namdar, D. Payer, I. Gheorghe, T. Lipan, K. Sheikh, J. Pingot, H. Paananen, M. Littow, M. Cloutier, and E. MacRobbie, "A 43 mW Bluetooth Transceiver with -91 dBm Sensitivity," in IEEE Int. Solid-State Circuits Conf. Dig. Tech. Papers, 2003.
- [108] S. Verma, J. Xu, M. Hamada, and T. H. Lee, "A 17mW 0.66mm<sup>2</sup> Direct-Conversion Receiver for 1Mb/s Cable Replacement," in IEEE Int. Solid-State Circuits Conf. Dig. Tech. Papers, 2005.
- [109] S. Khorram, H. Darabi, Z. Zhou, Q. Li, B. Marholev, J. Chiu, J. Castaneda, H.-M. Chien, S. B. Anand, S. Wu, M.-A. Pan, R. Roofougaran, H. J. Kim, P. Lettieri, B. Ibrahim, J. J. Rael, L. H. Tran, E. Geronaga, H. Yeh, T. Frost, J. Trachewsky, and A. Rofougaran, "A Fully Integrated SOC for 802.11b in 0.18 $\mu$ m CMOS," IEEE Journal of Solid-State Circuits, vol. 40, no. 12, pp. 2492– 2501, December 2005.
- [110] A. A. Emira, A. Valdes-Garcia, B. Xia, A. N. Mohieldin, A. Valero-Lopez, S. T. Moon, C. Xin, and E. Sanchez-Sinencio, "A Dual-Mode 802.11b/Bluetooth Receiver in 0.25 $\mu$ m BiCMOS," in IEEE Int. Solid-State Circuits Conf. Dig. Tech. Papers, 2004.
- [111] T. Aytur, H.-C. Kang, R. Mahadevappa, M. Altintas, S. ten Brink, T. Diep, C.-C. Hsu, F. Shi, F.-R. Yang, C.-C. Lee, R.-H. Yan, and B. Razavi, "A Fully Integrated UWB PHY in 0.13 $\mu$ m CMOS," in IEEE Int. Solid-State Circuits Conf. Dig. Tech. Papers, 2006.
- [112] Lee, F.S.; Chandrakasan, A.P.; , "A 2.5 nJ/bit 0.65 V Pulsed UWB Receiver in 90 nm CMOS," Solid-State Circuits, IEEE Journal of , vol.42, no.12, pp.2851-2859, Dec. 2007.
- [113] Crepaldi, M.; Chen Li; Dronson, K.; Fernandes, J.; Kinget, P.; , "An Ultra-Low-Power interference-robust IR-UWB transceiver chipset using self-synchronizing OOK modulation," Solid-State Circuits Conference Digest of Technical Papers (ISSCC), 2010 IEEE International , vol., no., pp.226-227, 7-11 Feb. 2010.

- [114] N.M. Pletcher, S. Gambini, and J. Rabaey, "A 52  $\mu$ W Wake-Up Receiver With -72 dBm Sensitivity Using an Uncertain-IF Architecture," *Solid-State Circuits, IEEE Journal of*, vol.44, no.1, pp.269-280, Jan. 2009.
- [115] S. Drago, D.M.W. Leenaerts, F. Sebastiano, L.J. Breems, K.A.A. Makinwa, and B. Nauta, "A 2.4GHz 830pJ/bit duty-cycled wake-up receiver with -82dBm sensitivity for crystal-less wireless sensor nodes," *Solid-State Circuits Conference Digest of Technical Papers (ISSCC), 2010 IEEE International*, vol., no., pp.224-225, 7-11 Feb. 2010.
- [116] J. Zyren and A. Petrick, "Tutorial on basic link budget analysis," Application note AN9804.1, Jun. 1998, Altera Application note.
- [117] R. Dokania, X. Wang, C. Dorta-Quinones, W. Godycki, S. Tallur, A. Apsel, "A 6 $\mu$ W, 100Kbps, 3-5GHz, UWB Impulse Radio Transmitter", *International Symposium on Low Power Electronics and Design*, August 18-20, Austin, Texas 2010.
- [118] R. Dokania, X. Wang, W. Godycki, C. Dorta-Quinones, A. Apsel, "PCO based Event Propagation Scheme for Globally Synchronized Sensor Networks" *IEEE Global Communications Conference 2010 (GLOBECOM 2010)*, Miami, Florida, December 6-10, 2010.
- [119] X. Wang, R. Dokania and A. Apsel, "Implementation of a Global Clocking Scheme for ULP Radio Networks", *IEEE International Symposium on Circuits and Systems*, 24-27 May 2009, Taipei, Taiwan.
- [120] A. Apsel, R. Dokania and X. Wang, "Ultra-Low Power Radios for Ad-Hoc Networks", *IEEE International Symposium on Circuits and Systems*, 24-27 May 2009, Taipei, Taiwan.
- [121] A. Apsel, R. Dokania, X. Wang, "Low Power Radio Links", To Appear in 2011 *Mc-Graw Hill Year Book of Science and Technology*.